Single Droplet Drying at High Temperatures

Andrew Bayly

PhD students: Wael Ebrahim, Tien Nguyen

Institute of Particle Science and Engineering

School of Chemical and Process Engineering

University of Leeds

UK

IFPRI Annual Meeting, 2017, Philadelphia, USA

Spray Drying Activity Update

UNIVERSITY OF LEEDS

IFPRI
International Fine Particle Research Institute

Modelling PhD recruited – Tien Nguyen

ADDPT
ADVANCED DIGITAL DESIGN OF PHARMACEUTICAL THERAPEUTICS

EPSRC
Engineering and Physical Sciences Research Council

Droplets to Structure

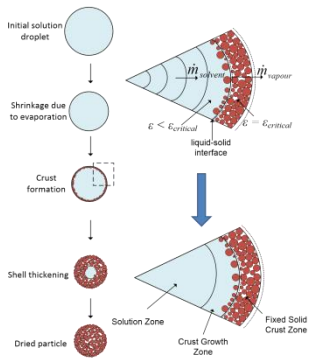

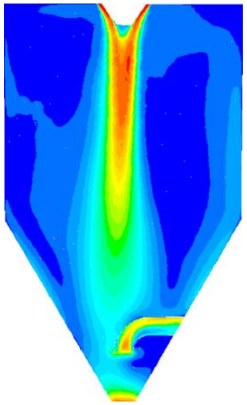

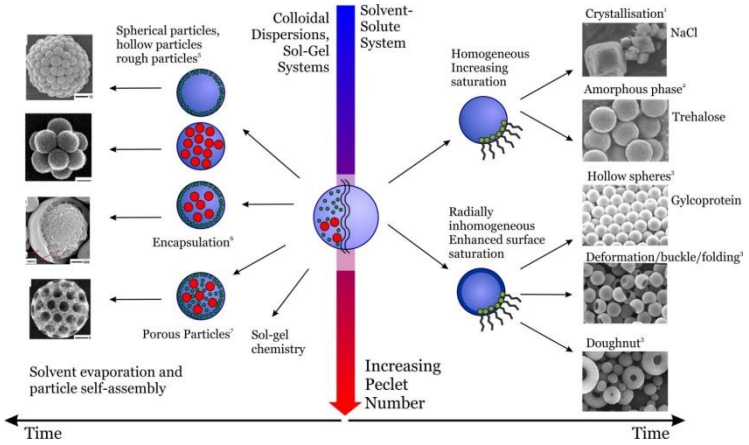

What is different about high temperatures?

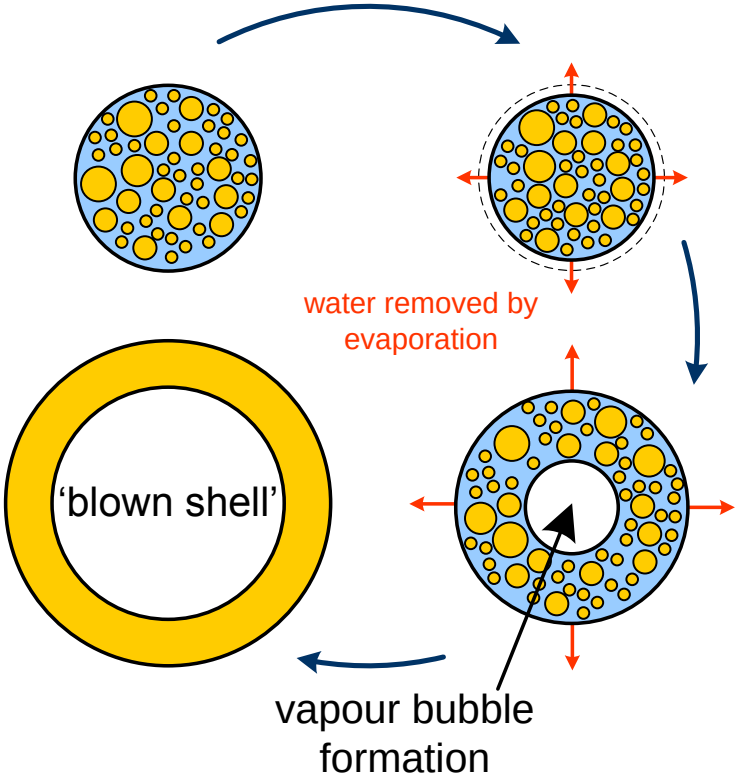

Bubble nucleation leads to mechanical deformation, puffing, and very significant changes in physical and functional properties

Work Programme

UNIVERSITY OF LEEDS

Goal: regime map based on material properties

- Drying rig development for experimental mapping
- Material property method development
- Modelling – incorporation of structural development

Material Categories

UNIVERSITY OF LEEDS

- Skin forming/plastic/polymeric
- Suspensions and colloids
  - diffusivity a function of packing, primary particle size
- Crystallizing
  - nucleation and growth

Material Categories

UNIVERSITY OF LEEDS

- Skin forming/plastic/polymeric - HPMC
- Suspensions and colloids - Ti02, silica
  - diffusivity a function of packing, primary particle size
- Crystallizing – Na2SO4, Sucrose, Ascorbic Acid
  - nucleation and growth

Mapping behaviours

UNIVERSITY OF LEEDS

Even on a relatively uniform spray dryer. The morphologies are different, significant distribution of properties.

Why:
- drop size
- distributed drying histories
- stochastic nature of structure development

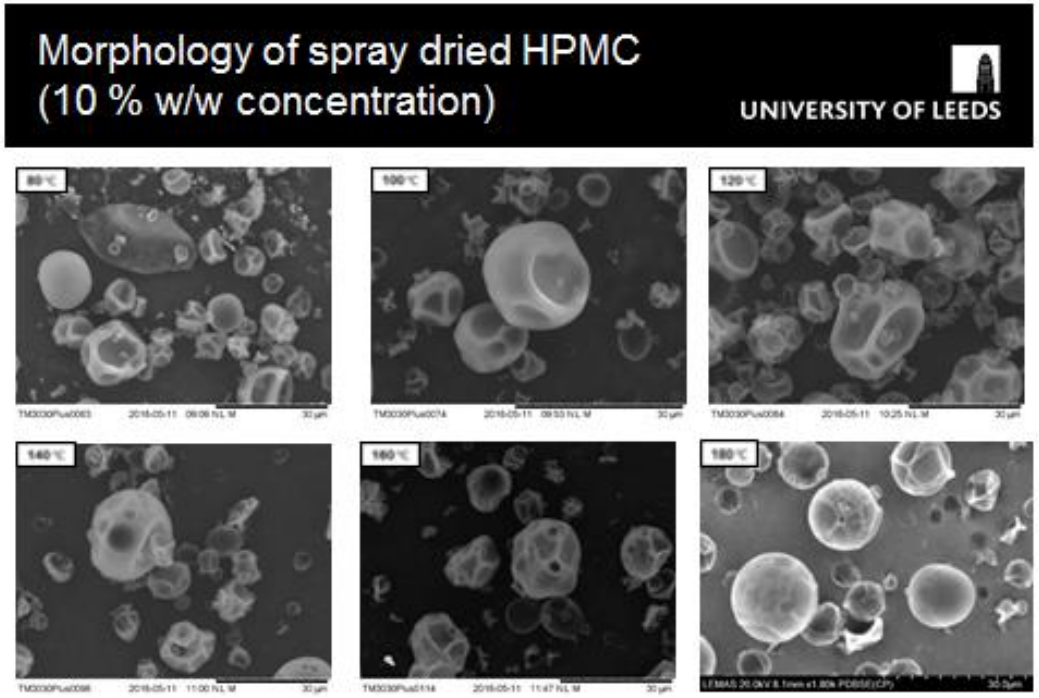

Establish method with controlled drying single or mono-dispersed droplets

Drying Methods

UNIVERSITY OF LEEDS

- Suspended droplet/filament
- Drop tube/chain
- Levitator
  - Acoustic
  - Electrodynamic balance (EDB)

Filament Drying Rig

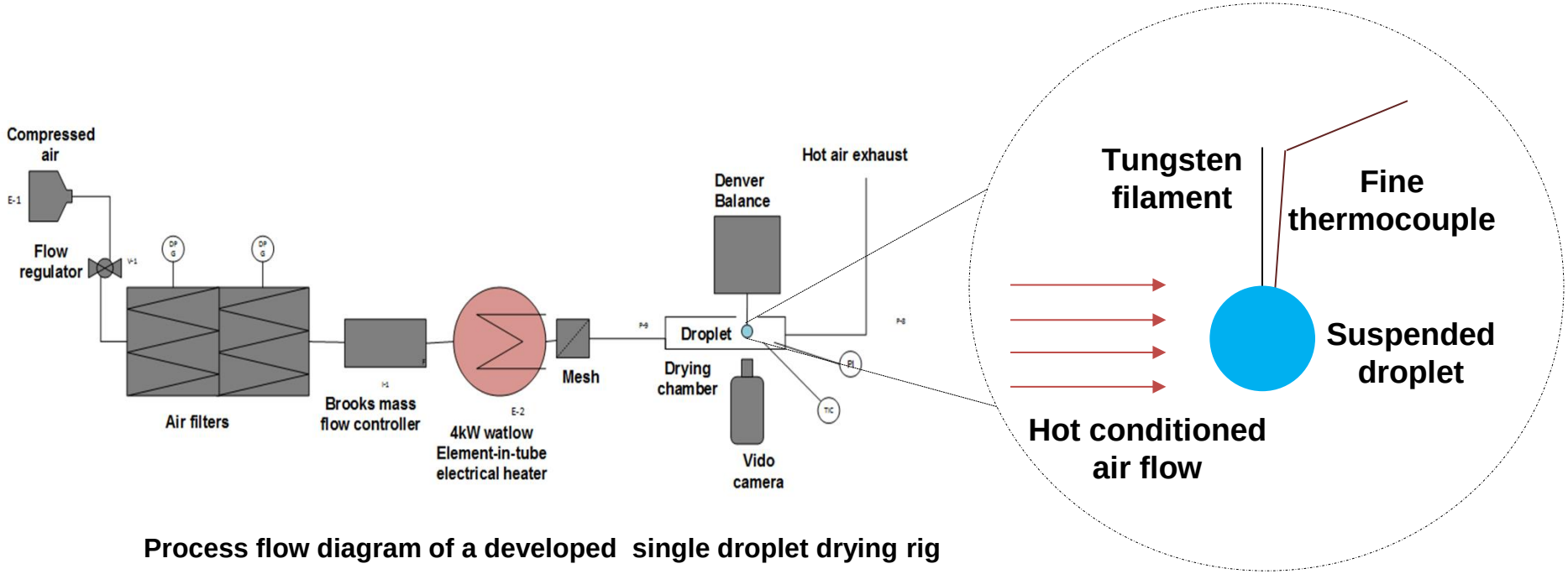

Process flow diagram of a developed single droplet drying rig

Filament Drying Rig

UNIVERSITY OF LEEDS

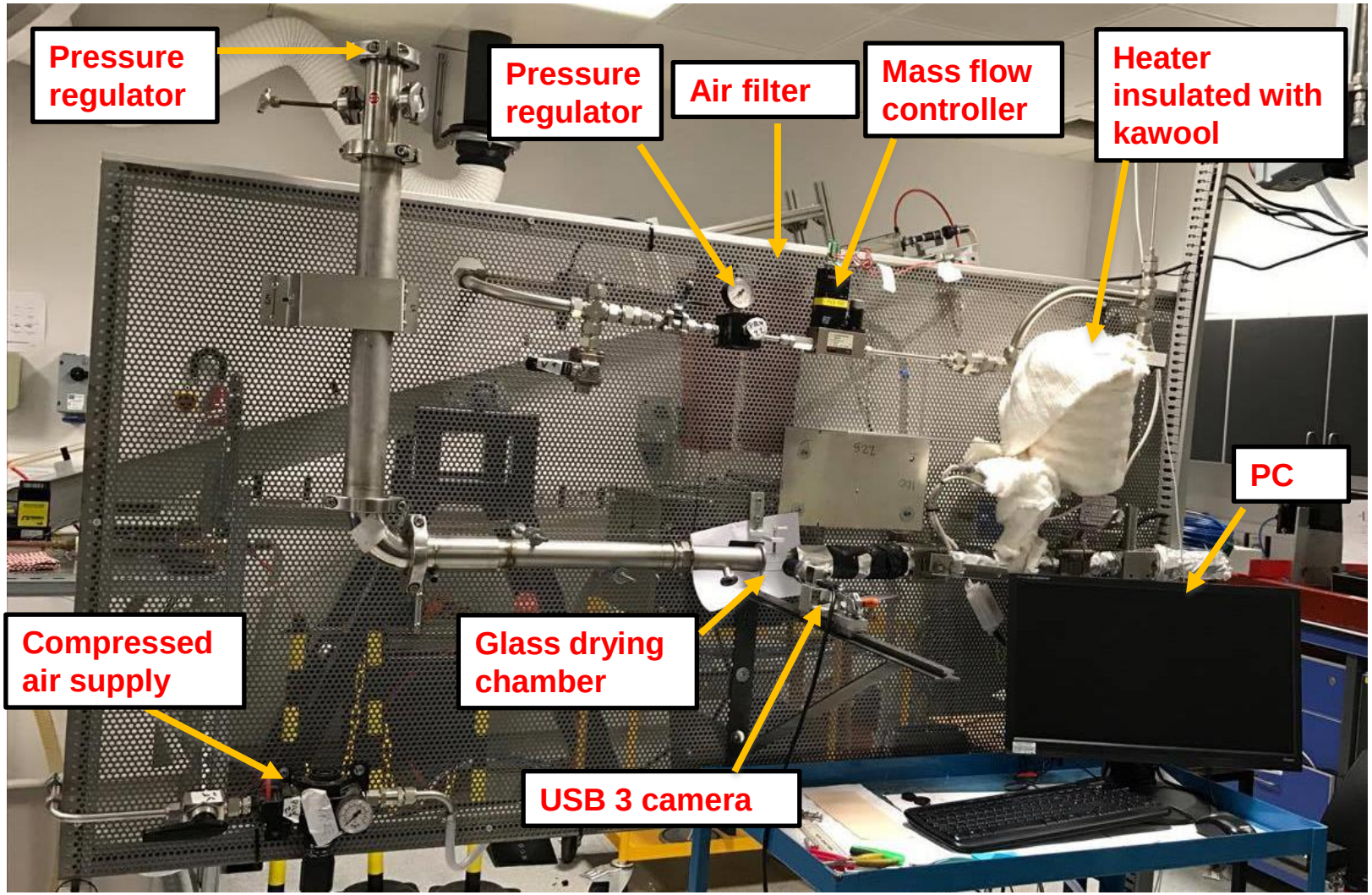

Mark 2 - Version

Sucrose - T_{air} = 190° C , 45 %, d_{init} = 1.5 mm inflation/defalation cycles

Sucrose - T_{air} = ?° C , 45 %, d_{init} = 1.5 mm
inflation/defalation cycles

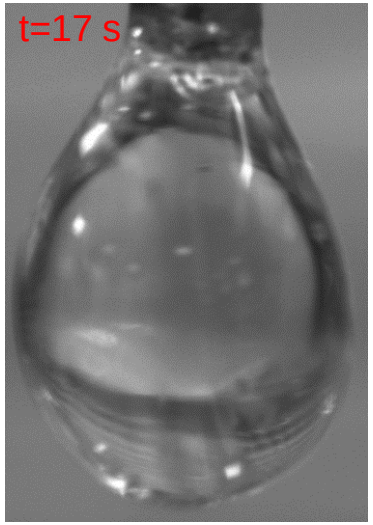

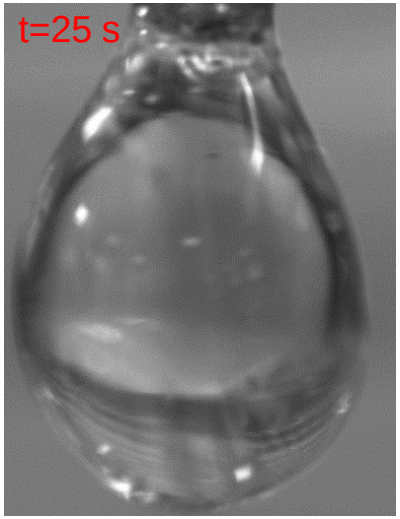

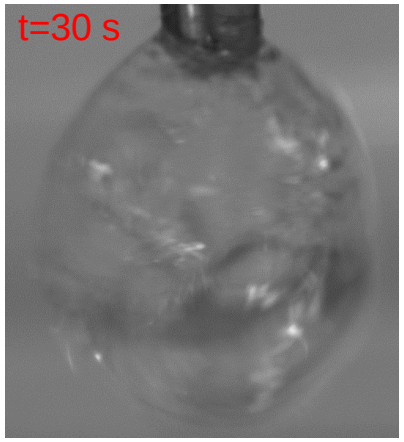

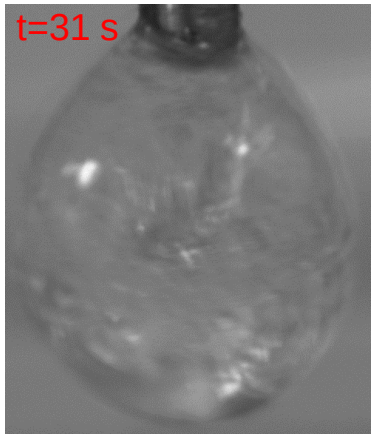

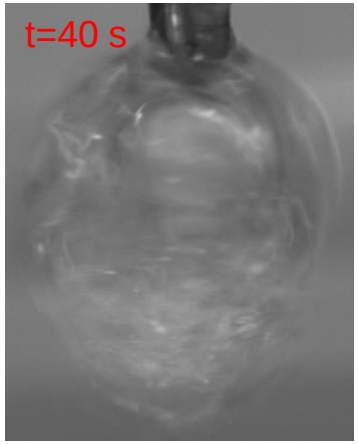

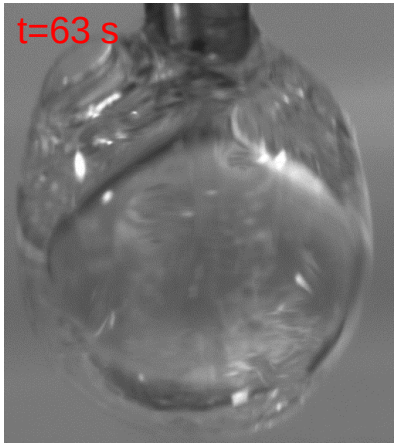

Na_2SO_4 - T_{air} = 190 ° C , 10 %, d_{init} = 1.4 mm supersaturation and crystalization

Na_2SO_4 - T_{air} = 190 ° C , 10 %, d_{init} = 1.4 mm supersaturation and crystalization

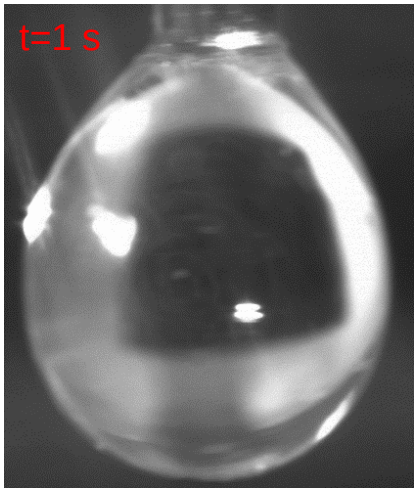

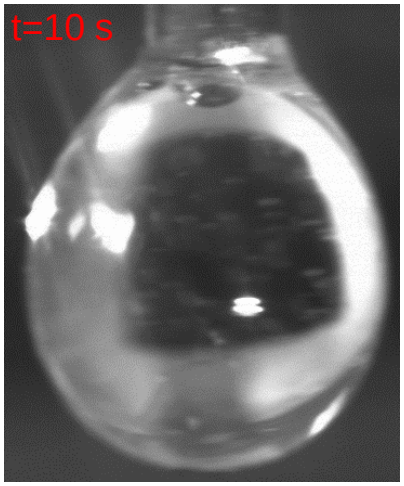

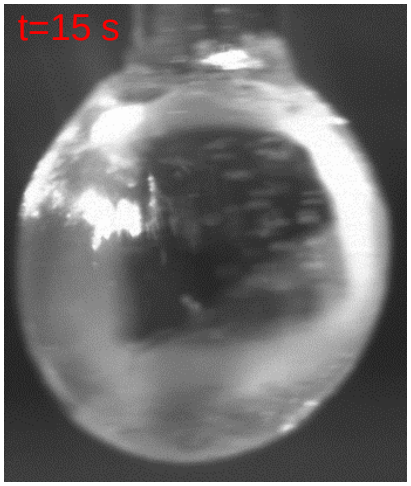

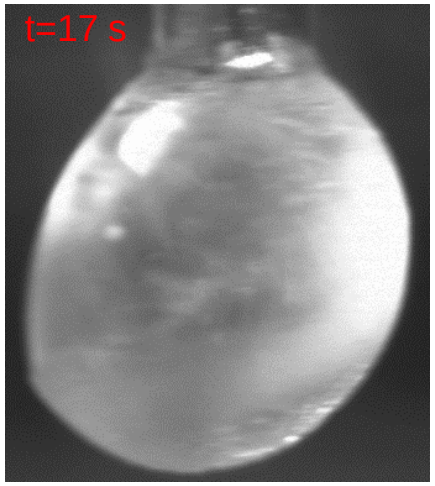

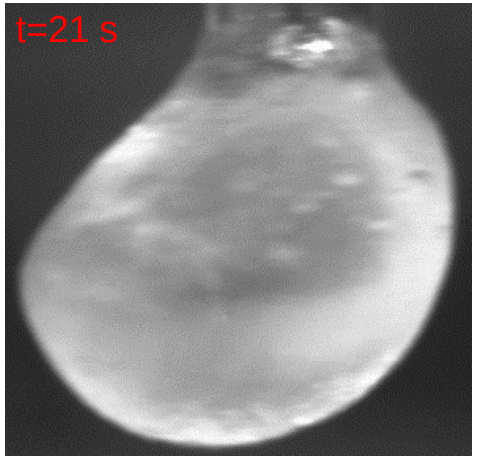

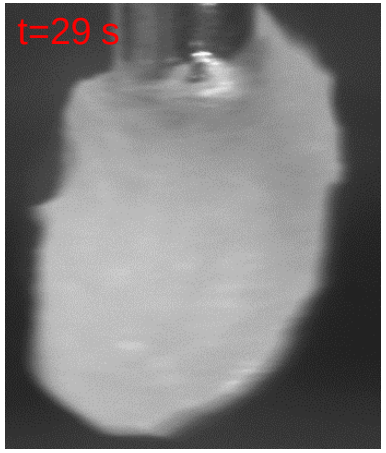

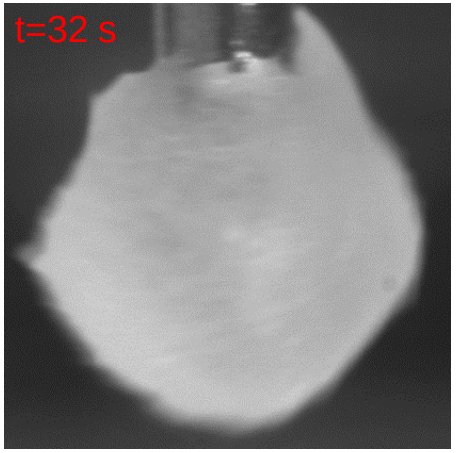

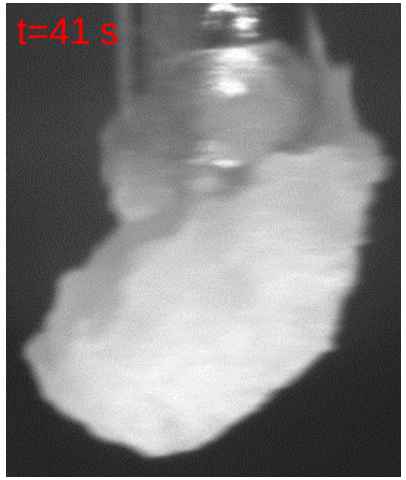

HPMC - T_{air} = 190 ° C , 5 %, d_{init} = 1.4 mm
inflation and rupture

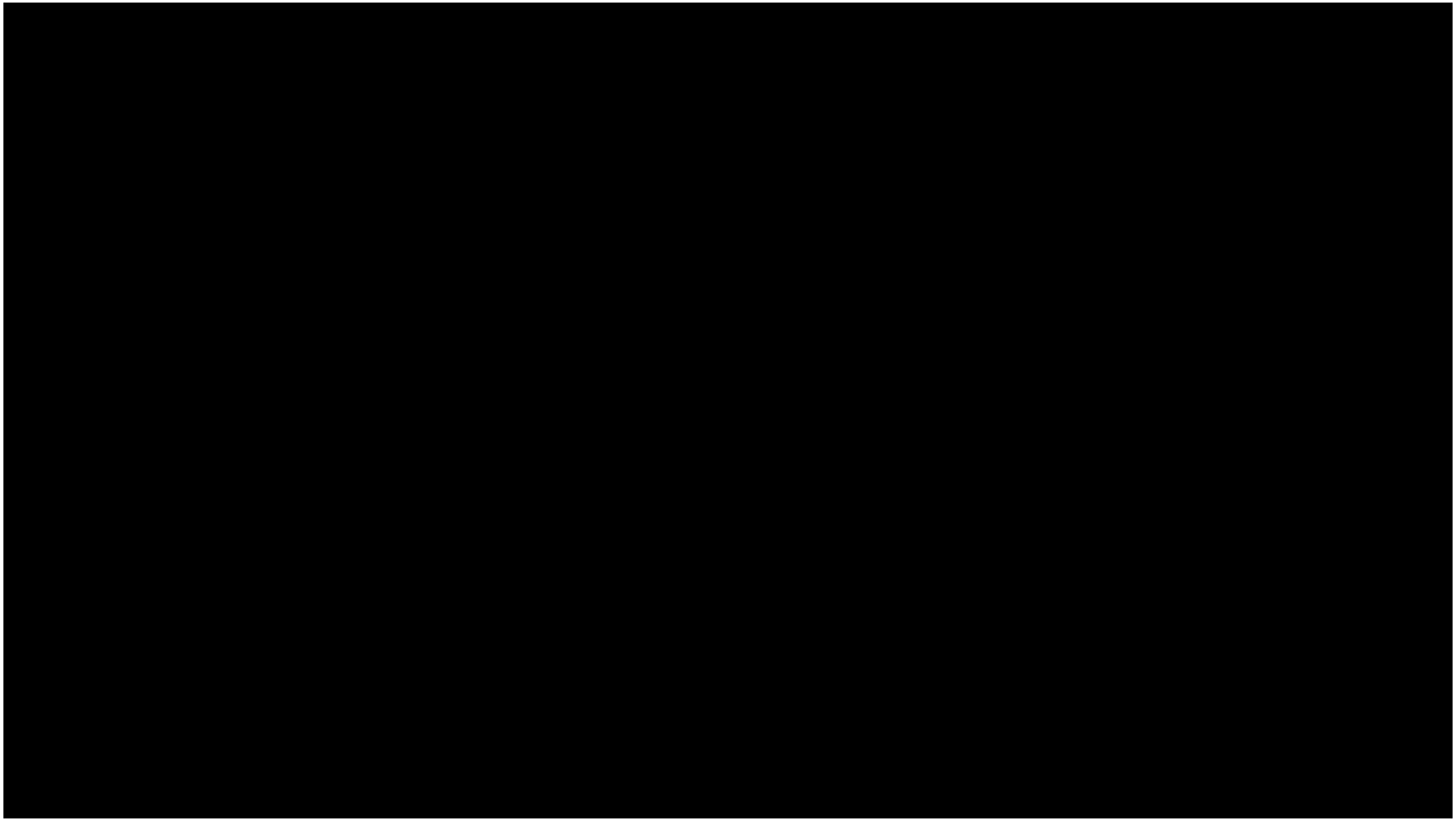

HPMC - T_{air} = 190 ° C , 5 %, d_{init} = 1.4 mm
inflation and rupture

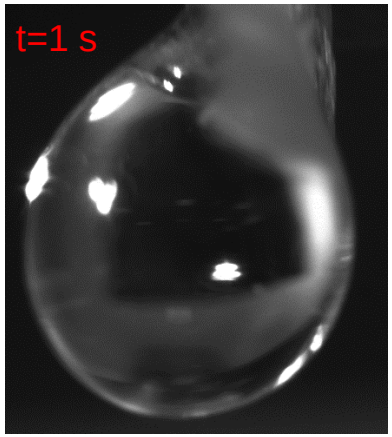

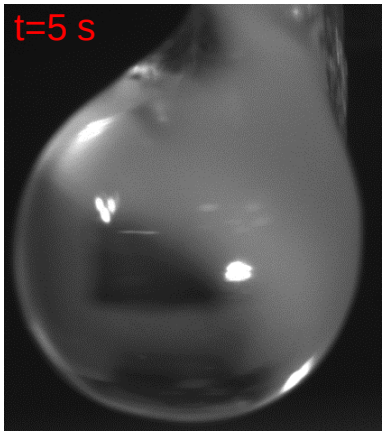

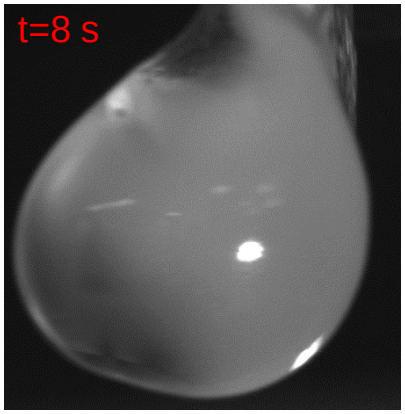

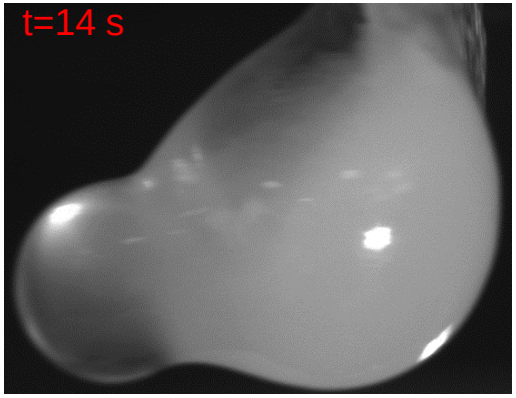

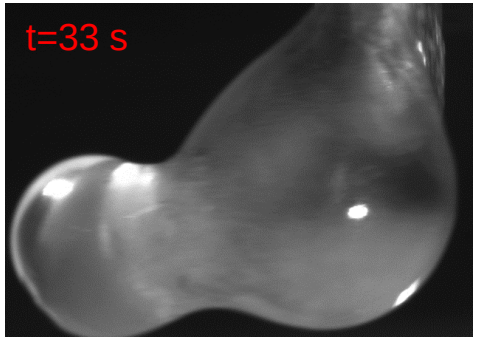

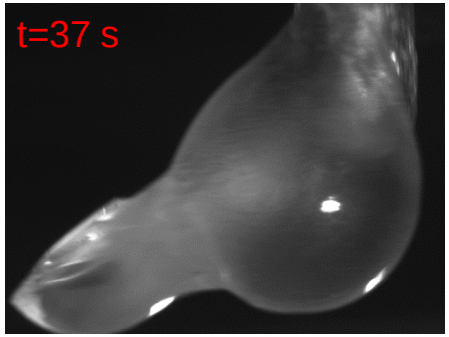

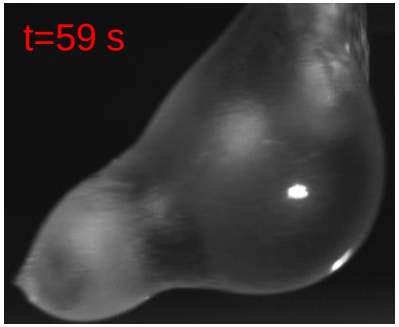

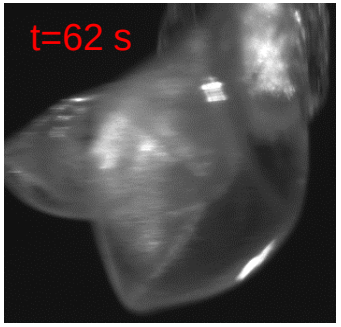

Spray Dryer & Drop Tube

UNIVERSITY OF LEEDS

- Bench marking ProCept spray dryer
- High temperature loss!
- Convert to drop tube

Heat loss on Spray Dryer

UNIVERSITY OF LEEDS

Position of thermocouples for temperature mapping on top of spray dryer

Temperature Profile for an Inlet Temperature of 80°C (Air Speed: 0.3 m³/min)

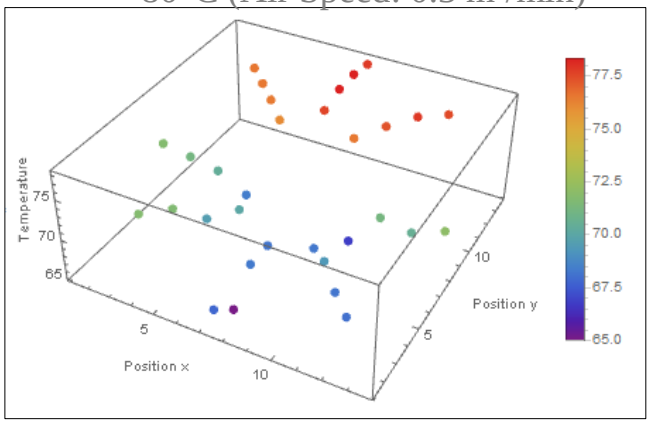

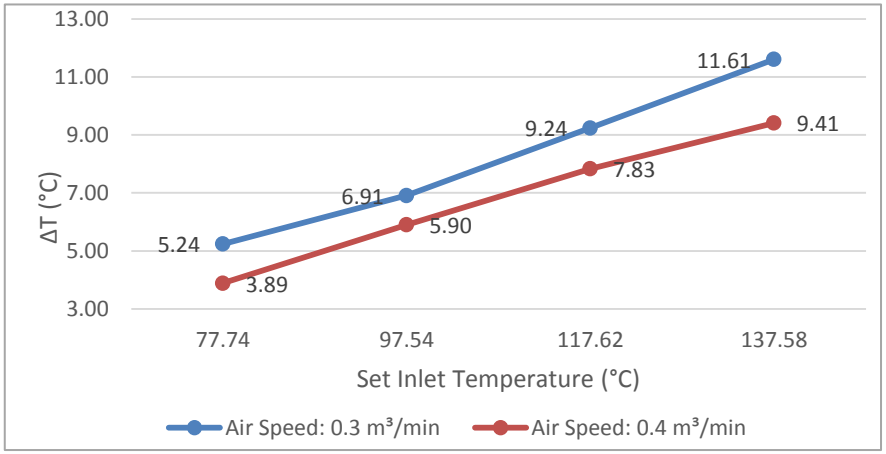

Difference between actual and set temperature

CFD Modelling of Procept Spray Drier

UNIVERSITY OF LEEDS

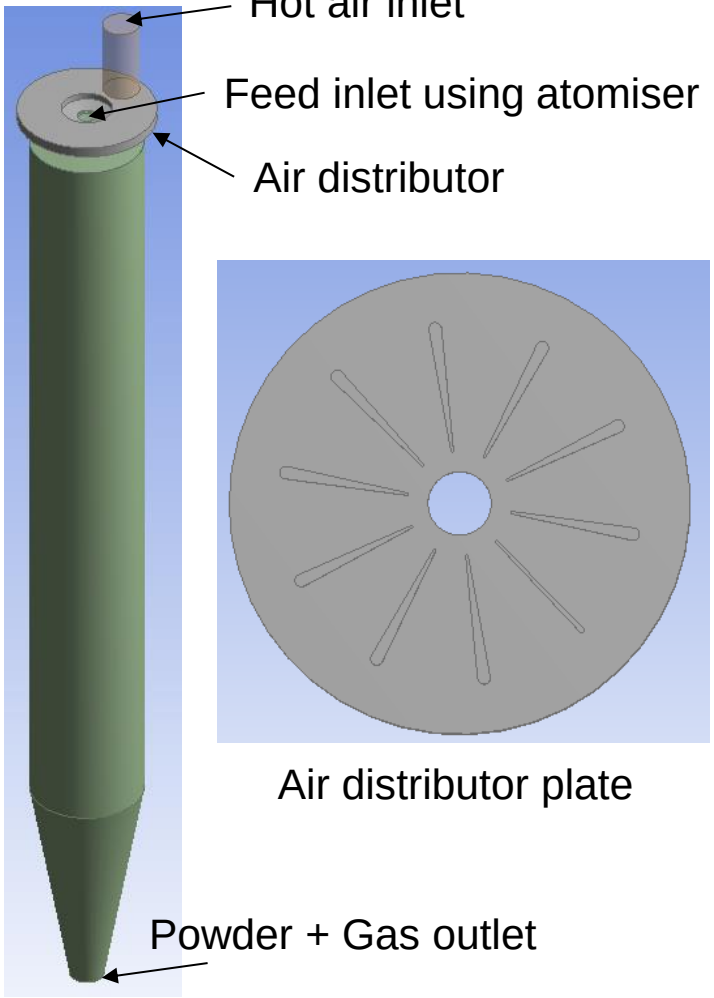

Air distributor plate

Procept Spray Dryer Geometry

- A series of wire mesh below the distributor plate modelled as porous zone
- CFD modelling is carried out using Realizable k-ε model
- Commercial CFD software Ansys Fluent is used

CFD Modelling of Procept Spray Drier

UNIVERSITY OF LEEDS

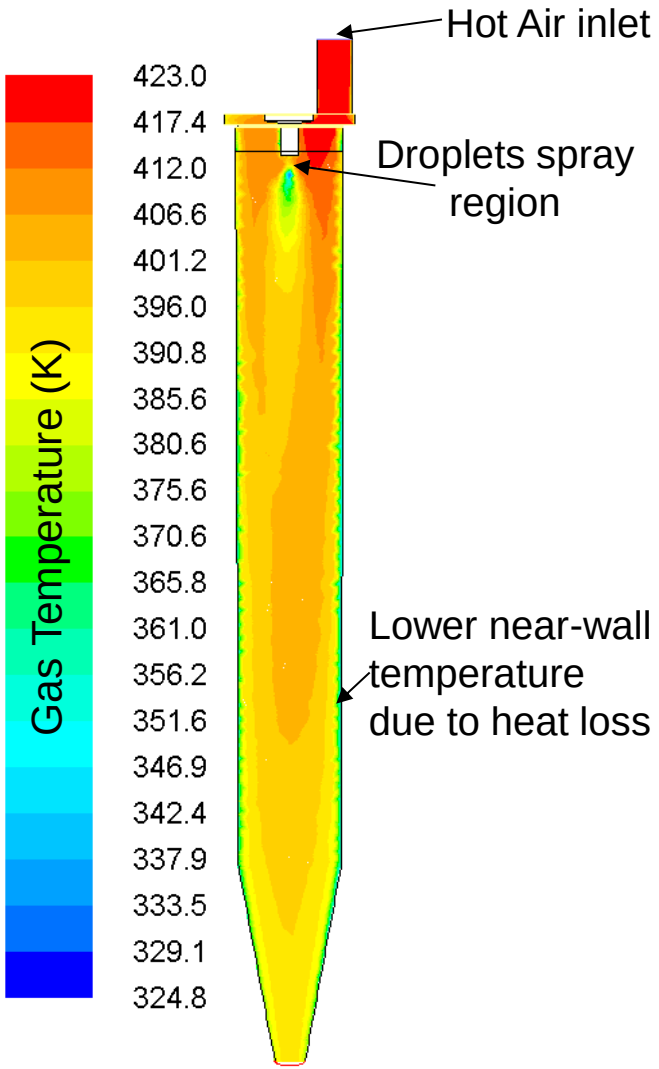

Gas Temperature Profile

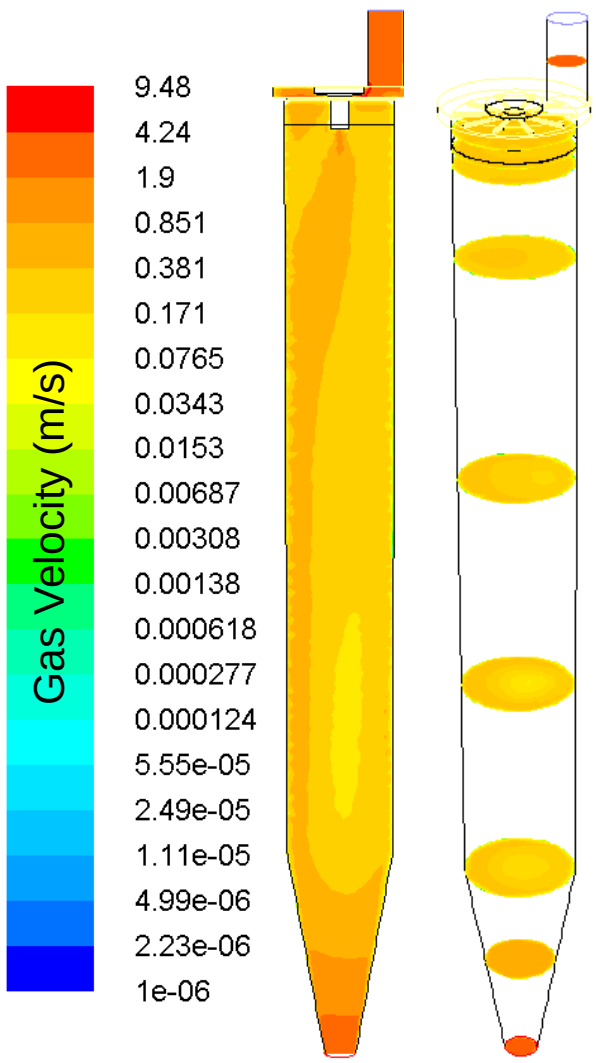

Gas Velocity Profile

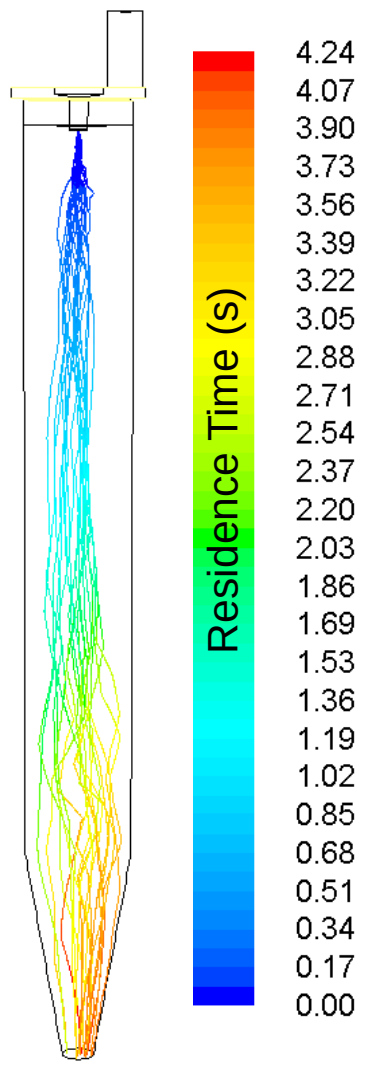

Droplets Residence Time

CFD Modelling of Procept Spray Drier

UNIVERSITY OF LEEDS

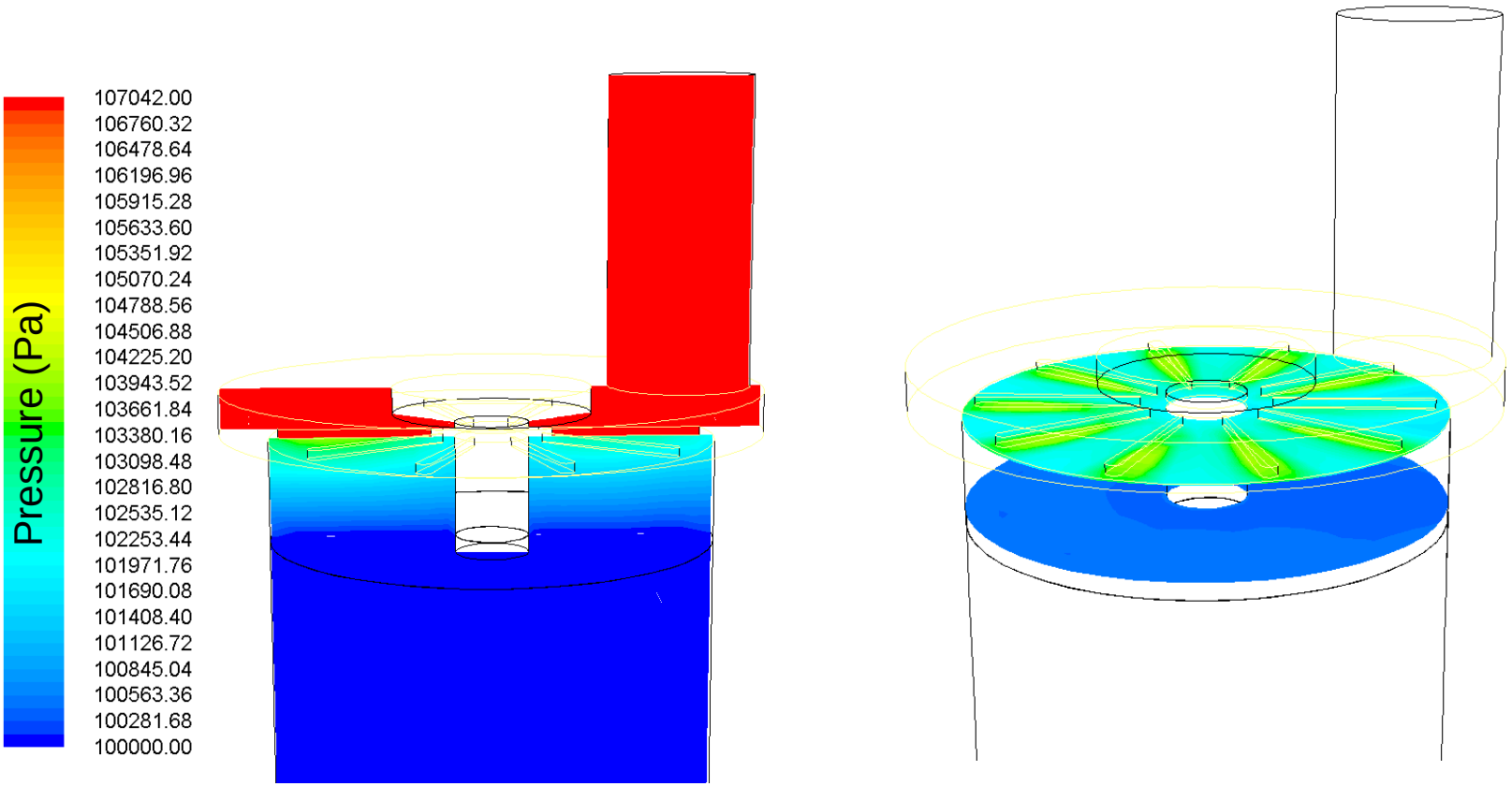

Pressure Profile

CFD Modelling of Procept Spray Dryer

UNIVERSITY OF LEEDS

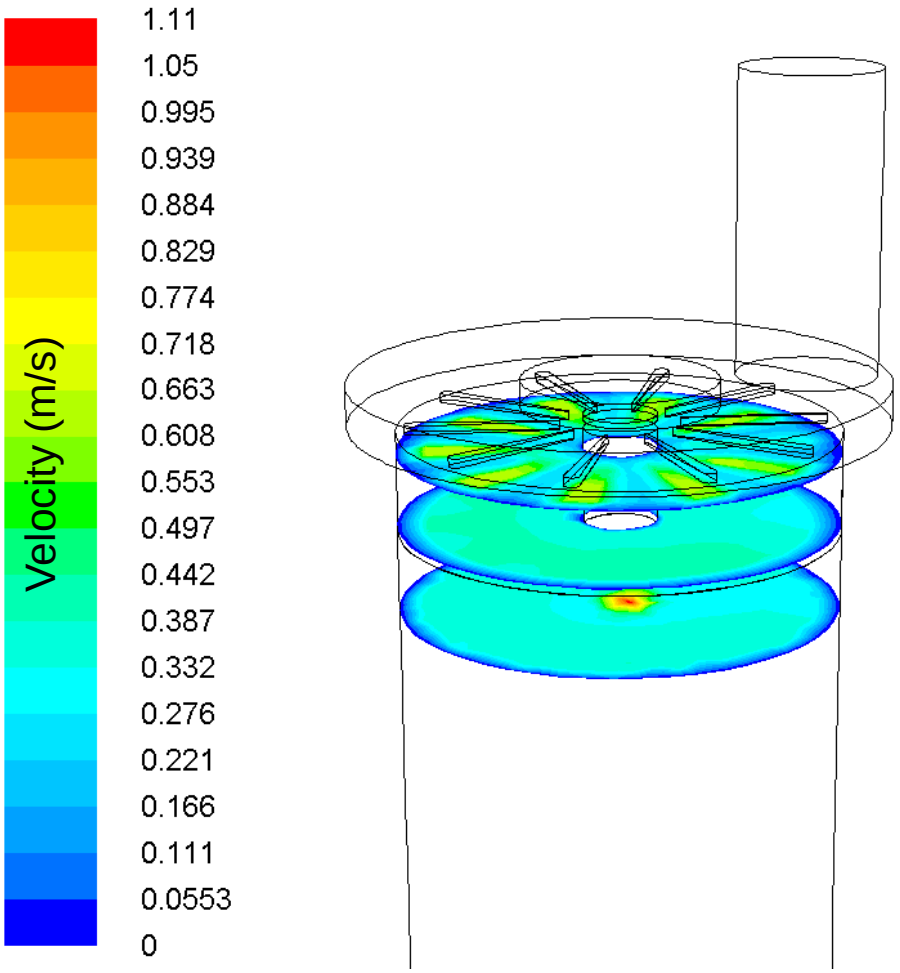

Velocity Distribution

CFD Modelling of Procept Spray Dryer

UNIVERSITY OF LEEDS

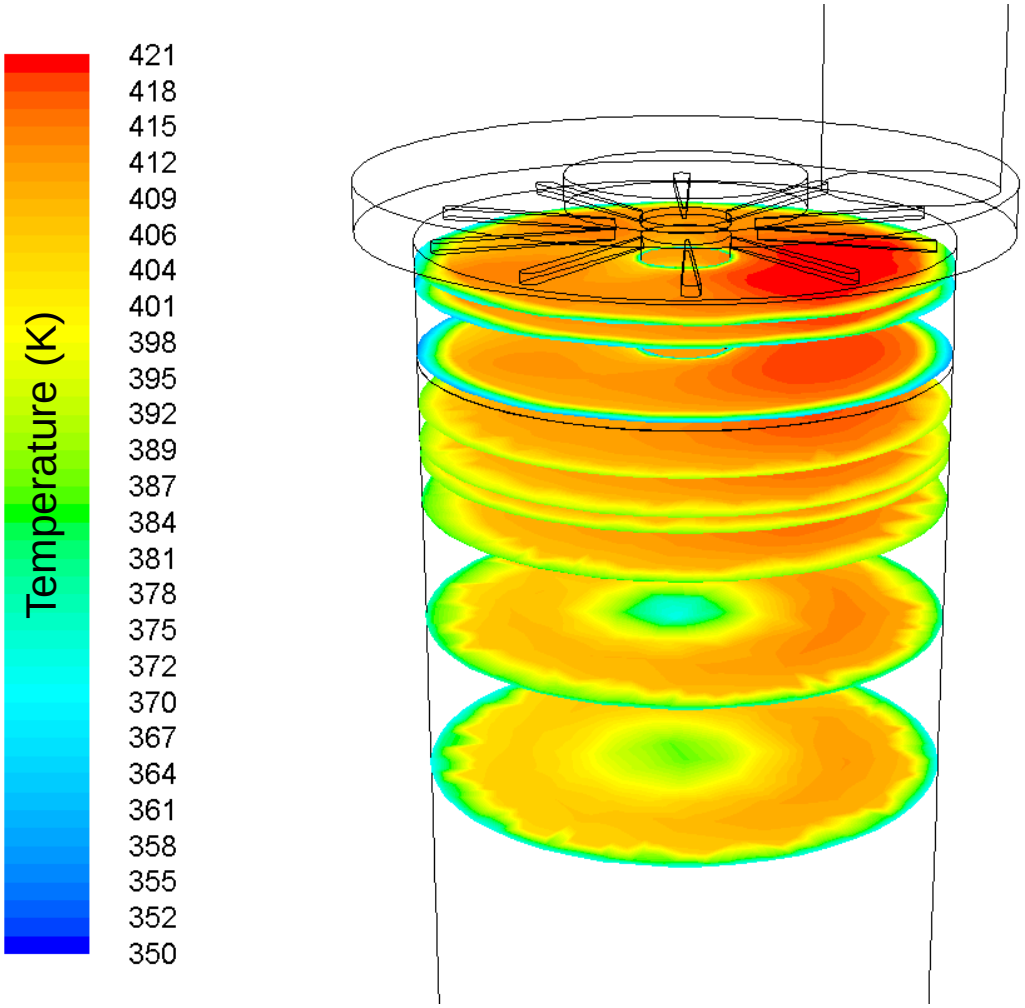

Temperature Distribution

Atomiser Selection

UNIVERSITY OF LEEDS

- Challenge – fluid viscosity
- Commercial systems reviewed
- UoL custom atomiser selected

Atomisers	Droplet size (µm)	Viscosity (cPs)	Operating temperature (°C)
MicroFab: MJ-A-Dispensing Device	10 - 150	< 20	< 50
FMP: MTG-01-G3	40 - 1000	1 - 150	20 - 80
Microdrop: MD-K-130	30, 50 & 70	0.4 - 20	10 - 80

MicroFab: MJ-A-Dispensing Device

Figure 4. MJ-AB type device with wires and connector

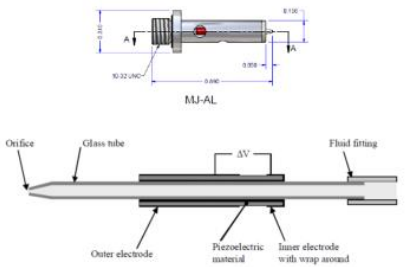

FMP: MTG-01-G3

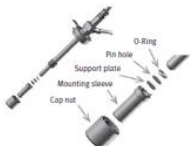

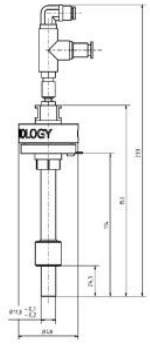

Microdrop: MD-K-130

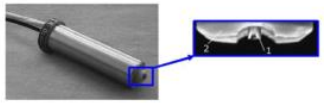

Droplet generator rig schematic

UNIVERSITY OF LEEDS

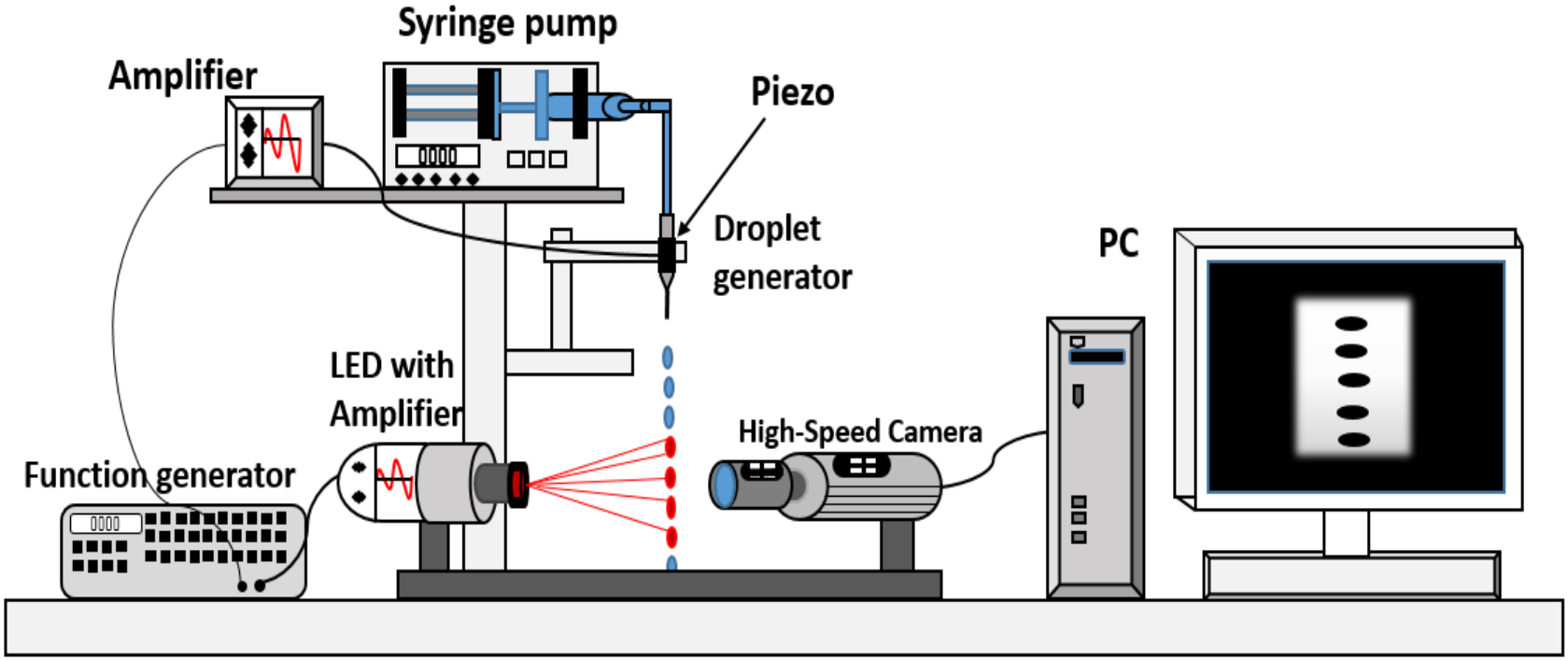

Droplet generator rig

UNIVERSITY OF LEEDS

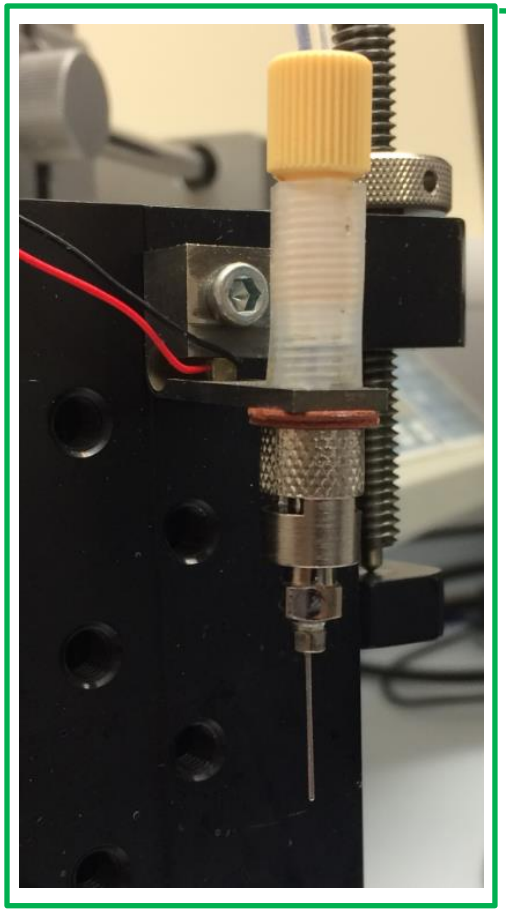

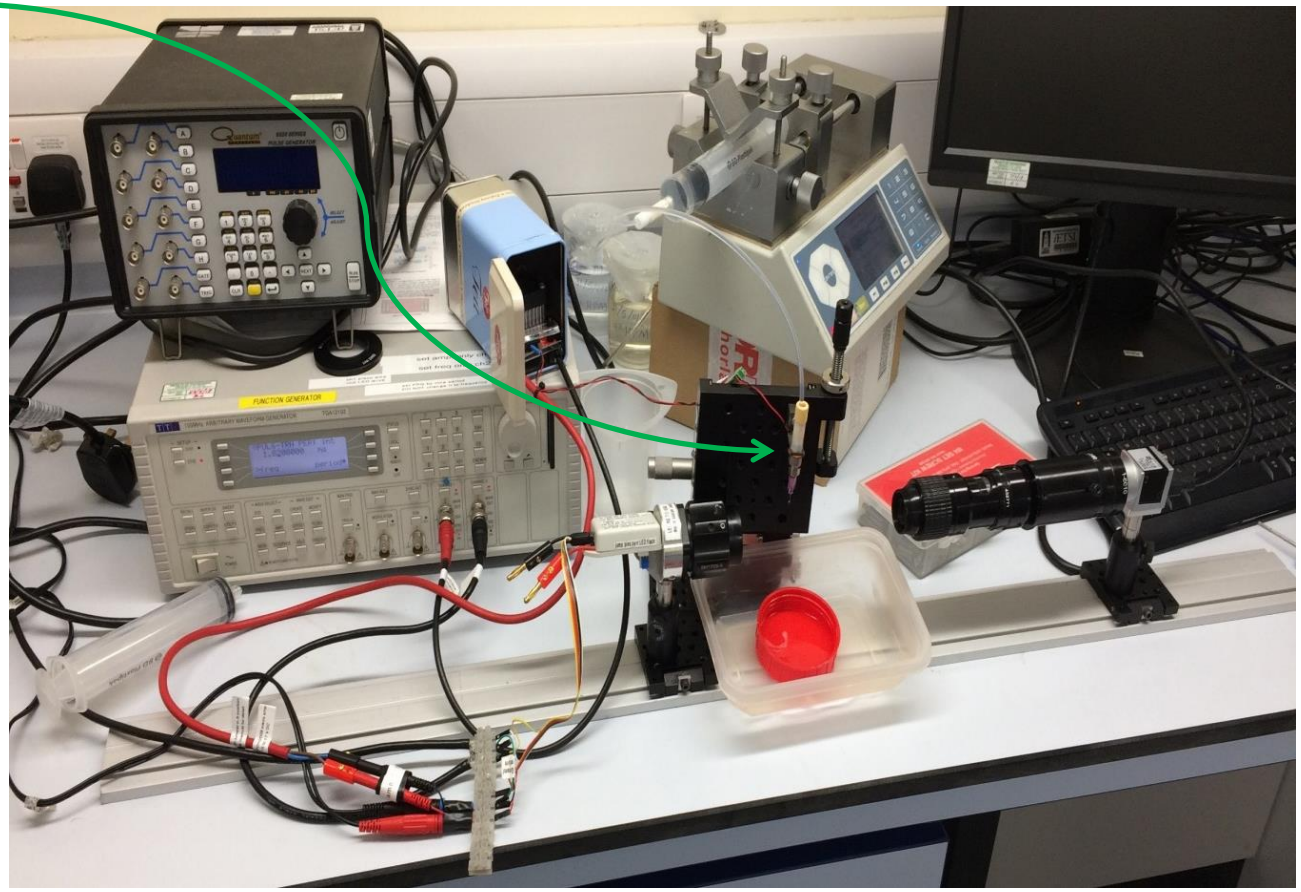

Examples of jet break-up

UNIVERSITY OF LEEDS

Water at 5ml/min from nozzle gauge of 23 (D_{in}= 0.337mm)

5% HPMC at 3 ml/min from nozzle gauge 30 (D_{in}= 0.159mm)

5% HPMC at 5 ml/min from nozzle gauge 30 (D_{in} = 0.15mm)

5% HPMC at 10 ml/min from nozzle gauge 23 (D_{in} = 0.337mm)

Nozzle D_{in}= 0.159 mm		Nozzle D_{in}= 0.337 mm	
Flow rate (ml/min)	f **(ms)** @ $\delta_\circ$ = 3mVpp	**Flow rate (Ml/min)**	f **(ms)** @ $\delta_\circ$ = 4mVpp
3	1.52	6	Low flow rate
4	1.7	7	1.1
5	2.16	8	1.5
6	No break-up	10	Difficult to break-up

The sensitivity of the amplitude seems to be mostly for the nozzle diameter $\text{amplitude}(\delta_\circ) = \frac{d_j}{2} e^{-7.68+2.66\ln(Oh)}$

Importance of material properties

UNIVERSITY OF LEEDS

Material properties of the system as it dries determine behaviour:

Transport - diffusivity

Thermodynamics - water activity

Mechanics – mechanical properties

Microwave rig

UNIVERSITY OF LEEDS

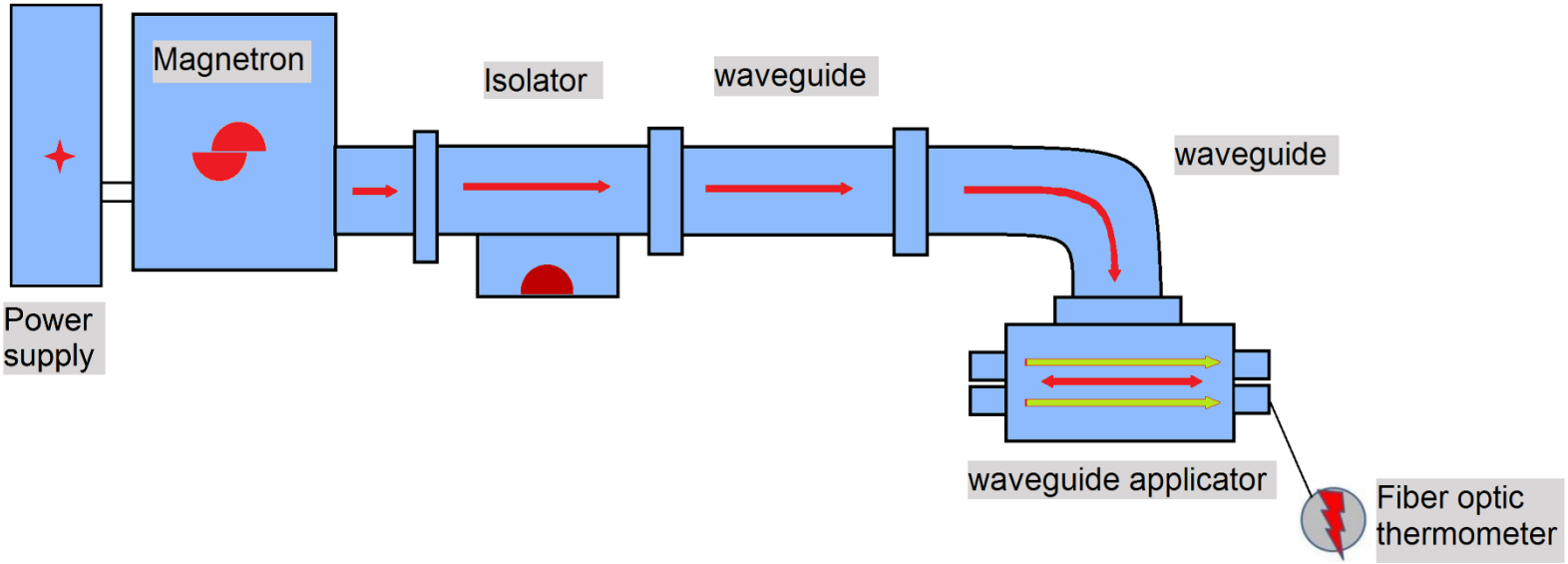

Microwave Rig

UNIVERSITY OF LEEDS

Test 1. 40 mL (water + sugar) in Teflon

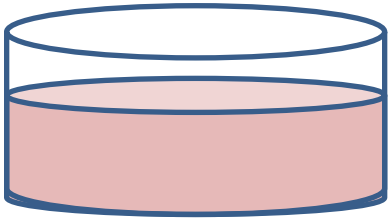

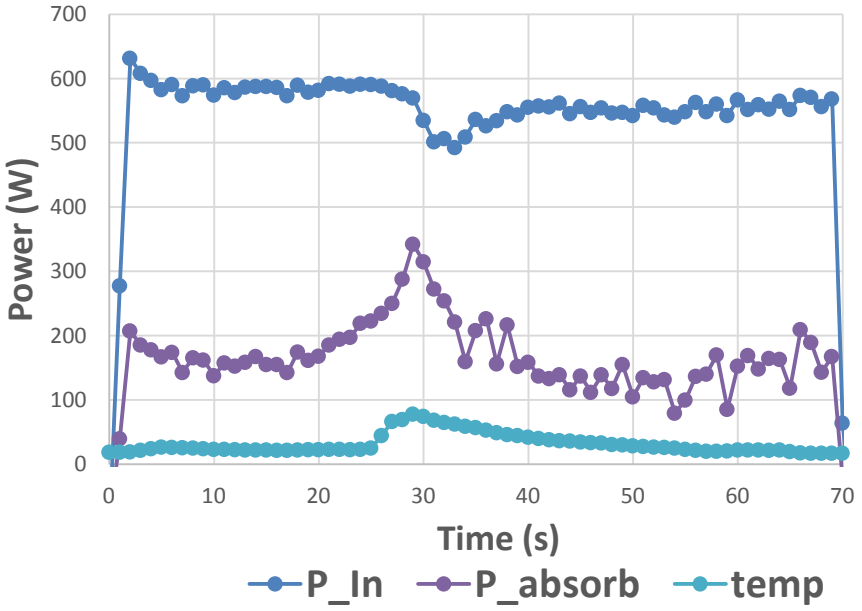

Test 2. Droplets (water + sugar) in Teflon

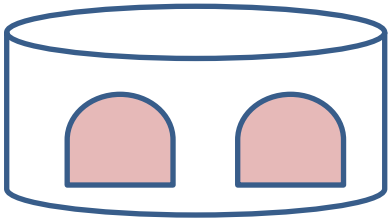

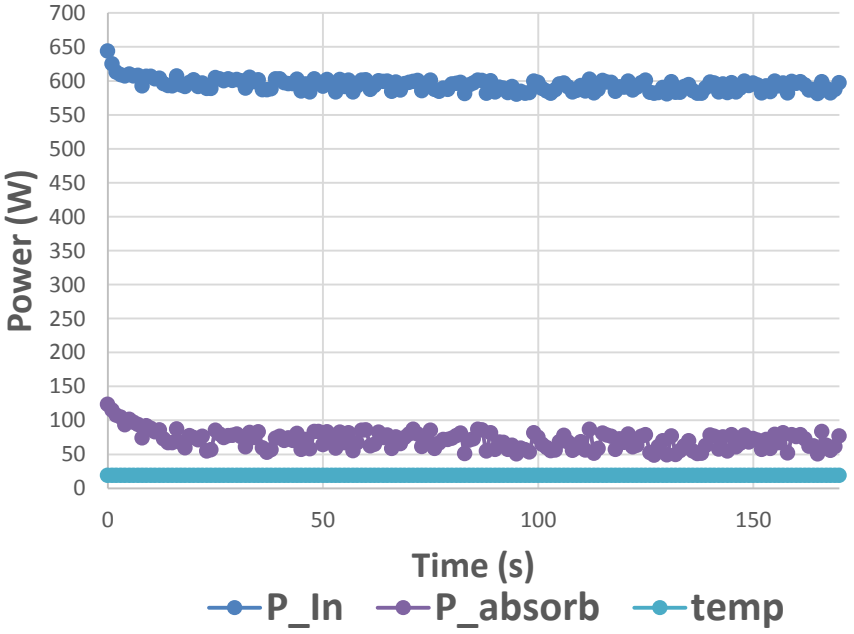

Material Properties – Next Steps

UNIVERSITY OF LEEDS

Alternative techniques

- EDB and tweezers
- rig modification and development

University of BRISTOL

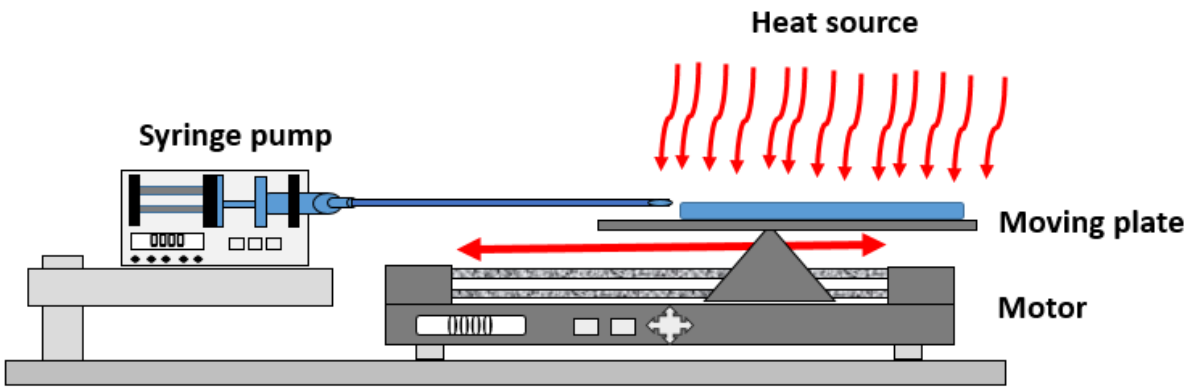

Modelling Approach

UNIVERSITY OF LEEDS

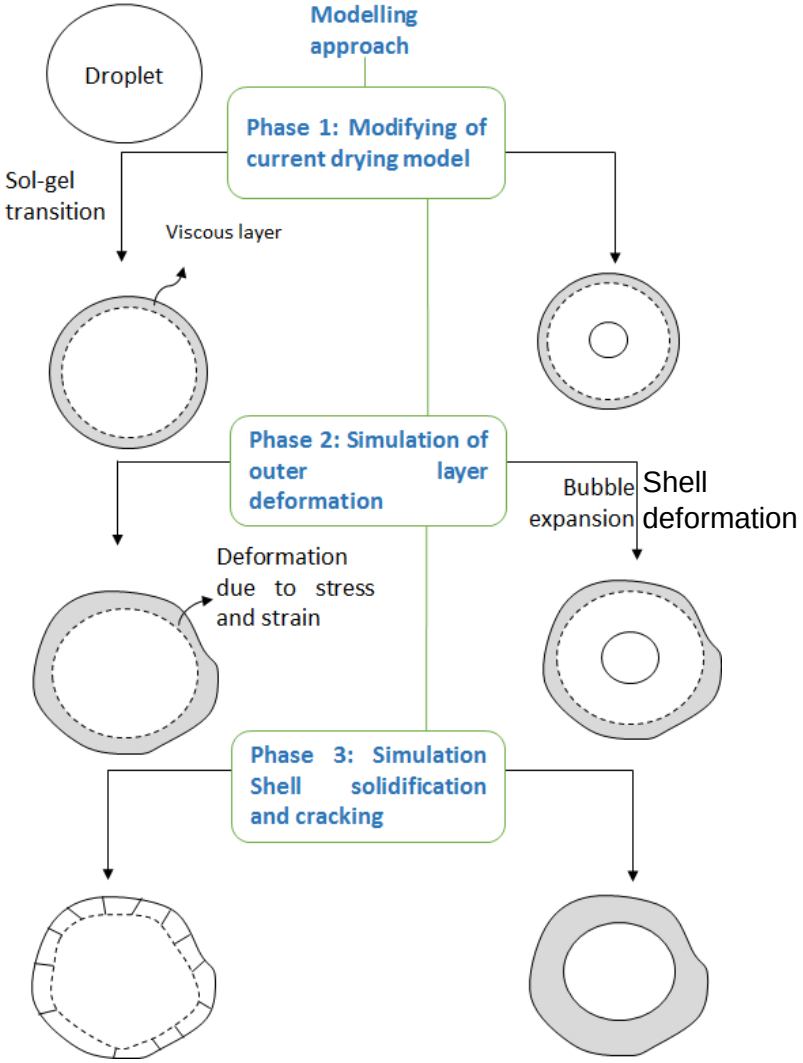

Challenges:

- Material property definition
- Numerical methods

Initial Approach

UNIVERSITY OF LEEDS

- Apply Rayleigh- Plesset approach to bubble in drop

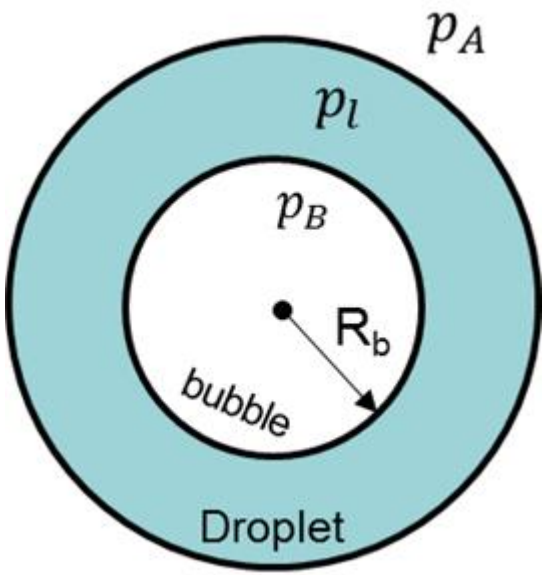

$$p_B - p_A = \left[R_D\rho_A + \rho_L\left(1 - \frac{R_D}{R_B}\right)\right]\frac{d^2R}{dt^2} + \left[\frac{3}{2}(\rho_A + \rho_L) \pm 2\rho_L\frac{R_B}{R_D} + \frac{\rho_L}{2}\left(\frac{R_B}{R_D}\right)^4\right]\left(\frac{dR}{dt}\right)^2 + 2S\left(\frac{1}{R_B} + \frac{1}{R_D}\right) + 4\left(\frac{\mu_A}{R_D} + \frac{\mu_L}{R_B}\right)\frac{dR}{dt}$$

Symmetrical Assumption?

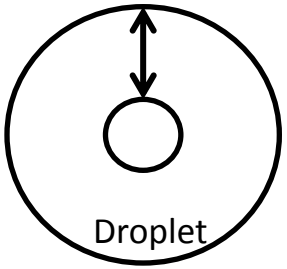

$$C_D = \frac{1}{18}\frac{d_0^2 g(\rho_l - \rho_g)}{\mu}$$

$$\tau_{dry} = \frac{\lambda \rho r_0^2}{2k(T_g - T_p)}$$

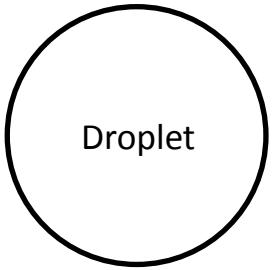

Time for rising bubble to surface vs droplet size in log scale

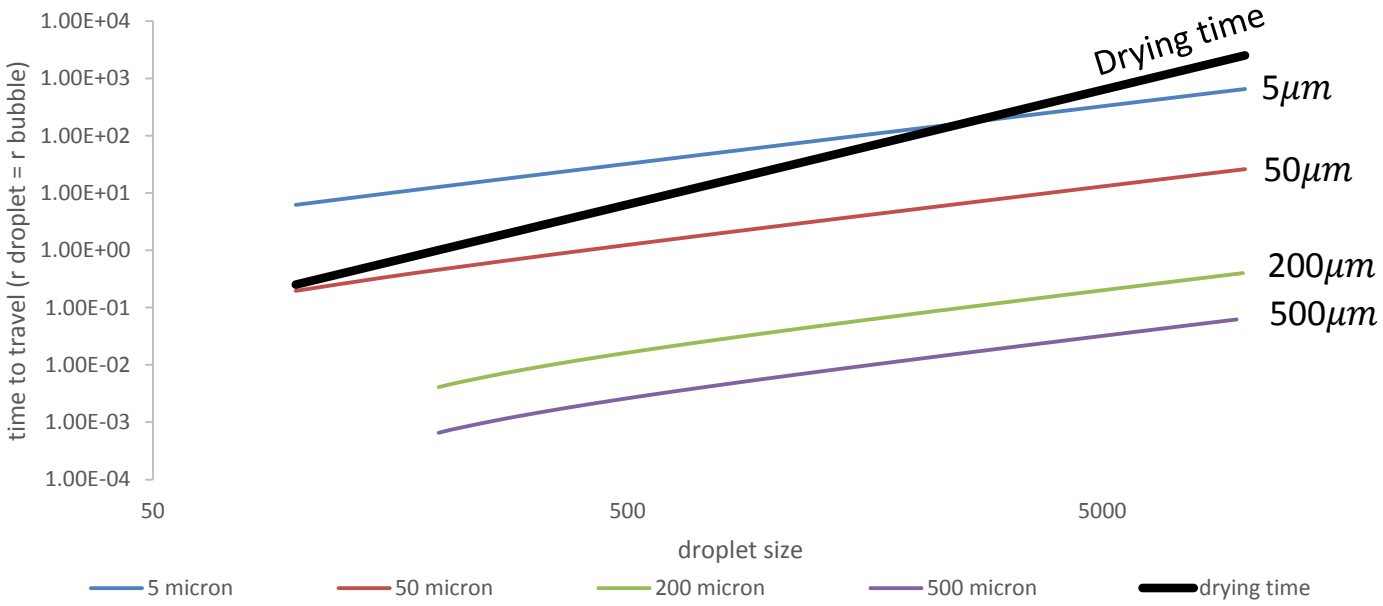

Towards a regime map

UNIVERSITY OF LEEDS

Capture link between material thermodynamic properties, transport properties and drying history

- Will a droplet boil?
  - Influence of material properties
  - Influence of size
- Properties at boiling
  - Droplet averaged
  - Surface

Drying above boiling

UNIVERSITY OF LEEDS

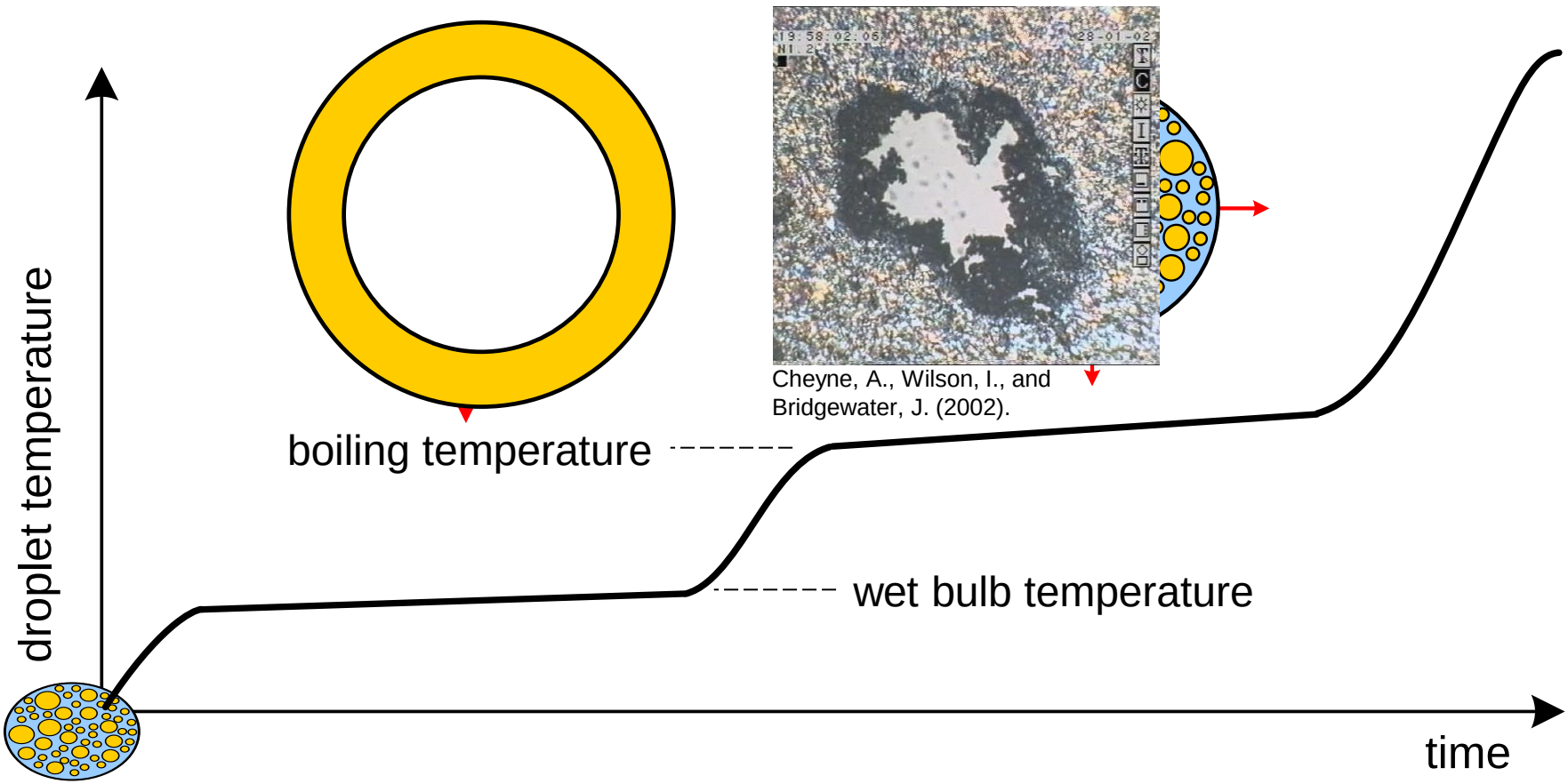

Cheyne, A., Wilson, I., and Bridgewater, J. (2002).

Will the droplet temperature exceed the solution boiling point?

Moisture Content at Boiling

UNIVERSITY OF LEEDS

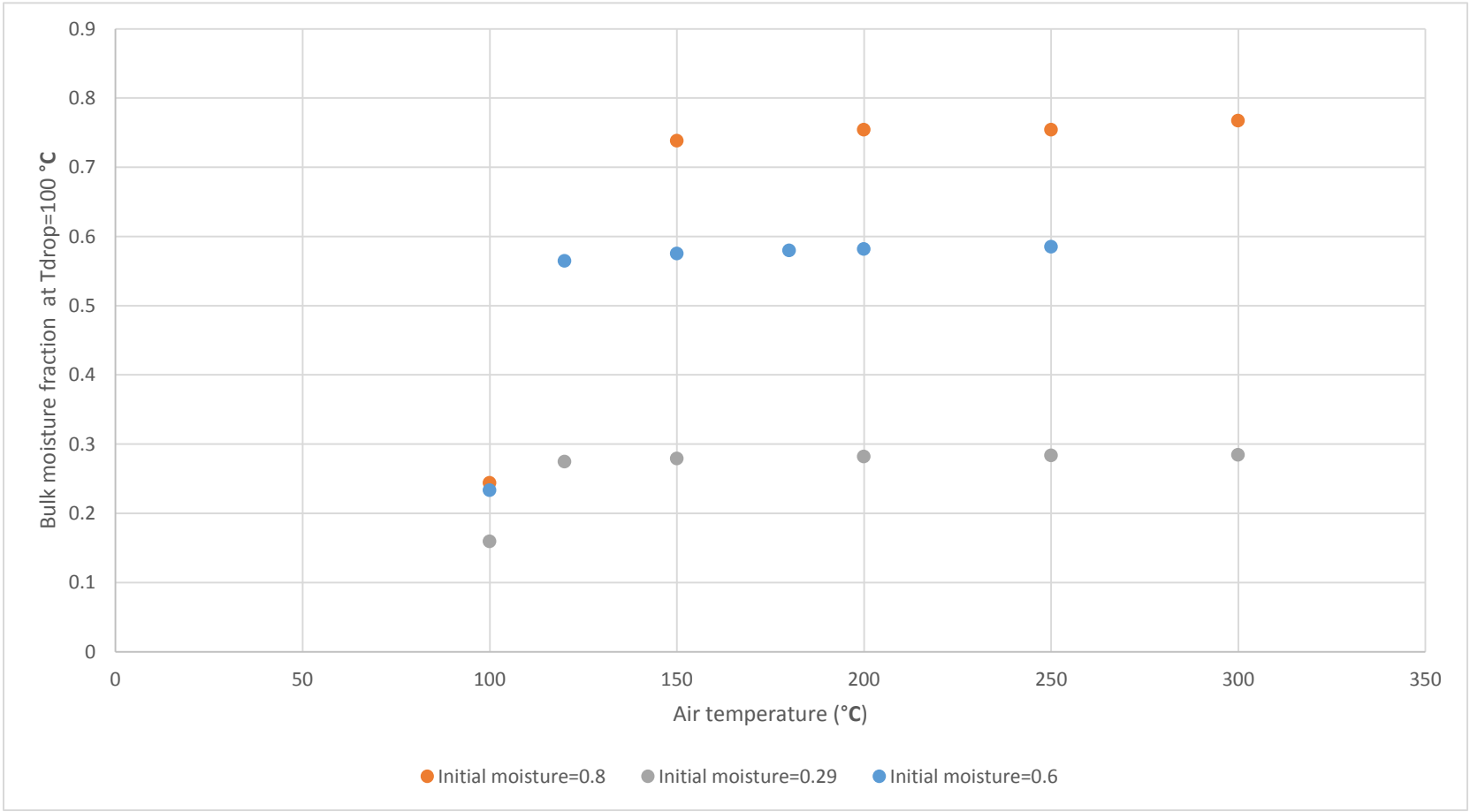

Summary

UNIVERSITY OF LEEDS

Goal: regime map based on material properties

- Filament rig – experimental mapping
- Drying rig development – drop tube
- Material property method evaluation
- Modelling – developing a resolved model

Acknowledgements

Group:
Dr. Muzammil Ali – CFD modelling supervision
Karrar Al-Dirawi – atomization rig development

Masters and Placement:
Khairul Mohd Faris – CFD of pilot spray dryer
Daniella De La Vega – Temperature profiling and atomizer evaluation
Dan Wesley – rig design
Leeds technicians – rig builds

Leeds academics:
Prof. Phil Threfall Holmes – atomiser, drying rig expertise
Prof. Nik Kapur – atomiser expertise

Funding: IFPRI, EPSRC, University of Leeds,

See you at the poster

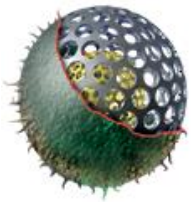

INSTITUTE OF
PARTICLE SCIENCE
& ENGINEERING

UNIVERSITY OF LEEDS

NC STATE UNIVERSITY

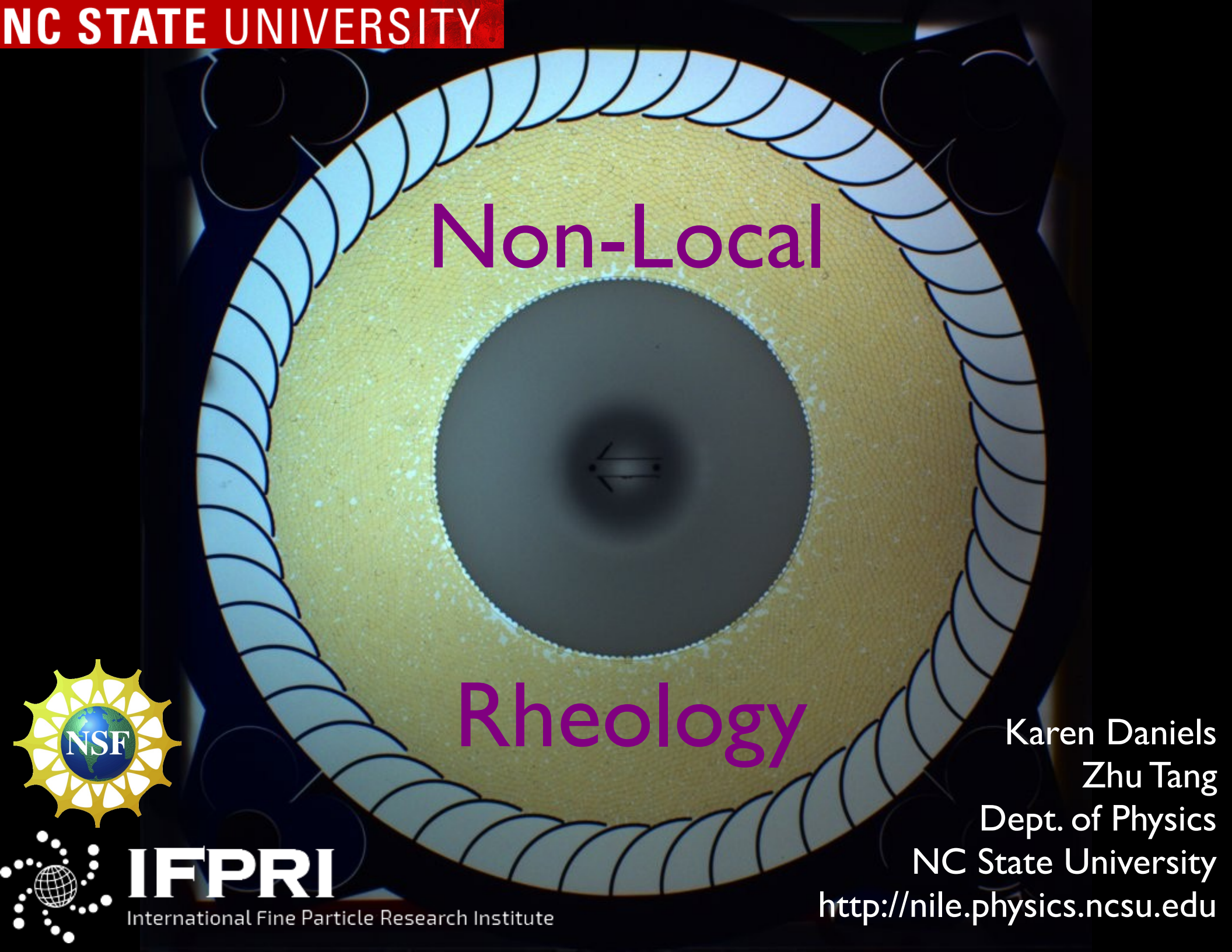

Non-Local Rheology

Karen Daniels
Zhu Tang
Dept. of Physics
NC State University
http://nile.physics.ncsu.edu

NSF
IFPRI
International Fine Particle Research Institute

Problem Statement

- There is no first-principles, general theory of intermediate granular flow that predicts the rheological response as a function of particle size/shape/friction
- Currently: use empirical relations fit to bulk data for that particular flow geometry and particles
- Needed: An improved understanding of how particle properties control the rheology of granular materials, independent of geometry

Kamrin & Koval. PRL (2012)

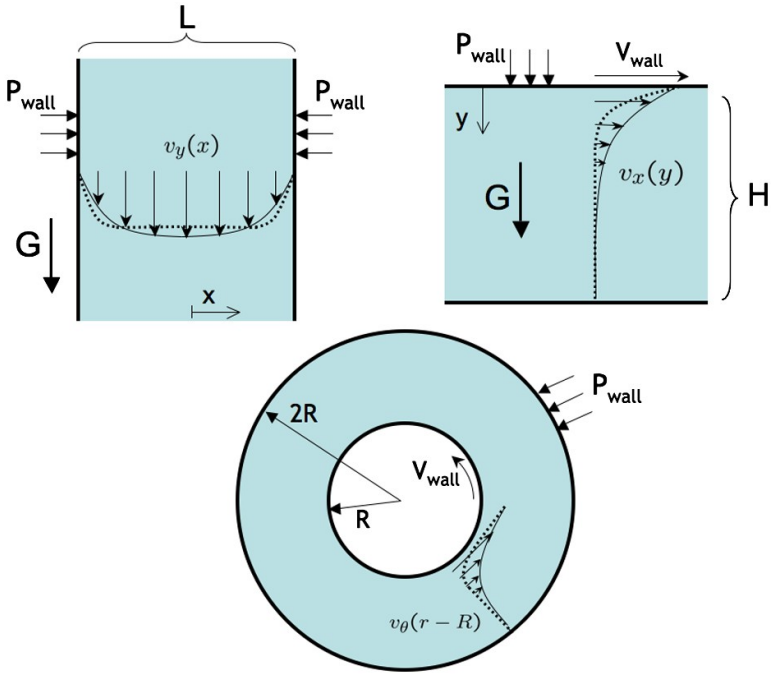

Local Granular Rheology

- inertial number: ratio $I = \frac{\dot{\gamma}\, d}{\sqrt{P/\rho}}$ between
  - micro timescale to squeeze a particle into a hole
  - macro timescale of deformation
  - large I corresponds to rapid flow

- stress ratio: ratio $\mu = \frac{\tau}{P}$ between
  - shear stress
  - normal pressure

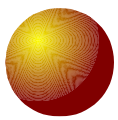

density ρ
diameter d

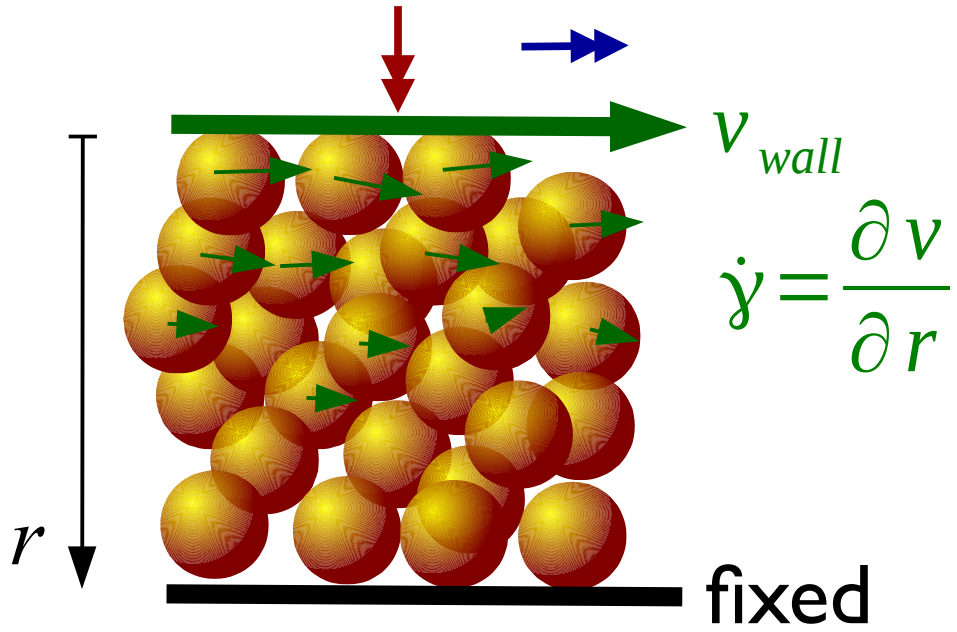

$$\mu(r) = \frac{\tau(r)}{P}$$

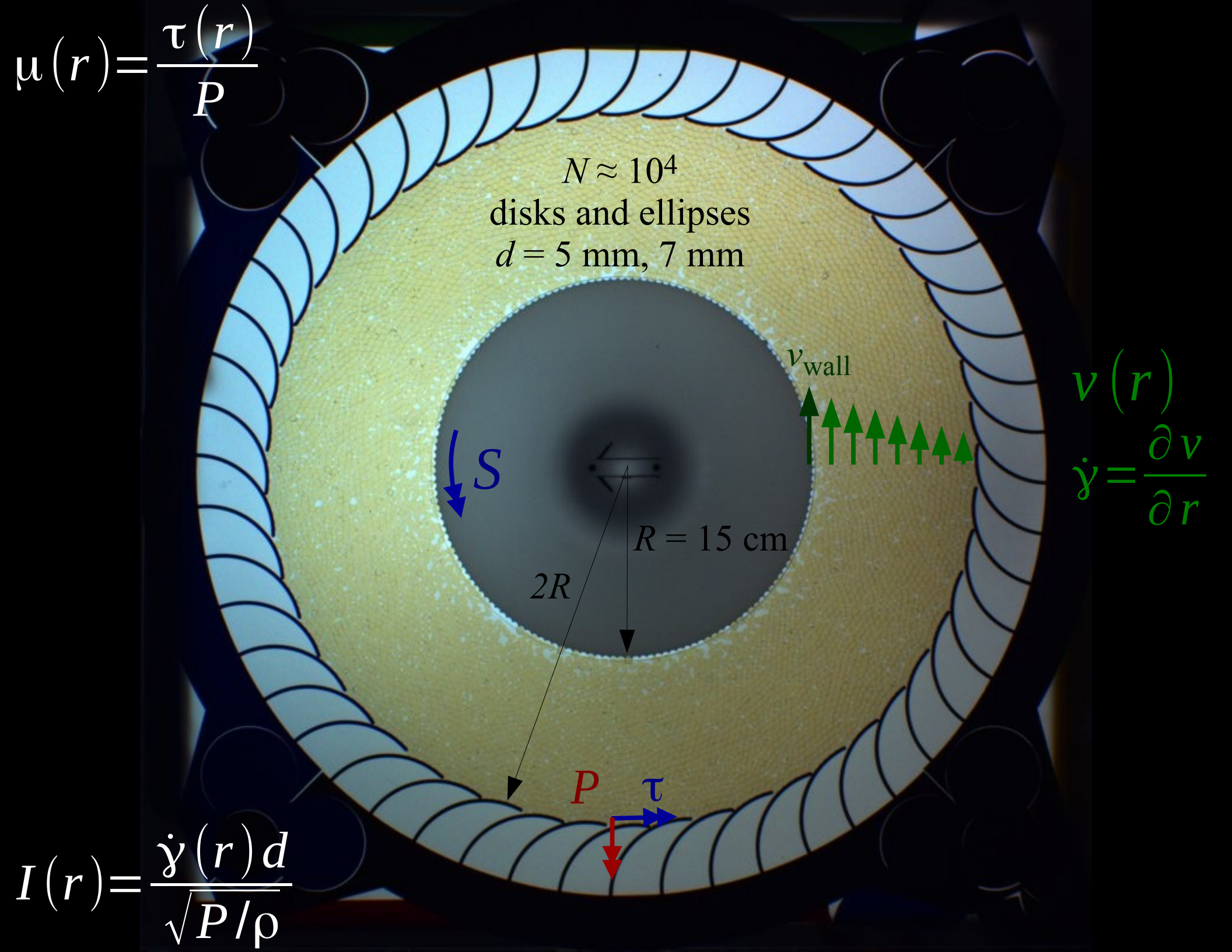

$$v(r)$$

$$\dot{\gamma} = \frac{\partial v}{\partial r}$$

$$I(r) = \frac{\dot{\gamma}(r)\, d}{\sqrt{P/\rho}}$$

Two Nonlocal Rheologies

cooperative model

Kamrin & Koval (PRL 2012)

$$g \equiv \frac{\dot{\gamma}}{\mu}$$

$$\xi^2 \nabla^2 g = (g - g_{loc})$$

$$g_{loc}(\mu, P) = H(\mu - \mu_s)\frac{\mu - \mu_s}{b\mu T}$$

$$\xi = A\sqrt{\frac{1 + H(\mu_s - \mu)}{|\mu - \mu_s|}}d$$

granular fluidity

gradient model

Bouzid et al. (PRL 2013)

$$f = \frac{\sigma_y}{\sigma}\dot{\gamma} = \frac{\mu_s P}{\sigma}\dot{\gamma}$$

$$0 = \dot{\gamma} - \frac{\mathcal{I}(f)}{T} + l^2 \nabla^2 f$$

$$\mathcal{I}(f) = \frac{Tf}{1 - aTf}$$

both: Laplacian term accounts for nonlocal effects

- based on extending a local Bagnold-type granular flow law
- length scale ξ diverges at μ_s
- fit parameters: A, b, μ_s

- based on gradient expansion
- length scale l is constant
- fit parameters: l, a, μ_s

Spring tips → normal & tangential force

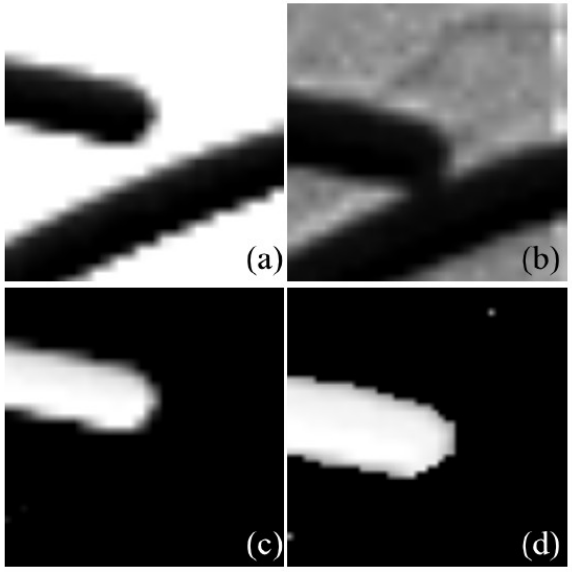

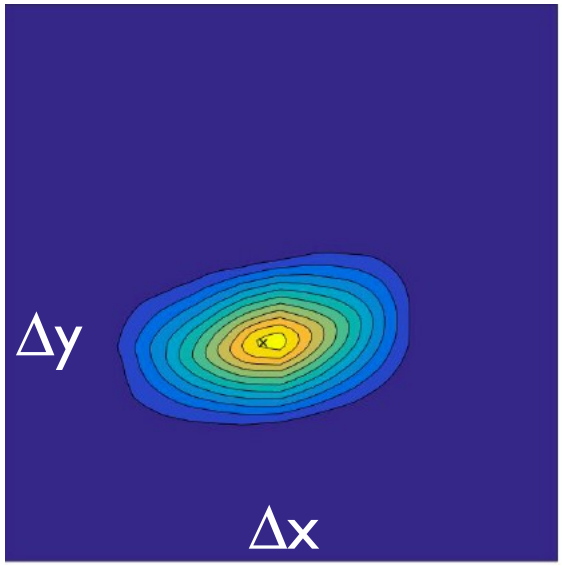

measure spring wall deformation in experiment by cross-correlation

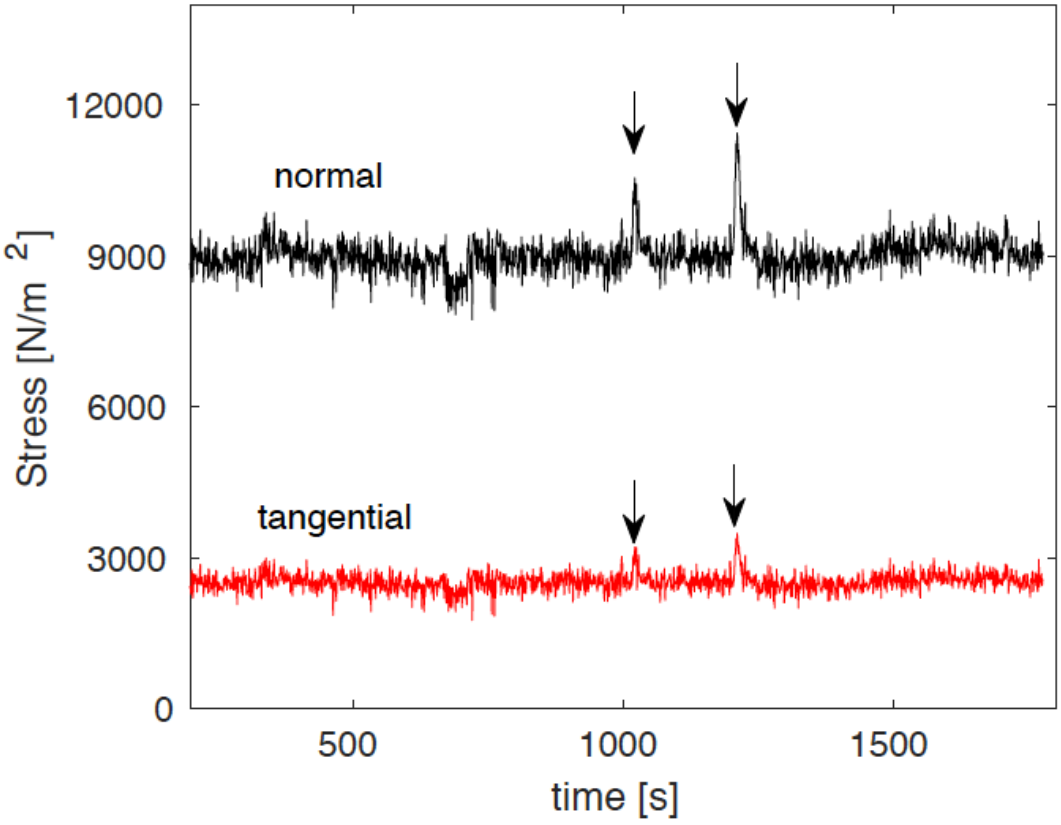

http://arxiv.org/abs/1704.08295

Calculate stress ratio: $\mu = \tau/P$

$$\tau(r) = S\left(\frac{R_i}{r}\right)^2 + \tau_0\left[1 - e^{-(r-R_i)/r_0}\right]$$

geometry basal friction

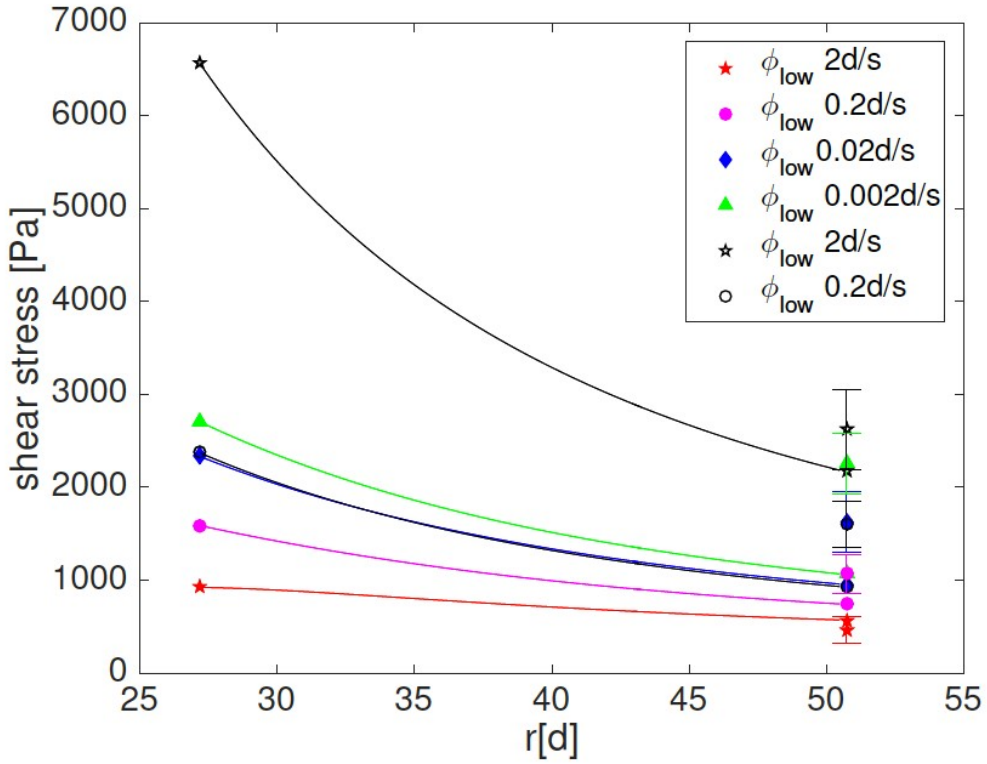

torque sensor

leaf springs

Testing the nonlocal models (I)

cooperative model – gradient model - - -

$$\mu(r) = \frac{\tau(r)}{P}$$

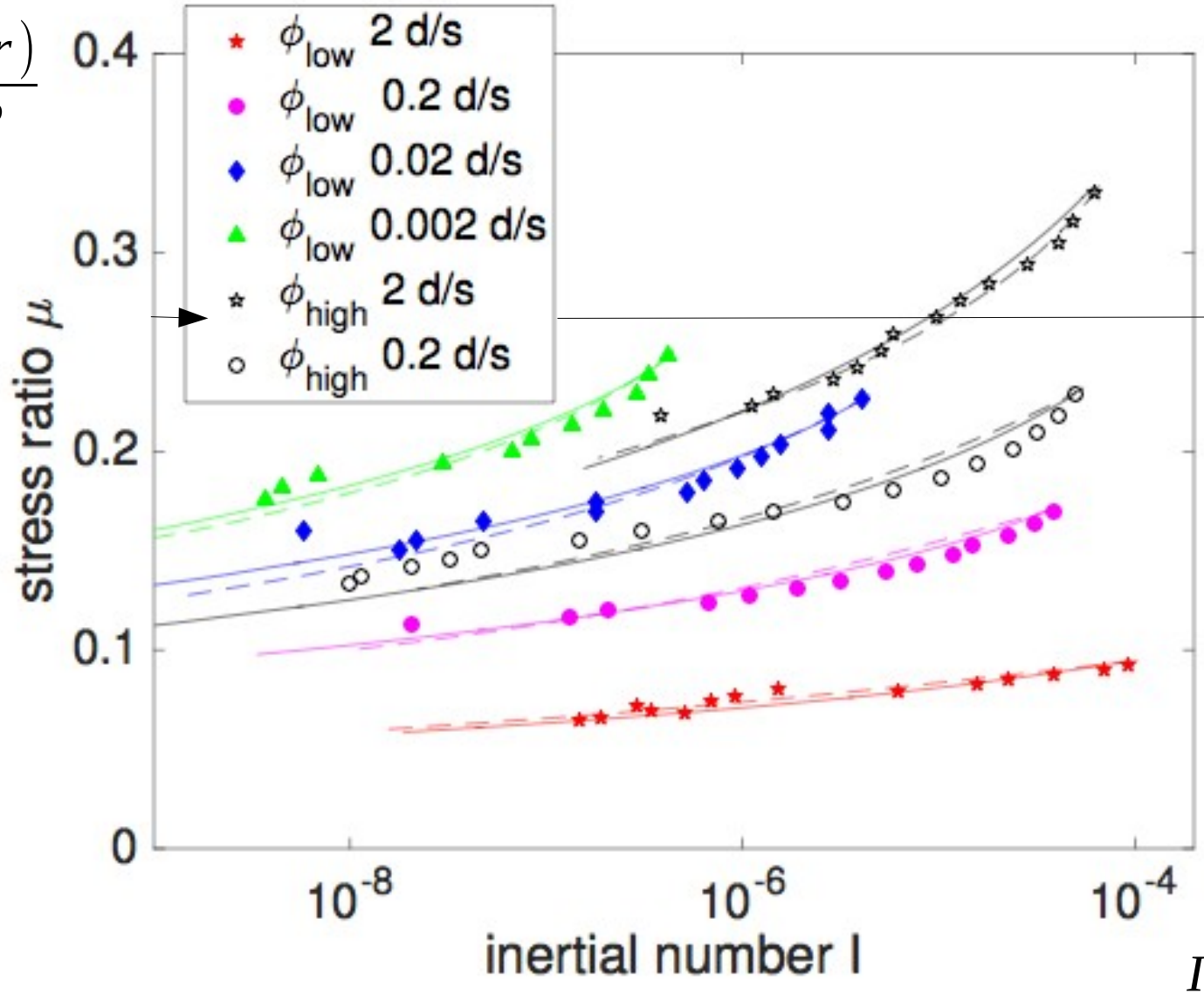

$\mu_s = 0.27$

$$I(r) = \frac{\dot{\gamma}(r)\, d}{\sqrt{P/\rho}}$$

Testing the nonlocal models (2)

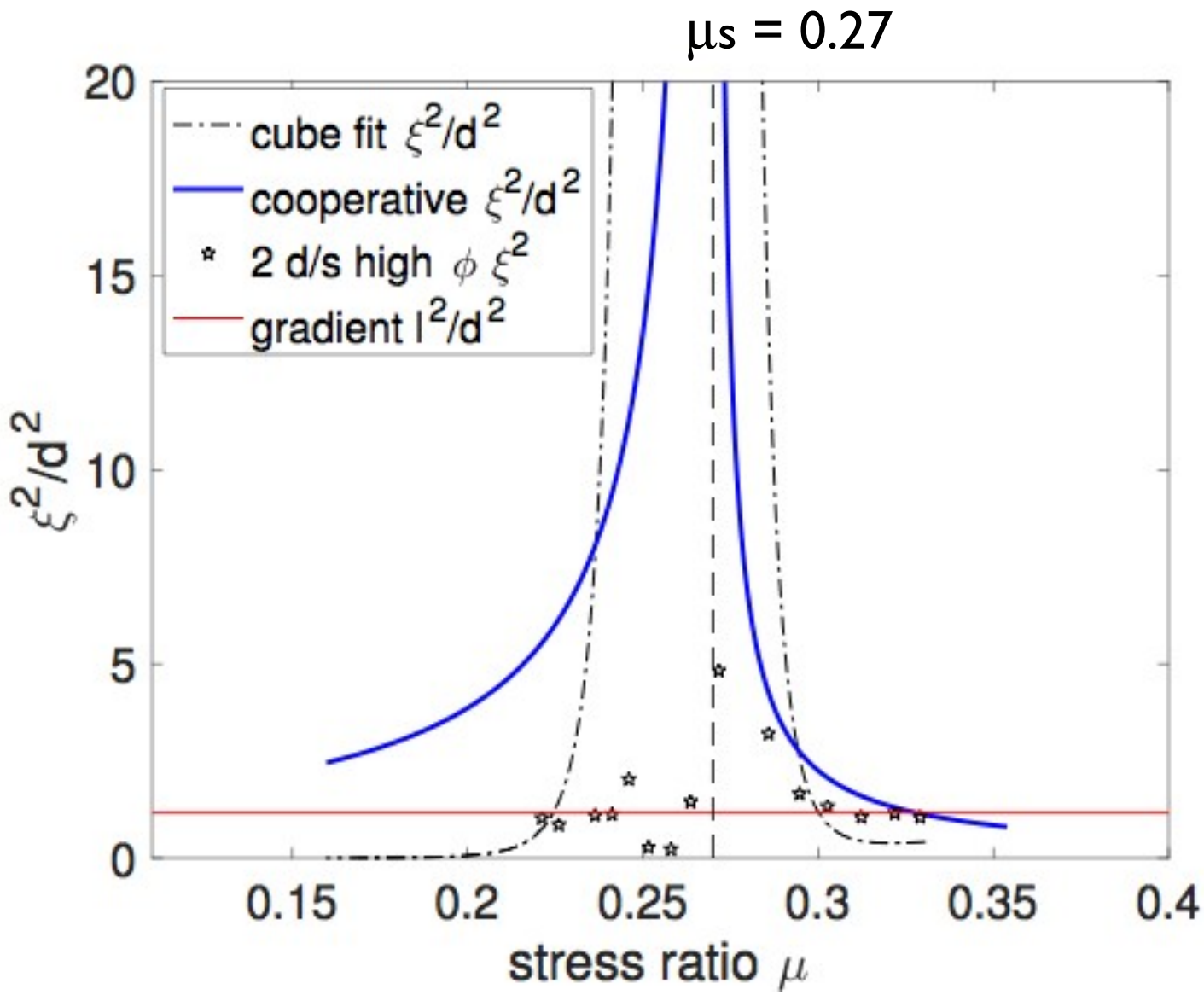

Conclusions

- calibrated leaf springs measure the normal & tangential stress dynamics
- modify two nonlocal rheologies to account for basal friction
- either nonlocal rheology can describe the $\mu(I)$ measurements (with a small # of fixed parameters)
- …but the presence of a diverging length scale favors the Kamrin model

Ongoing

- starting experiments on a variety of particle shapes → how do these affect the model parameters? choice of nonlocal model?

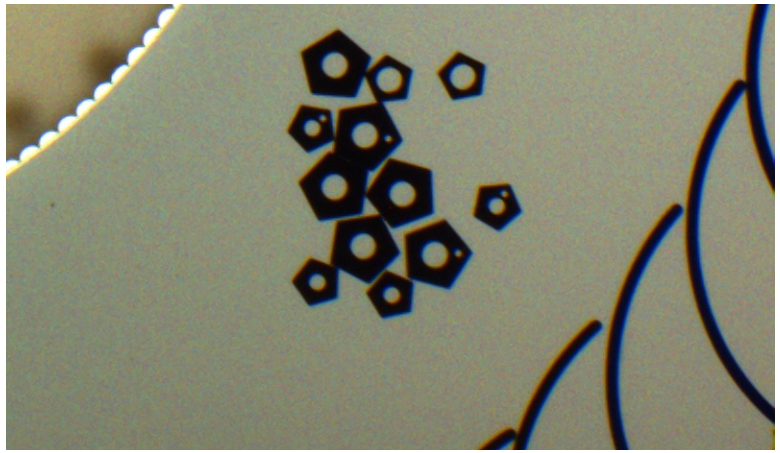

- are force chains the source of nonlocality?

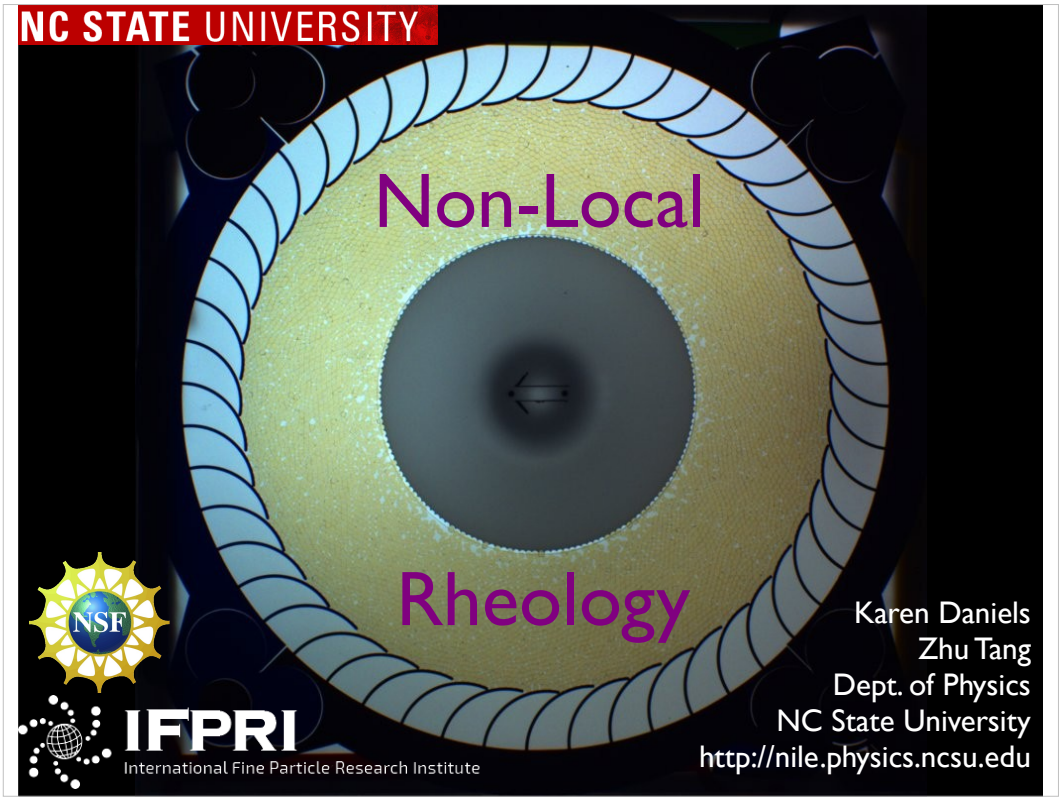
NC STATE UNIVERSITY
Non-Local
Rheology
NSF
IFPRI
International Fine Particle Research Institute
Karen Daniels
Zhu Tang
Dept. of Physics
NC State University
http://nile.physics.ncsu.edu

Problem Statement

- There is no first-principles, general theory of intermediate granular flow that predicts the rheological response as a function of particle size/shape/friction
- Currently: use empirical relations fit to bulk data for that particular flow geometry and particles
- Needed: An improved understanding of how particle properties control the rheology of granular materials, independent of geometry

Kamrin & Koval. PRL (2012)

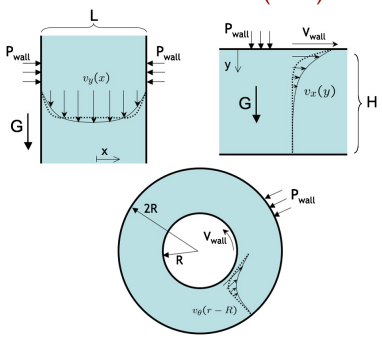

Local Granular Rheology

- inertial number: ratio $I = \frac{\dot{\gamma}\, d}{\sqrt{P/\rho}}$ between
  - micro timescale to squeeze a particle into a hole
  - macro timescale of deformation
  - large I corresponds to rapid flow
- stress ratio: ratio $\mu = \frac{\tau}{P}$ between
  - shear stress
  - normal pressure


density ρ
diameter d

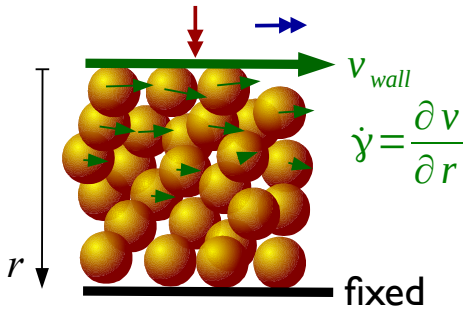

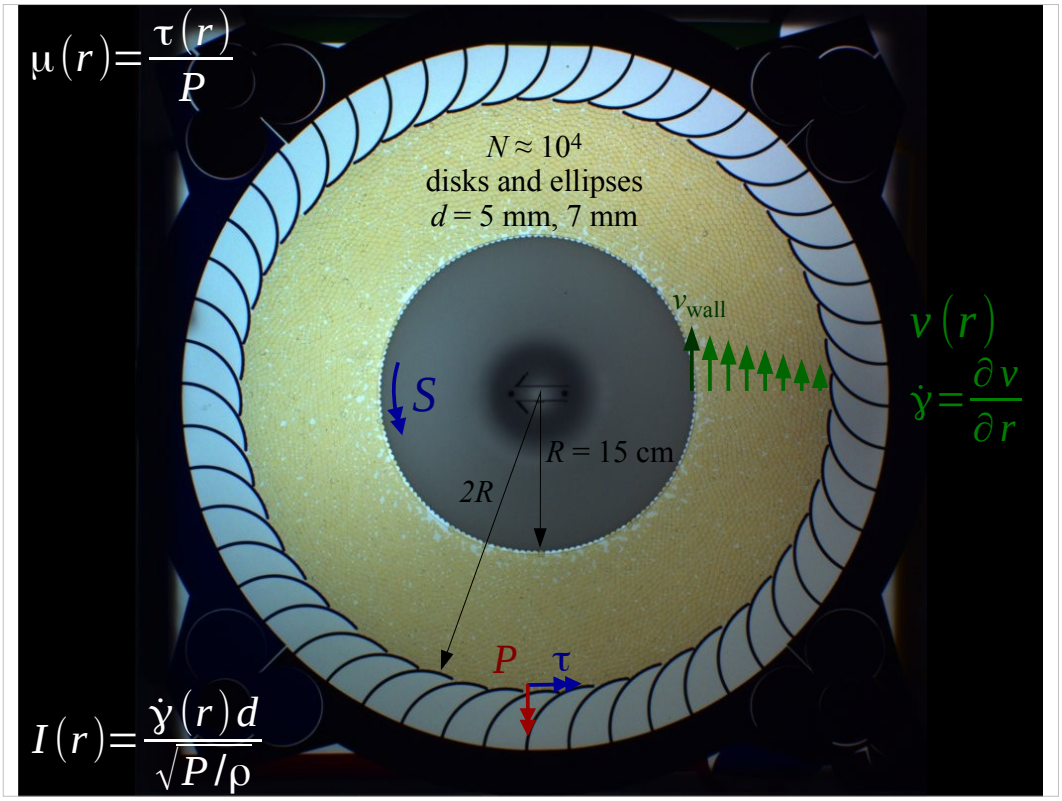
$\mu(r)=\frac{\tau(r)}{P}$
$N \approx 10^4$
disks and ellipses
d = 5 mm, 7 mm
v_{wall}
$v(r)$
$\dot{\gamma}=\frac{\partial v}{\partial r}$
S
R = 15 cm
$2R$
P
τ
$I(r)=\frac{\dot{\gamma}(r)d}{\sqrt{P/\rho}}$

Two Nonlocal Rheologies

cooperative model

Kamrin & Koval (PRL 2012)

$$g \equiv \frac{\dot{\gamma}}{\mu}$$

$$\xi^2 \nabla^2 g = (g - g_{loc})$$

$$g_{loc}(\mu, P) = H(\mu - \mu_s)\frac{\mu - \mu_s}{b\mu T}$$

$$\xi = A\sqrt{\frac{1 + H(\mu_s - \mu)}{|\mu - \mu_s|}}d$$

granular fluidity

gradient model

Bouzid et al. (PRL 2013)

$$f = \frac{\sigma_y}{\sigma}\dot{\gamma} = \frac{\mu_s P}{\sigma}\dot{\gamma}$$

$$0 = \dot{\gamma} - \frac{\mathcal{I}(f)}{T} + l^2 \nabla^2 f$$

$$\mathcal{I}(f) = \frac{Tf}{1 - aTf}$$

both: Laplacian term accounts for nonlocal effects

- based on extending a local Bagnold-type granular flow law
- length scale ξ diverges at μ_s
- fit parameters: A, b, μ_s

- based on gradient expansion
- length scale l is constant
- fit parameters: l, a, μ_s

Spring tips → normal & tangential force

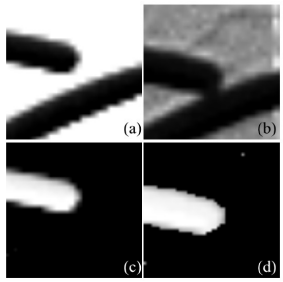

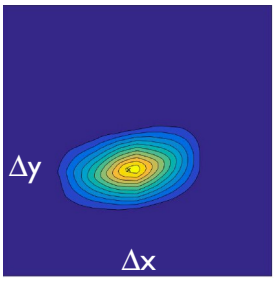

measure spring wall deformation in experiment by cross-correlation

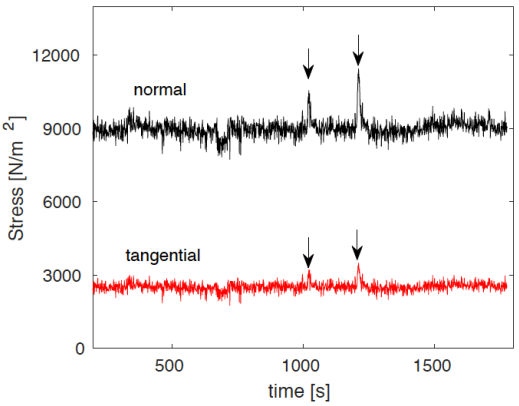

http://arxiv.org/abs/1704.08295

Calculate stress ratio: μ = τ/P

$$\tau(r) = S\left(\frac{R_i}{r}\right)^2 + \tau_0\left[1 - e^{-(r-R_i)/r_0}\right]$$

geometry basal friction

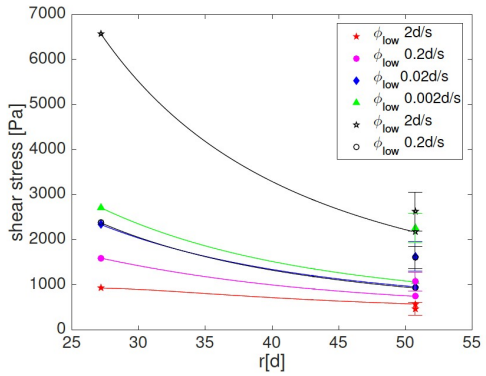

torque sensor

leaf springs

Testing the nonlocal models (1)

cooperative model – gradient model - - -

$$\mu(r)=\frac{\tau(r)}{P}$$

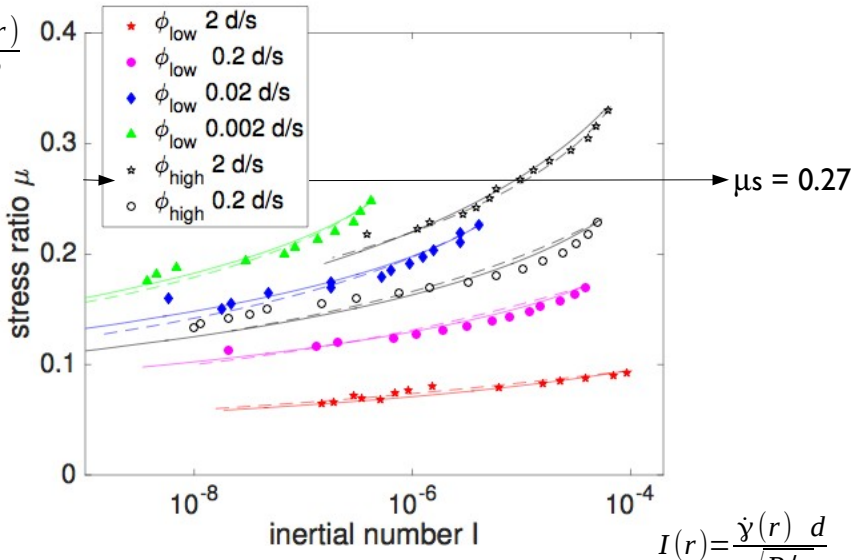

$$I(r)=\frac{\dot{\gamma}(r)\ d}{\sqrt{P/\rho}}$$

Testing the nonlocal models (2)

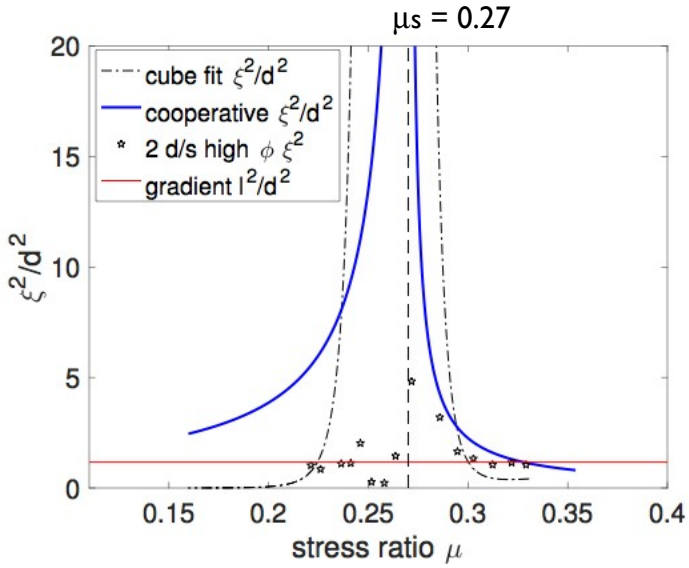

Conclusions

- calibrated leaf springs measure the normal & tangential stress dynamics
- modify two nonlocal rheologies to account for basal friction
- either nonlocal rheology can describe the $\mu(I)$ measurements (with a small # of fixed parameters)
- …but the presence of a diverging length scale favors the Kamrin model

Ongoing

- starting experiments on a variety of particle shapes → how do these affect the model parameters? choice of nonlocal model?

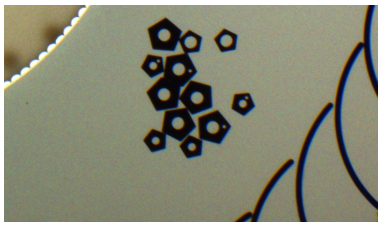

- are force chains the source of nonlocality?

MONASH University

Creating Tuneable Agglomerates via 3D Printing

Karen Hapgood, Deakin University

Mojtaba Ghadiri, Leeds University

Ruihuan Ge (PhD Student)

Zongyan Zhou, Monash University

IFPRI
International Fine Particle Research Institute

- **Experimental Breakage tests**
  - Quasi-static compression tests

    Tester: Instron 5566

    Load cell: 10000 N

    Cross head speed:

    0.02 mm/s 0.1 mm/s 0.5 mm/s
  - Drop weight impact tests

    Drop weight Impact energy: 1.6 J, 3.2 J

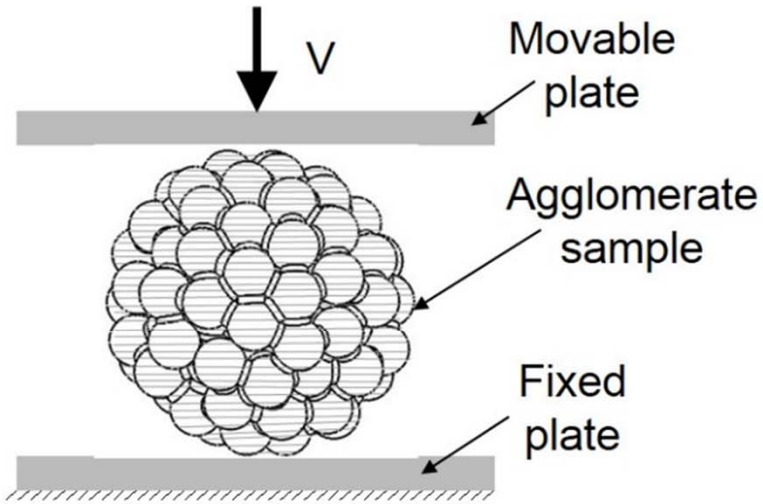

(a) Compression test

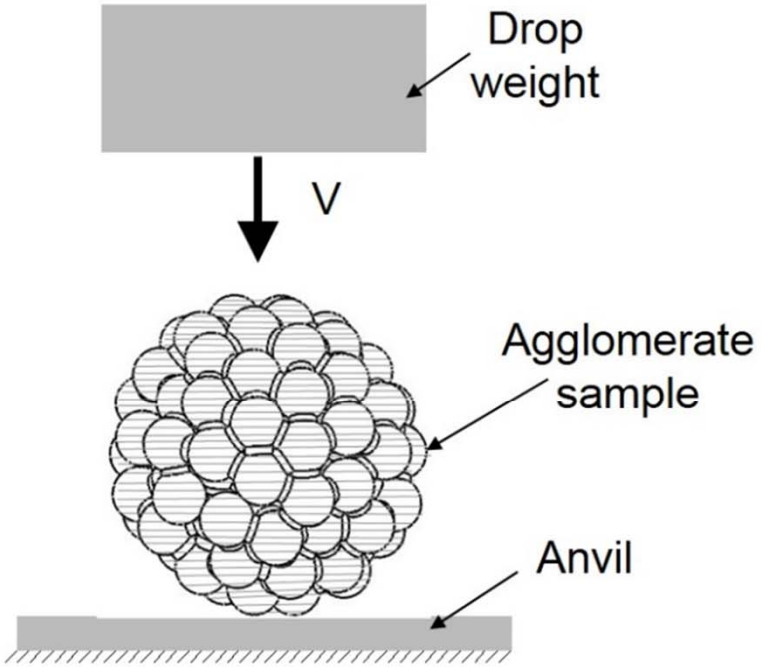

(b) Drop weight impact test

Six different agglomerate designs

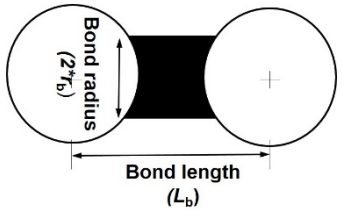

- Cubic tetrahedral structure (L_b =4.25 mm, r_b=1.3 mm)
- Random spherical structure ε=44% (L_b ~4 mm, r_b=1 mm)
- Random spherical structure ε=57% (L_b ~5.6 mm, r_b=1 mm)

	Cubic structure	Dense structure (ε=44 %)	Loose structure (ε=57 %)
Rigid bond (VeroWhitePlus™)	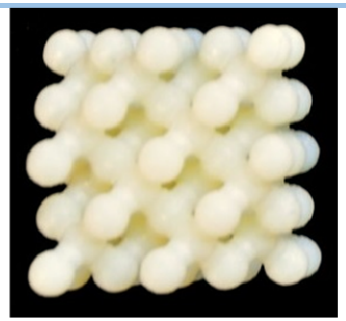		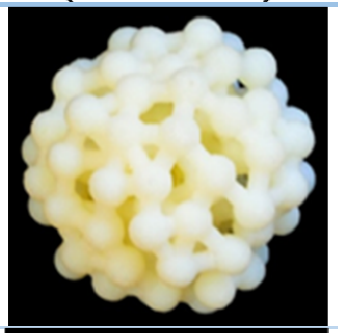
Soft bond (DM 9895)	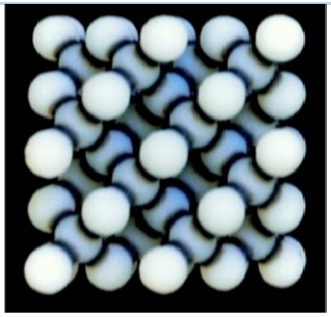		

DEM simulation setup

- Timoshenko Beam Bond Model (TBBM)

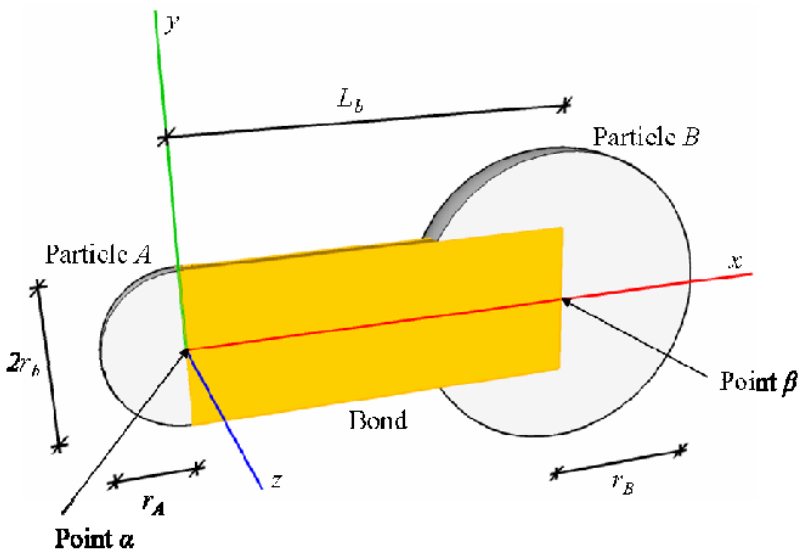

Brown *et al.* (2014)

Bonding parameters
Young's modulus (MPa)
Poisson's ratio
Mean compressive strength (MPa)
Mean tensile strength (MPa)
Mean shear strength (MPa)
Bond radius multiplier

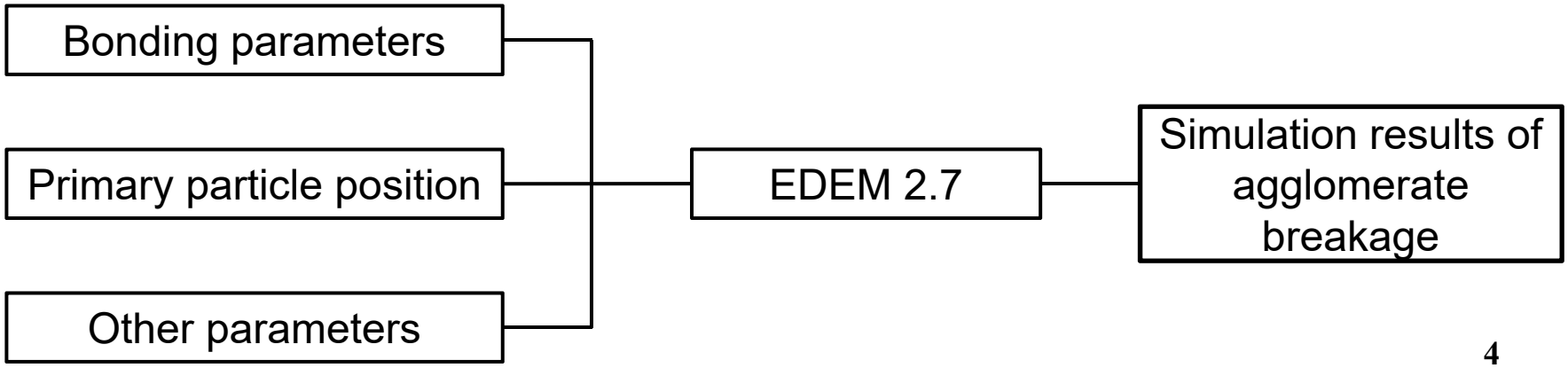

DEM simulation setup

- Bond parameter-Two bond materials i.e. **rigid bond** and **rubber-like bond** are used. The bonding parameters are based on experimental measurement and data offered by the vendor.

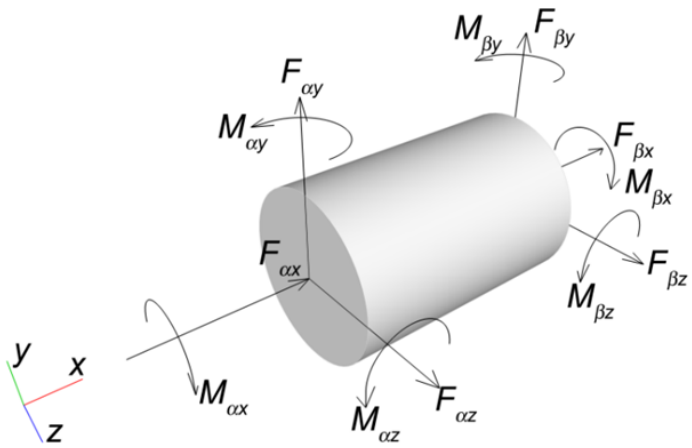

Description	Rubber-like bond
Young's modulus (MPa)	Varies with different bond geometry
Poisson's ratio	0.4
Compressive strength (MPa)	50
Tensile strength (MPa)	10
Shear strength (MPa)	10

DEM simulation setup-Other parameters

(1) Particle (Rigid 3D printing material)

Description	Value
Diameter	4 mm
Possion ratio	0.3
Shear modulus	0.37 GPa
Density	1200 kg/m^3

(2) Steel plate

Description	Value
Possion ratio	0.3
Shear modulus	70 GPa
Density	7800 kg/m^3

(3) Coefficient

Description	Value
Restitution	0.9
Rolling friction	0.01
Static friction	0.3

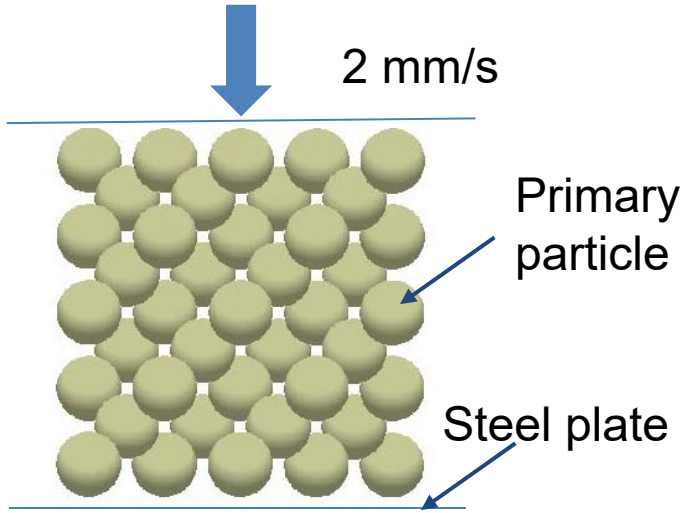

Bond Young's modulus used in simulation

To compensate the inappropriate use of the bond length in TBBM, the bond Young's modulus E_b was corrected using the doublet tensile test results considering different printing layer directions.

$$E_b = \frac{k_t \cdot L_b}{A_b}$$

$k_t = \frac{dF}{ds}$:Bond stiffness determined by doublet tests

L_b : Bond length in TBBM model.

$A_b = \pi r_b^2$: Bond cross-sectional area.

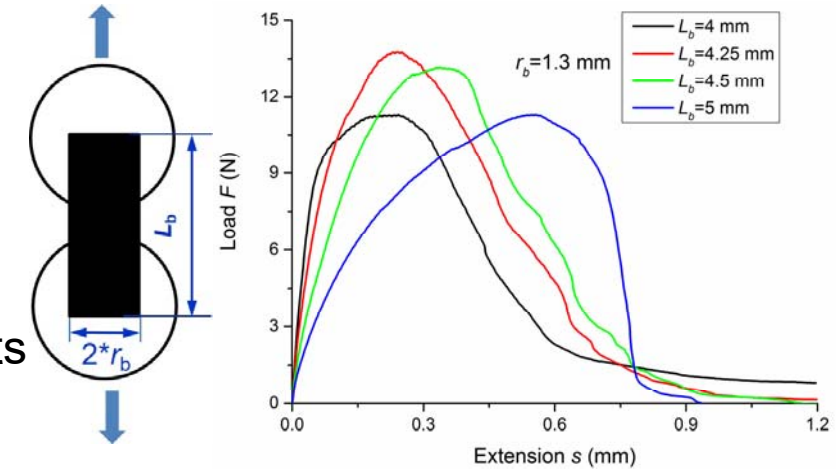

Doublet tensile test curves

	Parallel loading	Perpendicular loading
Cubic tetrahedral structure (L_b =4.25 mm, r_b=1.3 mm)	E_b = 116 MPa	E_b = 142 MPa
Spherical random structure (L_b =4 mm, r_b=1 mm)	E_b = 254 MPa	E_b = 195 MPa

Agglomerate structure and type

Tetrahedron structure

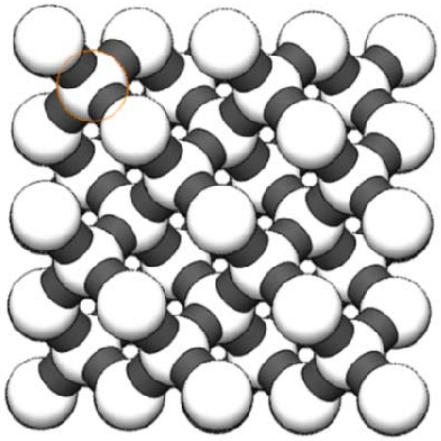

Random structure

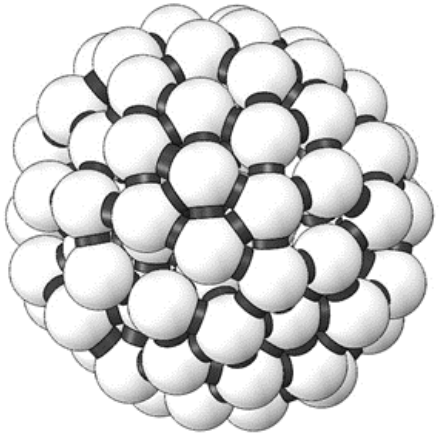

Primary particle	Agglomerate structure	Bond material	Bond dimension
Vero WhitePlus™	Tetrahedron structure	Rubber-like (DM 9895)	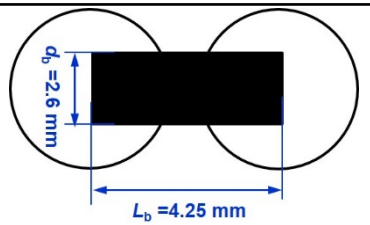
	Random structure	Rubber-like (DM 9895)	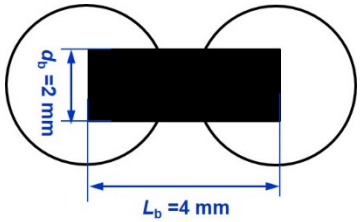

Estimating Youngs Modulus E_b

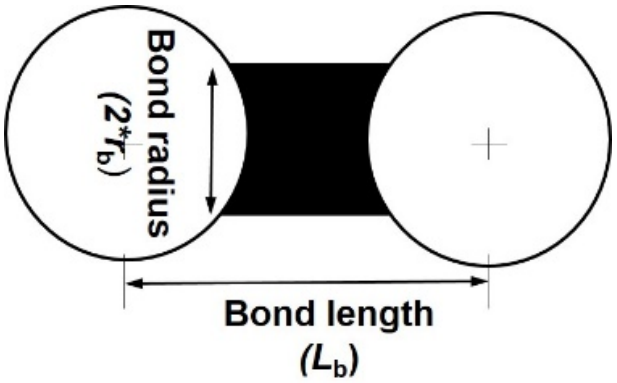

$$E_b = \frac{k_t \cdot L_b}{A_b}$$

k_t: Bond stiffness from doublet tests.

L_b : Bond length in TBBM model.

$A_b = \pi r_b^2$: Bond cross-sectional area.

Doublet type	Parallel loading	Perpendicular loading
Cubic tetrahedral structure (L_b =4.25 mm, r_b=1.3 mm)	E_b = 116 MPa	E_b = 142 MPa
Spherical random structure (L_b =4 mm, r_b=1 mm)	E_b = 254 MPa	E_b = 195 MPa

Cubic Tetrahedral breakage - DEM vs experiment

Compression then slip plane failure along 45 degree line

0 mm 3 mm 5 mm 7 mm 10 mm

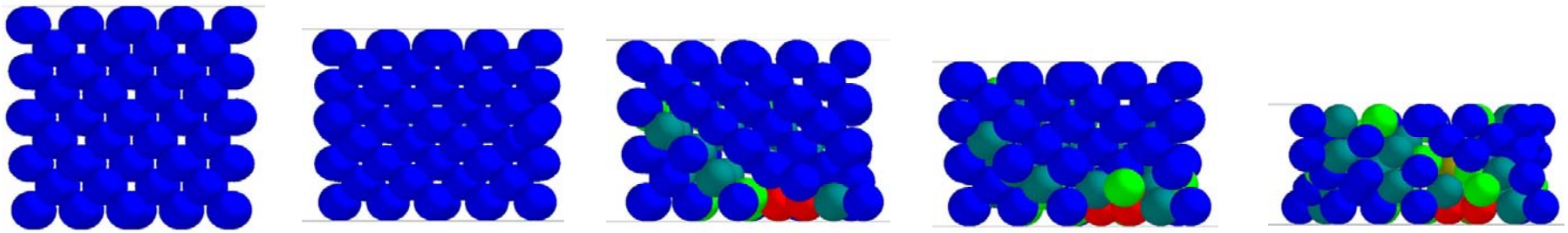

Simulation (E_b=116 Mpa)

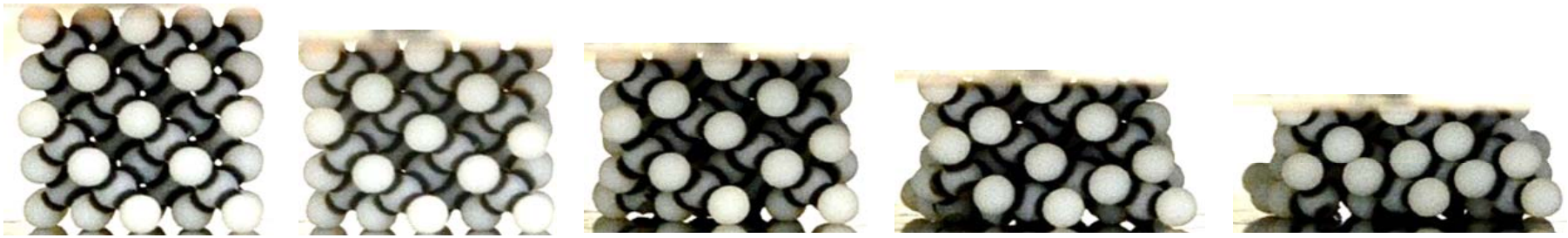

Experiment

Random spherical agglomerate breakage comparison

Meridian plane failure

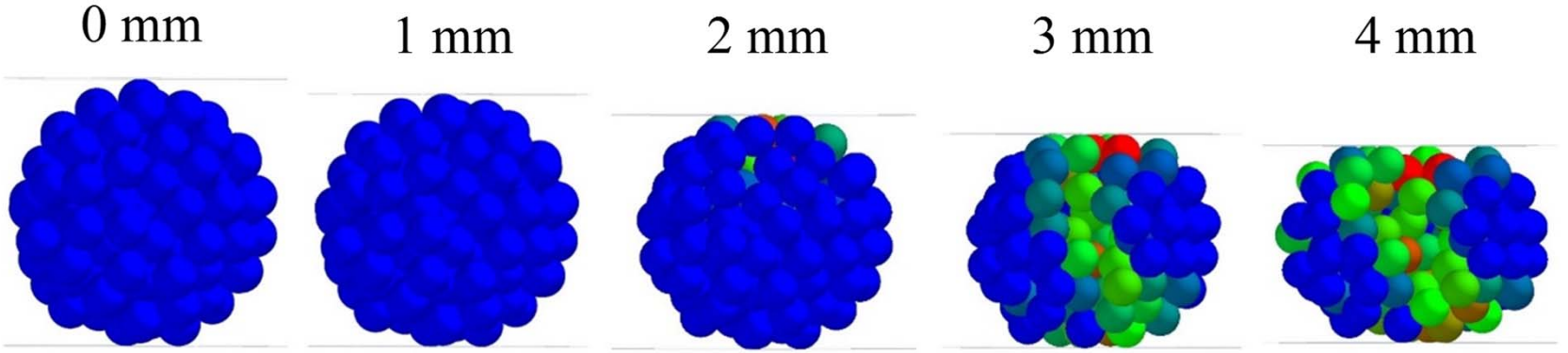

Simulation (E_b=195 Mpa)

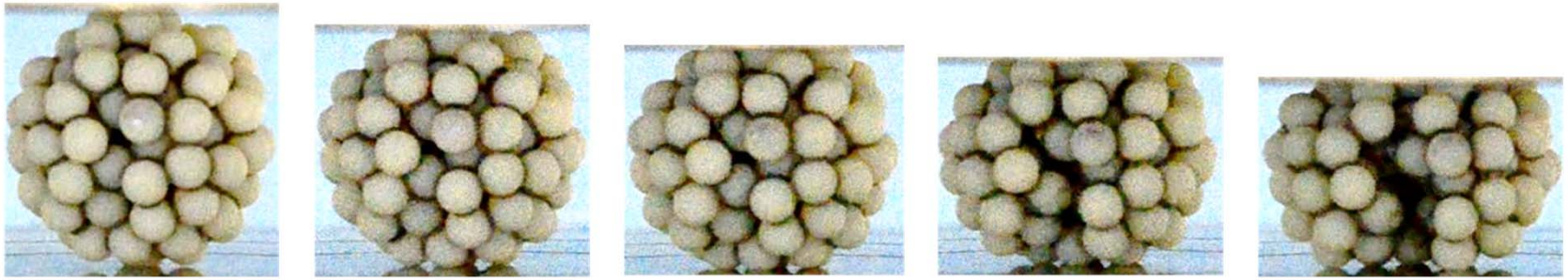

Experiment

Comparison of load-displacement curves - Tetrahedral

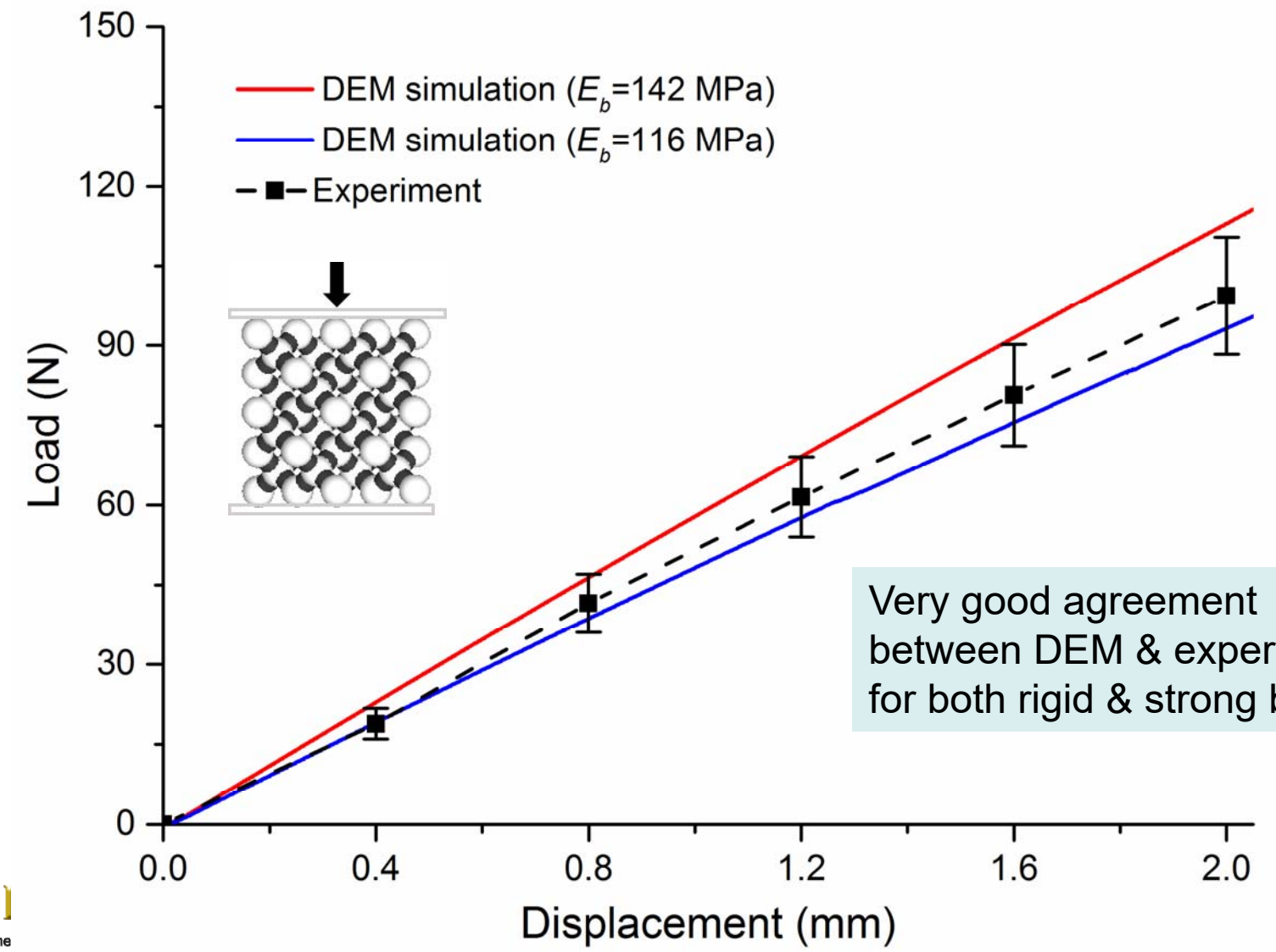

Very good agreement between DEM & experiment for both rigid & strong bonds

Comparison of load-displacement curves – random spherical

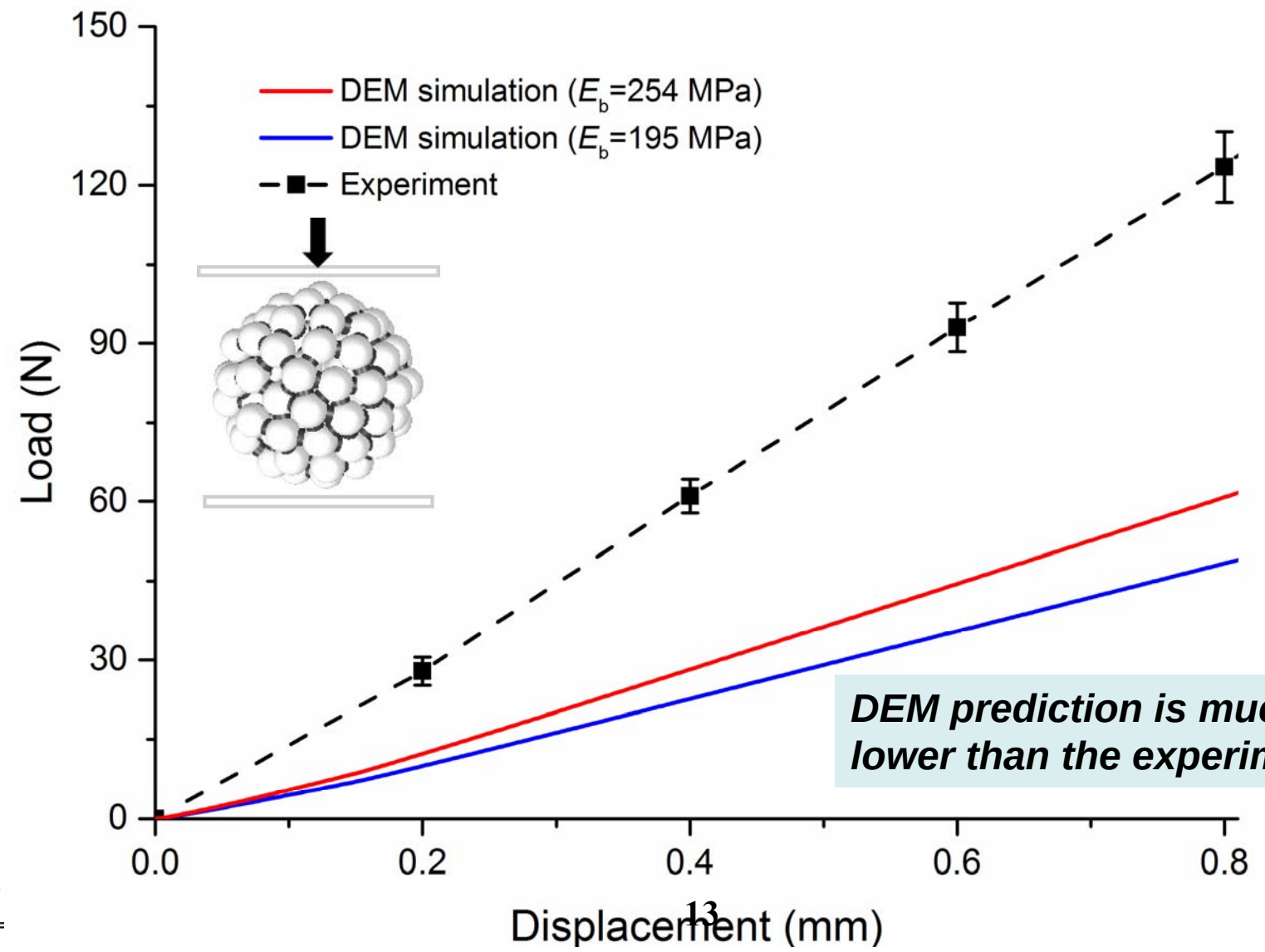

DEM prediction is much lower than the experiments

Bond geometry differences

MONASH University

- In TBBM contact model, for simplicity, it is assumed that the beam element connects to the centres of the two particles.
- The bond geometry definition will significantly influence the simulation results.

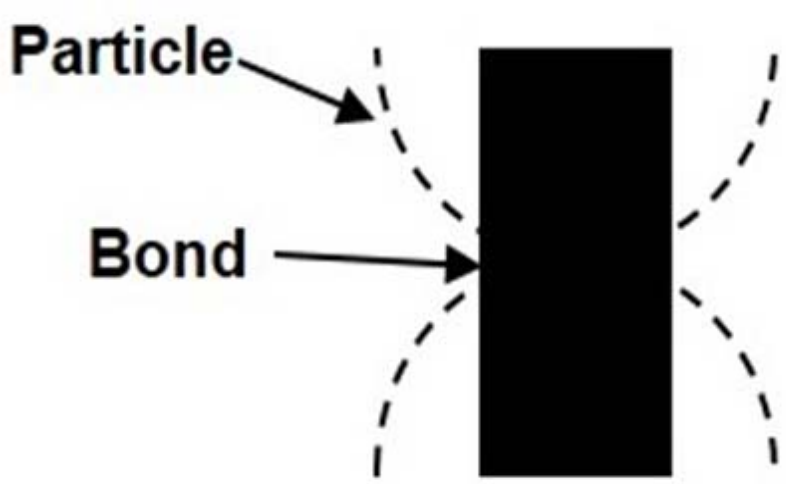

(a) TBBM model bond geometry

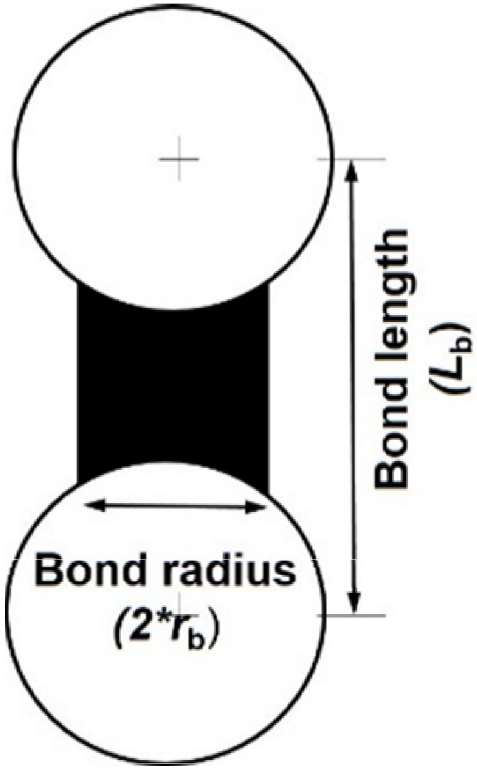

(b) Printed bond geometry

Flowability Assessment of Weakly Consolidated Powders

Colin Hare[1], Ali Hassanpour[2], Alexandros Stavrou[1]

[1]Department of Chemical and Process Engineering, University of Surrey
[2]Institute of Particle Science & Engineering, University of Leeds

The brief

- **In traditional flowability measurement devices:**
  - **Reproducibility of unconfined yield strength is greatly reduced at low stresses.**
  - **Or inconsistent with observed behaviour.**
  - **Materials found to be cohesionless may have practical differences.**
  - **Onset of flow is measured – may not be complete flow description.**

- **IFPRI seek to develop a theoretical understanding of flow of weakly consolidated & weakly cohesive powders.**
  - **Development of practical means of making measurement to support theory.**
  - **Results should be generalisable to broad class of powders.**

Our approach – ball indentation

- **Directly measures hardness[1], *H***
  - **related to unconfined yield stress**

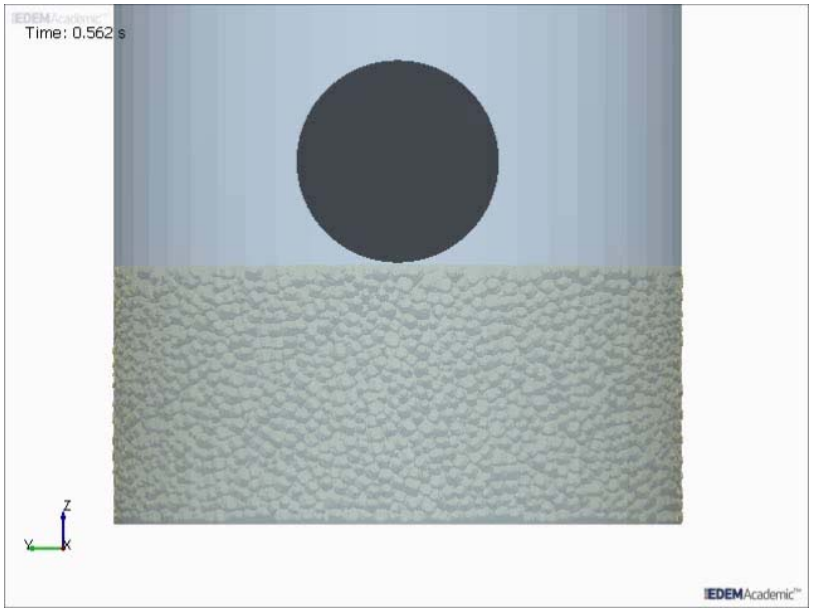

$$H = \frac{F_{max}}{A} = \frac{F_{max}}{\pi\left(2Rh - h^2\right)}$$

F = maximum force applied
A = projected area
R = indenter radius
h = final penetration depth

$$C = \frac{H}{\sigma_C}$$

C = constraint factor
σ_C = unconfined yield stress

- **Applicable at low stresses, with small sample**
- **Can operate at high strain rates**

[1] Hassanpour, A., Ghadiri, M. (2007). *Particle & Particle Systems Characterization*, 24(2), 117-123.

Constraint factor determination

- Unconfined yield stress measured stresses in a shear cell
  - Pre-shear stresses: 2, 4, 6, 8 kPa
- Hardness measured at relevant major principal stresses
- Materials tested
  - Silanised glass beads – 45-53, 53-63, 63-75, 75-90, 90-106 µm
  - Silanised glass beads – 63-75, 53-90, 45-106 µm
  - Titania, alumina, limestone
  - Maize starch, pea protein, sweetener

Constraint factor - previous

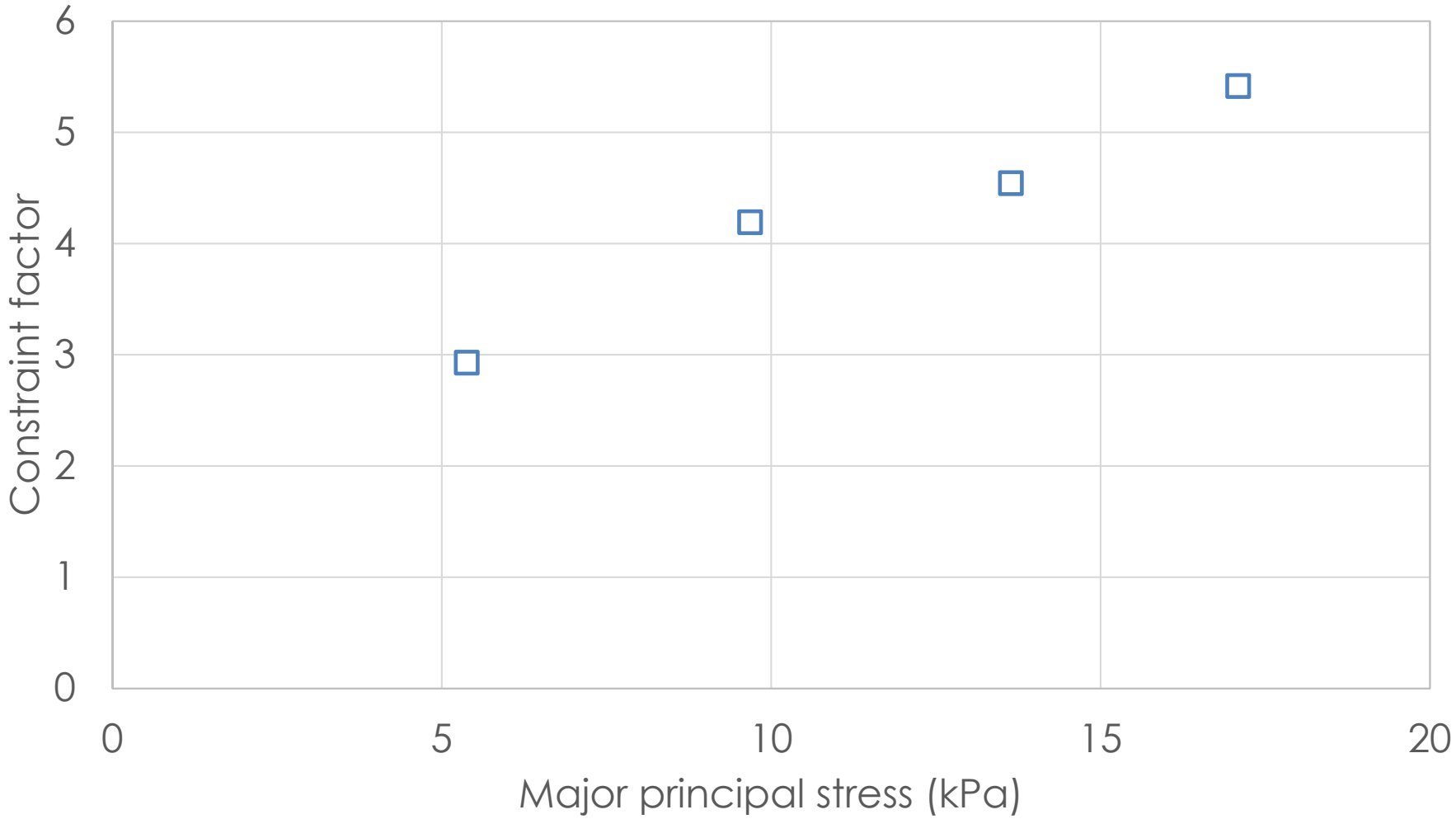

Alumina (CT800 SG)

Yield locus extrapolation

- **At some pre-shear stresses: applied normal stresses not suitable**
- **Yield locus extrapolated to find σ_c**

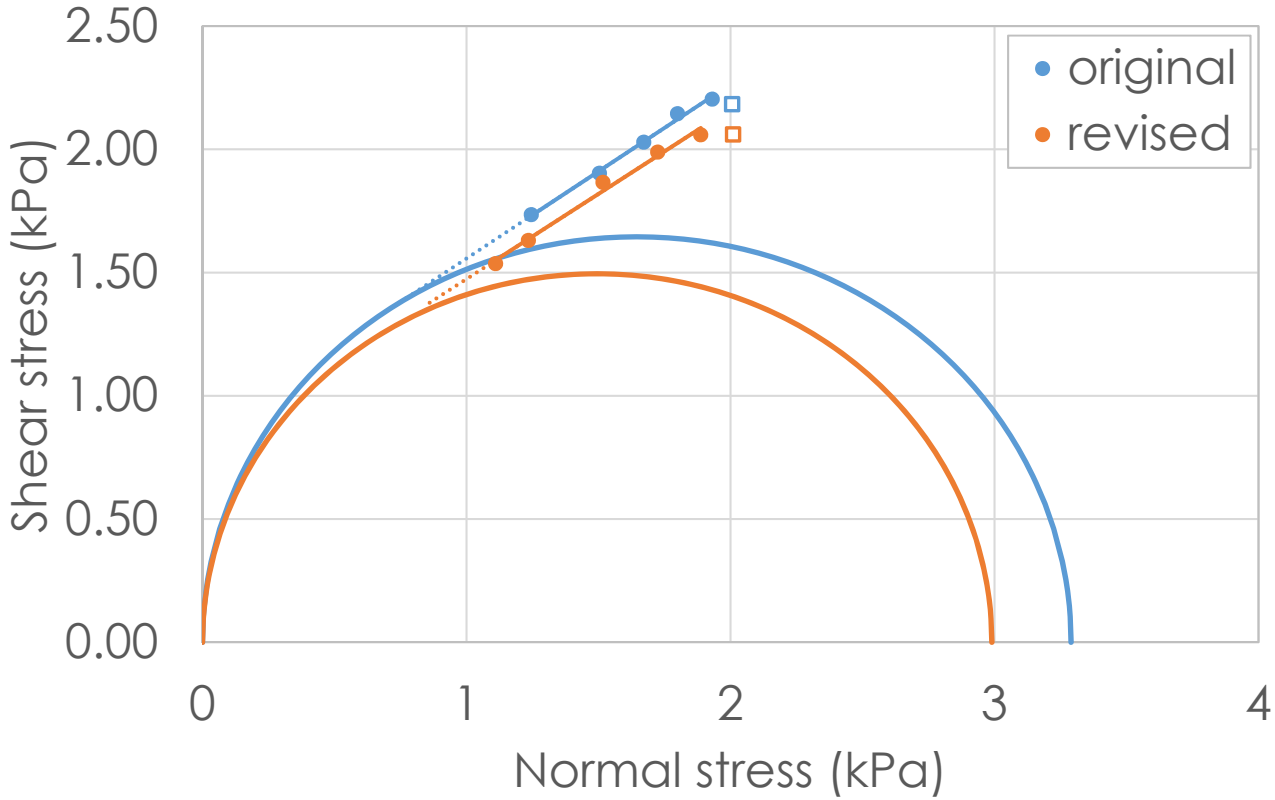

Constraint factor - revised

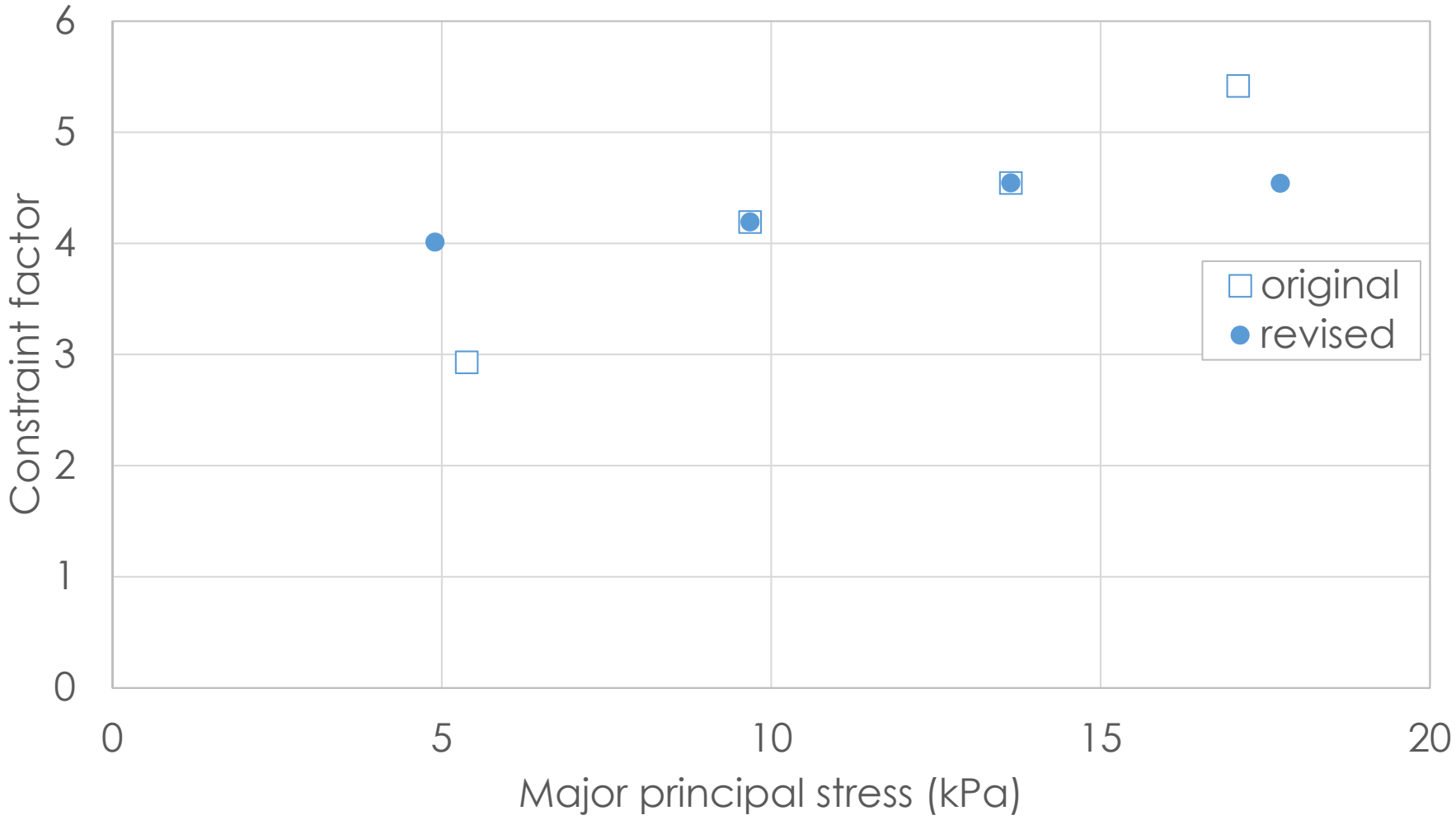

Alumina (CT800 SG)

Particle size effect

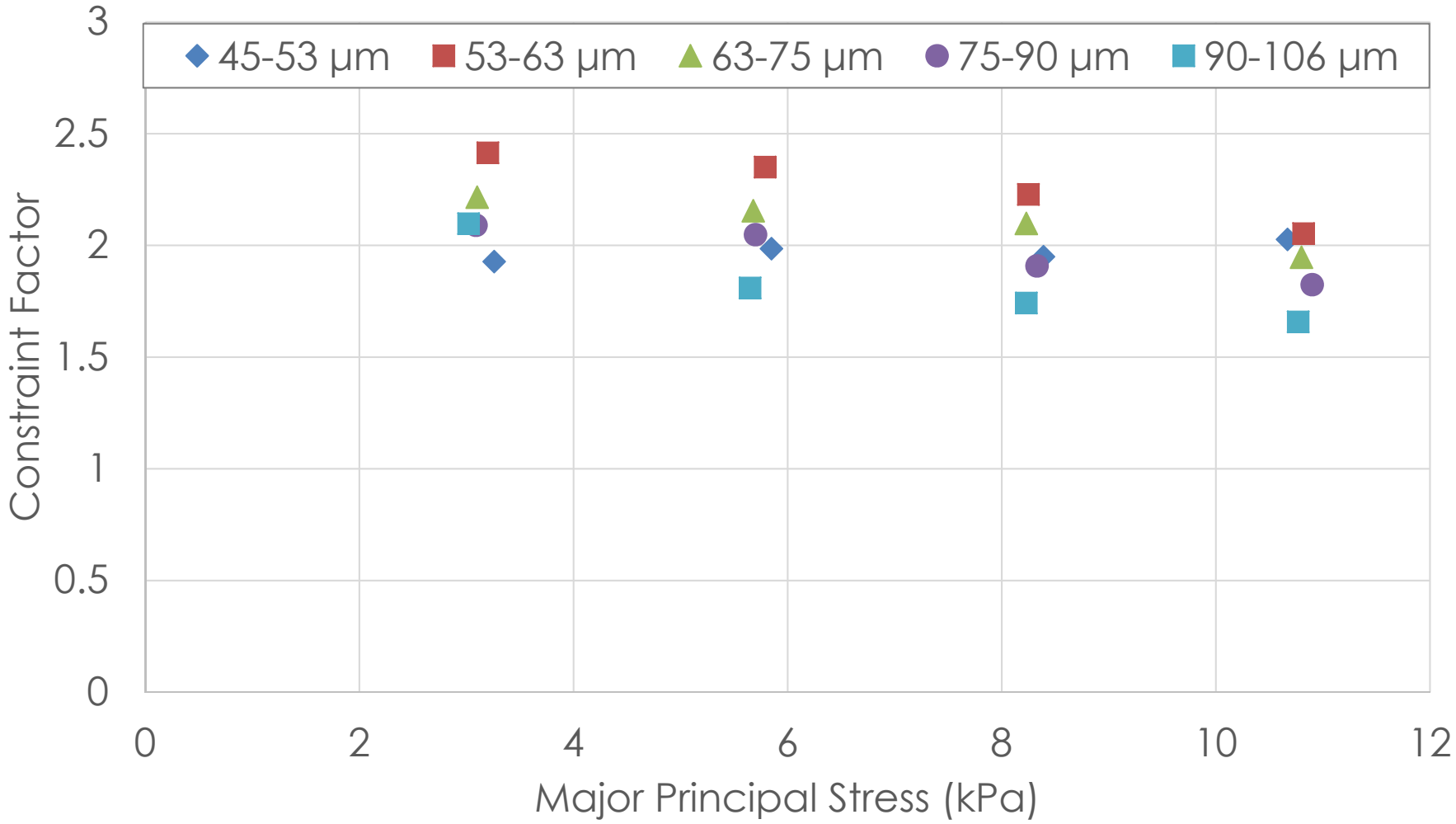

Silanised glass beads

Size distribution effect

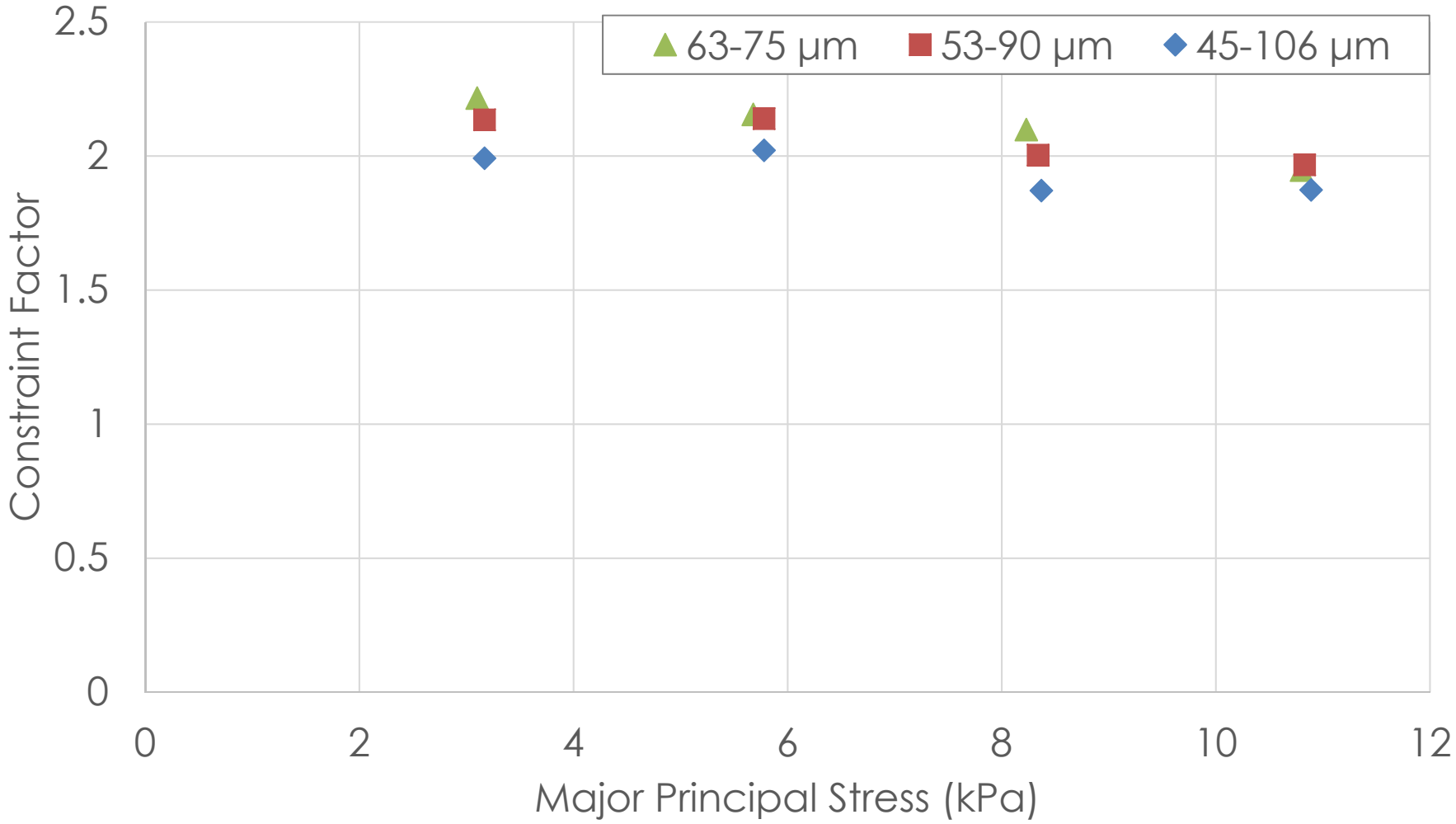

Silanised glass beads

Constraint factor – all materials

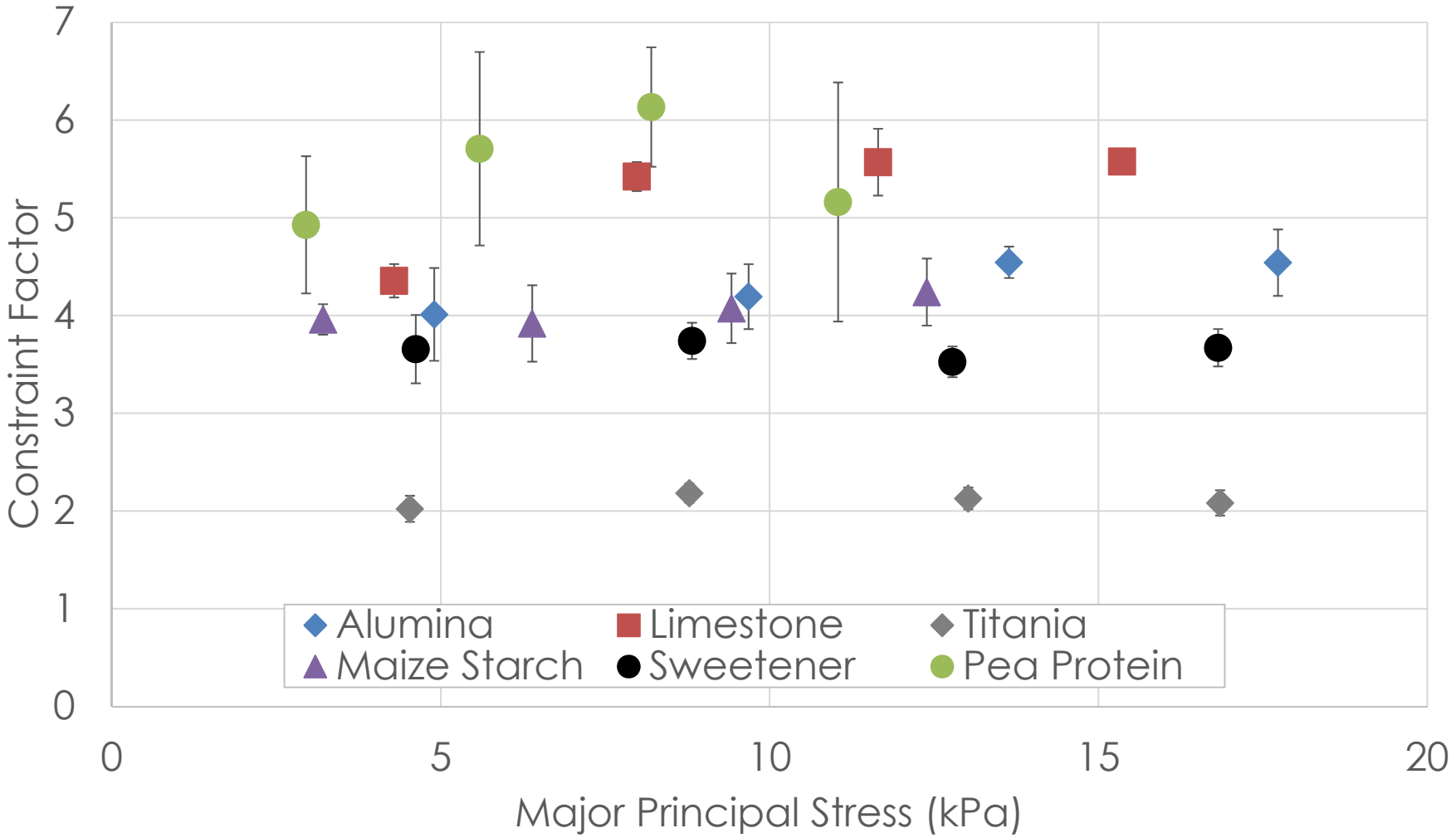

Inferred unconfined yield stress

- For most materials C is independent of stress
  - Can only be evaluated at stress levels where σ_c can be measured
- Measurement of σ_c at low stress problematic
- We infer σ_c from ball indentation measurements ($\sigma_c = H/C$)
  - Assuming C remains independent of stress
- Compared to shear cell measurements ≤ 1kPa pre-shear

Measurements at low stress

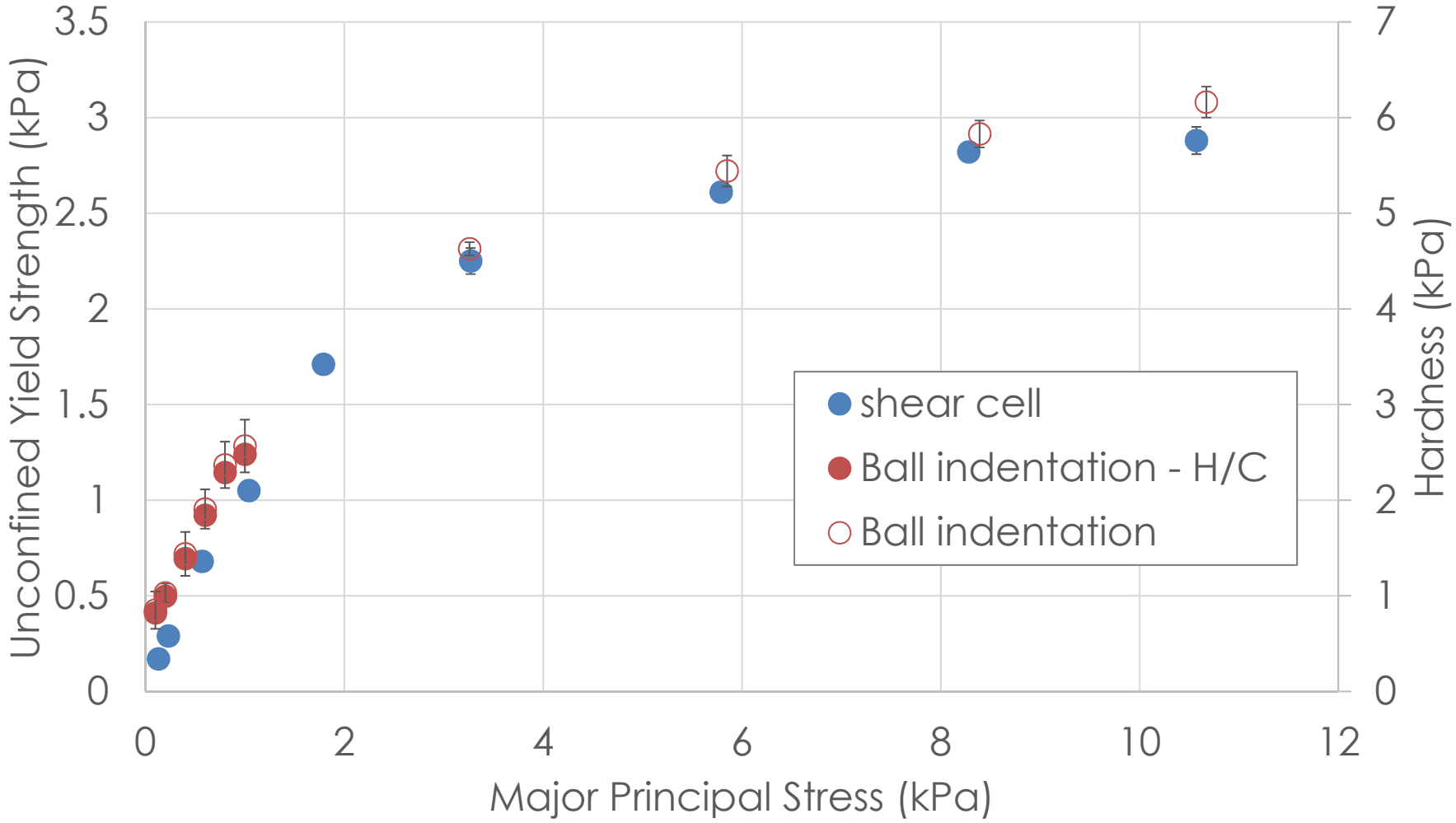

45-53 μm silanised glass beads

Future work

- Experimentally assess flowability dependency on:
  - Surface energy (silanised glass beads)
  - Particle shape (copper: spherical, irregular, dendritic)

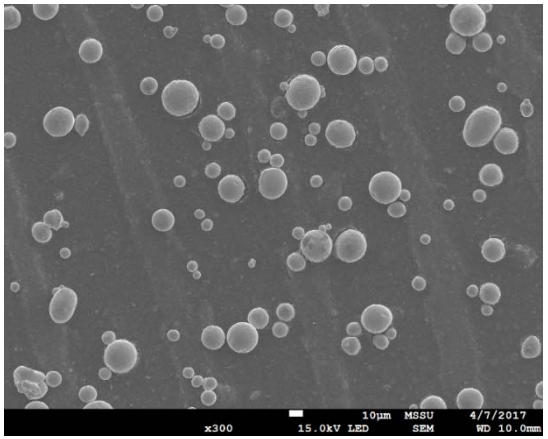

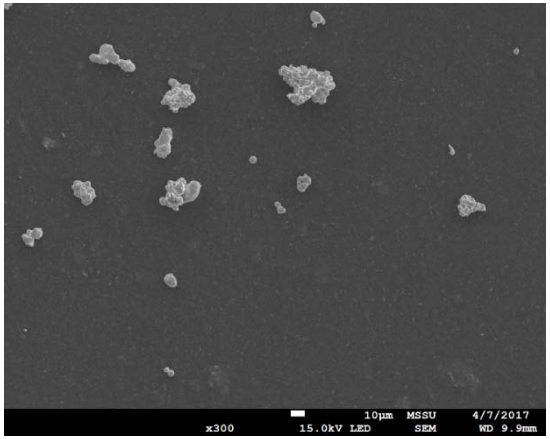

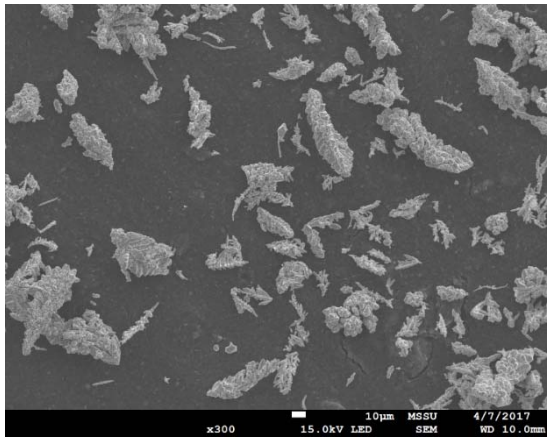

- DEM will be used to analyse C at low stresses
- Note: Project funded to Feb 2018

Renewal Proposal

Major principal stress direction

	Ball indentation	Uniaxial compression	Shear cell
Consolidation	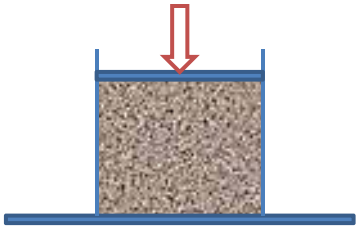	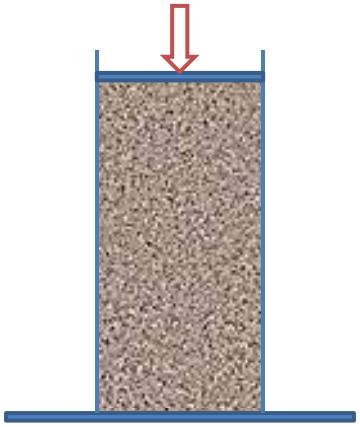	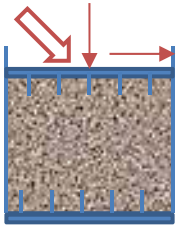
Failure	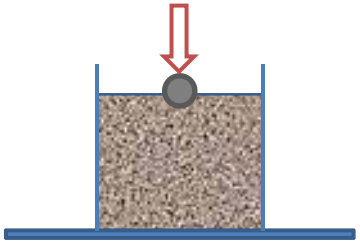	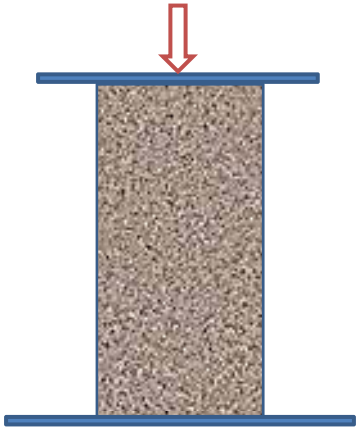	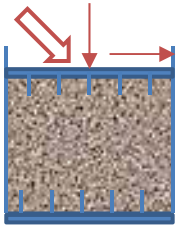

Major principal stress direction

	Ball indentation	Uniaxial compression	Shear cell
Consolidation	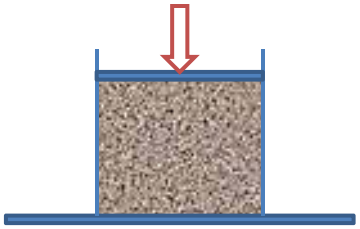	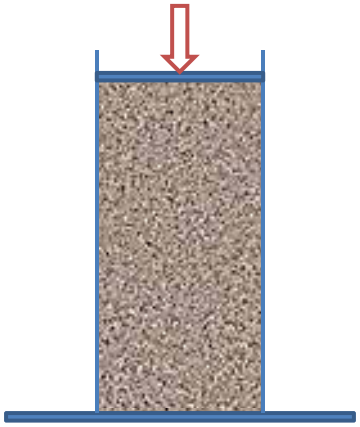	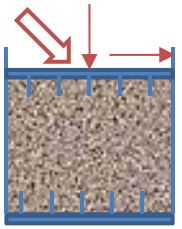
Failure	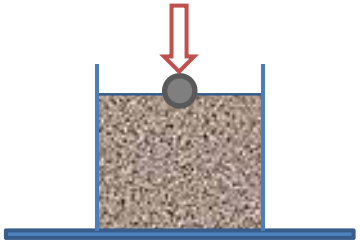	σ_1 in same direction as ball indentation: Both for consolidation and failure Known to underestimate σ_c 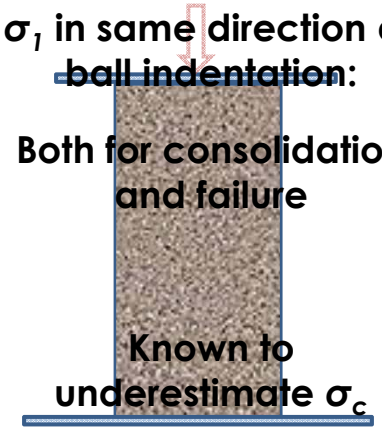	σ_1 in different direction to ball indentation: Both for consolidation and failure  Greater packing fraction for given σ_1

Constraint factor

- **Constraint factor determined in a number of ways:**

1. **Indentation at same σ_1 as shear cell**
2. **Indentation at same packing fraction as shear cell**
3. **Indentation at same σ_1 as uniaxial compression**

Shear cell method

- **Optimise pre-shear procedure at low stresses; vary**
  - **Number of pre-shear steps applied**
  - **Defined end point – i.e acceptable deviation to define steady state**
  - **Required agreement between consecutive pre-shears**

- **Ensure yield locus is reliable**
  - **Extrapolation to mohr circle should be minimised**
  - **Shear points should fit a line well (e.g. linear, Warren-Spring)**

Materials

- First funded period focussed on controlled particles
  - i.e. single property manipulated
- Wider range of powders to be investigated (~20)
  - Physical, mechanical and chemical properties measured
  - Statistical analysis of influential parameters on *C*

Lowest stress achievable

- All powders will be tested with the three techniques
  - Ball indentation, shear cell, uniaxial compression
- Range of low stresses investigated

- Determine, for each technique:
  - Lowest stress providing reliable result
  - As a function of particle properties

Packing fraction variation

- Bulk packing fraction measured for all three techniques
- Packing fraction in flowing zone may differ across techniques
- X-Ray Tomography to be carried out for all techniques
  - For key materials
    - Low constraint factor
    - High constraint factor

IFPRI
International Fine Particle Research Institute

POWDER STRUCTURE CONTROL

R. Kohlus, J. Harnacke

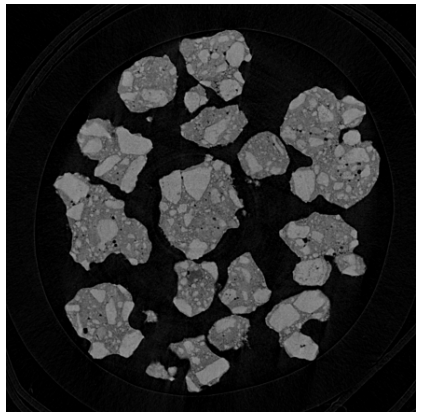

Introduction: Types of structure

- Different **types of structure** can occur in granules
- **Length scales** to describe spatial distribution of phases

Regular/
Homogeneous

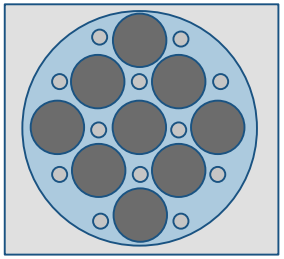

Random
-dense

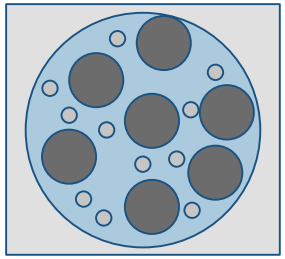

Random
-porous

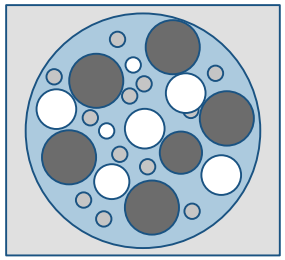

Clustered

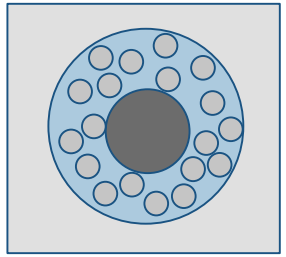

Structure – Process relation: Model structures

				Effect	structure measure
Twin screw extruder Dense Structures	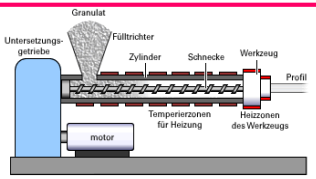	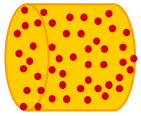		Diffusion	Nearest Neighbour
Low pressure extruder Fluid bed agglomeration Low moisture - open structure	 	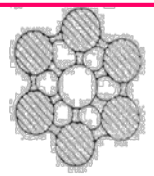		Dissolution Disinte-gration	Connectivity, CVF
Fluid bed Spray on granulation Dense tailored structures				Diffusion	RDF
High shear mixer granulation Brick and mortar structure	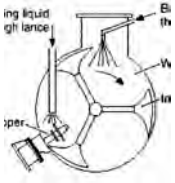	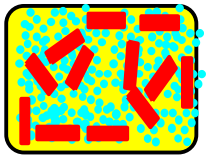	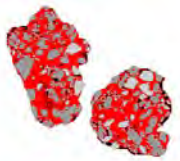	Strength	Contact number,…
Spray drying Porous structure	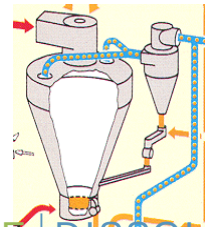			Strength, Dissolution	LP, CVF, RDF

Structure prediction : Covariance function

2nd order statistics

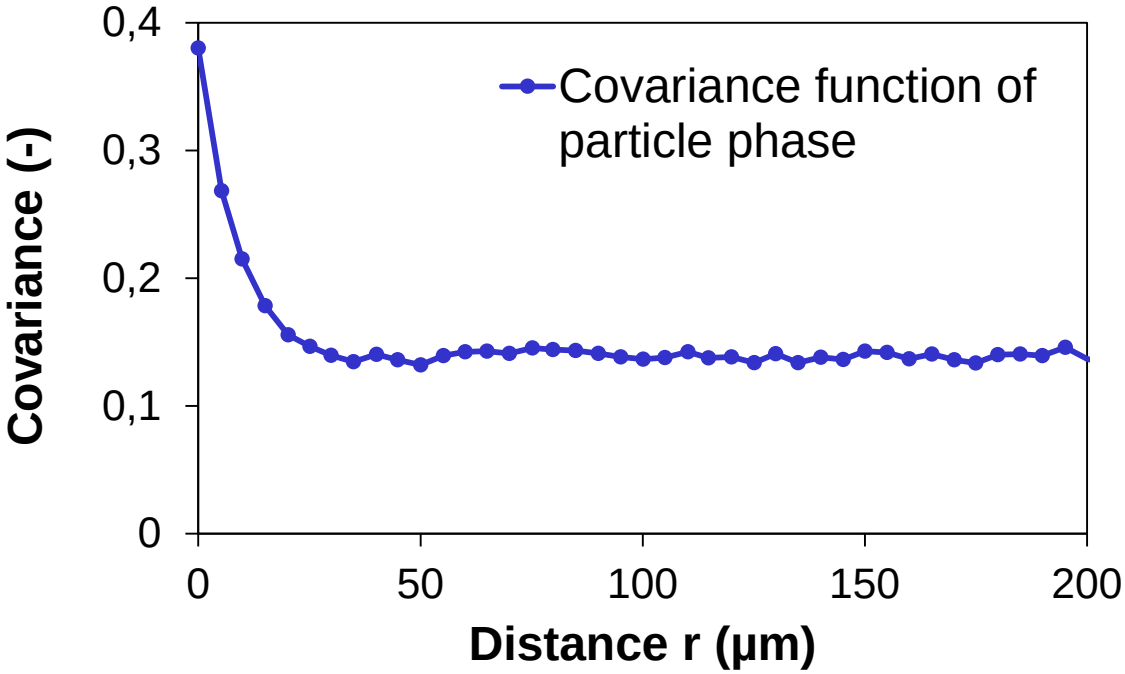

$$Cov(r) = (\Phi - \Phi^2) \cdot \exp\left(-3 \cdot \frac{r}{l}\right) + \Phi^2$$

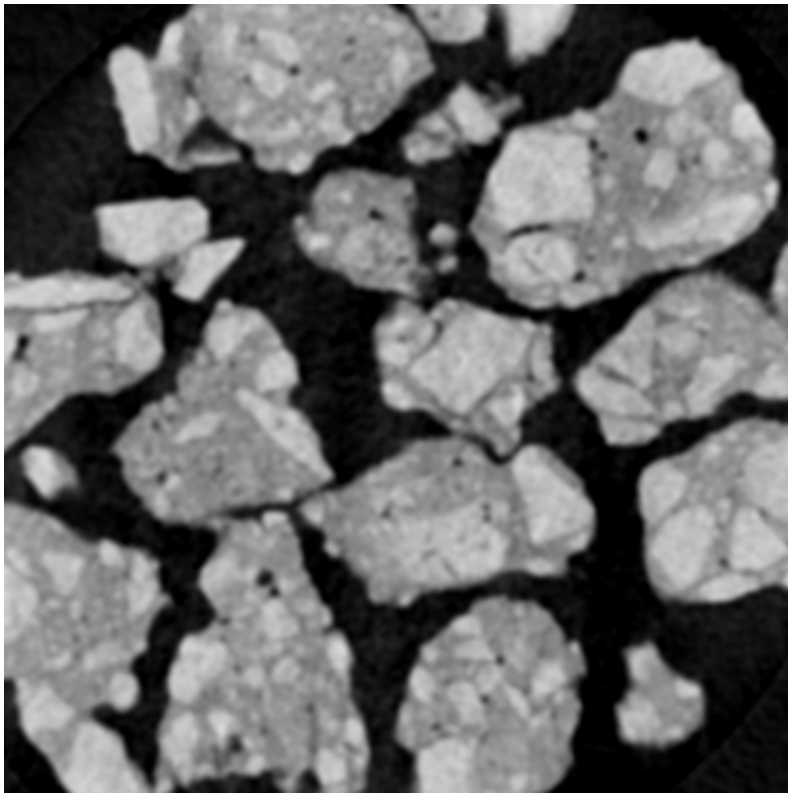

Parameter characteristic length l, Φ → CLD, pair correlation function, V*

Particle – particle distance d_{pp} from particle size distribution

- PSD of primary particles contains information about structure
- Packing of spheres: **randomly packed spheres** require a volume of 64 %
- Using **volume mean diameter** $d_{3,0}$ of coarse primaries to calculate their mean distance

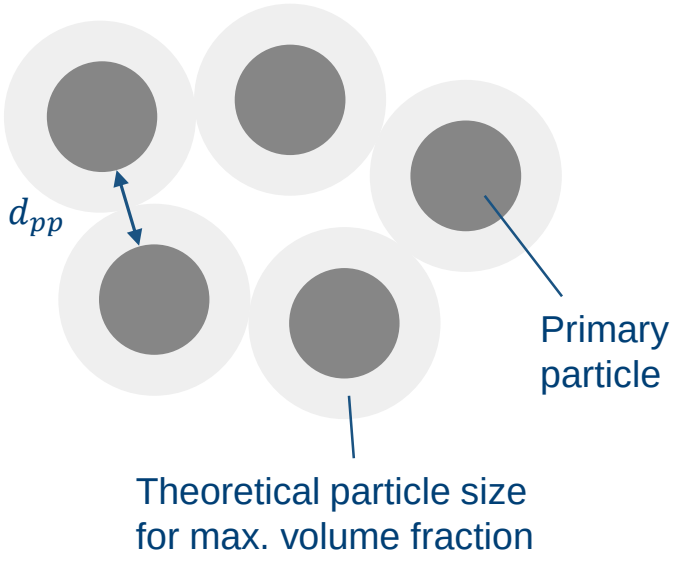

$$d_{pp} = d_{3,0} \cdot \left(\sqrt[3]{\frac{\phi_{max}}{\phi_c \cdot \rho_{tap}/\rho_{solid}}} - 1 \right)$$

Comparison between particle – particle distance from image analysis and from particle size distribution

Calculated and measured particle – particle distance is dependent on volume fraction of coarse primary particles

→ in good agreement

A low particle – particle distance is correlated with a high fraction of coarse primary particles

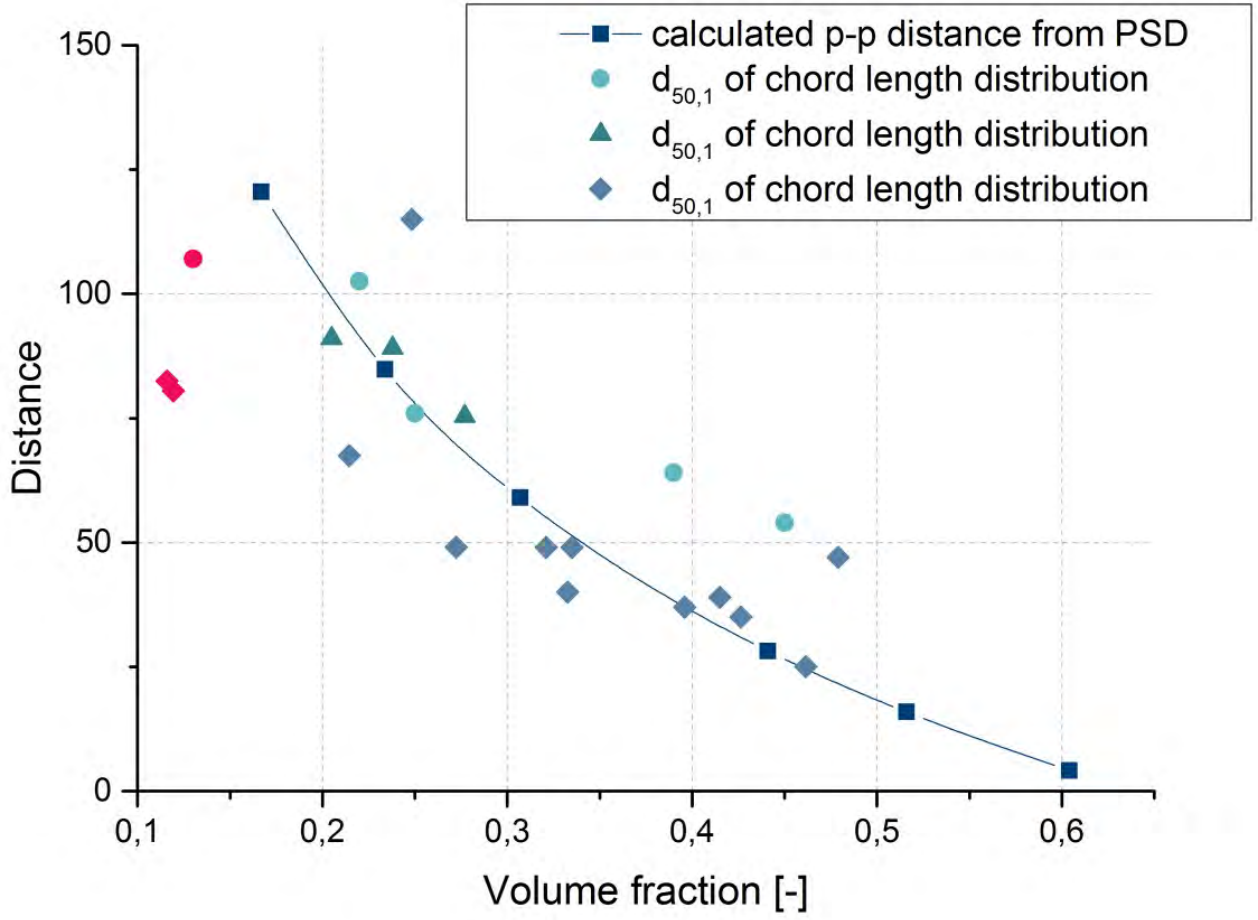

Dissolution behavior
Effective diffusion coefficient

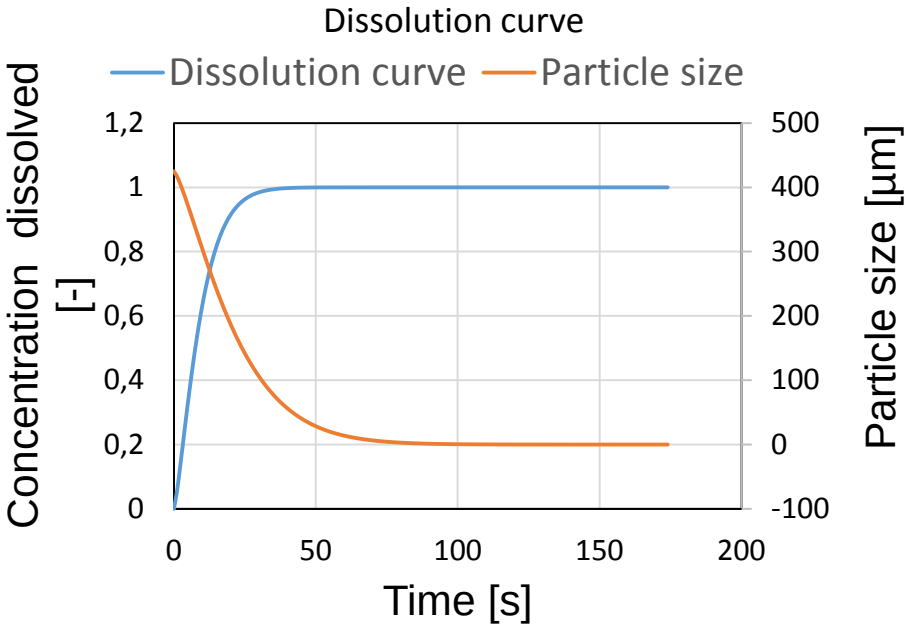

$$\dot{m} = \beta \cdot S \cdot (c_s - \bar{c})$$

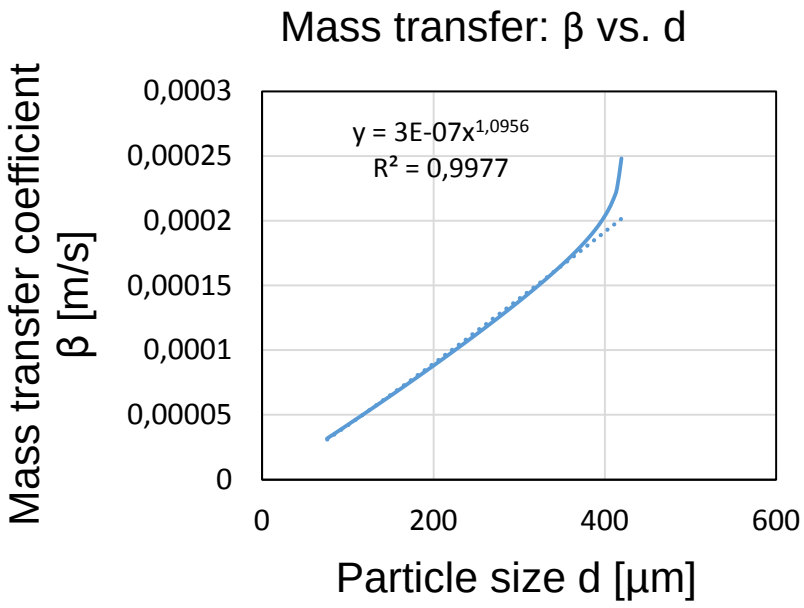

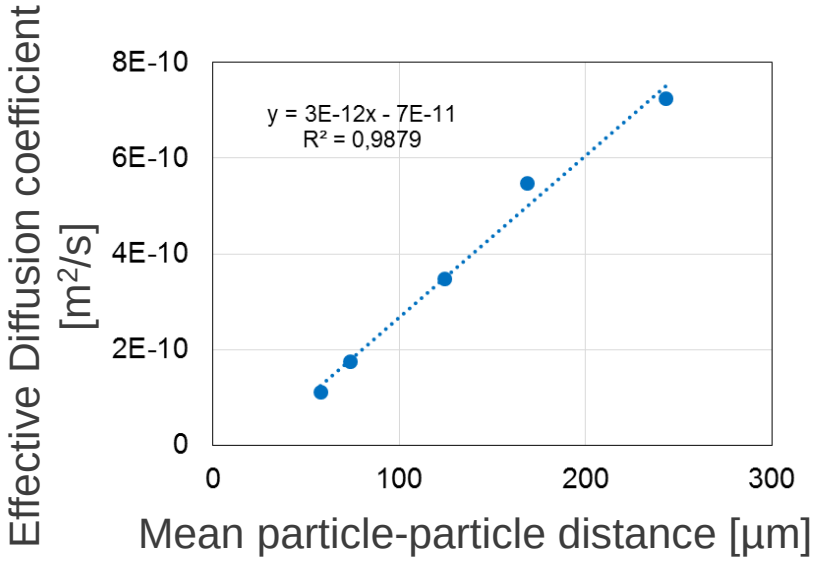

$$D_{\text{eff,structured}} = \left(\frac{\beta_{\text{structured}}}{\beta_{\text{homogene}}}\right)^{3/4} \cdot D_{\text{homogene}}$$

Assumption $Sh = f(Re) \cdot Sc^{0.33}$

β	mass transfer coefficient
S	particle surface
c	concentration of dissolving
D	diffusion coefficient

Random close structures

- Previous results: relationship between particle-particle distance and granule properties
- Dissolution faster for larger pore space = distance of insoluble material

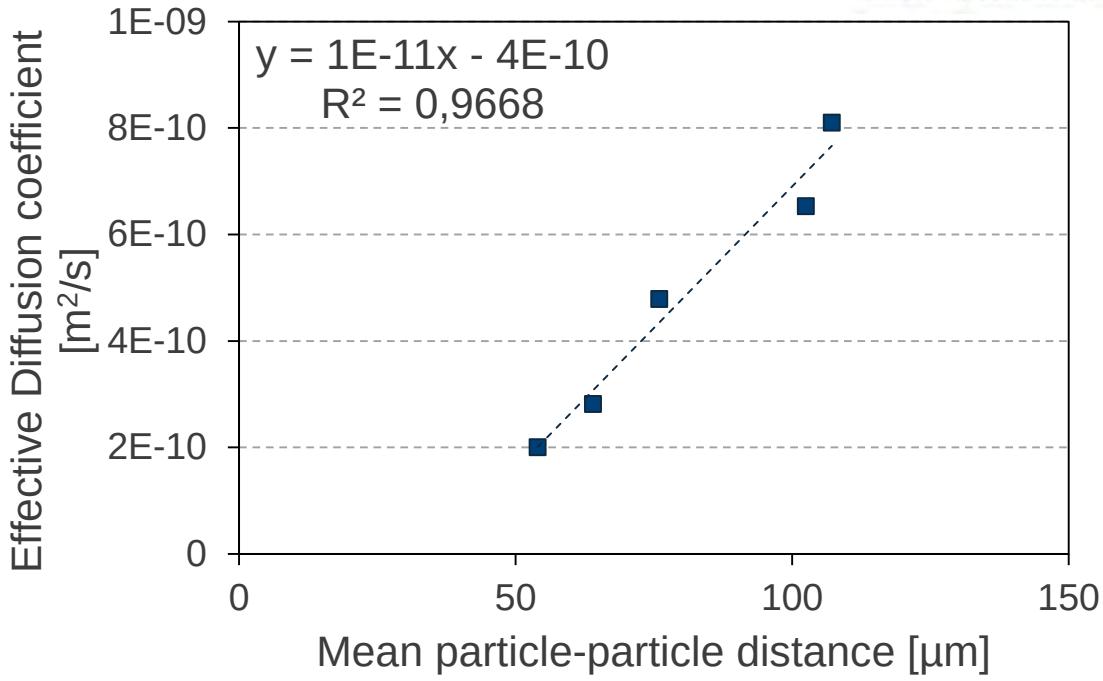

- Recent results variation of particle-particle distance
- Porous structures: pores as additional phase
- Layered structures: special case of clustered system

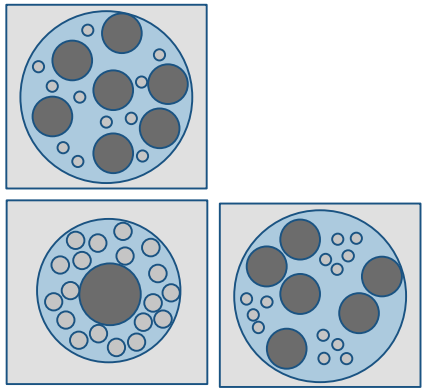

Dissolution: d_{pp} variation by choice of primary particle sizes (Limestone)

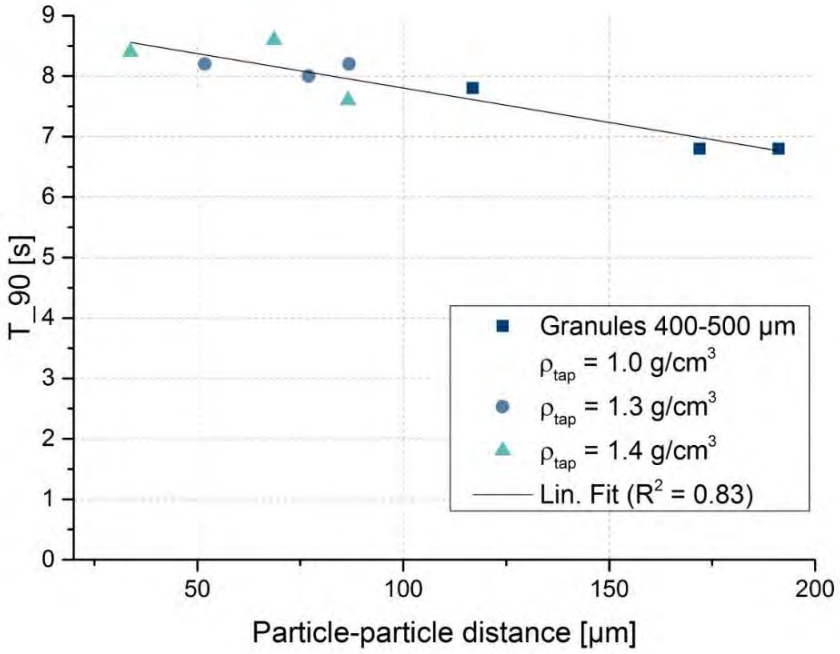

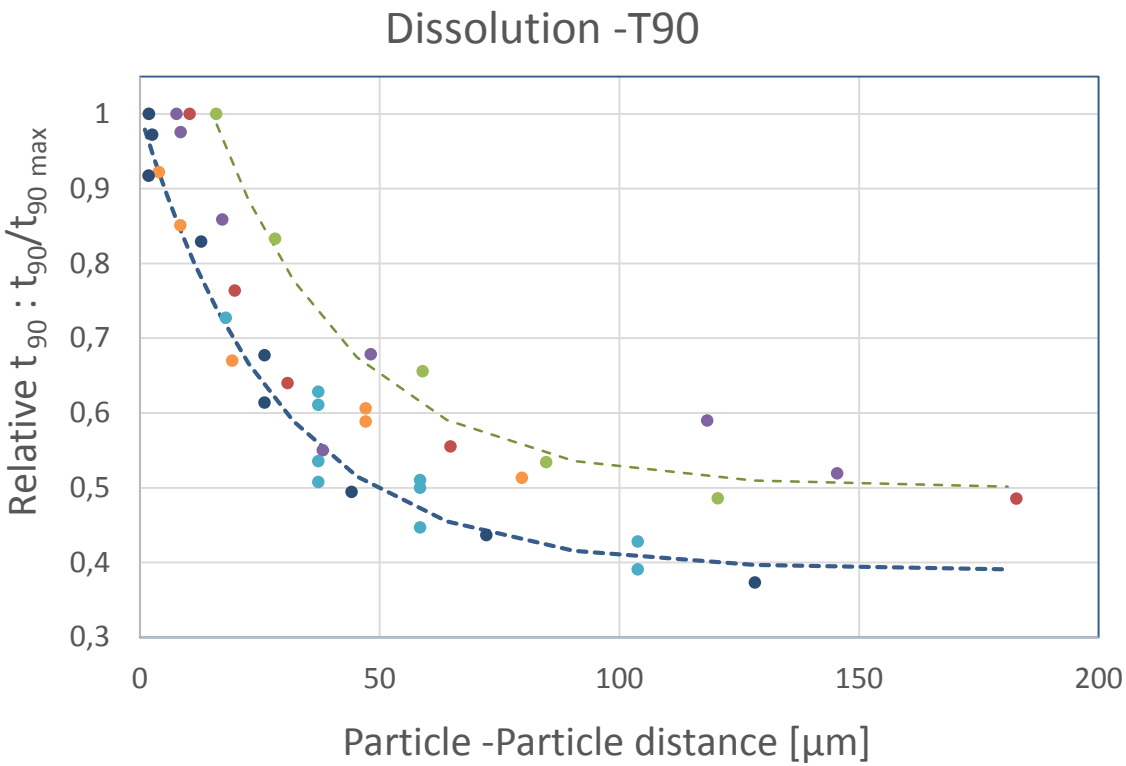

- Granule size 400-500 µm and 600-710 µm
- Variation of particle - particle distance between dense packing (d_{pp} ≈0) and $d_{pp} \approx d_{3,0}$
- t_{90} up to 80 s under stirred conditions

Physical properties: Single particle crushing

Measurement of crushing strength

of single granules with n > 100

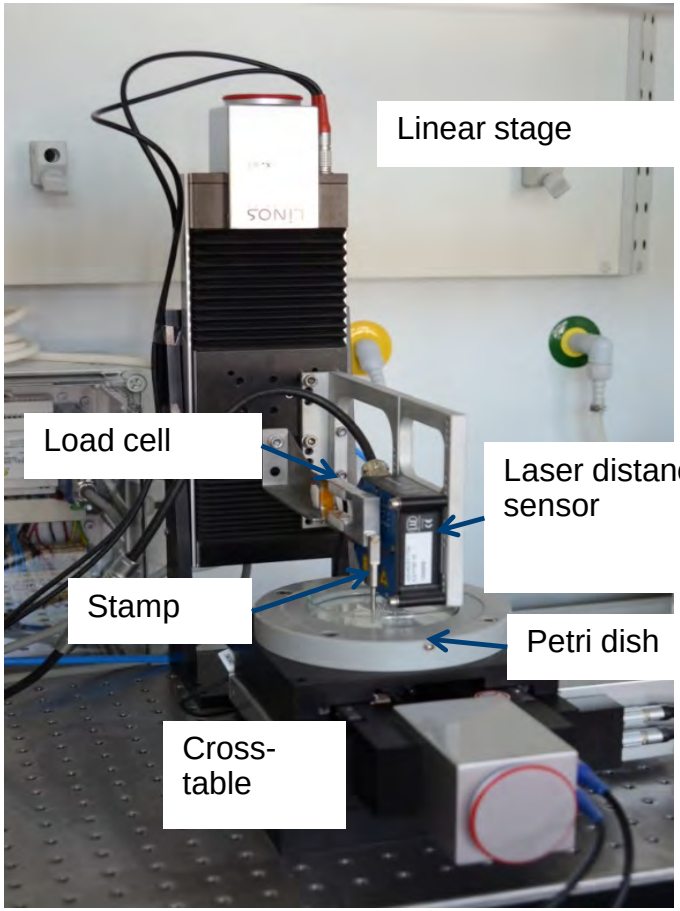

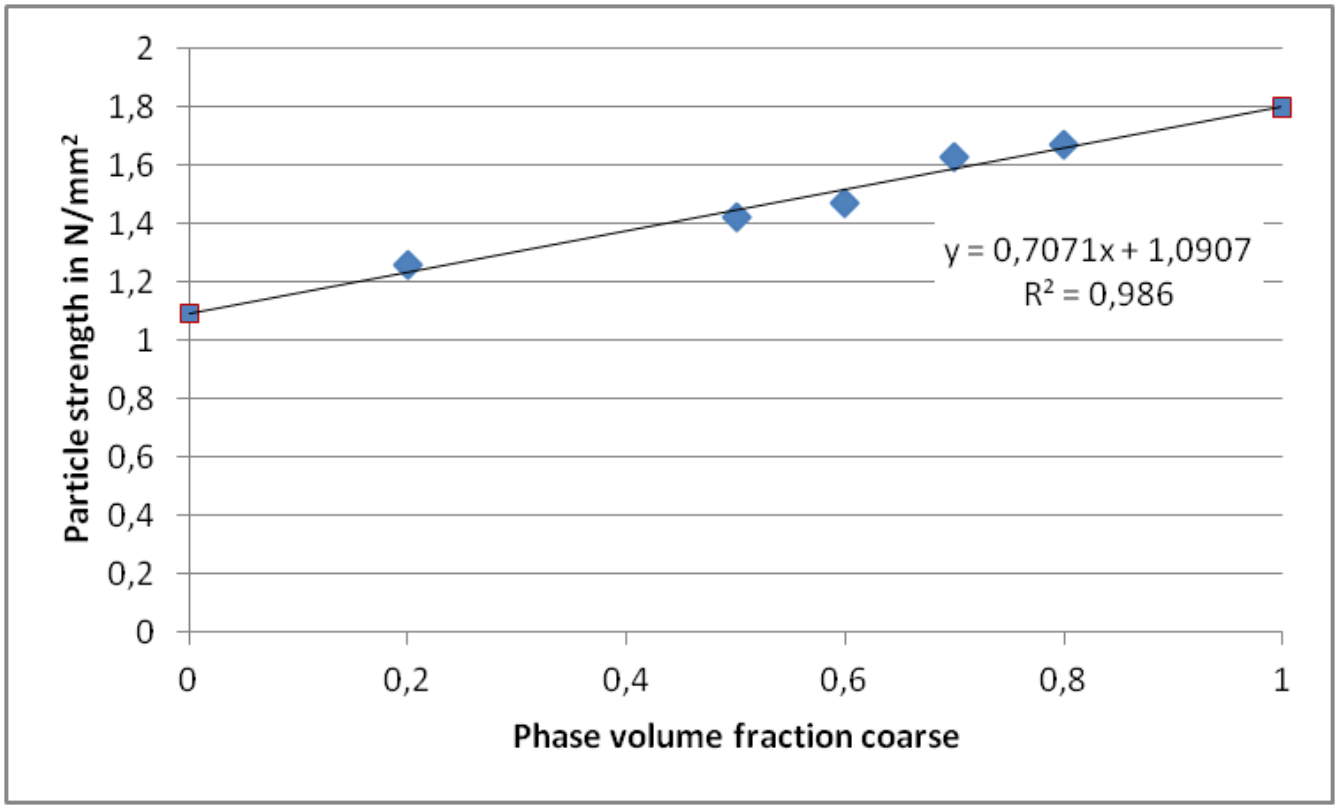

Phase volume changes mean also a shift in average chord length of binder- phase and total surface area.

Porous systems: Random loose structure

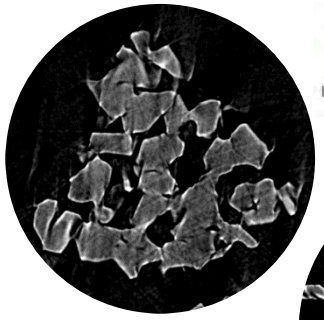

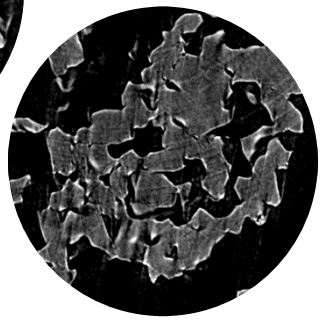

IFPRI International Fine Particle Research Institute

Sintered systems: sugar particles of different size classes

→ variation of pore sizes

Stored at high humidity → water uptake → building of bridges – V_{bridge} ca 2,2 V_{liquid}

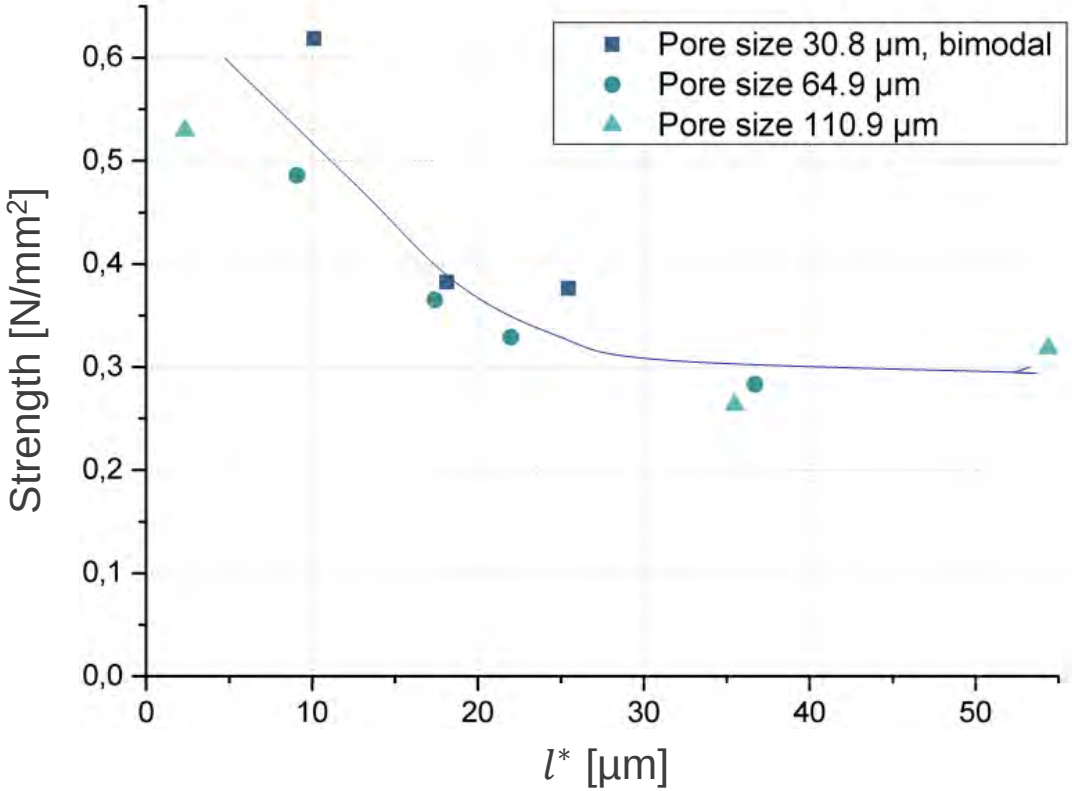

$$V^* = \frac{\pi}{3}\bar{l}^3$$

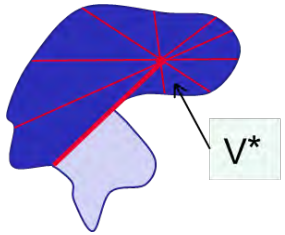

$$V^* = \frac{\pi}{3}\bar{l}^3 = \frac{\pi}{2}\bar{d}_{3,0}^3 \frac{\varepsilon}{1-\varepsilon}$$

$$\bar{l} = 1{,}15 \cdot \bar{d}_{3,0}^3 \sqrt[3]{\frac{1-\phi_s}{\phi_s}}$$

l^* mean minimum star volume length

Physical properties: particle strength

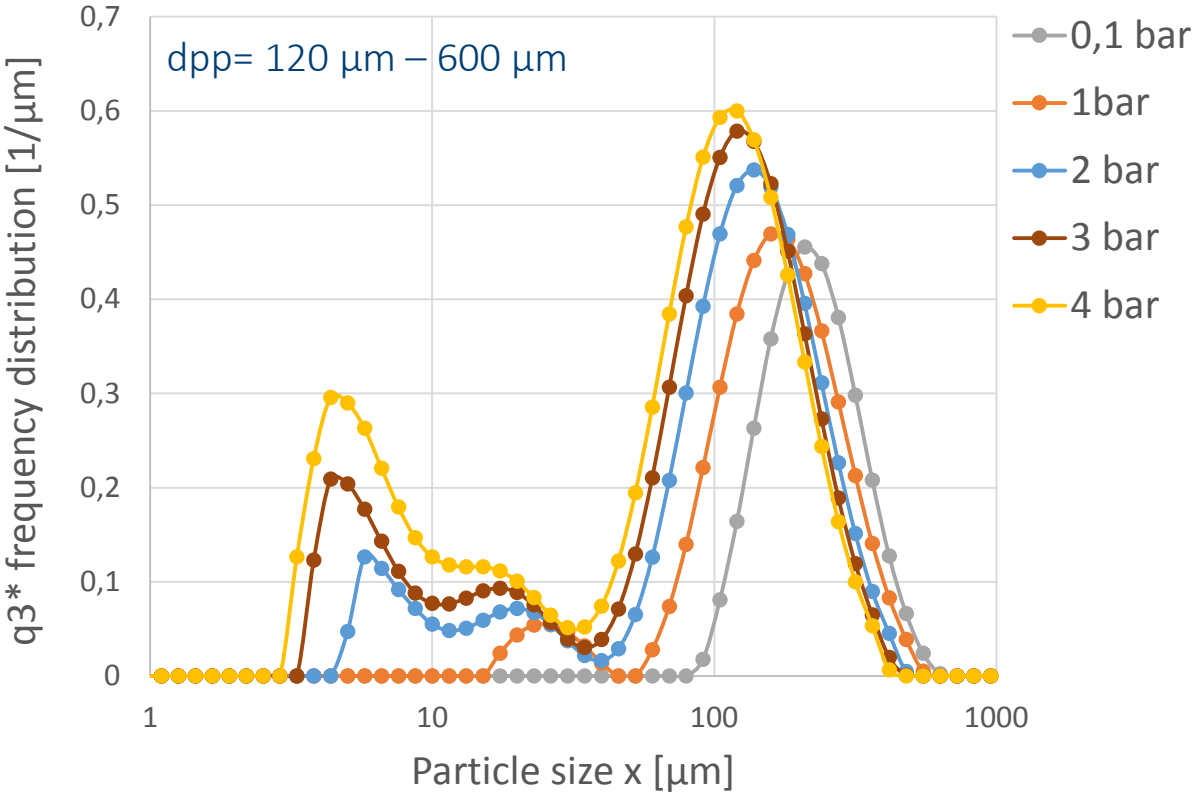

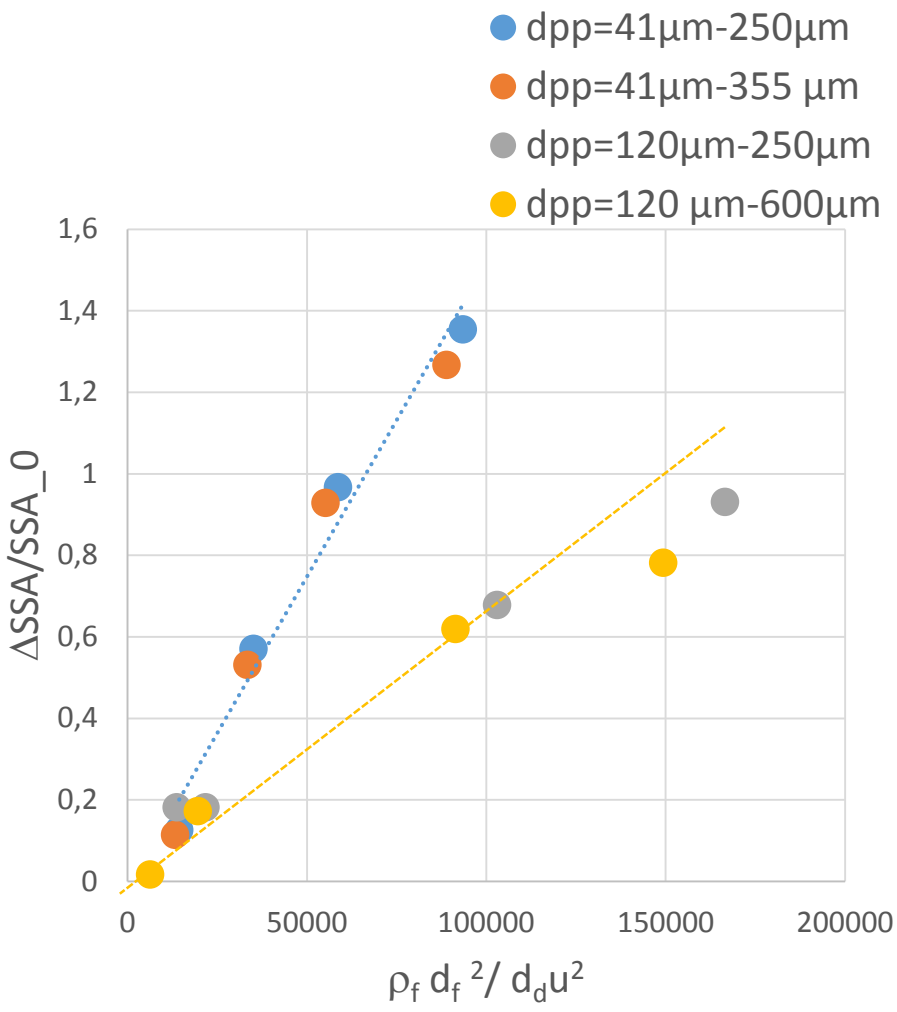

Fluid bed agglomerated systems, Binder PEG 4000, different particle size distributions of primary limestone.

Simulated dissolution by VOF

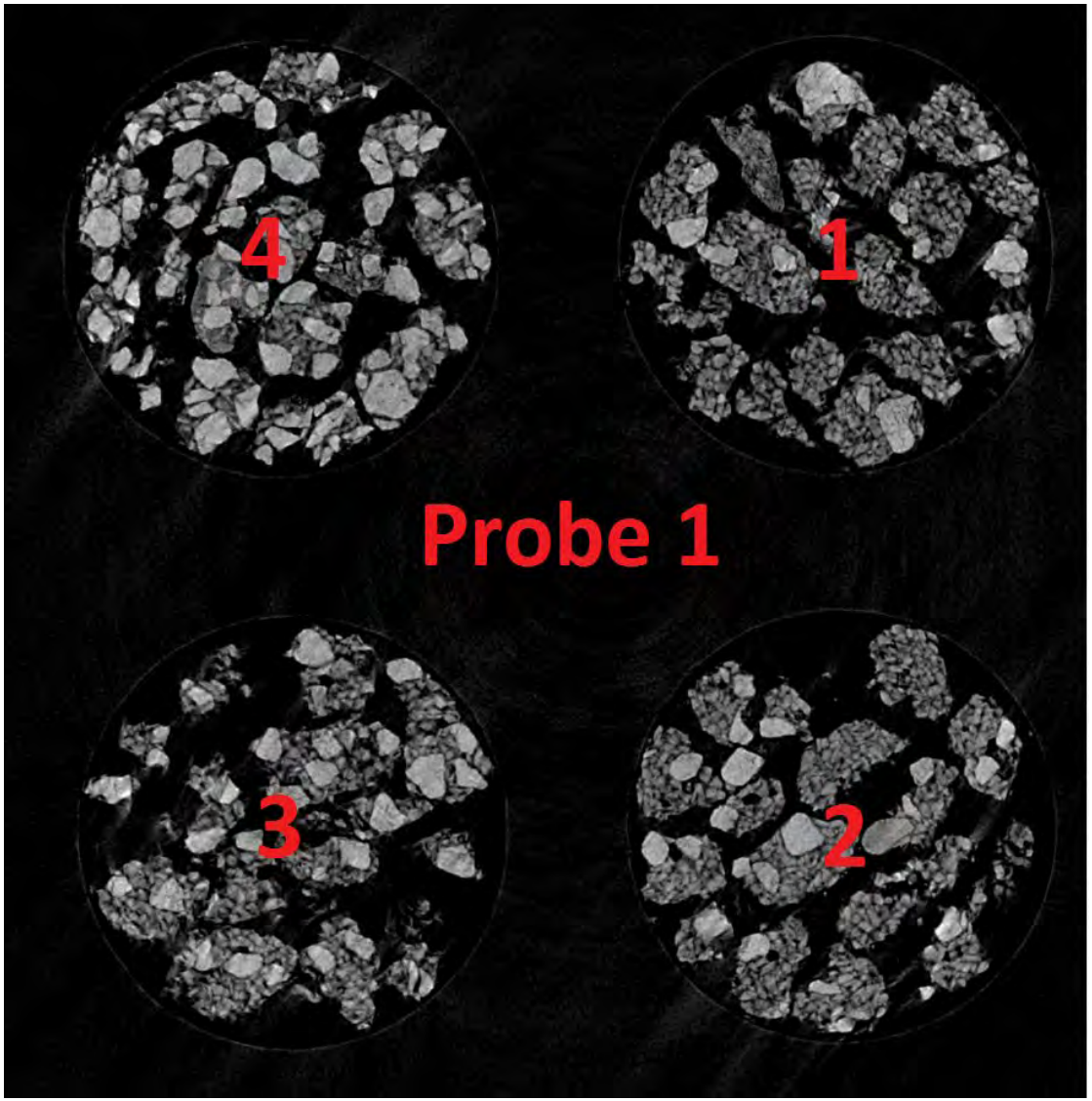

Dissolution simulation system:

- Limestone coarse
- Limestone fine
- Binder: PEG 4000
- NaCl particle –simulated

Unstructured (homogeneous) particle:

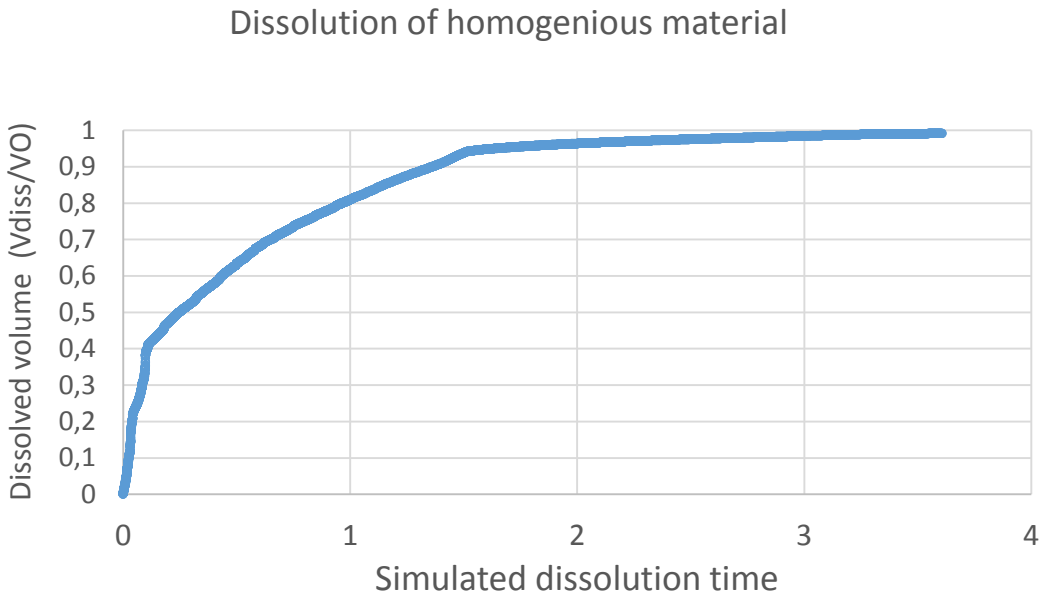

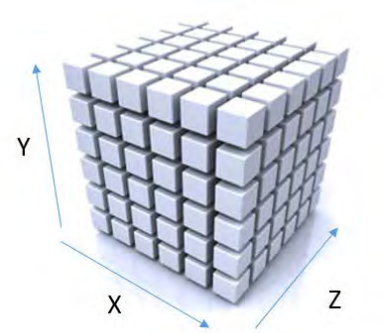

Simulated dissolution by VOF

$$\frac{\delta c}{\delta t} = D \cdot \left(\frac{\delta^2 c}{\delta x^2} + \frac{\delta^2 c}{\delta y^2} + \frac{\delta^2 c}{\delta z^2} \right)$$

2nd. Fickian law for diffusion

$$\frac{\delta c}{\delta t} = D \cdot \left(\frac{1}{\Delta x^2} c_{i+1,j,k} + \frac{1}{\Delta x^2} c_{i-1,j,k} - 2 \left(\frac{1}{\Delta x^2} + \frac{1}{\Delta y^2} + \frac{1}{\Delta z^2} \right) c_{i,j,k} + \frac{1}{\Delta y^2} c_{i,j+1,k} + \frac{1}{\Delta y^2} c_{i,j-1,k} + \frac{1}{\Delta z^2} c_{i,j,k+1} + \frac{1}{\Delta z^2} c_{i,j,k-1} \right)$$

2nd. Fickian law in form of a finite differences scheme

Each volume element with information on concentrations and phase volume ratio
Limestone- NaCl – Binder

Solved by Matlab (sparsely populated matrices)

Single particles ex µXRT

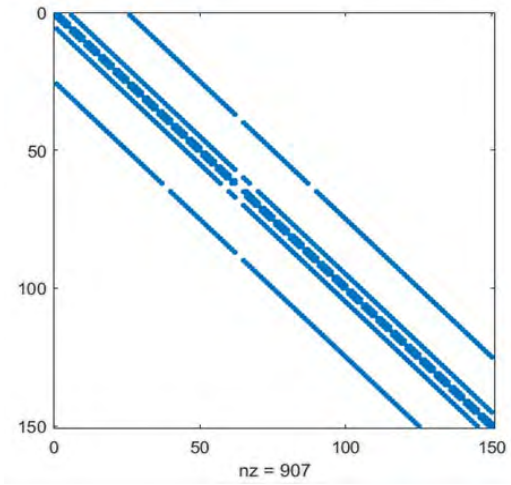

Simulated dissolution

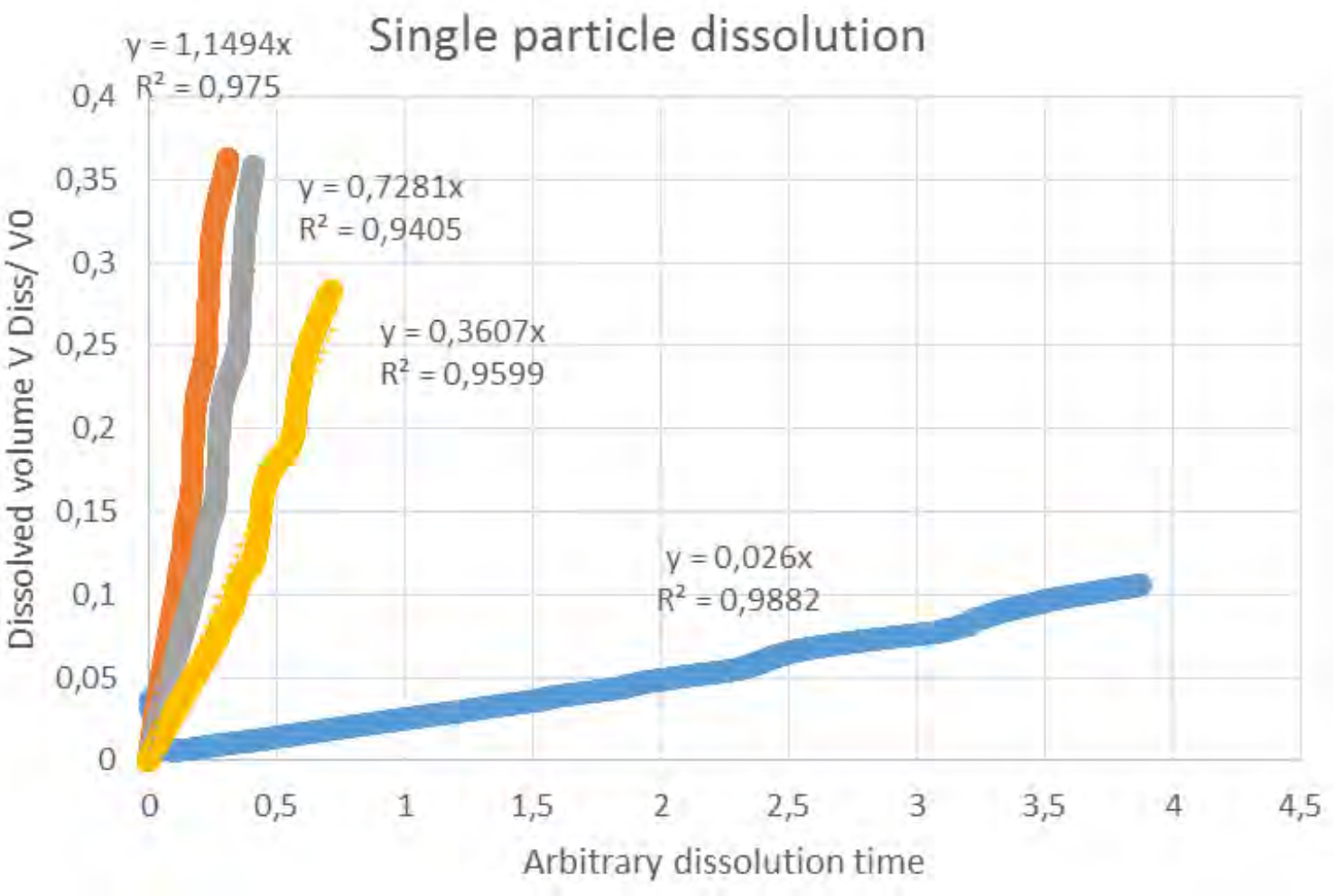

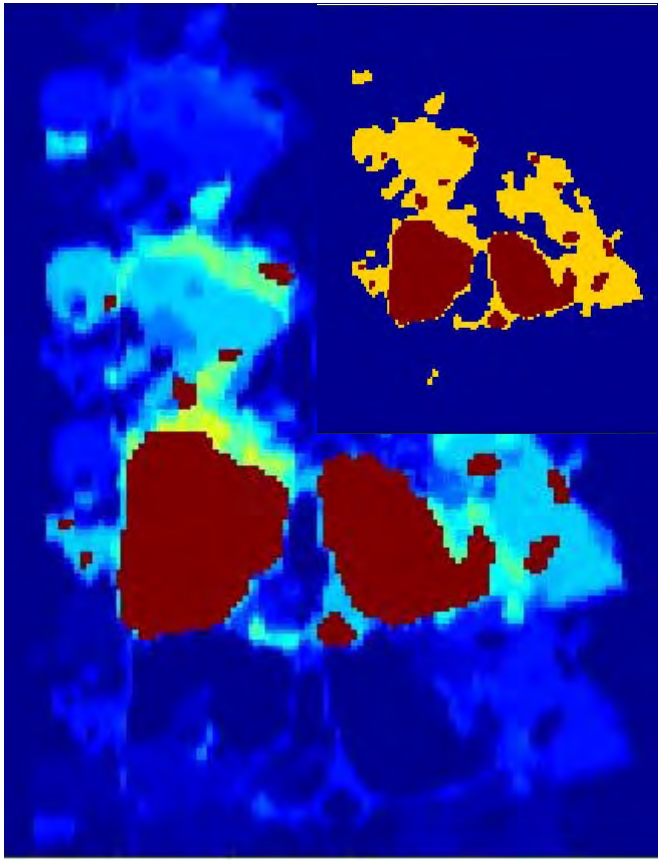

Linear slope of dissolution start of limestone, NaCl, PEG 4000 particle – spatial resolution 5 µm.

Simulated dissolution

Results are very noisy!
⇒ Averaging of high number of particles

Early state structure dependent
=> late state not representative

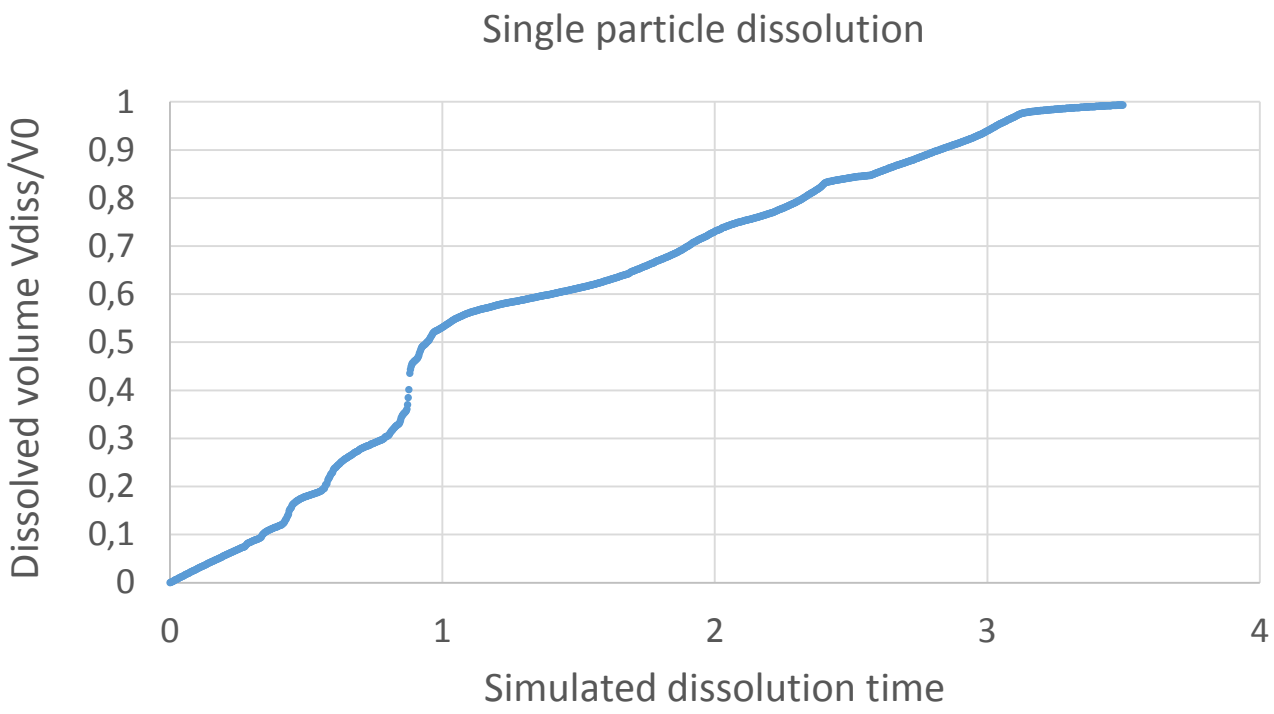

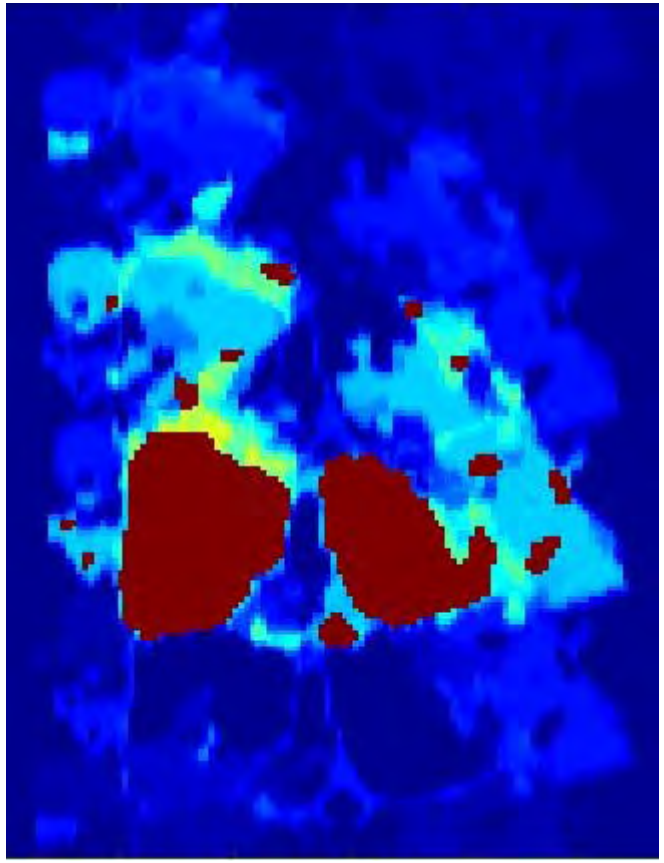

Powder Structure

Potential spatial arrangement of components

Type/Scale	Amount 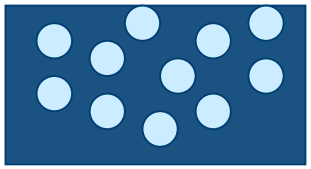	Size 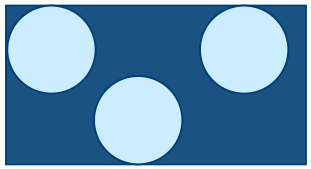	Distribution 
Macro Powder bed / Tablet	BD / Bed Porosity	Particle / Pore Size	Pore Size: Tablet / Powder Bed
Meso Granule	Phase Volume / Particle Porosity	Chord Length / CVF	CVF / Distance Distribution, RFD, Homogeneity
Micro Raw Materials / Molecular Level	Formulation	Raw Material characteristic (e.g. PSD solid)	Spacings, crystal forms etc.

CVF: Covariance function, PSD: Particle size distribution, RFD: Radial distribution function

Property functions

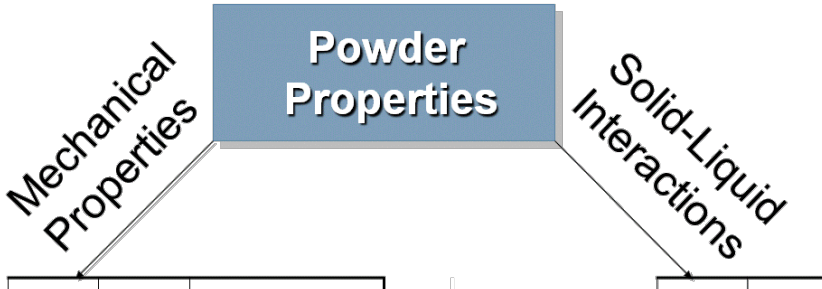

	PB	AG	Physical Effect
Bulk Density	✓	✓	Steric
Compaction	✓	±	Stress Chains
Tensile Strength	-	✓	Stress Chains

	PB	AG	Physical Effect
Wetting	✓	✓	Capillary Flow
Dispersion	✓	✓	Cohesive Forces
Dissolution	-	✓	Cohesive Forces

Blue: Promising areas for improvement by structure information

Structure depending properties. PB – Particle Bed, AG – Agglomerate

Property area	Characteristic
Mechanical:	E, ν (Poisson ratio), c compressibilty, deformation, fracture
Solid-liquid interaction:	dispersion, dissolution time, wetting, capillary pressure, diffusion, disintegration
Others:	thermal properties (λ heat conduction)

IFPRI
International Fine Particle Research Institute

Thank you for your attention!

Exploiting a Framework
for the Development of Segregation Rate Models

J. J. McCarthy

Department of Chemical Engineering
University of Pittsburgh

June, 2017

Quantitative Prediction of Segregation at Process Scale

- Identify critical **material and process parameters** that control the *extent* of powder segregation
- Develop **quantitative models that predict** segregation and possible re-homogenization within a process train
- **Validate** models with appropriate experiments
- Demonstrate that the models are applicable to **full-scale** processes
- In scope:
  - Dense flows
  - Formulated (i.e. multicomponent) mixtures
- Additional considerations:
  - Cohesive powders
  - Particle shape effects

Competing Timescales

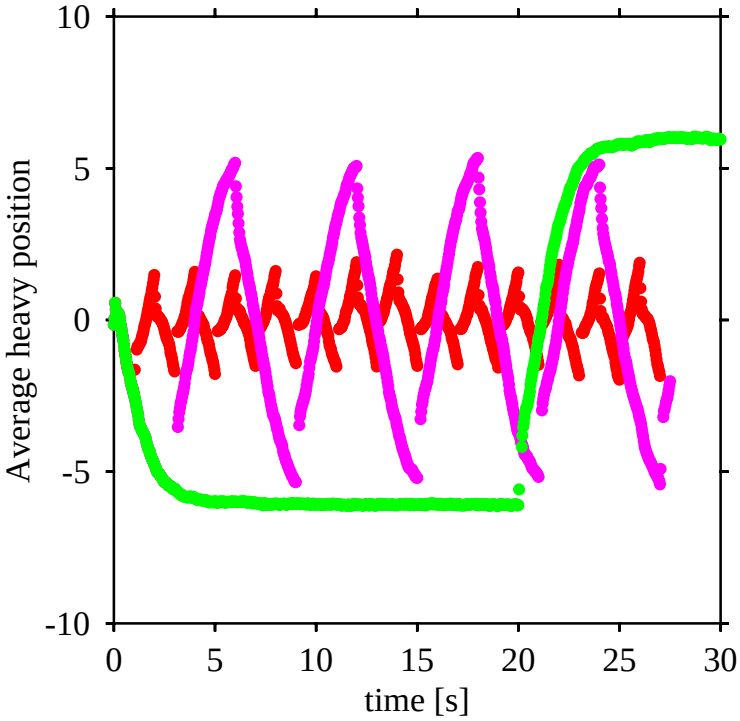

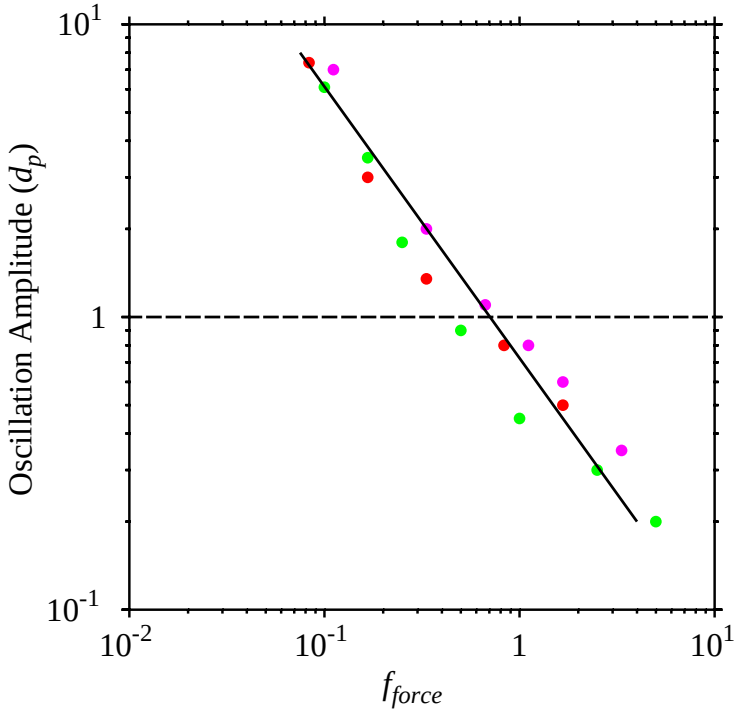

- "Asymptotic" segregation ↓ with ↑ forcing frequency
- If $t_{seg} \approx t_{forcing}$ balance of rates
  - We control $t_{forcing}$
  - Sensitive test of t_{seg} model
  - "Collapse" complex dynamic experiment onto "steady state" measurement

Indirect Forcing in a Baffled Tumbler

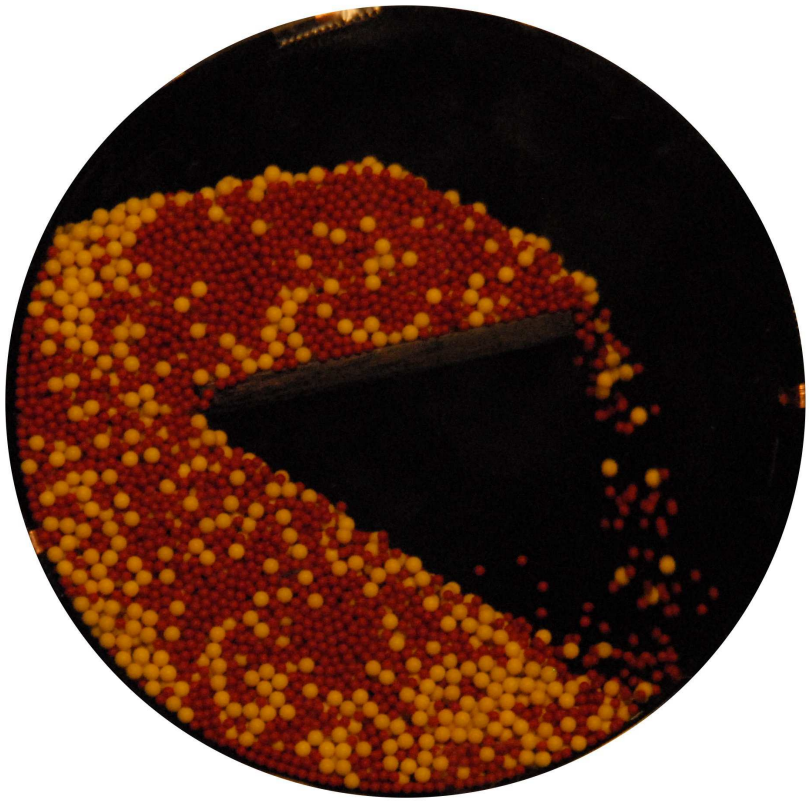

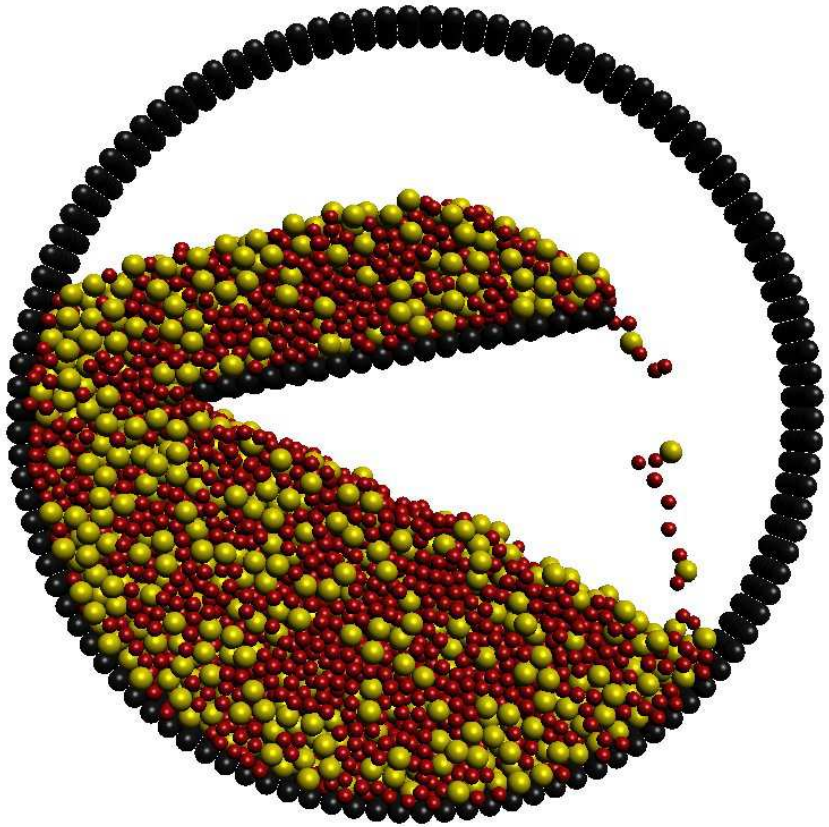

- Changing the rotation rate changes $t_{forcing}$

Model Predictions (Density Segregation)

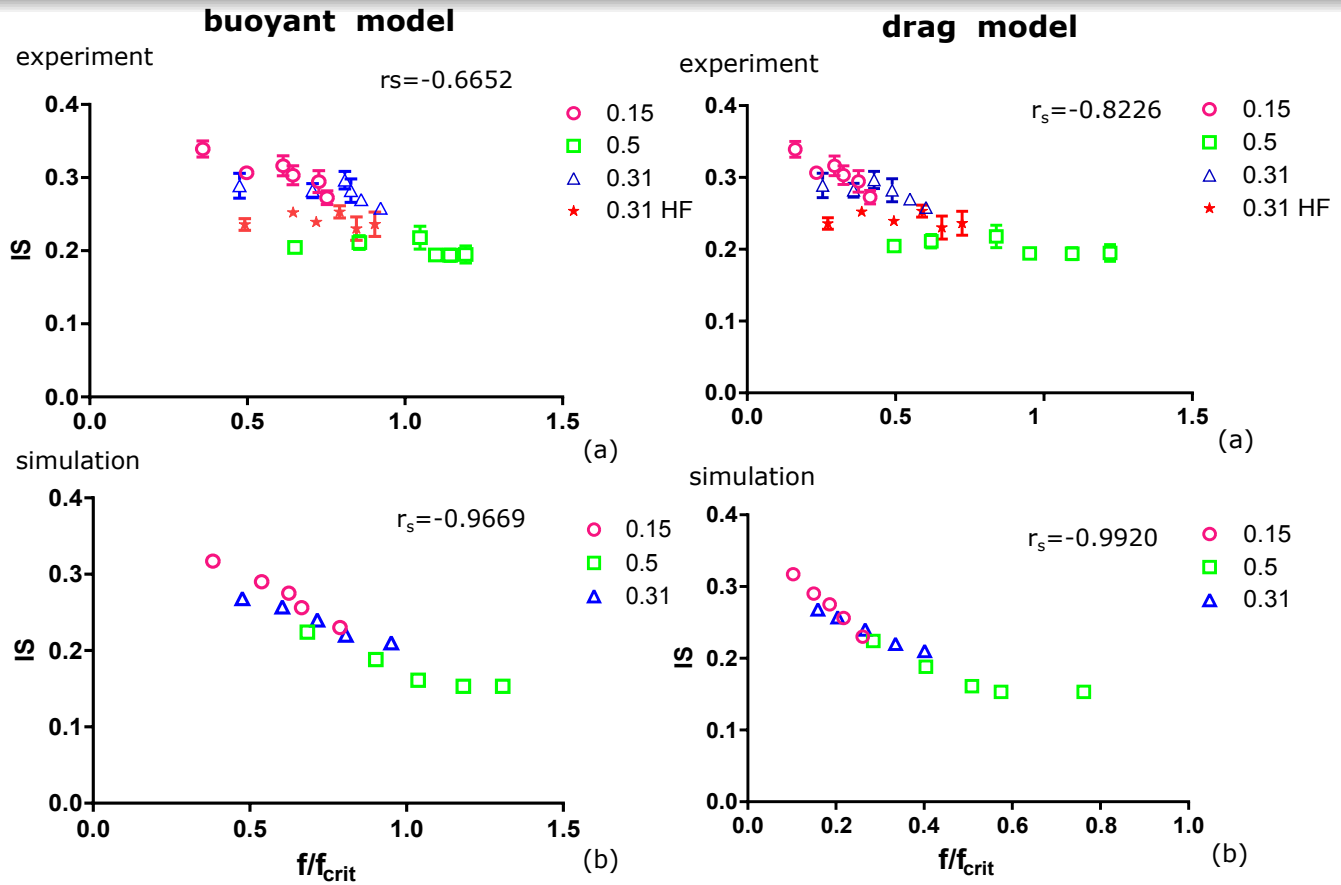

- Particle roughness suggested at AGM 2015
- "Proper" model will yield monotonic change in IS vs f/f_{crit}
- r_s for quantitative measure ($1 \rightarrow$ monotonic)

Model Predictions (Size Segregation)

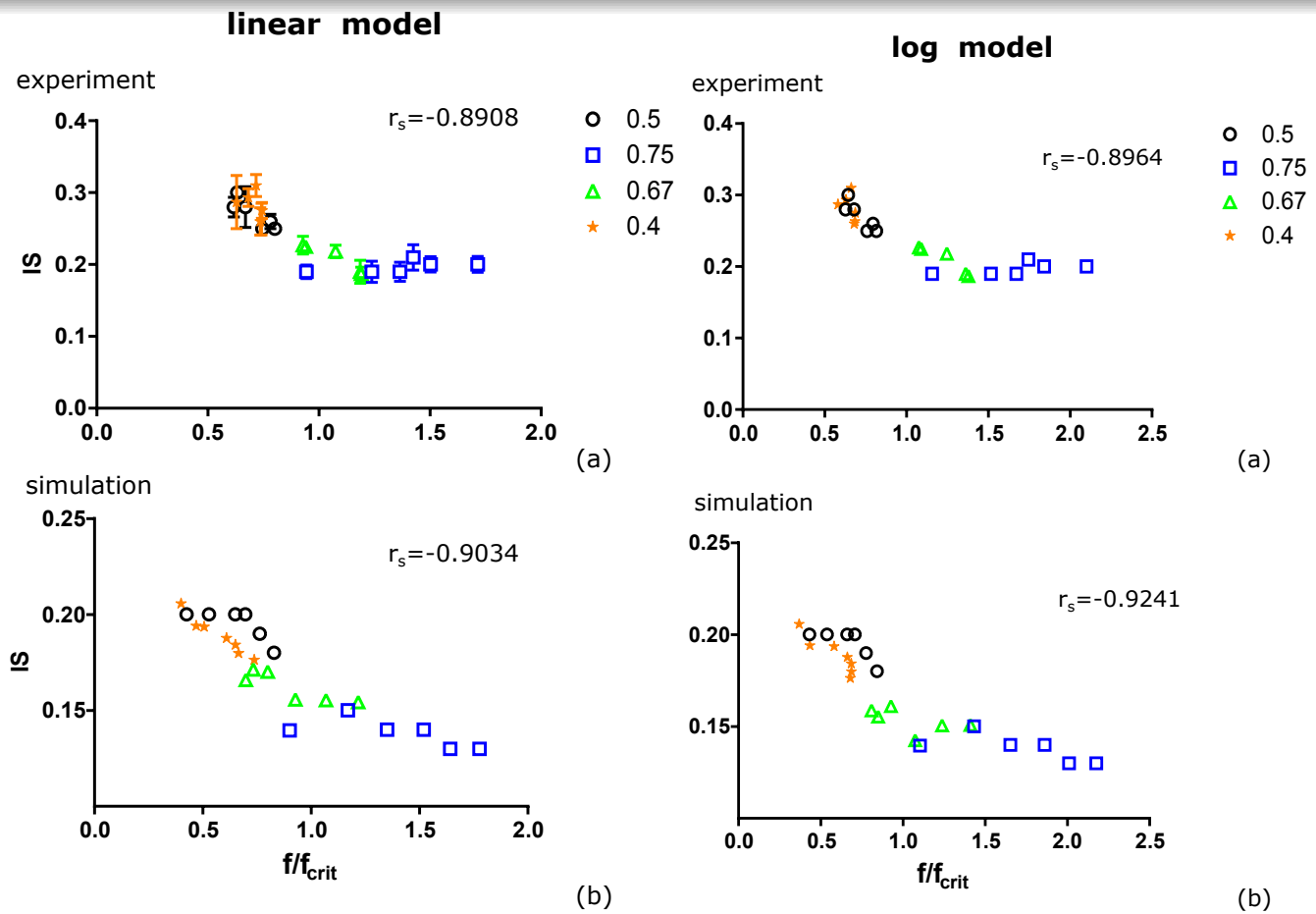

- "Proper" model will yield monotonic change in IS vs f/f_{crit}
- r_s for quantitative measure ($1 \rightarrow$ monotonic)

Preliminary Conclusions

- Competing timescales can *experimentally* discriminate between models (even in a tumbler)
- Density segregation:
  - No current model is great (best is 0.82 vs 1.0)
  - "Drag" is critical for capturing particle surface properties (0.82 vs 0.67)
  - Tumbler makes for a somewhat "messy" model system
- Size segregation:
  - Both linear and log models are OK (0.90)
  - Models are essentially the same for "reasonable" size ratios
- Better control of forcing frequency is required for better model validation/development

Direct Forcing in a Simulated Shear Cell

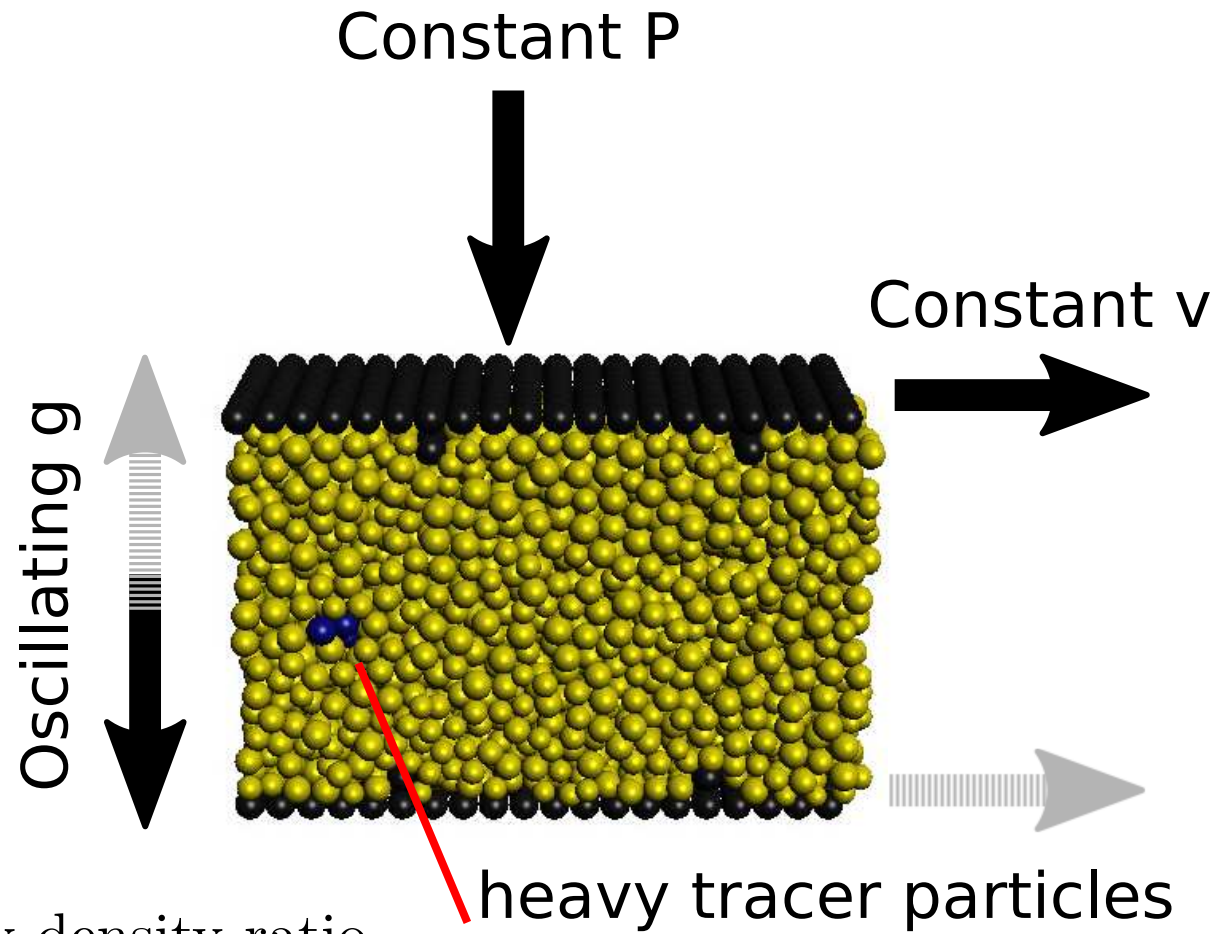

- Vary density ratio
- Vary shear rate (velocity)
- (Mostly) Constant pressure BC

Traditional Approach to Density Segregation

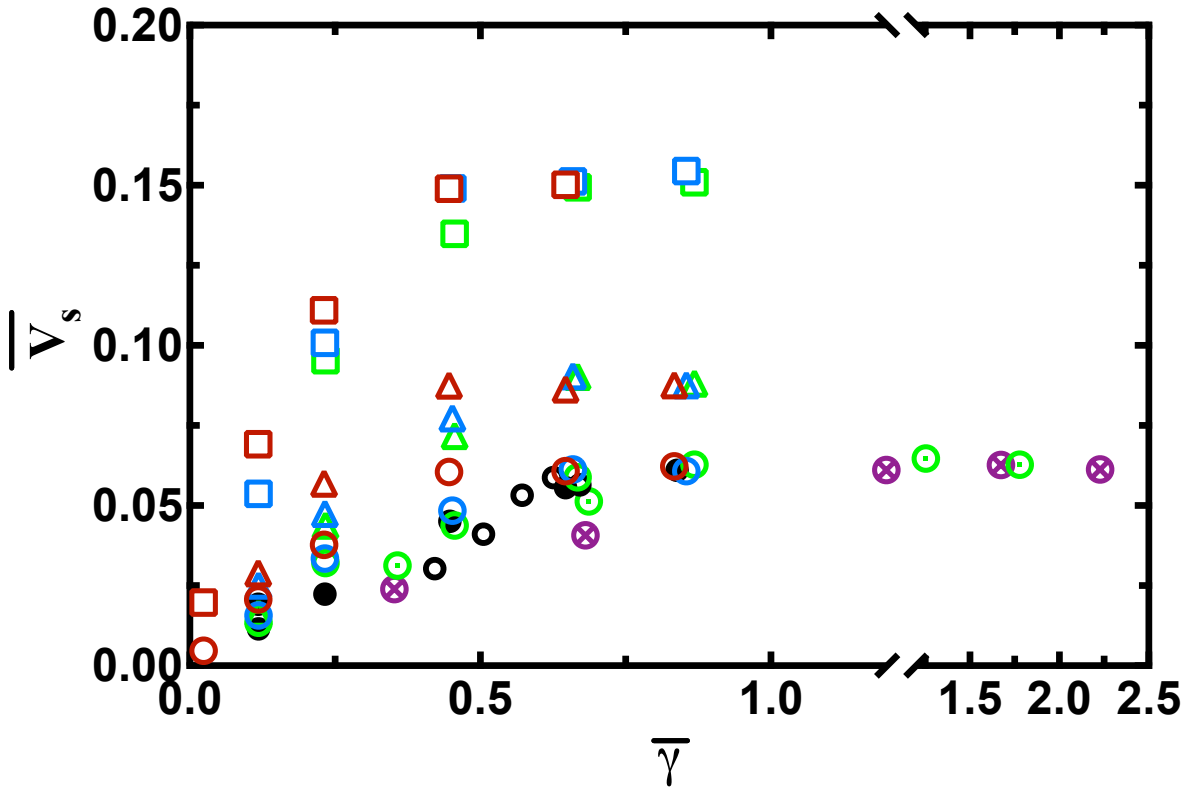

$$\bar{v}_s = \frac{v_s}{\sqrt{d_p g}}$$

$$\bar{\gamma} = \frac{\dot{\gamma}}{\sqrt{g/d_p}}$$

- Colors → density ratios
- Shapes → boundary conditions (mostly P, solid is CV)
- Differing circles: particle size, imposed gravity

Rheologically-inspired Scaling

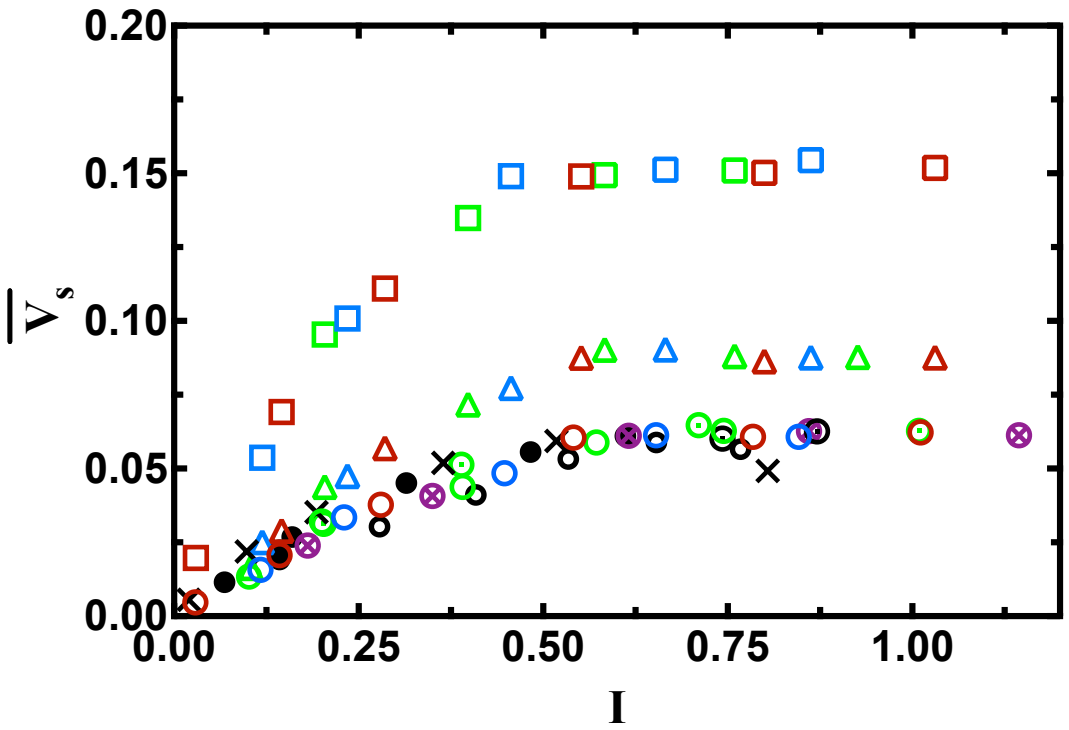

- Using the Inertia number, $I = \dot{\gamma} d_p \sqrt{\rho / P}$, collapses BC's
- Need scaling for density ratio

Fixing the Impact of Density Ratio

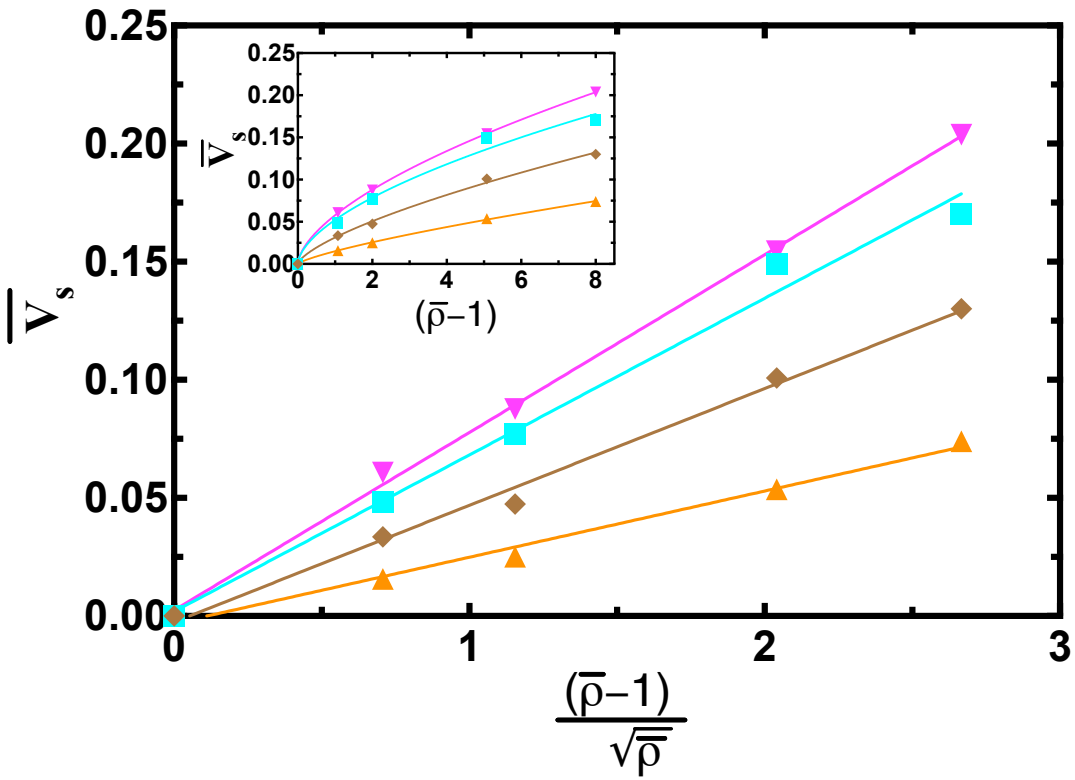

- Interestingly, typical density scaling doesn't fit
- "Added mass" scaling, based on energy balance works!

A Unified Model, Based on Rheology

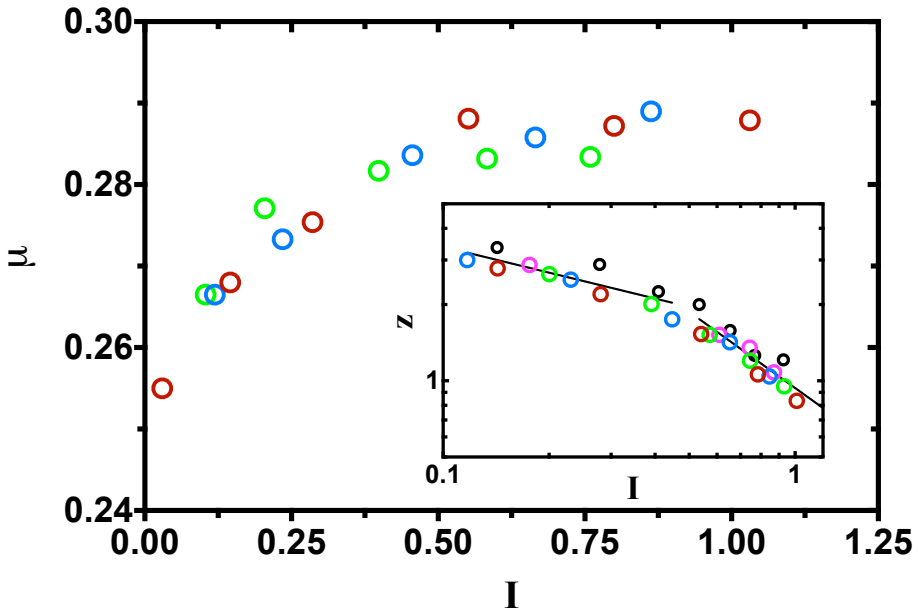

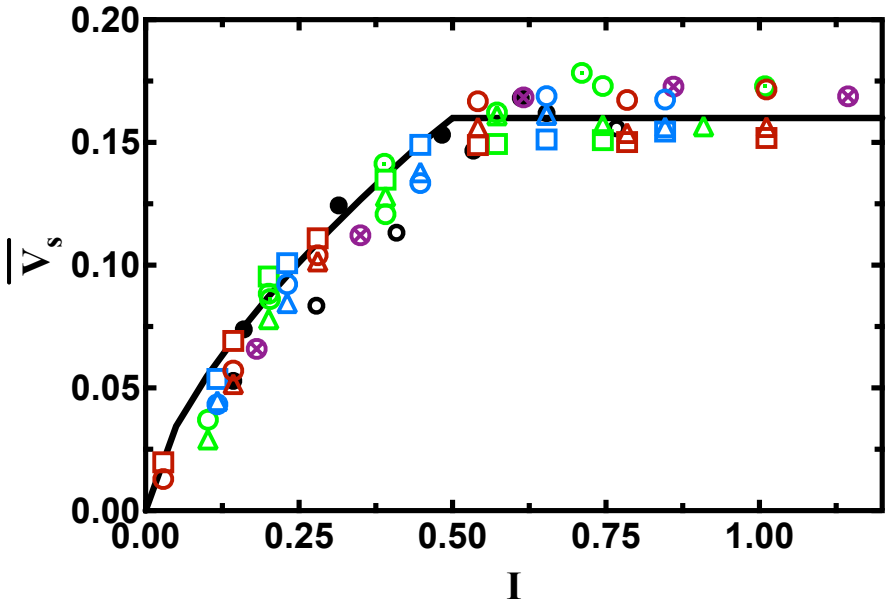

- Segregation saturation occurs at same location as frictional saturation
- Model based on coordination number fits **all** data

Testing Size Segregation

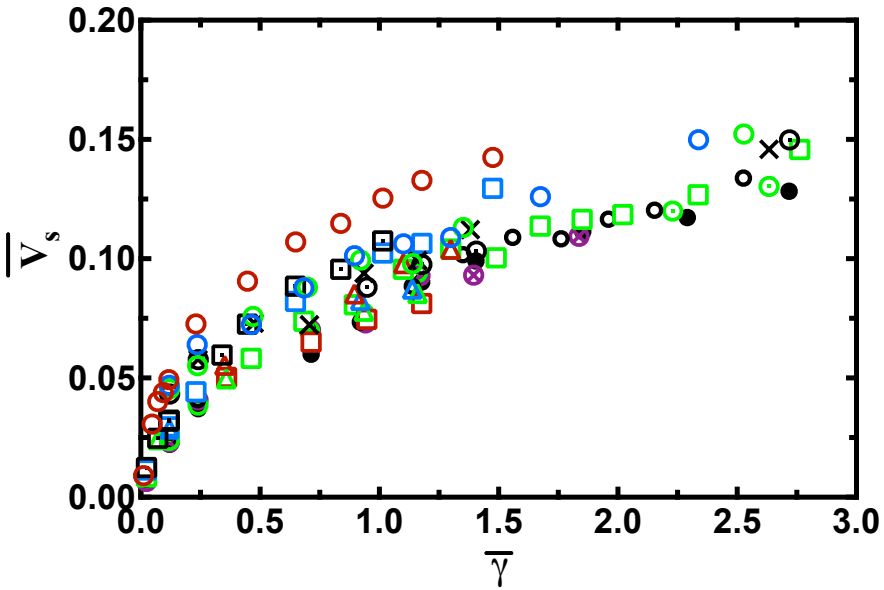

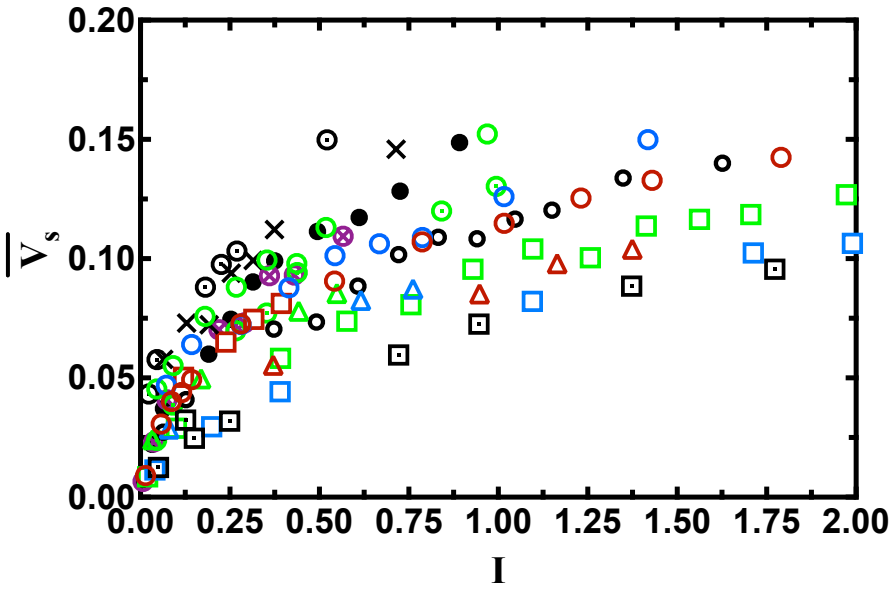

- Results are not linear with *either* $\dot{\gamma}$ or I
- Clearly we are missing some other rheological effect ...

A **Proposed** Approach for Shape Segregation

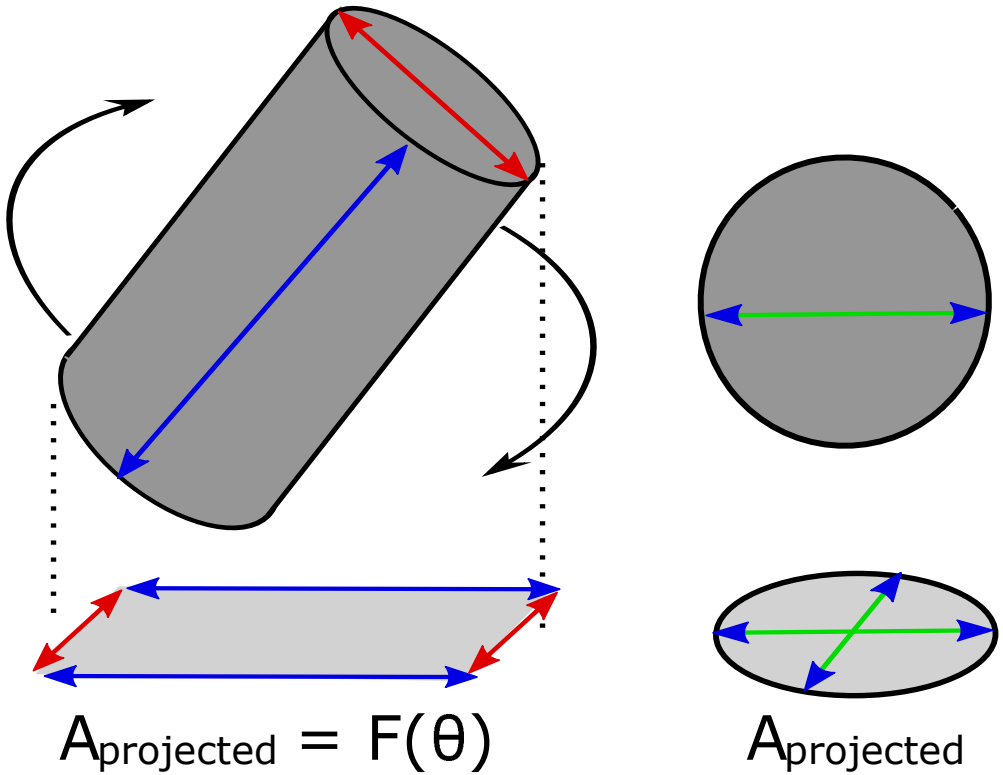

- If particles are able to freely rotate:

$$A_{eff} = A_{avg_\theta}$$

- Use this approach to predict segregation direction

Preliminary Work on Shape Segregation

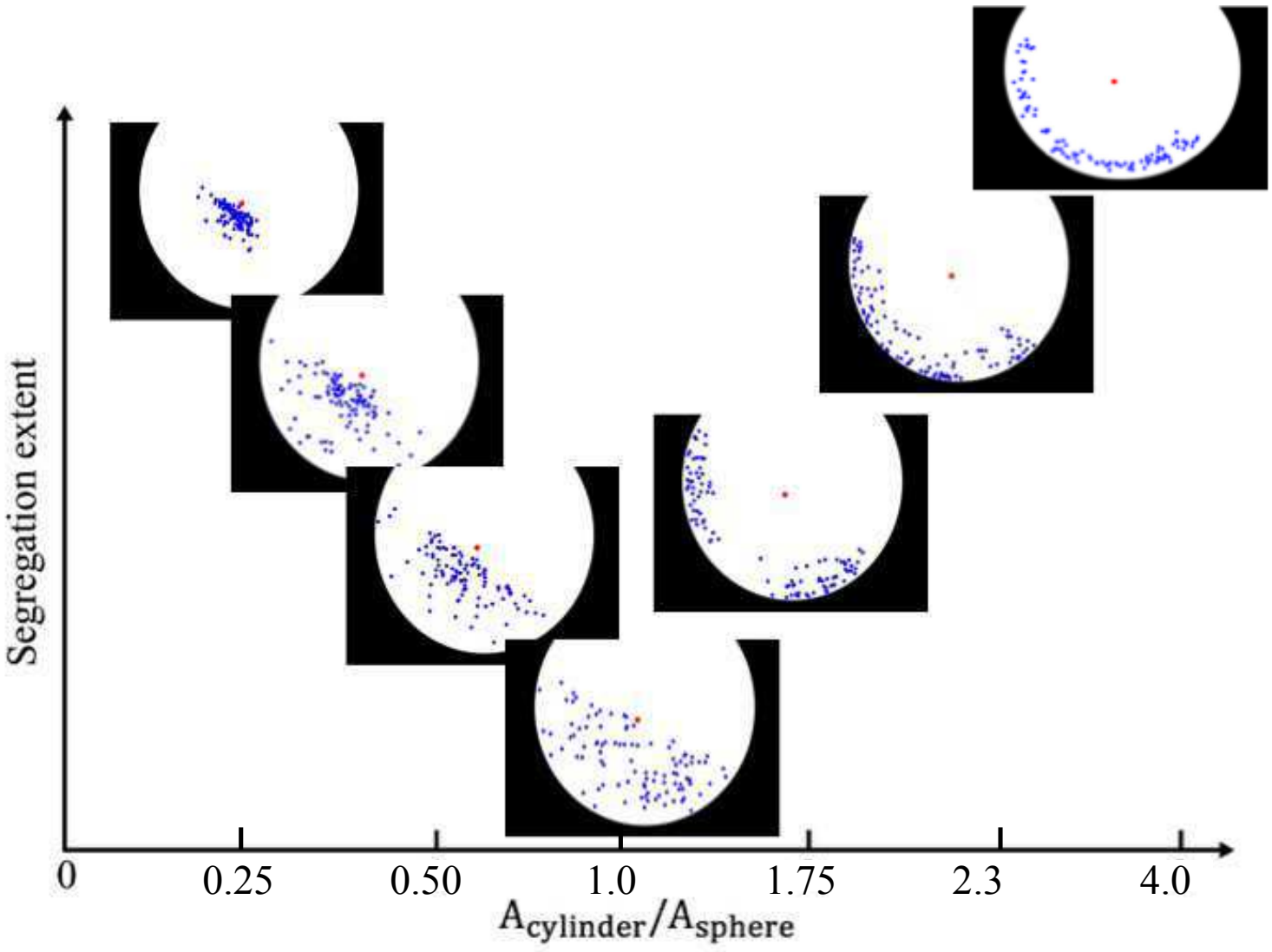

A **Proposed** Cohesive Density Segregation Model

- Force balance on particle **with cohesion**

$$0 = F_w - F_b - F_c + F_d$$

where F_c is the total cohesive force (new!)

- Taking a single heavy (H) particle in a "sea" of light (L)

$$0 = m_H g - m_L g - z F_c + c\pi\eta d_p v_{seg}$$

where z is the average coordination number (number of cohesive interactions)

- Solving for v_{seg}

$$v_{seg} = -\frac{W_L}{c\pi d_p \eta}\frac{(W_H - W_L - zF_c)}{W_L}$$

so v_{seg} will be linear with $\frac{(W_H - W_L - zF_c)}{W_L}$

Proposed Segregation Model (cont.)

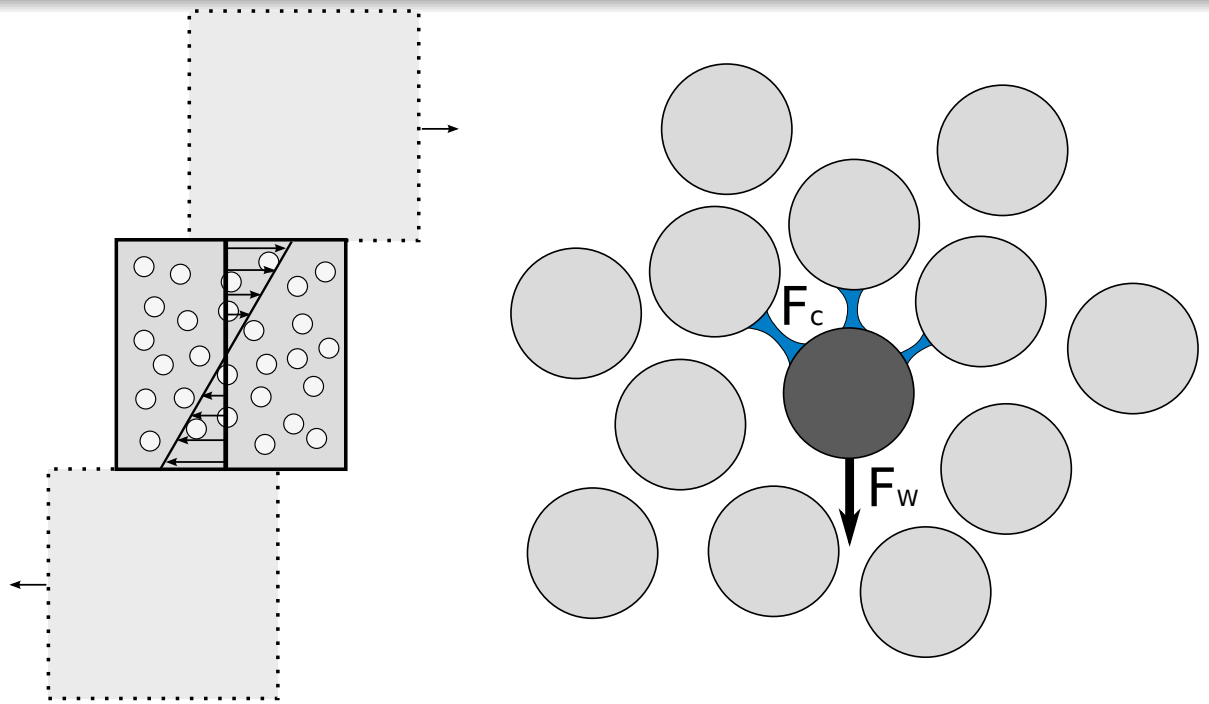

- Lees-Edwards bc eliminate need for "viscosity" (stays constant)
- Liquid bridges chosen as model cohesion

Testing Cohesive Density Rate Model (computationally)

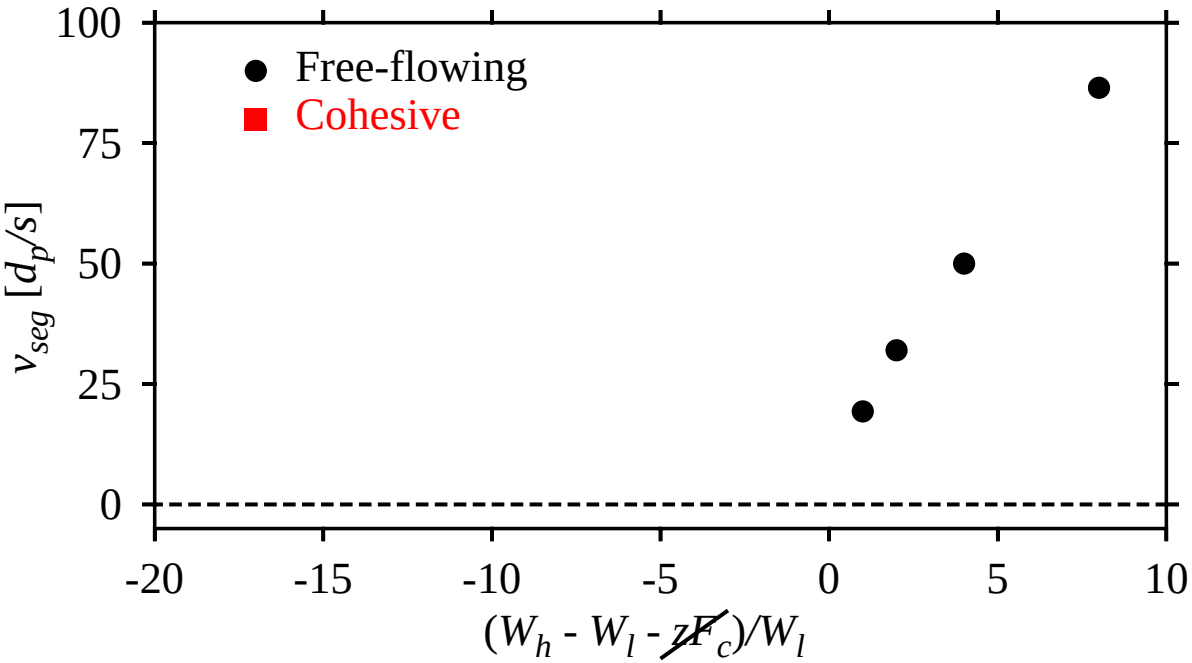

- Proposed model matches "new" model well
- Neither have been tested experimentally
- Segregation control framework should (finally) make this "easy"!

Testing Cohesive Density Rate Model (computationally)

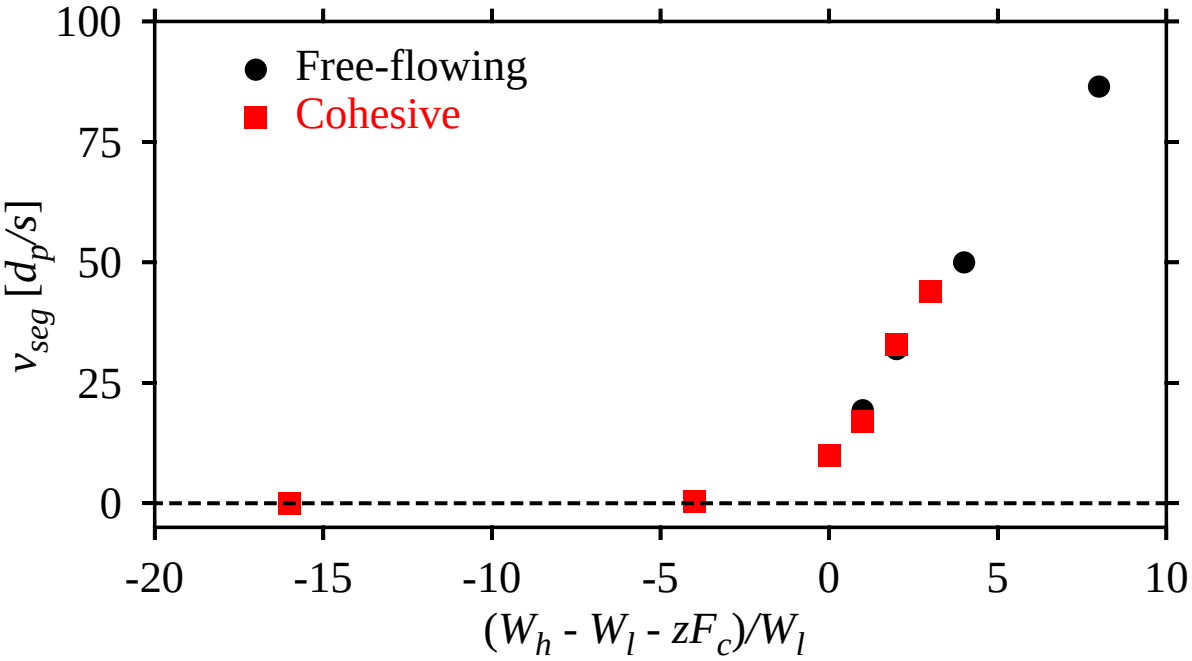

- Proposed model matches "new" model well
- Neither have been tested experimentally
- Segregation control framework should (finally) make this "easy"!

Testing Cohesive Density Rate Model (computationally)

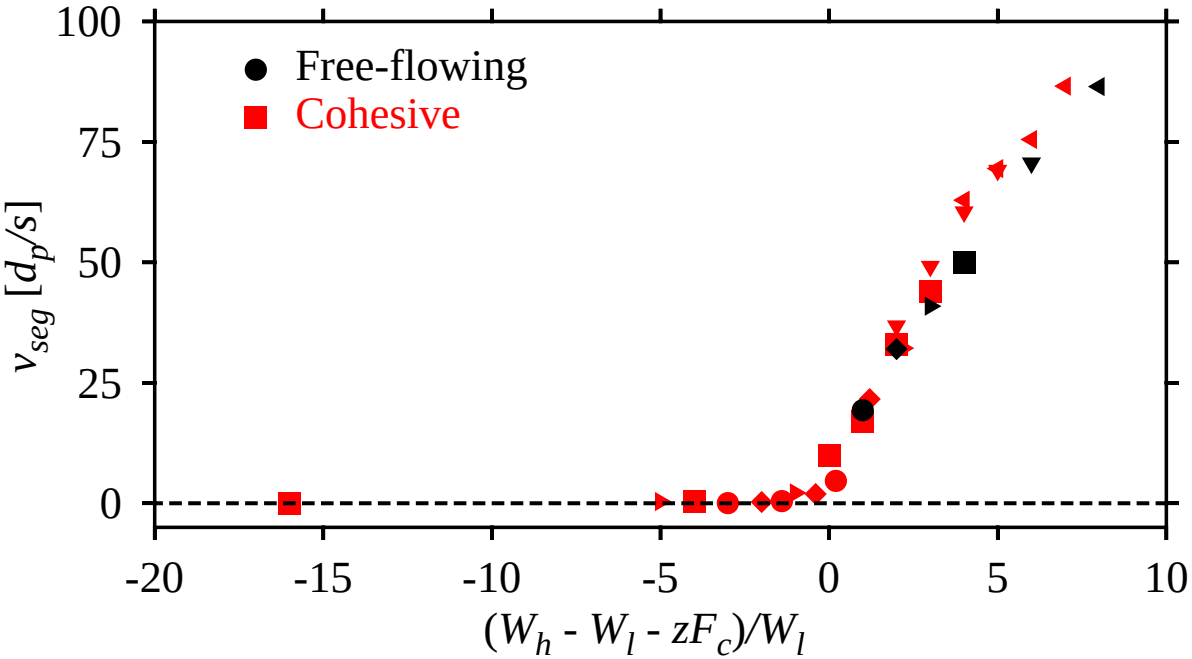

- Proposed model matches "new" model well
- Neither have been tested experimentally
- Segregation control framework should (finally) make this "easy"!

An "Easy" Set of Cohesion Experiments

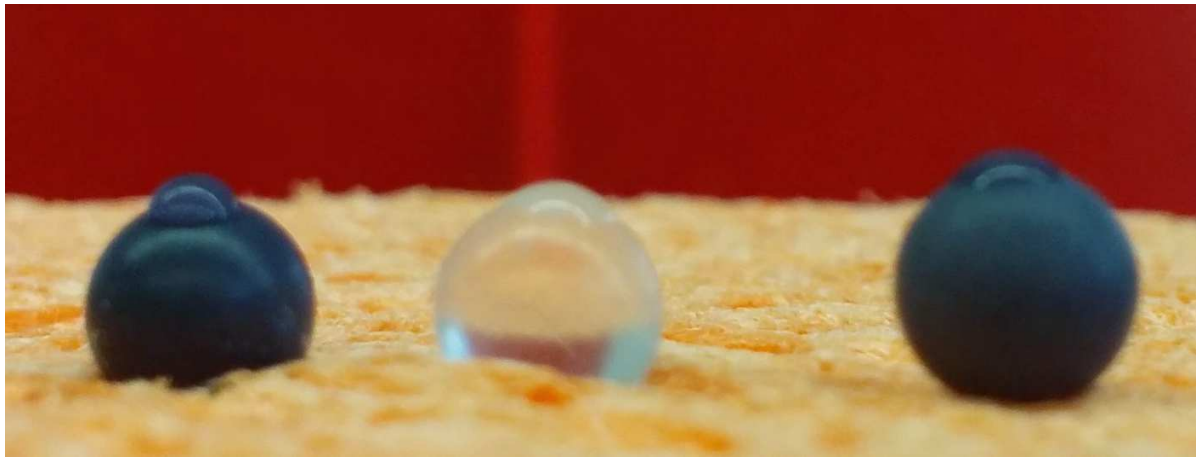

- Changing density → changing wetting
- Use TEOS to build a "silica skin"
- Further surface modification allows additional control

A Holistic Approach for the Model-based Control of Crystal Size, Shape and Purity in Integrated Batch and Continuous Crystallization - Wet Milling Systems

Botond Szilagyi, Zoltan K. Nagy

Purdue University, Davidson School of Chemical Engineering, West Lafayette

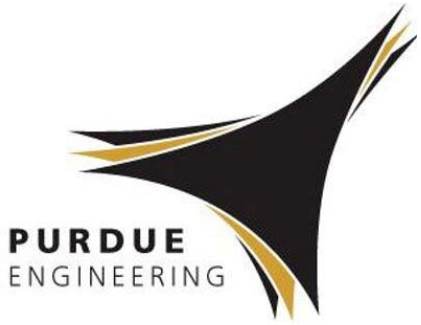

Outline

Project objectives

… and main deliverables

Current realizations

… and how our recent results fit into the project objectives

Short term plans

… how are we planning to extend the research

Project objectives

Well-known phrases

- Key unit operation in fine chemical industry
- Its driving force is the supersaturation
- Crystal size and shape: increasing significance
- Distribution - size, shape
- ***Control!***

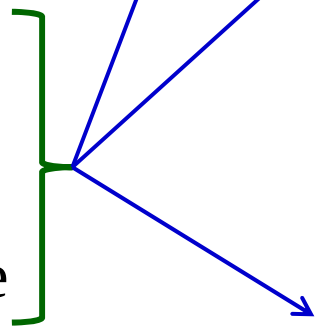

Physical properties

- Porosity
- Specific surface
- Mechanical properties

Product quality

- Adsorption properties
- Polymorphism
- Dissolution rate

Technological issues

- Efficiency, batch time
- Filterability, drying

Project objectives

- Many technology and economic drivers
- 70% of all solid products & 90% of APIs involve a crystallization step
- Control of crystalline properties (CSD, shape, polymorphic form, purity, etc.) important
  - Product effectiveness (dissolution, bio-availability, tablet stability)
  - Efficient downstream operations (filtration, drying)

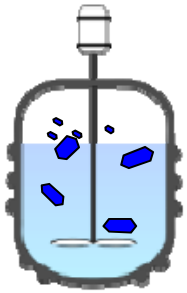

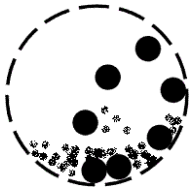

Crystallization → Downstream processes → Final product

Control of crystal properties is critical for product functionality and operational efficiency

Project objectives

- **Crystal size, shape and purity is often not achieved in the crystallizer →innovative technologies are required. We propose the followings:**

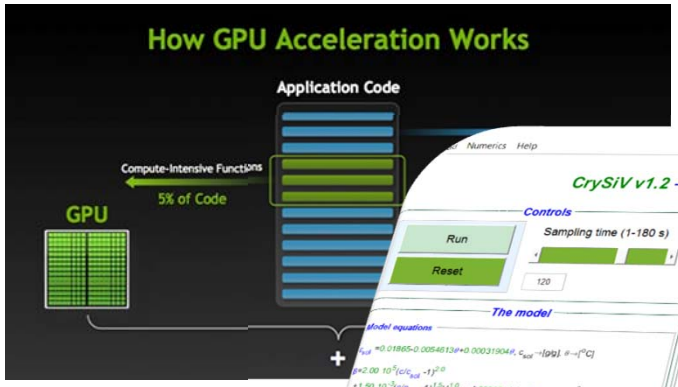

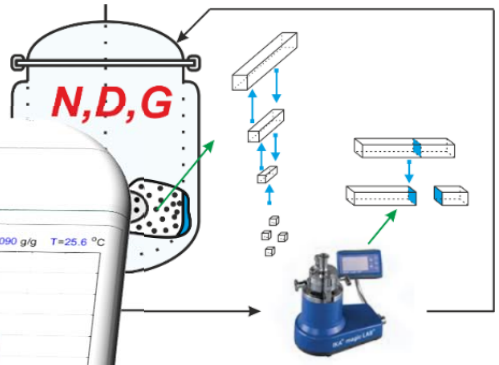

Advanced compute… improved si…

…d recirculation … flexibility

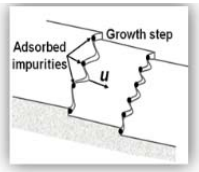

Competitive adsorption model:

- **multi-component (*j*)**
- **multi-site (*k*)**
- **multi-face (*i*)**

Projection based 2D CSD →CLD, ARD transformation with real time applicability potential for MPC applications

Application additives for purity control and manipulation of crystallization kinetics

The CrySiV

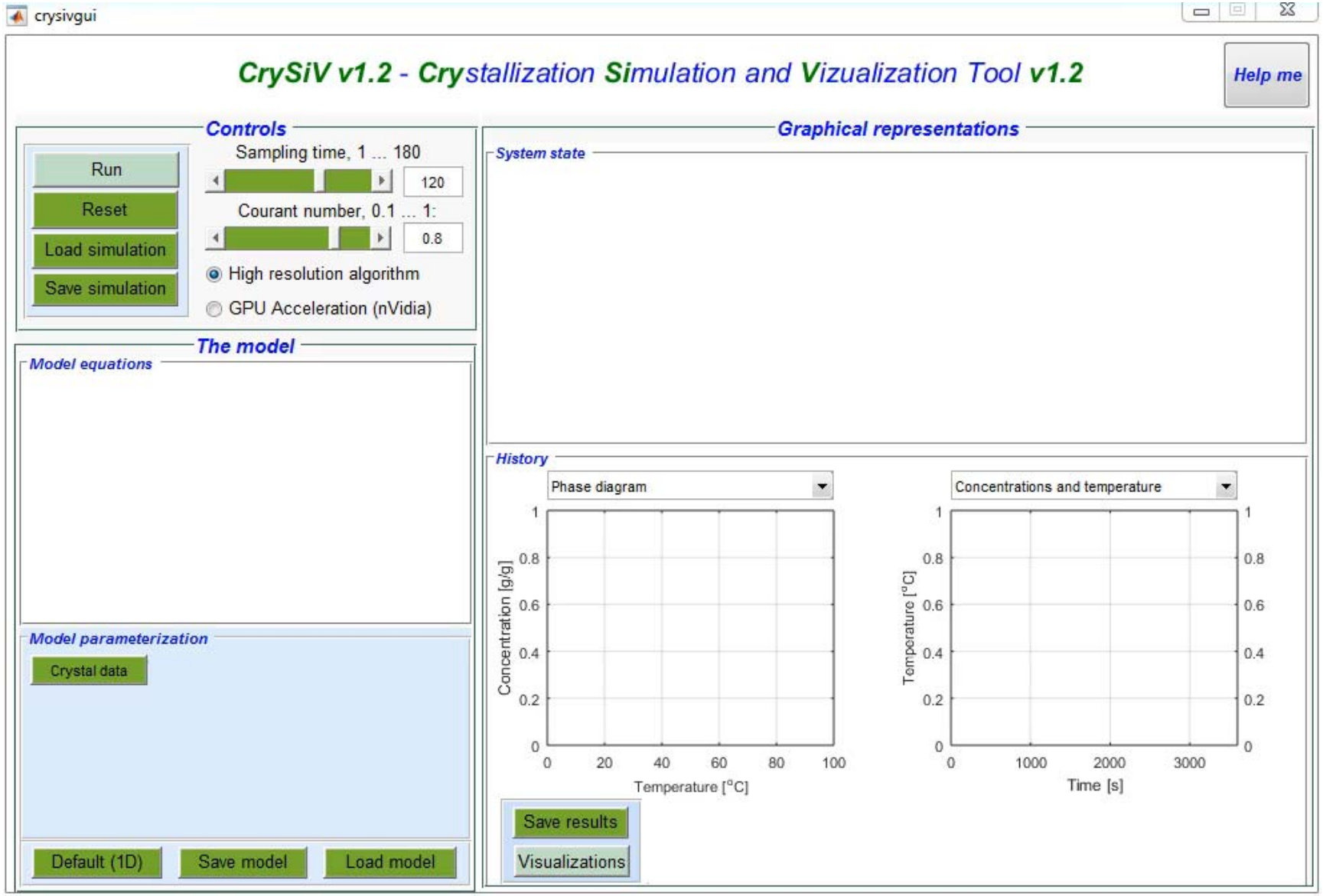
crysivgui
CrySiV v1.2 - Crystallization Simulation and Vizualization Tool v1.2
Help me
Controls
Run
Reset
Load simulation
Save simulation
Sampling time, 1 ... 180
120
Courant number, 0.1 ... 1:
0.8
High resolution algorithm
GPU Acceleration (nVidia)
The model
Model equations
Model parameterization
Crystal data
Default (1D)
Save model
Load model
Graphical representations
System state
History
Phase diagram
Concentration [g/g]
Temperature [°C]
Concentrations and temperature
Temperature [°C]
Time [s]
Save results
Visualizations

Project objectives

Main deliverables:

- A model based optimization case study for the optimization of temperature and GM concentration profiles for crystal shape control using 2D/nD PBM models (3 year)
- Efficient nD PBM-based simulation, optimization and control platform (1 year)
- FBRM-PVM sensor model for quantitative use of these technologies (1 year)
- Simulation case studies for NMPC of CSD and shape for the batch and continuous integrated crystallization-wet milling processes (2 year)
- First proof-of-concept experimental implementation of a full 2D PBM based real-time predictive control of CSD and shape during crystallization in impure media, using in line real-time image analysis (3 year)
- High quality journal and conference publications (2-3 year)

Recent results – GPU accelerated PBM solution

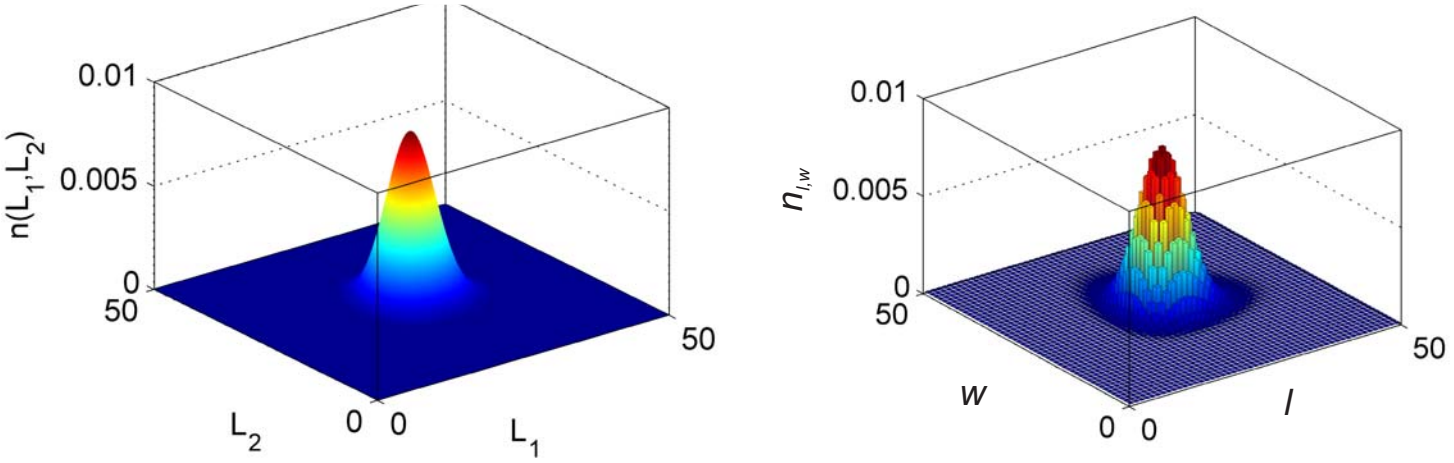

Figure. Finite Volume discretization of a continuous 2D CSD

Mass balance
Energy balance

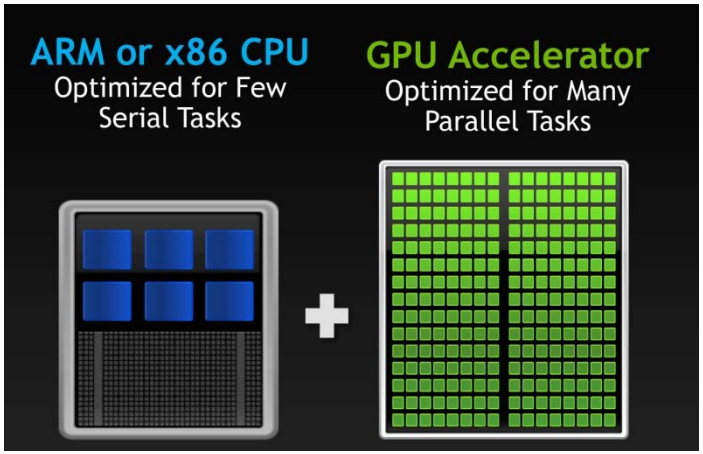

Integrals
Population balance

Figure. Typical CPU and GPU architecture

Recent results – GPU accelerated PBM solution

- **2D batch PBM with primary and secondary nucleation and growth,**
- **Full-discrete HR-FVM solution**

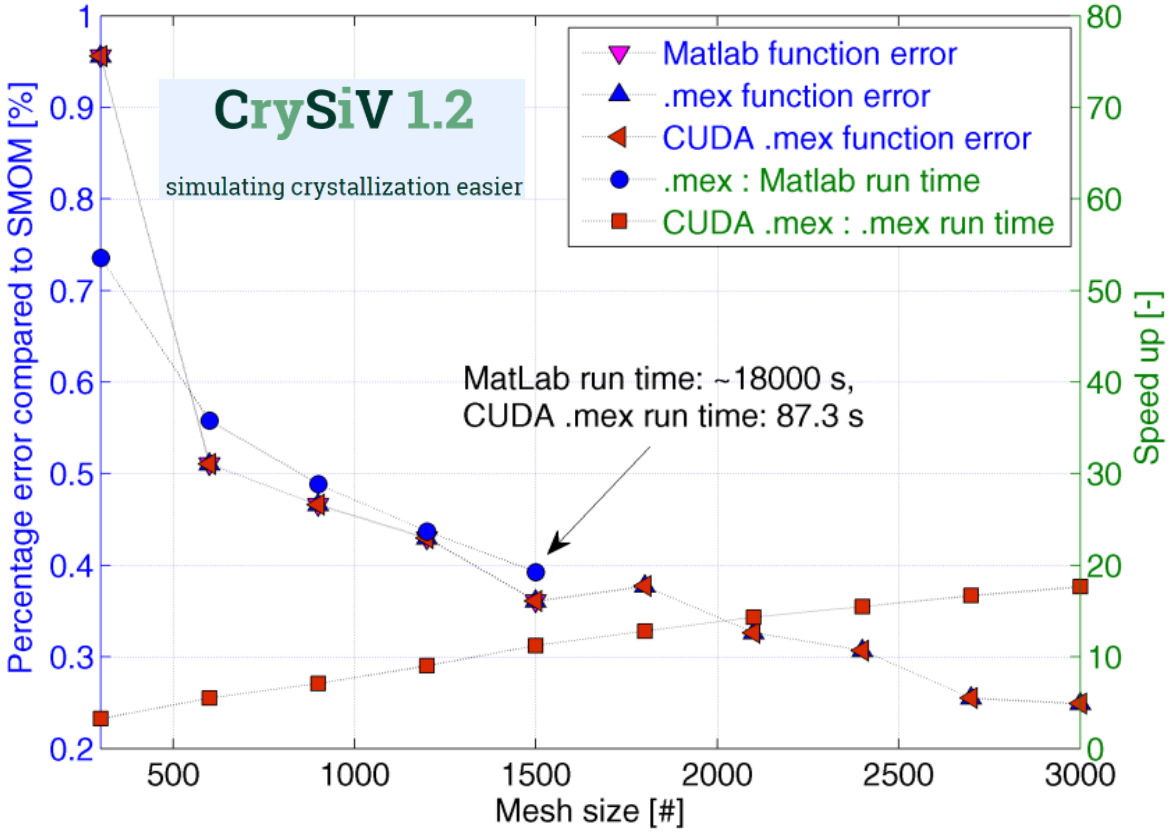

Figure. Comparing the MatLab, serial C (.mex) and hybrid CPU-GPU (CUDA .mex) accuracy and compute performance. Low cost CPU and GPU (~100 USD both)

Recent results – soft-sensor for 2D crystals

- **CLD calculation of a single crystal: map all possible "chord length" of all possible 2D projections (pre-computed)**

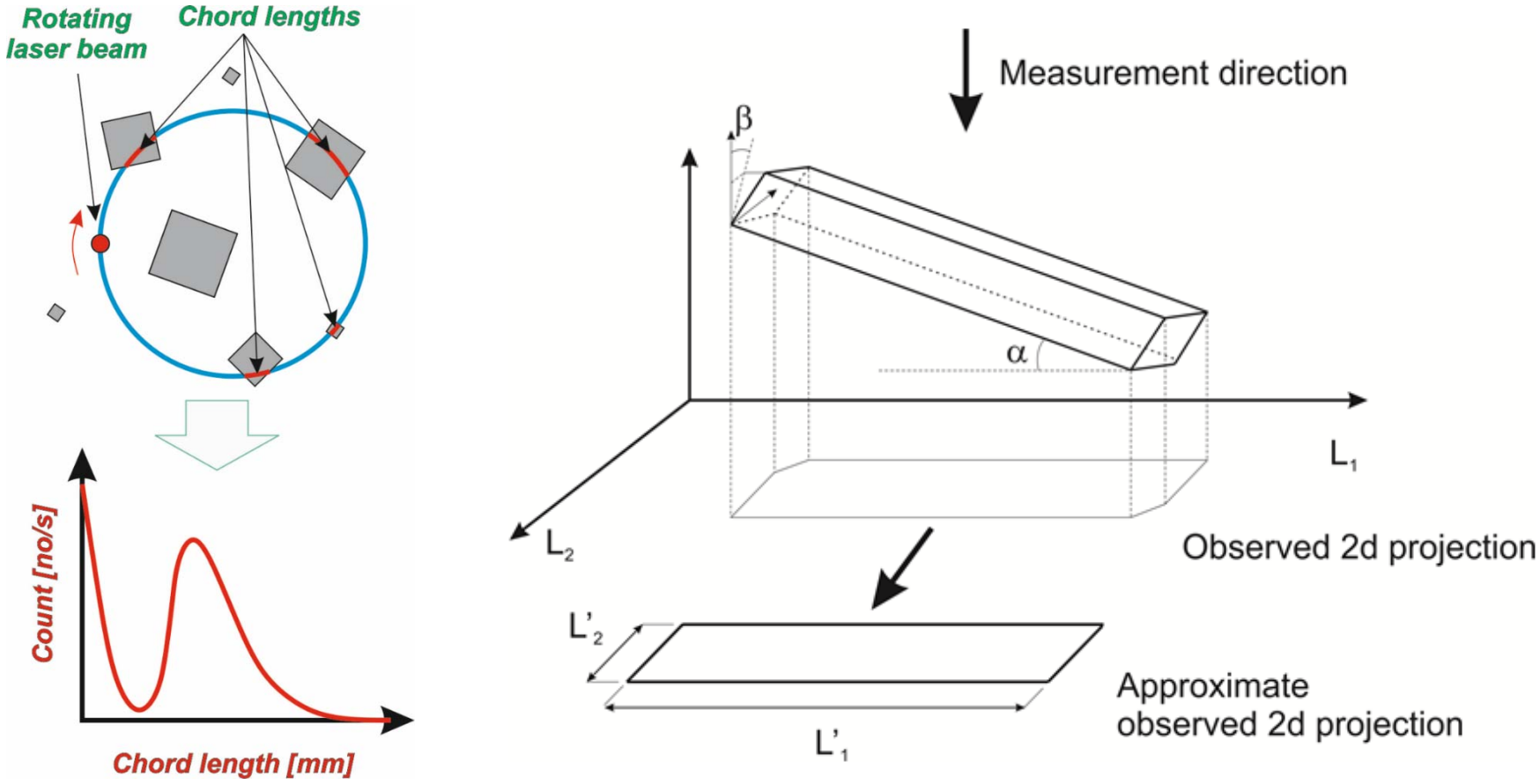

Figure. Working principle of the FBRM and the CLD simulation of a single crystal

Recent results – soft-sensor for 2D crystals

- **CLD calculation of a crystals population: weighted sum of individual crystals CLDs (real time calculation)**

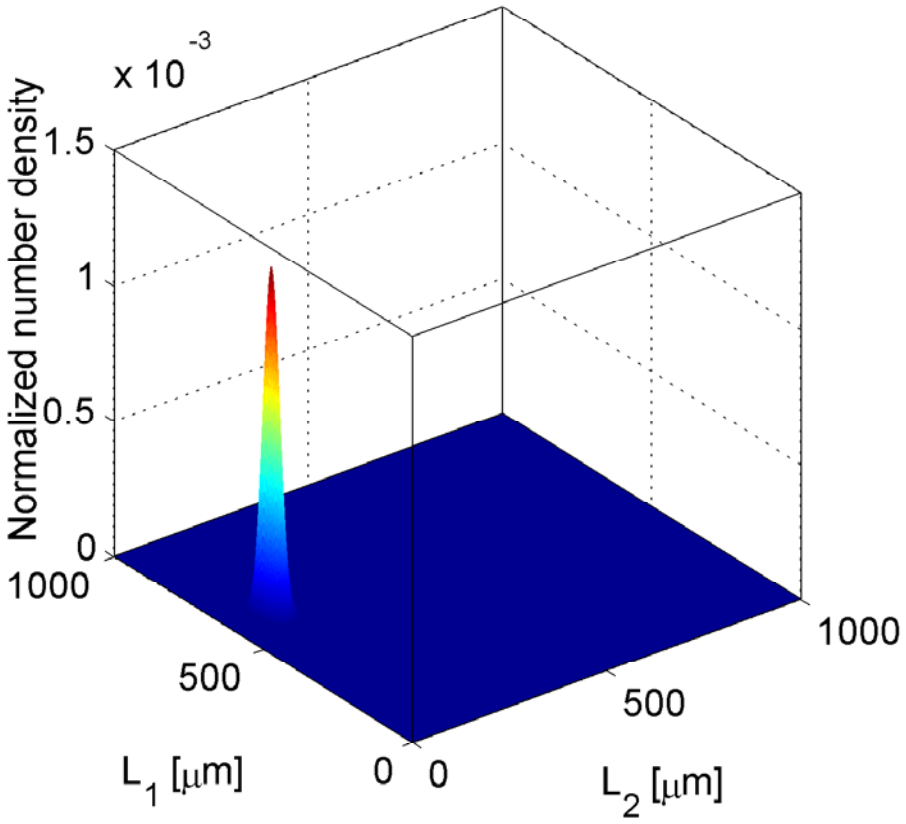

Figure. Typical 2D CSD of high aspect ratio crystals

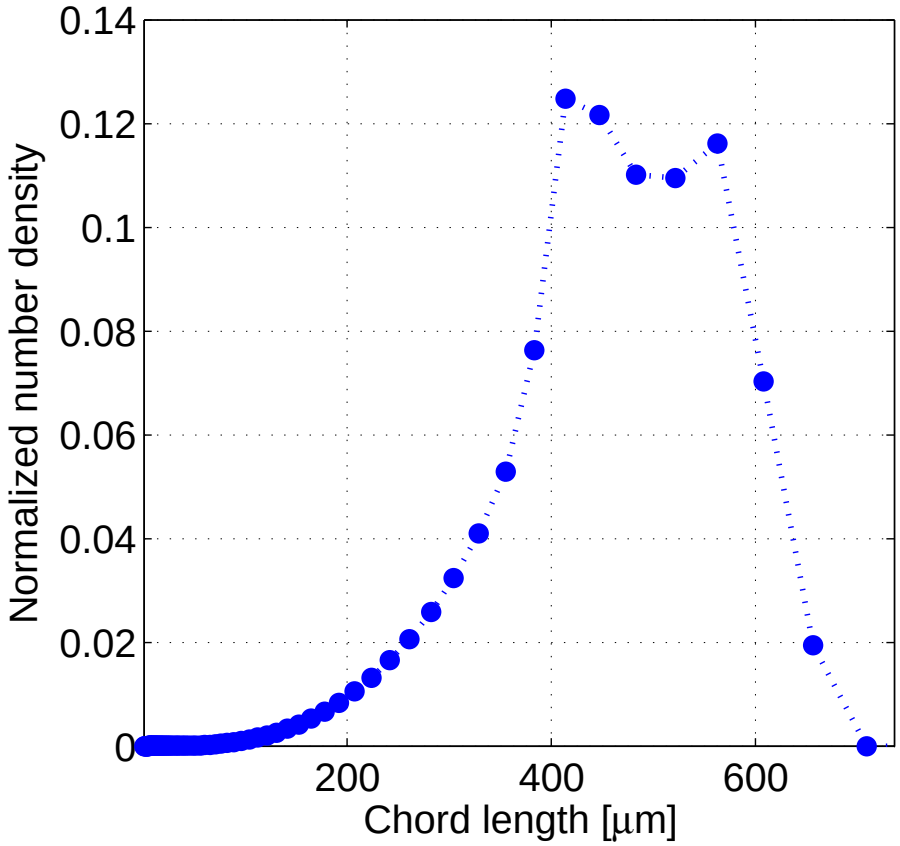

Figure. The simulated (bimodal) CLD

Recent results – soft-sensor for 2D crystals

- **ARD calculation of a crystals population: weighted sum of individual crystals ARDs (real time calculation)**

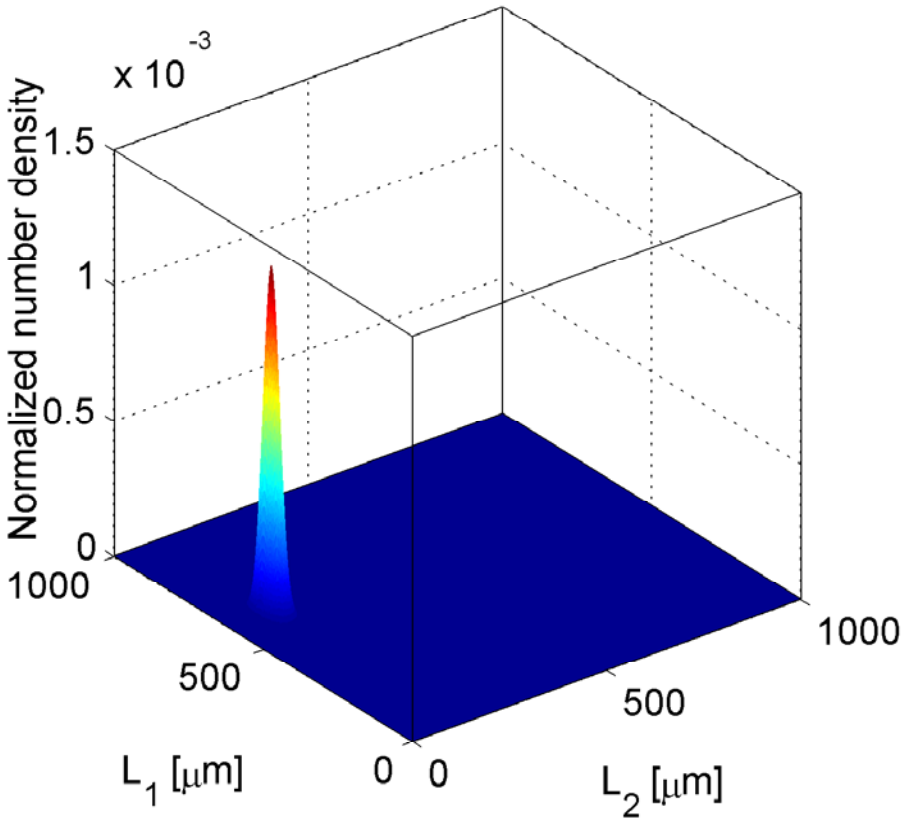

Figure. Typical 2D CSD of high aspect ratio crystals

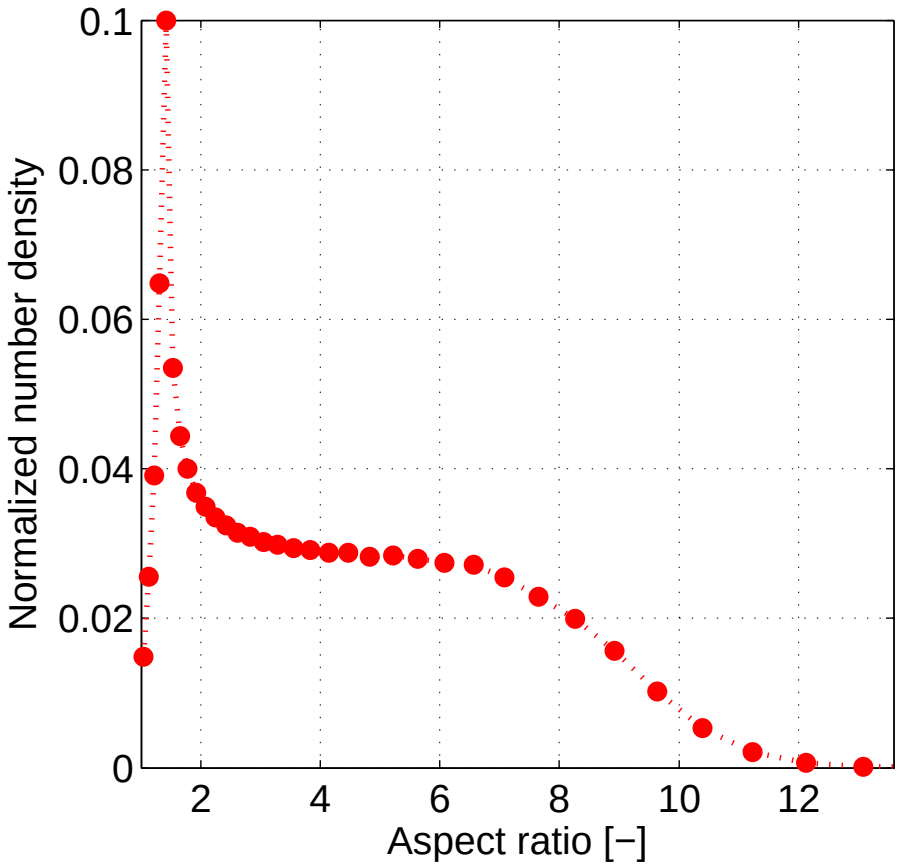

Figure. The simulated ARD

Recent results – soft-sensor for 2D crystals

- KDP crystallization kinetics
- Using the PVM soft-sensor (projection based ARD estimation, then mean AR calculation)

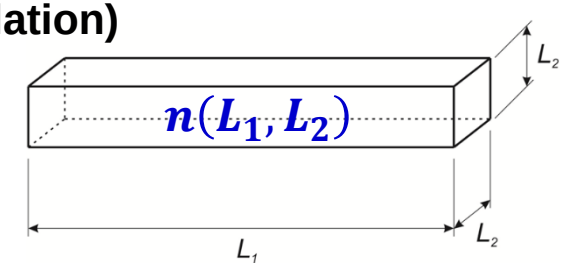

$$AR_{ideal} = \frac{\langle L_1 \rangle}{\langle L_2 \rangle}; \quad AR_{corr} = \frac{\langle L_1 \rangle + \langle L_2 \rangle}{2\langle L_2 \rangle}$$

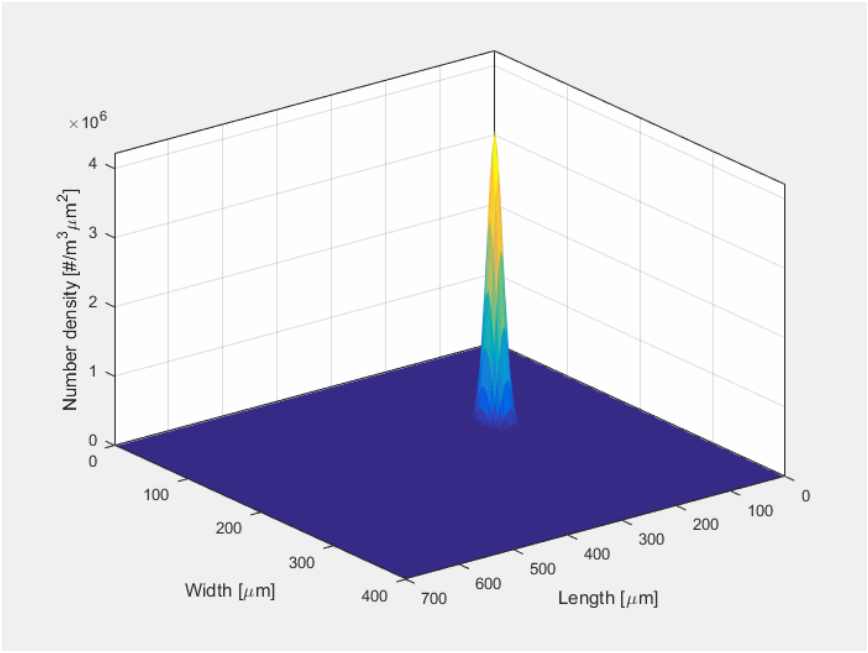

Animation. CSD evolution of fast cooling batch

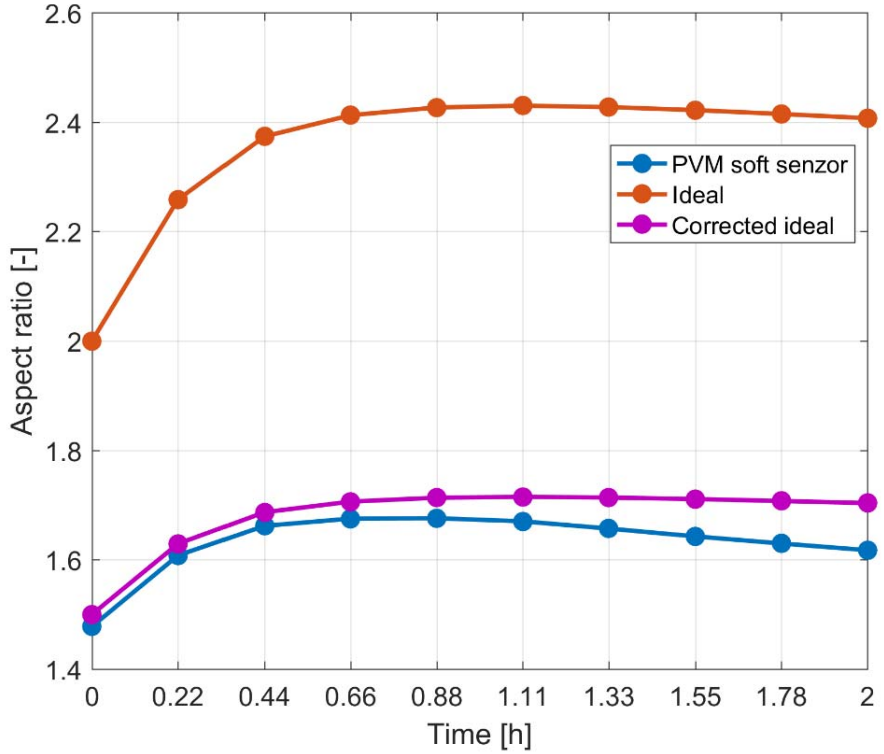

Figure. AR evolution of fast cooling batch

Recent results: crystallizer-wet mill optimization

- **Crystallizer: crystallization only**
  - **- primary nucleation**
  - **- growth**
  - **- dissolution**

  } **oABA**
- **Wet-mill: breakage only**
  - **- fragmentation**
  - **- attrition**
- **Temperature: controller, no energy balance written up**

Un-seeded system!!

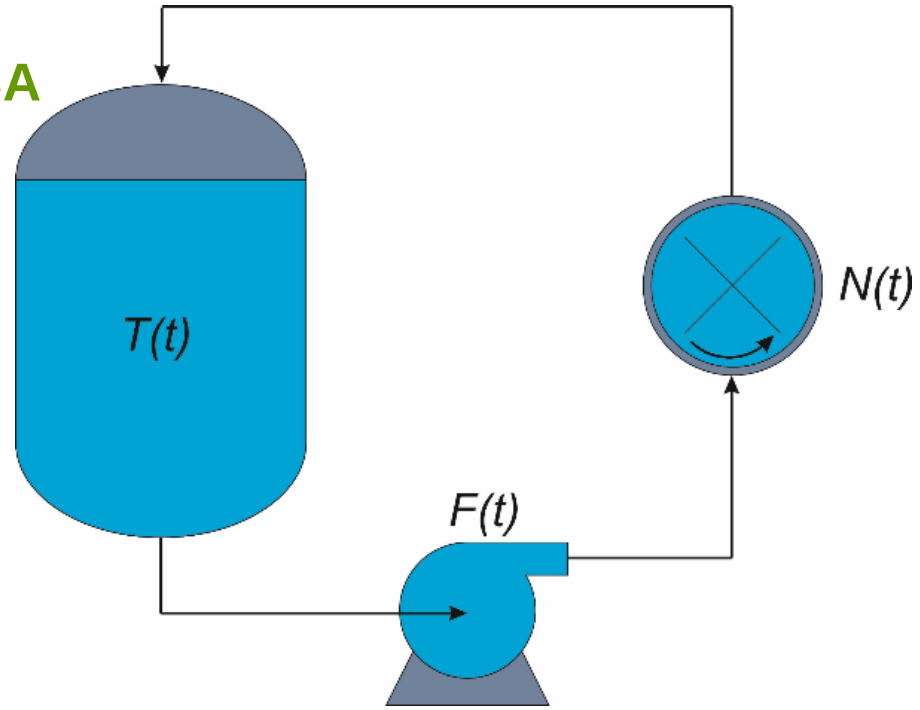

Figure. Scheme of the integrated crystallizer-wet mill system with the most important design parameters

Recent results: crystallizer-wet mill optimization

- **Selection function**

$$S(\lambda) = \lambda^{\beta} \frac{\rho_{imp} l_{imp}^2 h_{imp} N_{imp}^3 d_{imp}^5}{768\pi}$$

- **Breakage function (fragmentation)**

$$b_f(L|\lambda) = k_f \frac{1}{\sqrt{2\pi\sigma_f^2}} exp\left[-\frac{(L-\lambda/2)^2}{2\sigma_f^2}\right]$$

- **Breakage function (attrition)**

$$b_a(L|\lambda) = k_a \delta(L - L_n)$$

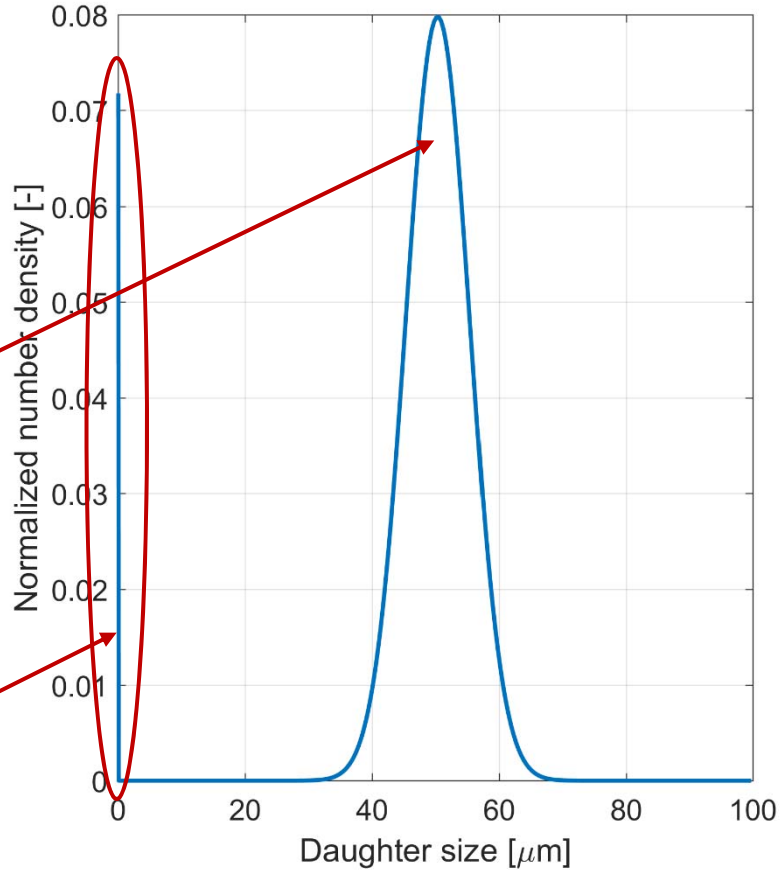

Figure. Daughter distribution of a λ = 100 μm crystal

Recent results: crystallizer-wet mill optimization

- **Grid: discretization of space and time: fine vs. coarse**

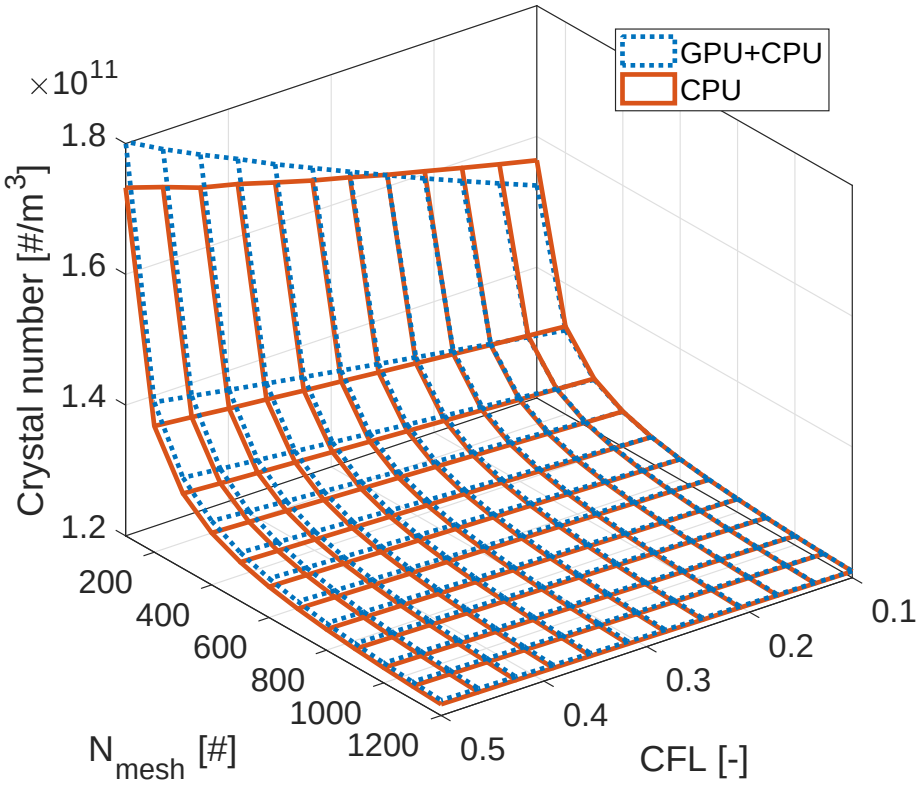

Figure. Predicted crystal number as a function of time and space discretization. **Differences in coarse domain due to different numerical implementation.**

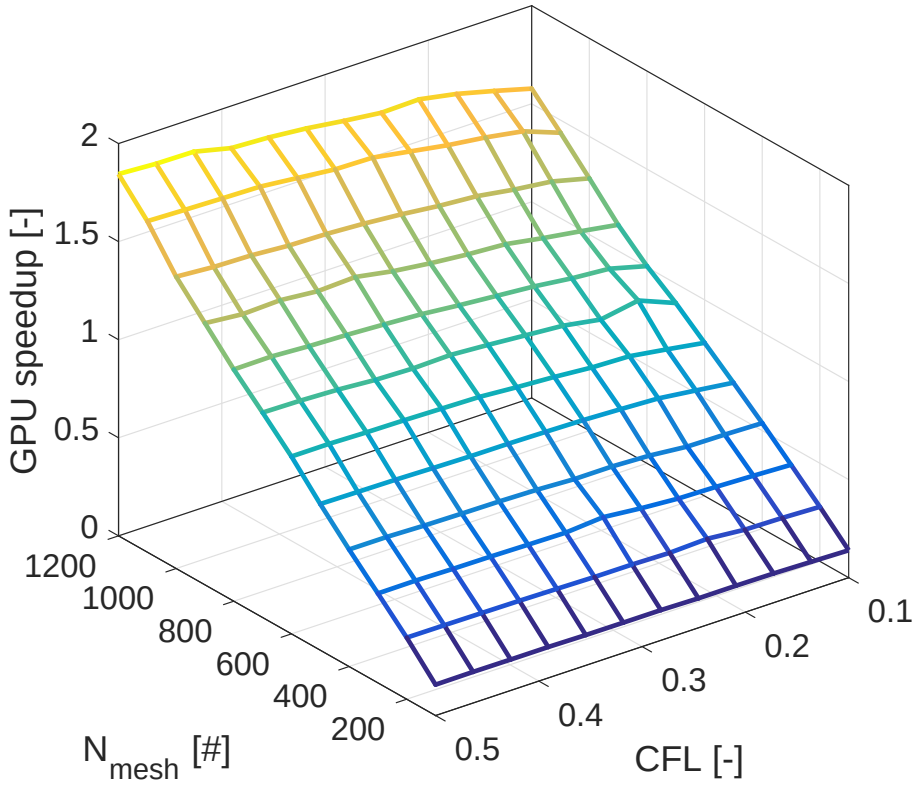

Figure. Solution time by the CPU and CPU+GPU solvers

Recent results: crystallizer-wet mill optimization

- ***System optimization with multiple objectives***

$$SSE(\boldsymbol{T},\boldsymbol{F},\boldsymbol{N}) = \underbrace{\int_0^{L_{max}} \left[\frac{|n_T(L,t_{end}) - n(L,t_{end})| + \varepsilon}{n_T(L,t_{end}) + \varepsilon}\right]^2 dL}_{\text{Target CSD realization}} + \underbrace{\int_0^{t_{end}} \left[w_1\left(\frac{dT}{dt}\right)^2 + w_2\left(\frac{dF}{dt}\right)^2 + w_3\left(\frac{dN}{dt}\right)^2\right] dt}_{\text{Smooth profiles}} + \underbrace{\int_0^{t_{end}} [w_4 F + w_5 N]\, dt}_{\text{Minimal flow and stirring}} + T_{fin} \stackrel{!}{=} min$$

- ***Numerical details***

Table. Potential accuracy domains

Accuracy	CFL	Mesh size	Compute platform
Low	CFL > 0.5	N < 500	CPU only
Moderate	CFL > 0.3 CFL < 0.5	N > 500 N < 1000	CPU + GPU; CPU only
High	CFL < 0.3	N > 1000	CPU+GPU

Table. Multi-level optimization

Level	Accuracy	Algorithm	Points/profile
1	Low	Interior-point	15-25
2	Moderate	Interior-point	20-30
3	High	SQP	25-35

Recent results: crystallizer-wet mill optimization

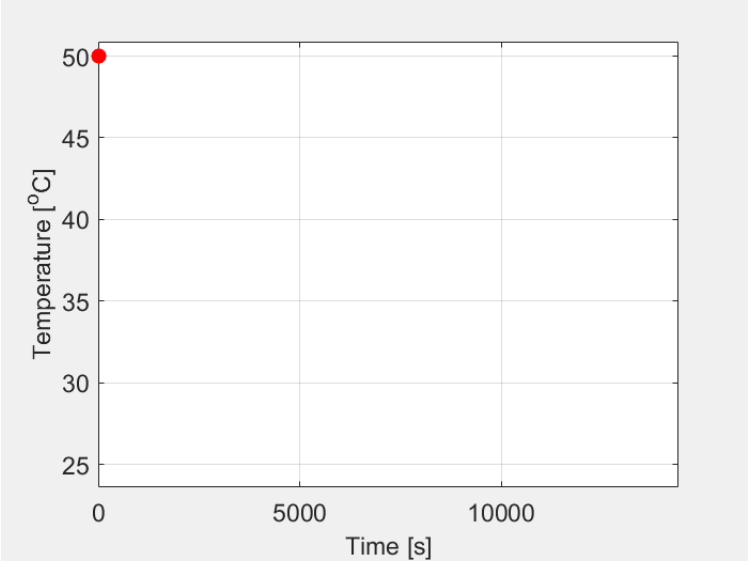

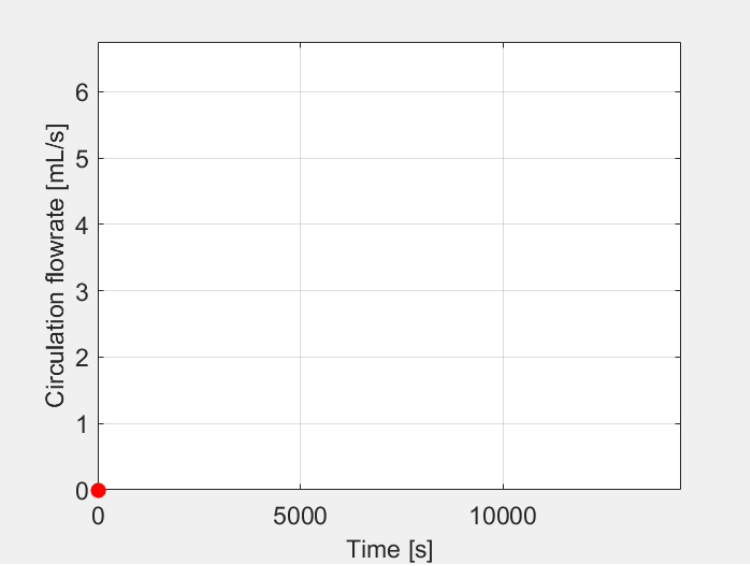

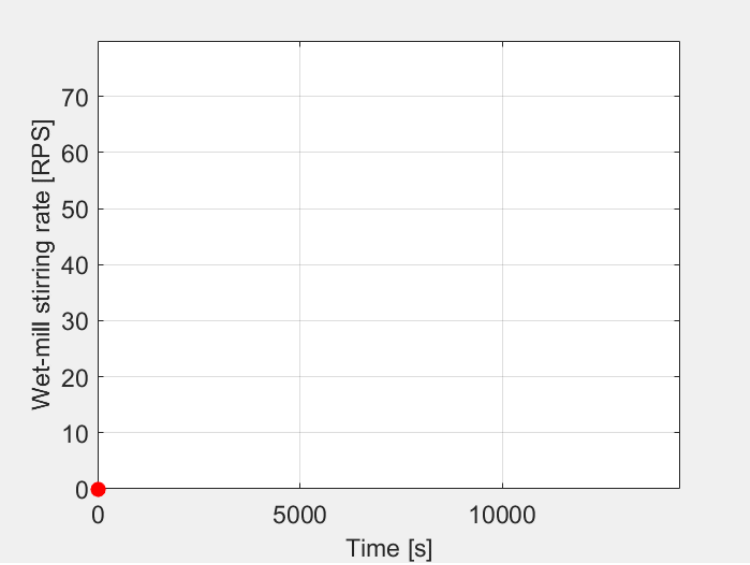

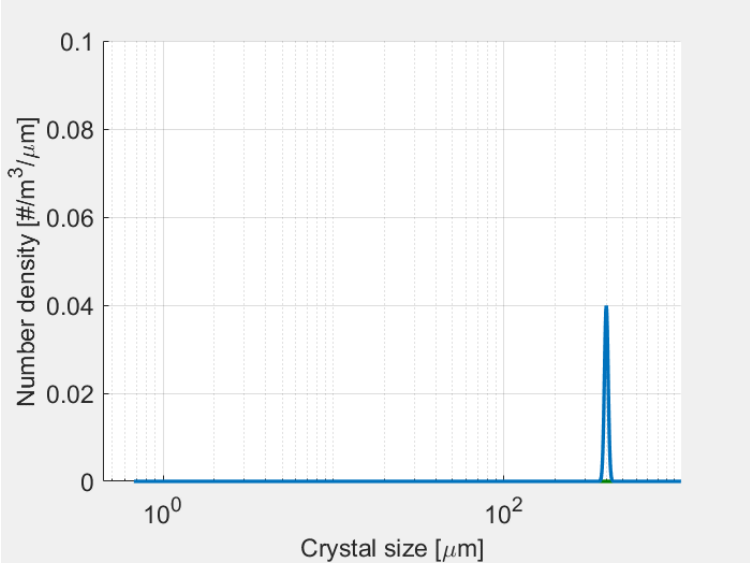

Short term plans (~1 year)

CLD of sphere/cylinder shape

… since these are typical 1D and 2D shapes

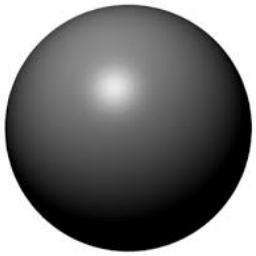

ANN for soft-sensor simulation

… to avoid the large matrixes for the pre-calculated individual CLD's

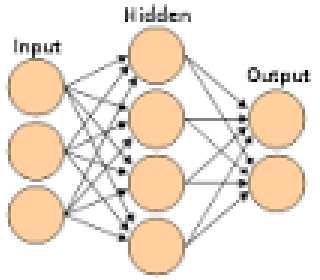

1D MPC implementation

… with high accuracy full PBM, for ascorbic acid

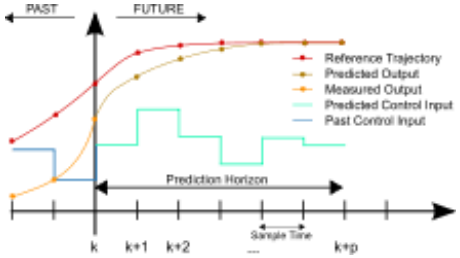

2D wet-mill model

… CPU only and CPU+GPU implementation

A Holistic Approach for the Model-based Control of Crystal Size, Shape and Purity in Integrated Batch and Continuous Crystallization - Wet Milling Systems

Botond Szilagyi, Zoltan K. Nagy

Purdue University, Davidson School of Chemical Engineering, West Lafayette

Thank you for your attention!
Questions?

IFPRI 39th Annual General Meeting

Project Reporting:

Milling and Material Grindability

J.Y. Ooi, X.Z. Chen, L.G. Wang, J.F. Chen*, J. Sun

University of Edinburgh, UK

*Queen's University Belfast, UK

Philadelphia, June 2017

Project Overview

- Overall goal is to develop a generic methodology to characterise grindability of particulates in milling, through:
  - Understanding particle dynamics in a mill from computational modelling and experiments
  - Develop grindability measures to characterise the comminution behaviour of particulates
  - Hierarchical verification and validation leading to robust evaluation of milling performance
- Project commenced January 2013
- A 5th Year summary is presented

Multiscale Modelling of Grindability

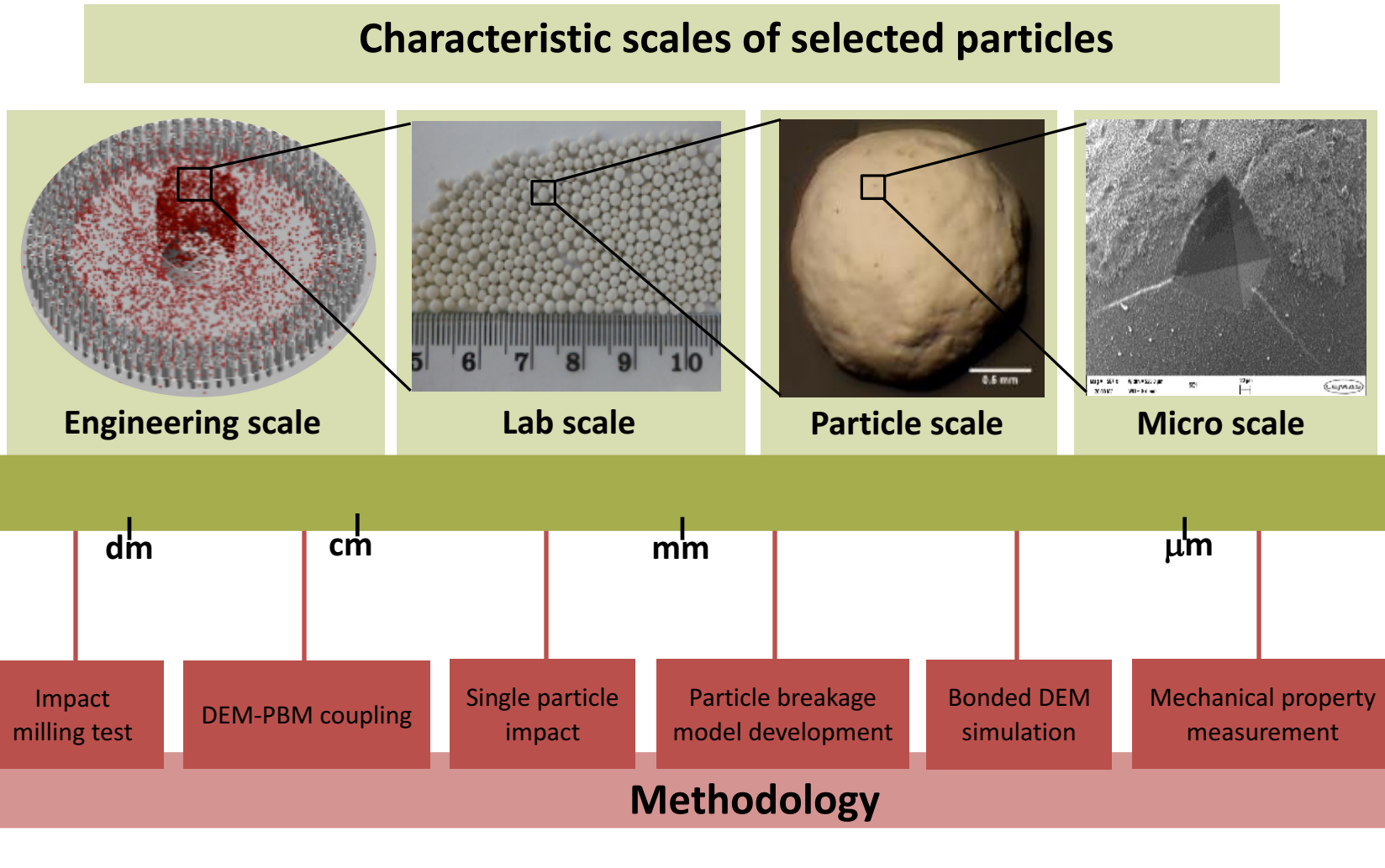

Schematic illustration of multiscale modelling of material grindability

DEM-PBM Coupling Framework

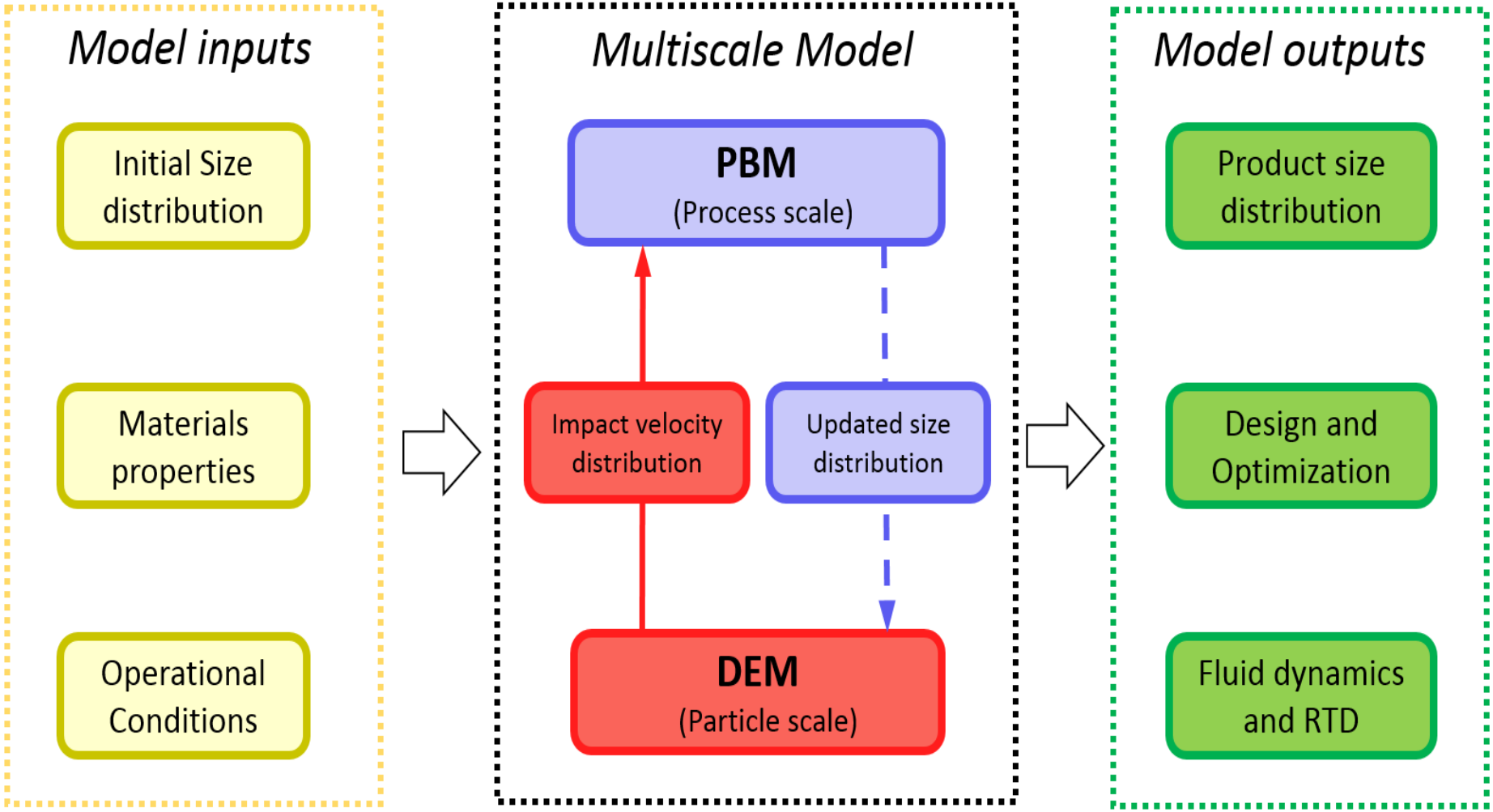

- DEM provides particle dynamics for mechanistic kernels
- PBM is empirical but provides the evolved particle size distribution

Impact Milling Tests

Alumina particles were milled under varying rotary speed and feed rate using impact pin mill UPZ 100

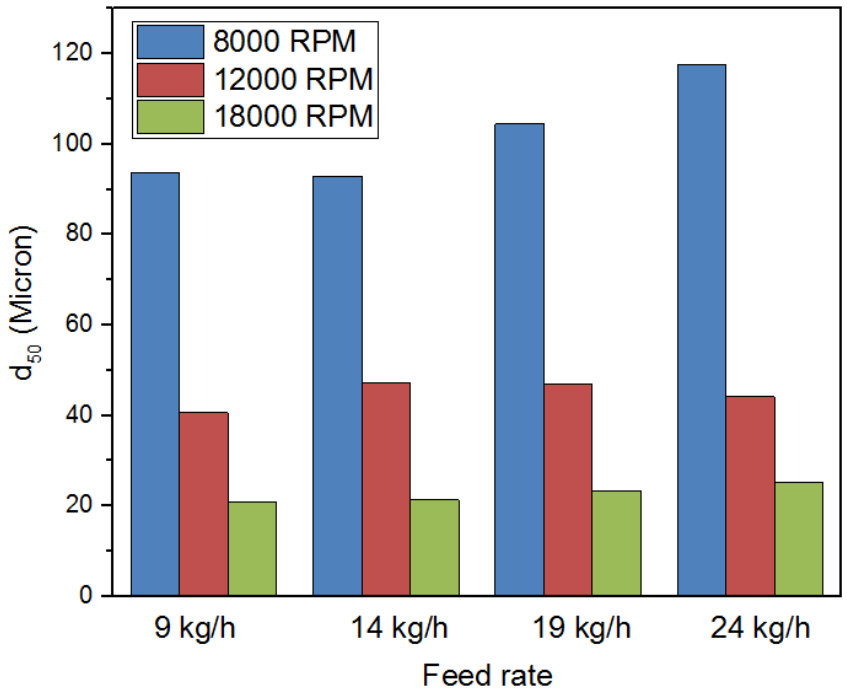

Median size d_{50} of milled alumina under varying Rotary speed and feed rate

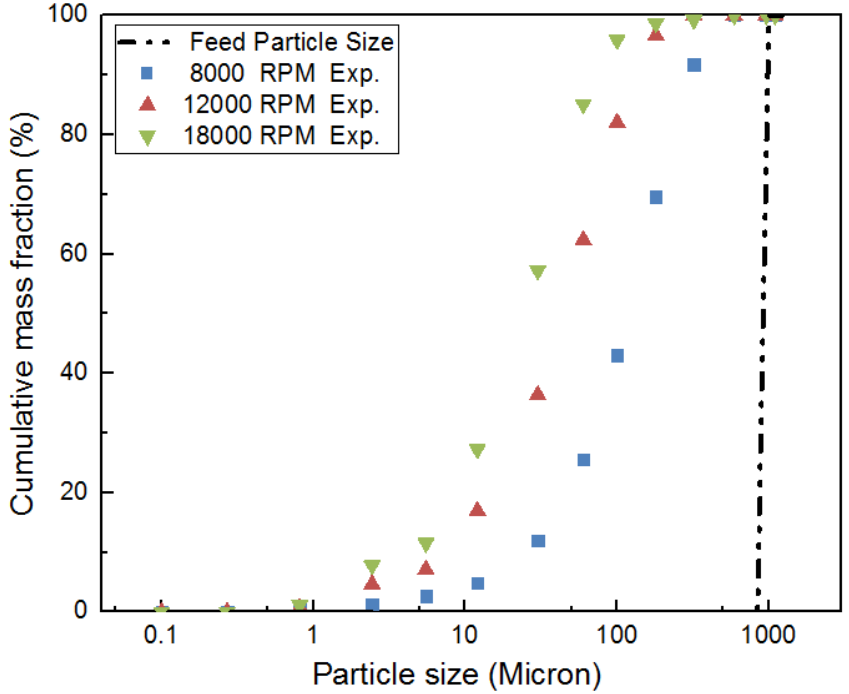

PSD of milled alumina under varying rotary speed at 24 kg/h

DEM Simulation of Impact Pin Mill

- UPZ100 mill was simulated
- Particle impact velocity extracted from DEM is employed in selection function of PBM
- Average particle velocity increases with increasing rotary speed

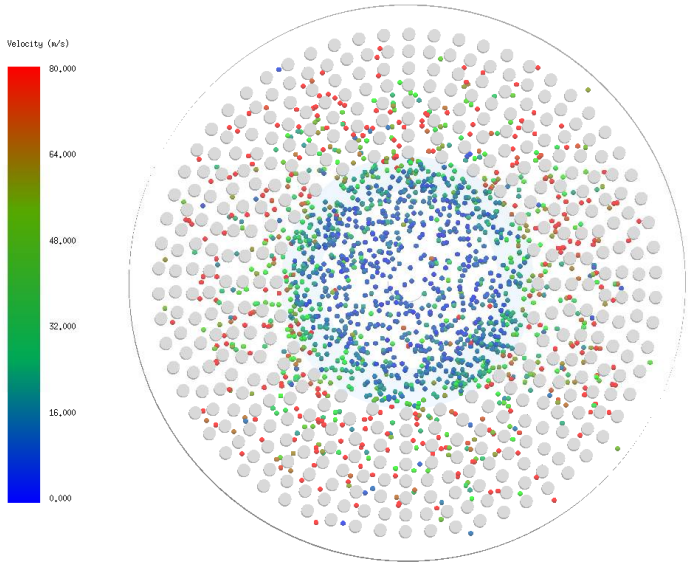

Velocity distribution of particles

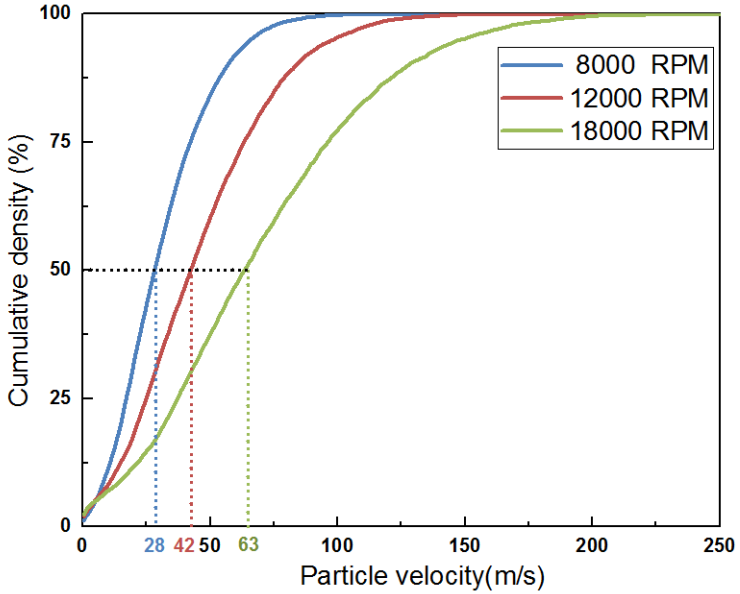

Particle velocity cumulative distribution

DEM Results: Feed Rate and Rotary Speed

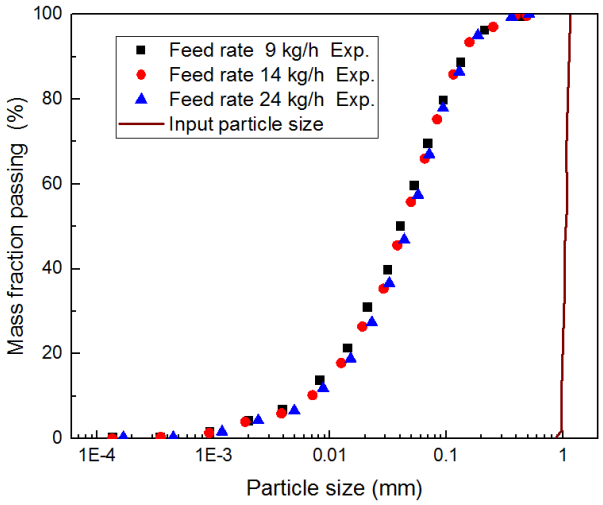

Exp. results: different feed rate under 8000RPM

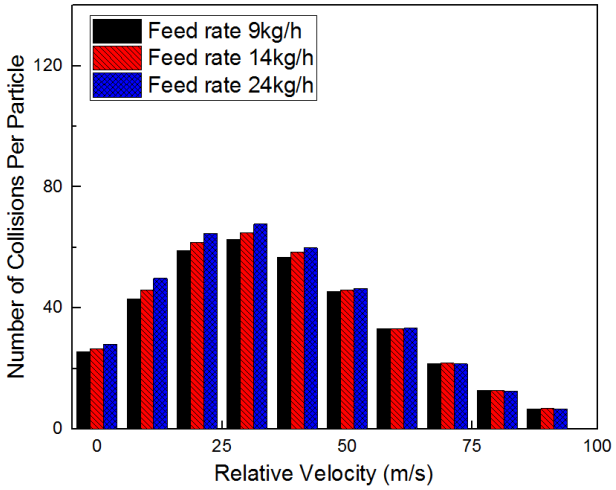

DEM simulation: different feed rates under 8000RPM

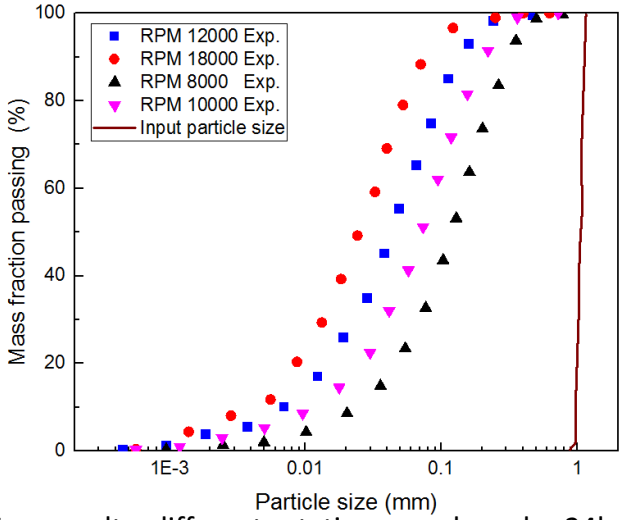

Exp. results: different rotation speeds under 24kg/h

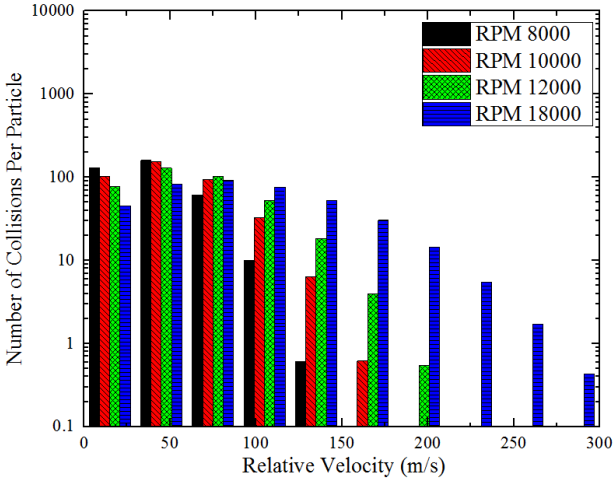

DEM simulation: different rotation speeds under 24kg/h

- DEM simulation results are consistent with experimental observations

DEM-PBM Coupling to Predict PSD

Breakage rate

$$S_M(x) = Sc_M\left[1-\exp\left(-f_{mat}x\left(W_{m,kin}-W_{m,\min}\right)\right)\right]$$

Cumulative breakage Distribution

$$B_M(x,y) = \frac{1}{2}\cdot\left(\frac{x}{y}\right)^q\cdot\left(1+\tanh\left(\frac{x-x'}{x'}\right)\right)$$

Sc_M: impact frequency $W_{m,kin}$: Impact energy

Red variables---machine dependent --- obtained from DEM simulation of mill

Blue variables---material dependent --- Estimated from 12000 RPM milling test

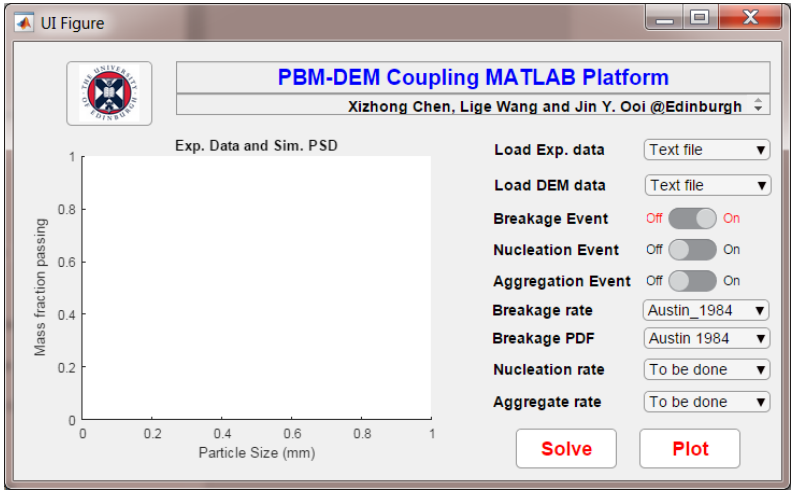

A MATLAB code is developed to solve PBM

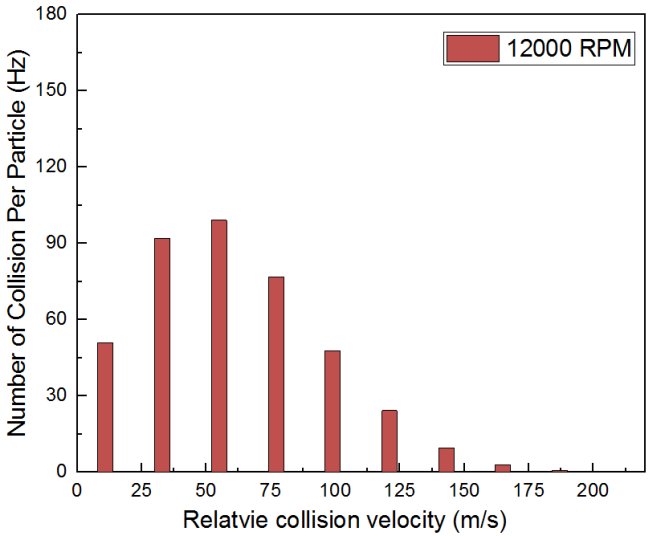

Impact velocity distribution from DEM

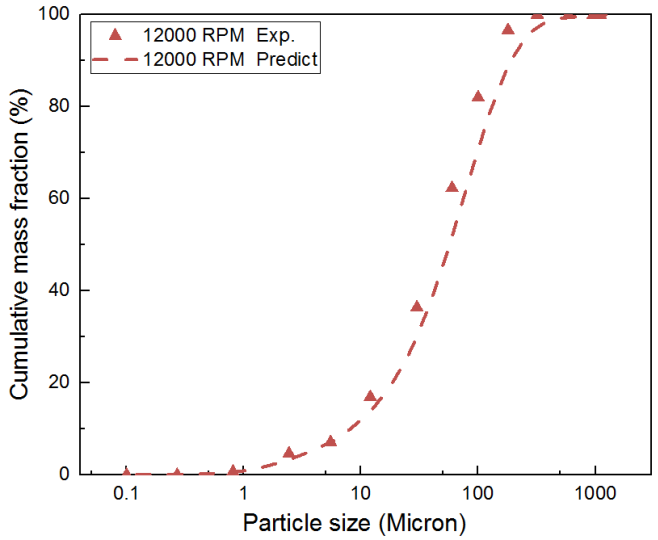

Product particle size distribution predictions

DEM-PBM Coupling to Predict PSD

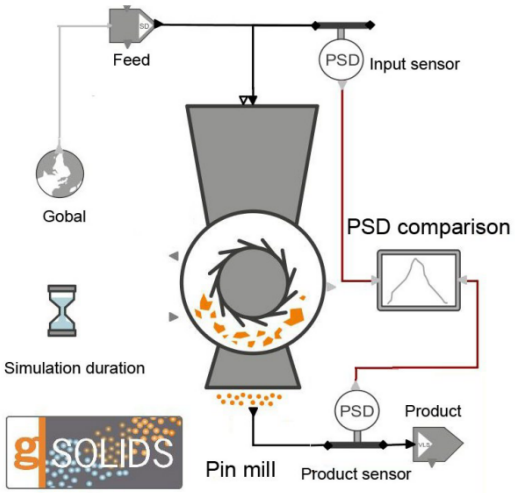

Flowsheet simulation of milling process

gSOLIDS from PSE is used to verified the MATLAB code

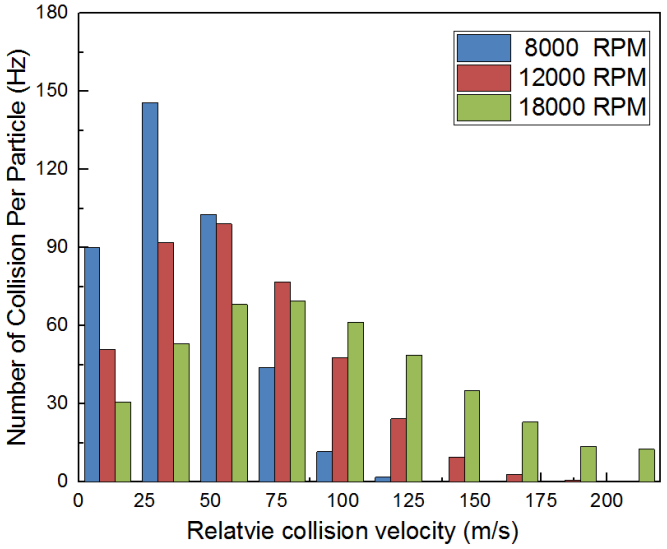

Impact velocity distribution from DEM

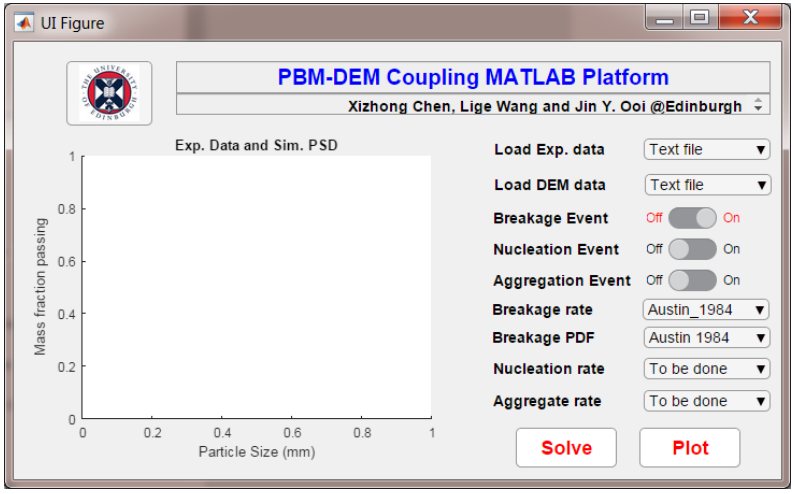

A MATLAB code is developed to solve PBM

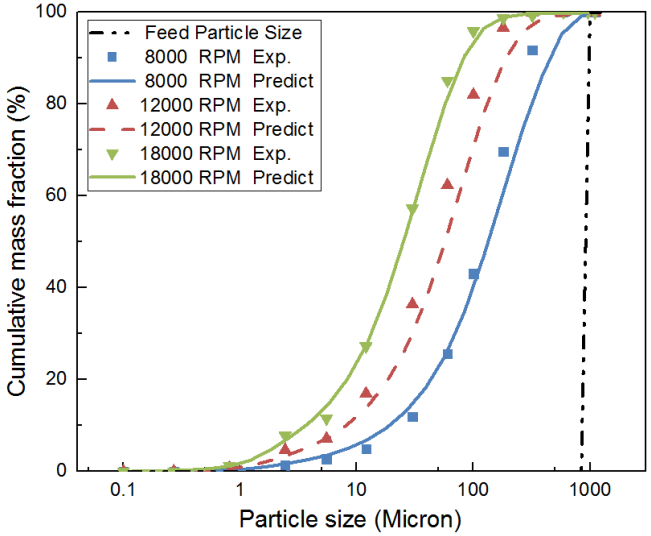

Product particle size distribution predictions

Scale-up in DEM-PBM Coupling

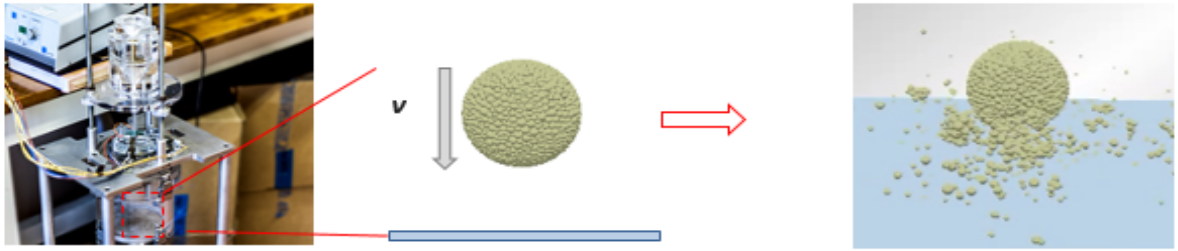

a) **Single particle breakage:** Use experiment measurement to calibrate DEM
   - **Output:** Impact energy e_k with breakage probability P_k and distribution b_{ij}

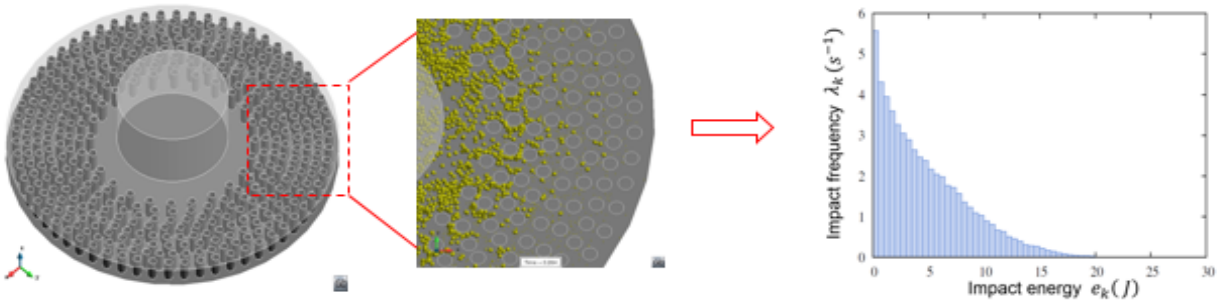

b) **Impact mill DEM simulation:** Coarse-graining the key parameters
   - **Output:** Impact frequency λ_k with energy e_k distribution

$$\frac{dM_i(t)}{dt} = -S_i M_i(t) + \sum_{j=1}^{i-1} S_j b_{ij} M_i(t), \quad S_i = \sum_{k=1}^{N} \lambda_k P_k$$

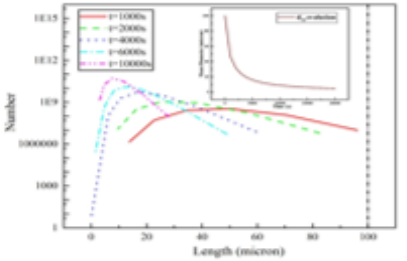

c) **PBM prediction:** Integration the outputs of the previous two processes
   - **Output:** Time evolution of particles size distribution at system scale

Single particle impact for parameters estimation

Scaling-up

Particle dynamics from DEM

procedure

DEM-PBM coupling for PSD prediction

Conclusions

- A multiscale framework of DEM-PBM coupling was proposed to predict the milling behaviour of impact pin mill
- The particle dynamics were computed from DEM and introduced in PBM for PSD prediction
- The DEM-PBM coupling shows good agreement of product size prediction with milling results

Next Step

- Improving parameter evaluation from bonded contact model
- Two-way coupling of PBM with DEM to predict the evolution of PSD in milling

Thank you!

Acknowledgement:

International Fine Particles Research Institute, IFPRI

Hosokawa Micron Ltd. UK

DEM Solution Ltd. UK

Process System Enterprise, UK

The long-term stability of colloidal gels

Destruction by gravity and hydrodynamics

Wilson Poon
Xuemao Zhou, Joost de Graaf and Michiel Hermes

EPSRC
Engineering and Physical Sciences Research Council

IFPRI

Colloidal gel

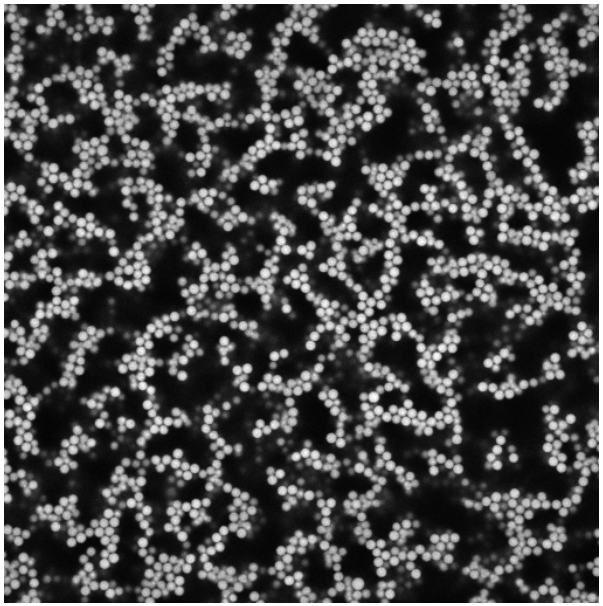

Space-spanning network of attractive particles …
… stabilises against sedimentation/creaming …
… but still has low enough yield stress to flow in use

Key control parameters

$\boxed{\frac{U_0}{k_{\mathrm{B}}T}}$

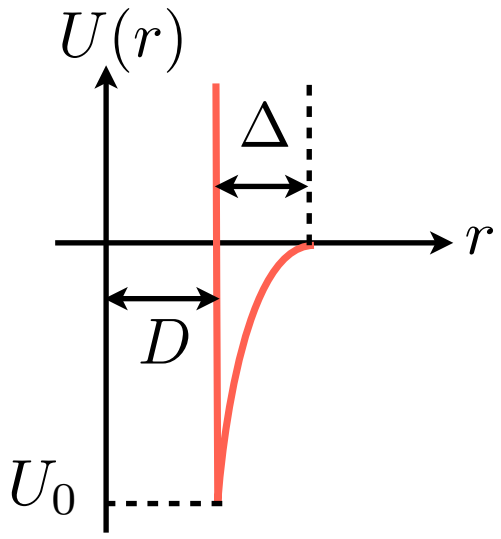

$\boxed{\frac{\Delta}{D}}$

$$\text{Gravitational Pélect no.} = \frac{\text{time to sediment own size}}{\text{time to diffuse own size}}$$

$$\boxed{\mathrm{Pe}_g = \frac{4\pi}{3} g \Delta \rho k_B T a^4}$$

Two generic collapse mechanisms

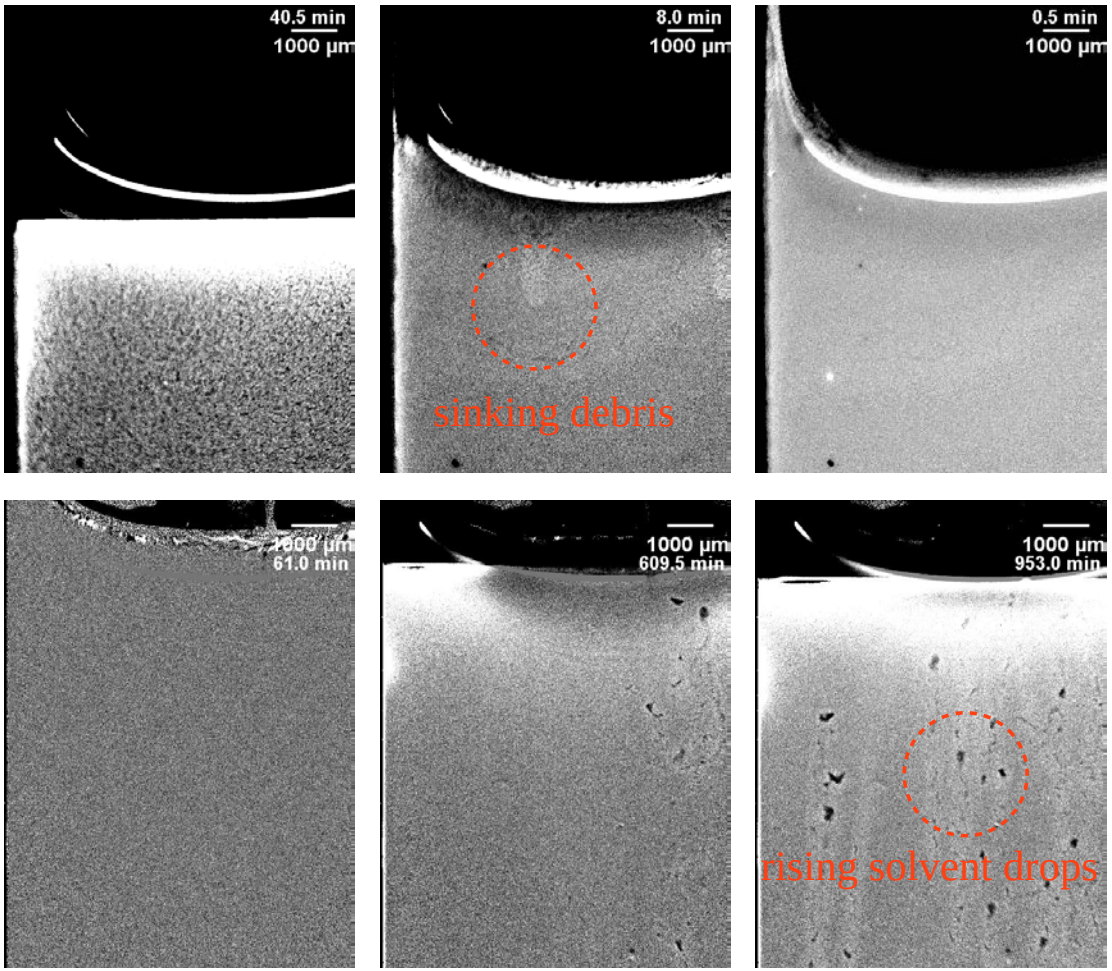

$$\mathrm{Pe} = 2.25, U_0/k_\mathrm{B}T \approx 10, \Delta/D = 0.05T$$

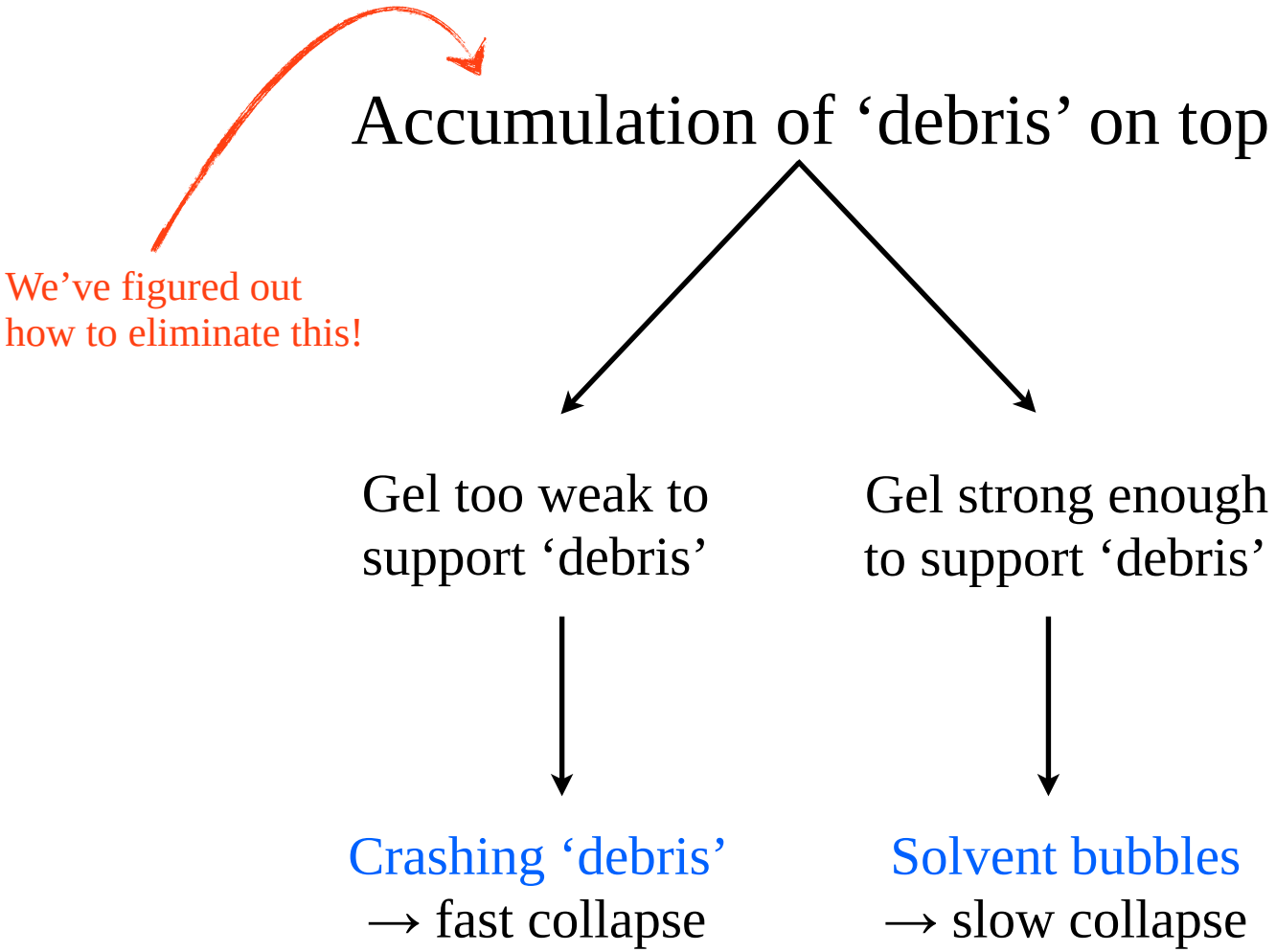
Accumulation of ‘debris’ on top
We’ve figured out
how to eliminate this!
Gel too weak to
support ‘debris’
Gel strong enough
to support ‘debris’
Crashing ‘debris’
→ fast collapse
Solvent bubbles
→ slow collapse

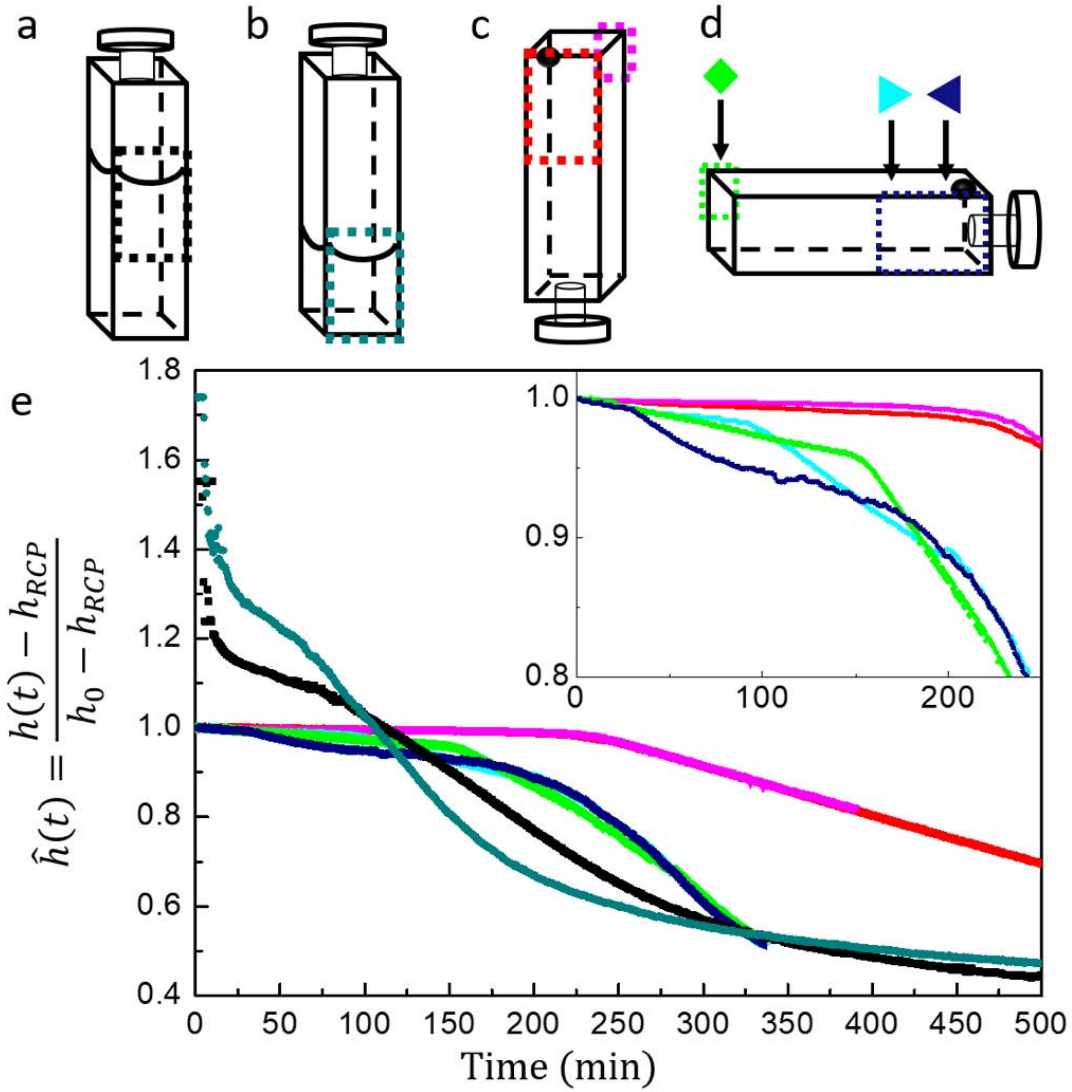

$$\mathrm{Pe} = 2.25, U_0/k_\mathrm{B}T \approx 18, \Delta/D = 0.05T, \phi = 0.23$$

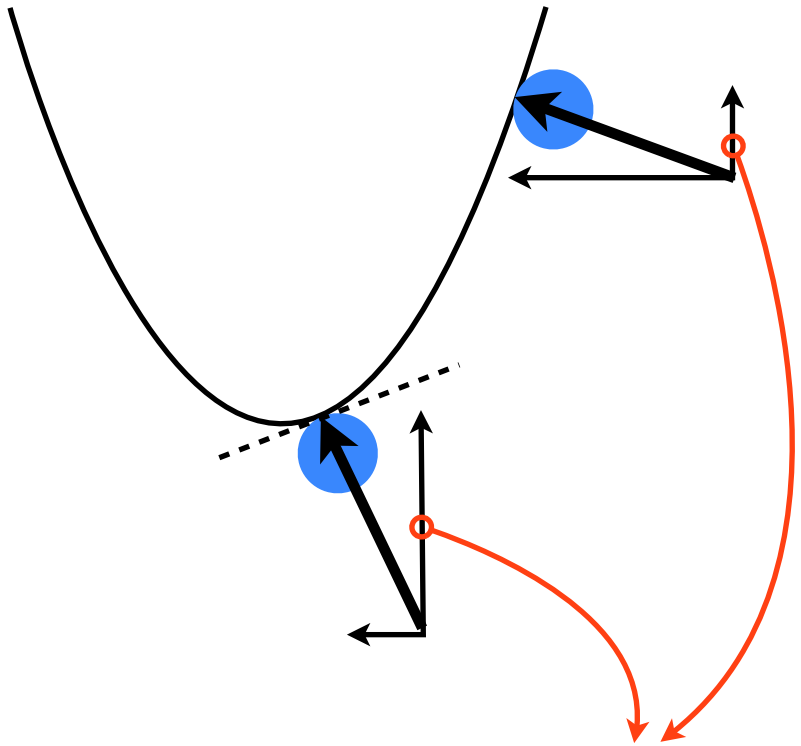

Decreasing vertical force holding particles to interface
→ gel will always tear off upper parts of the meniscus

Imaging: Back flow (and ∴hydrodynamic) plays key role ...

→ Lattice Boltzmann (LB) simulations

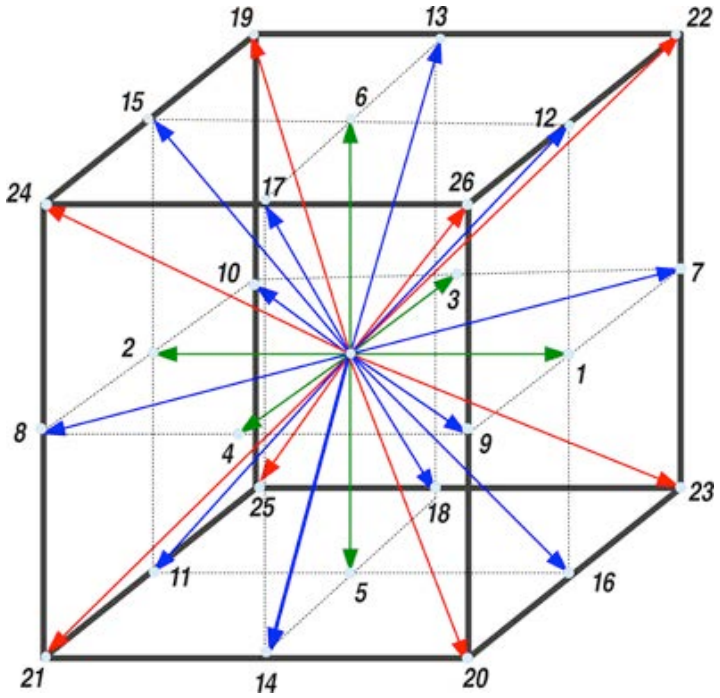

$$\phi = 0.1 - 0.2, U_0 = 10 k_{\mathrm{B}} T, \Delta / D = 0.06$$

Hydrodynamics → fast and chaotic backflow

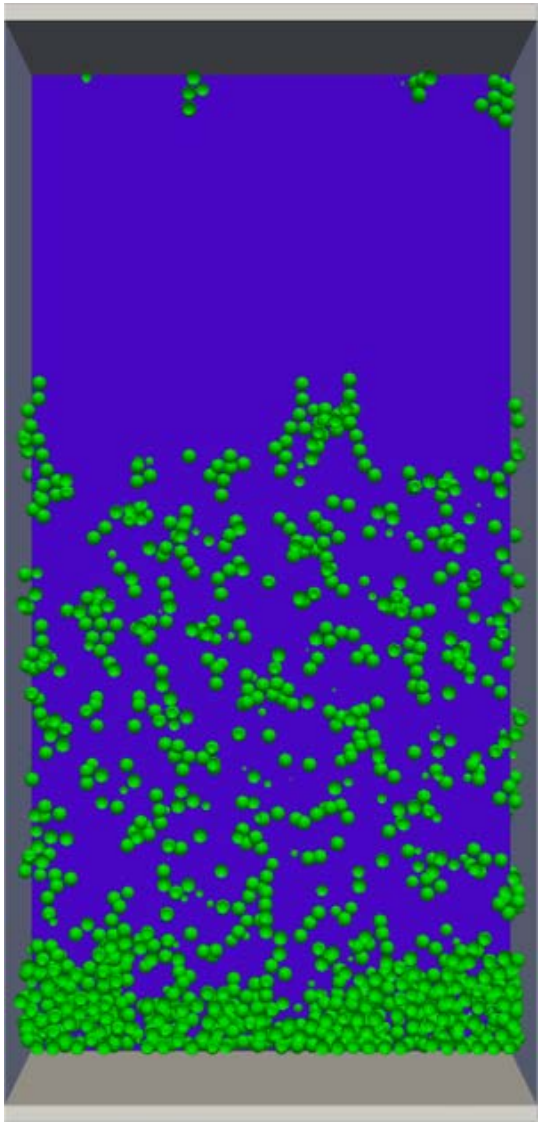

(movies)

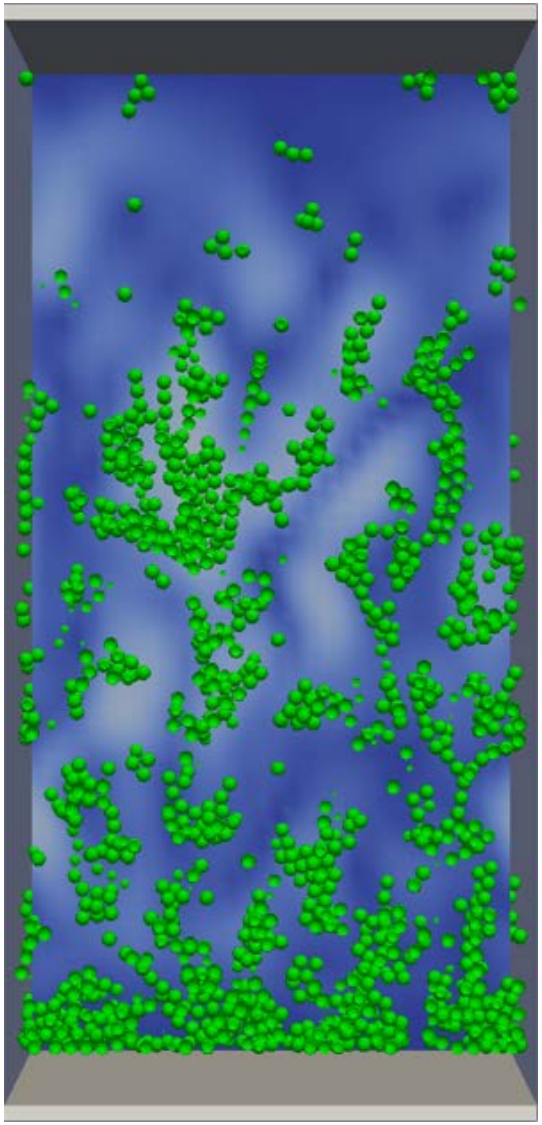

Hydrodynamics drives gel structure coarsening

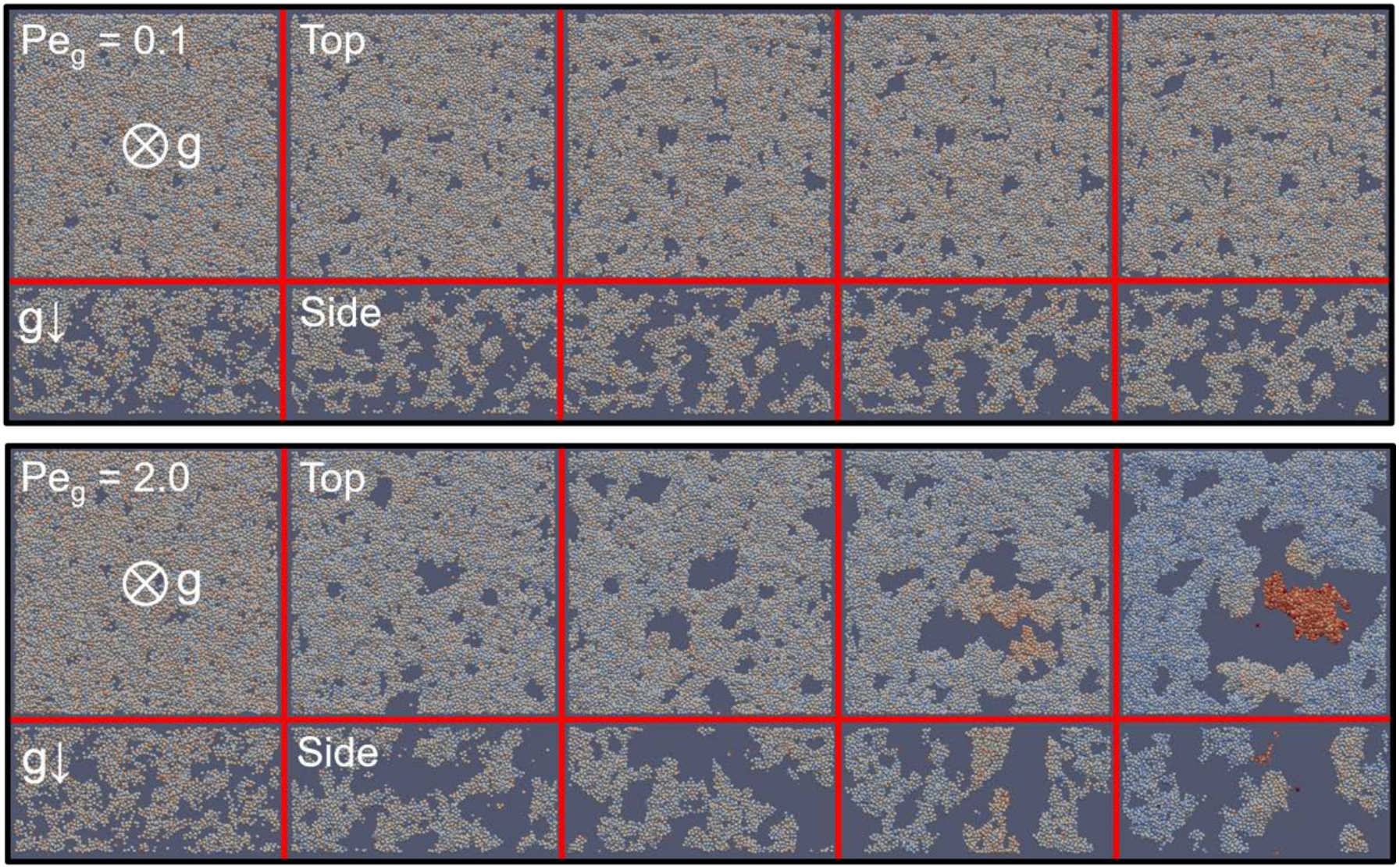

(movies)

Density profile (with hydrodynamics)

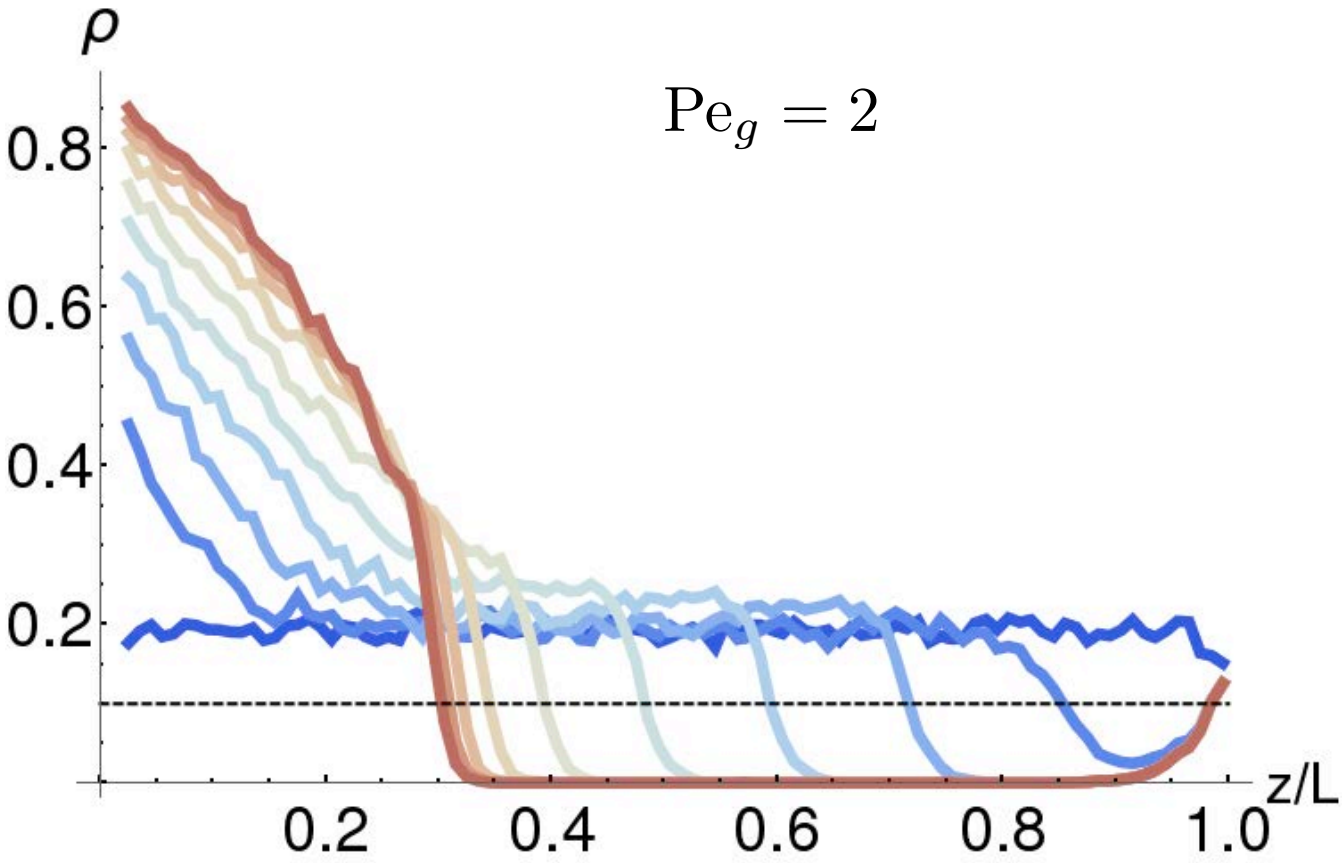

(Time = blue to red)

Number of particles in largest cluster

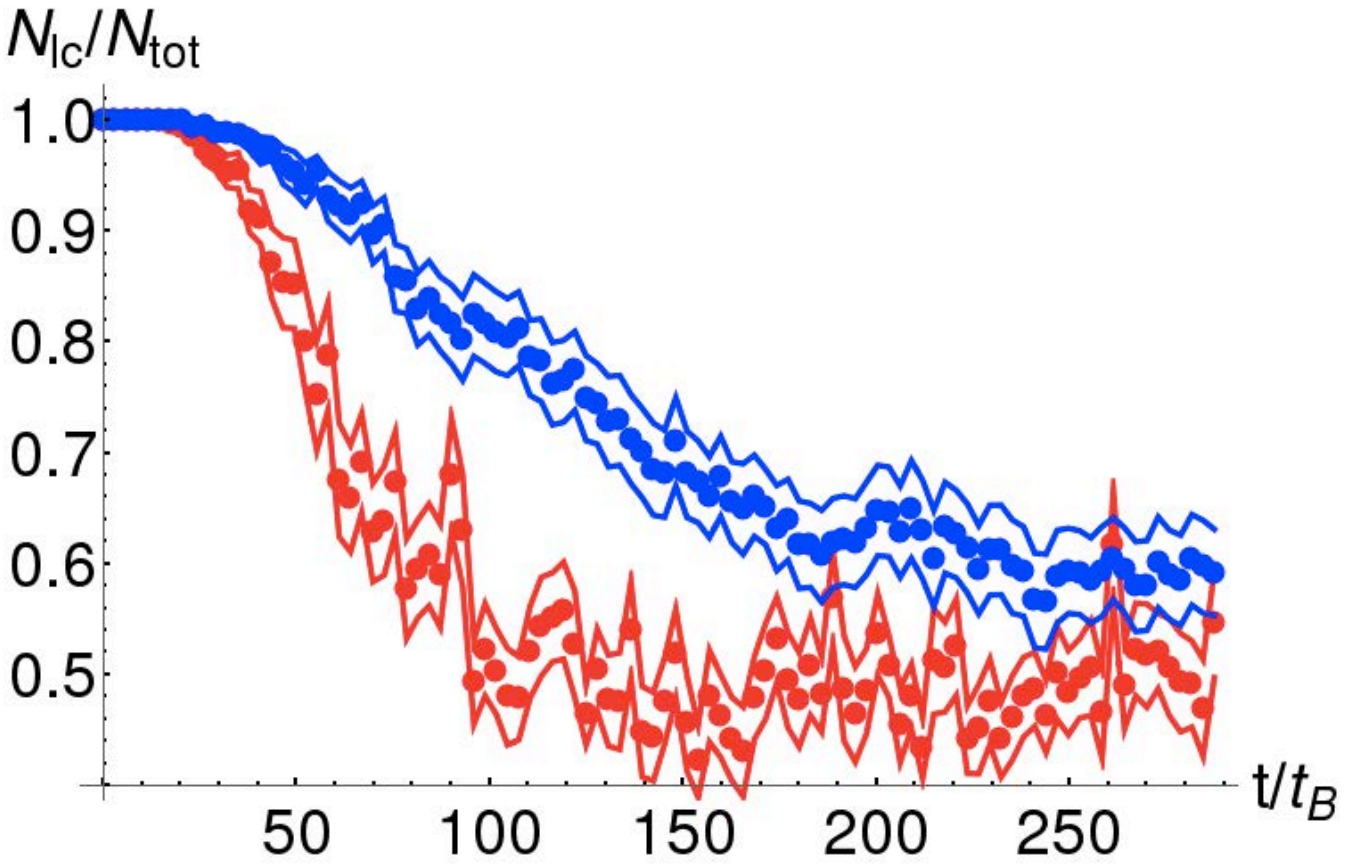

$\mathrm{Pe} = 2, N = 10^4, N = 2.5 \times 10^4$

Inverse collapse onset time *vs* gravitational Péclet number

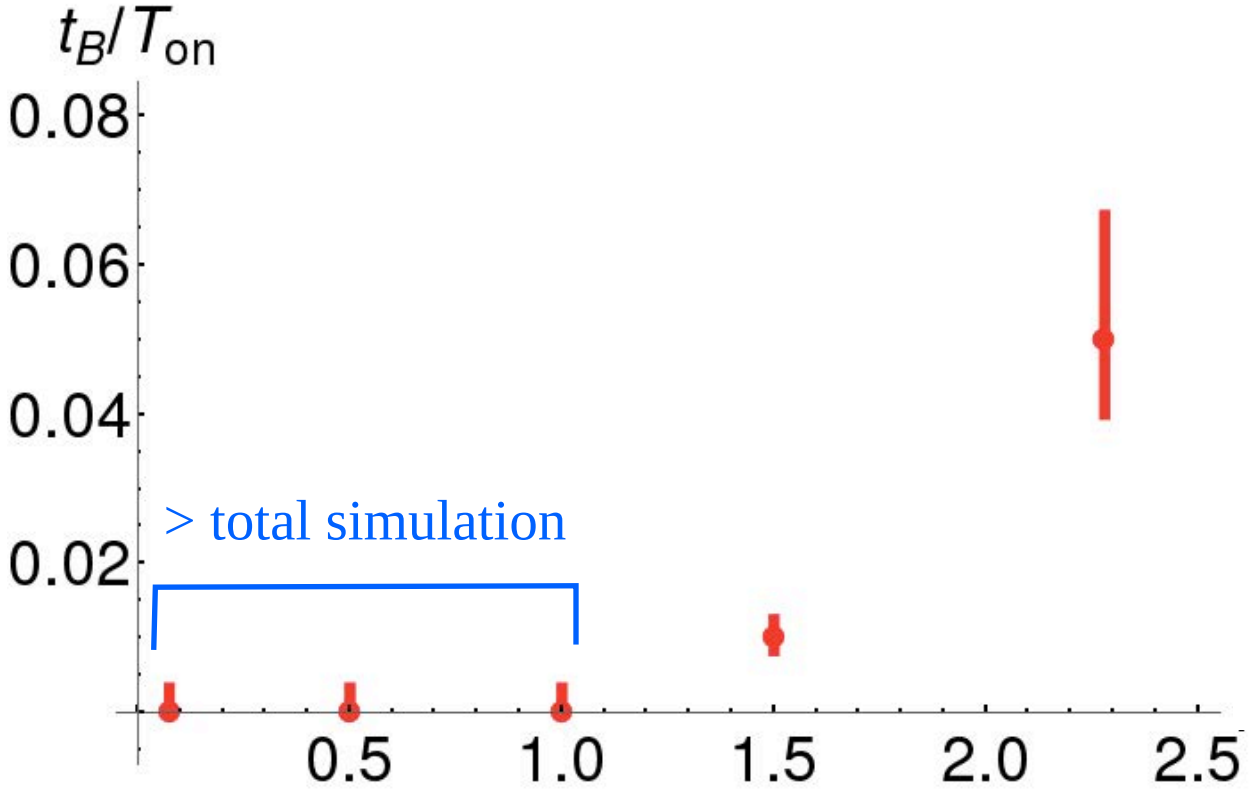

$$\mathrm{Pe}_g = \frac{4\pi}{3} g \Delta\rho k_B T a^4$$

Summary & conclusions

- Rapid collapse can be delayed by getting rid of curved meniscus
- Gravity speeds up coarsening
- Back flow destroys gel structure

Self-Assembled Monolayers as Nucleating Surfaces to Study Early Formation Pathways of Crystal Polymorphs

Zihao Zhang, Katherine P. Barteau, Lara A. Estroff, & Uli Wiesner

Materials Science and Engineering

ubw1@cornell.edu

IFPRI 39th Annual General Meeting, Philadelphia PA, June 18-22, 2017

This work made use of the Cornell Center for Materials Research Shared Facilities which are supported through the NSF MRSEC program (DMR-1120296).

Research Project Brief

- Fund project to understand and control crystallinity, polymorphism, and particle morphology in the *early formation stages*.
- Use advanced techniques like cryo-TEM, synchrotron derived pair-correlations, solid-state C^{13} NMR, and in-situ AFM, to visualize these stages.
- High level objectives of this project:

  - *identify appropriate model system(s)* to study, adapt and apply characterization techniques to describe early particle formation stages;

  - collect data that is relevant for the development of molecular dynamic simulation or other computational physics models.

Proposed Approach

- Here: Use of self-assembled monolayers (SAMs) to study the relationship between nucleation event and polymorph selection.

- Advantages: (i) Enables establishment of scientific correlations between nucleation and observed polymorph and (ii) provides access to polymorphs not accessible via solution methods.

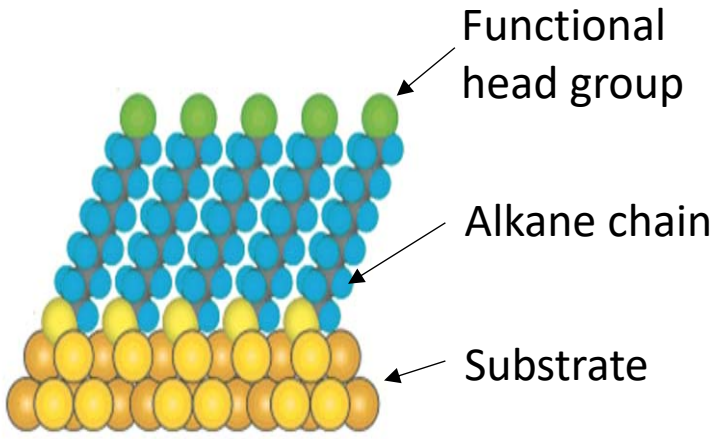

J.C. Love et al., *Chem. Rev.* 2005, **105**, 1103−1169.

Experimental Design – Drug Choice

Acetaminophen (Paracetamol, ACM)

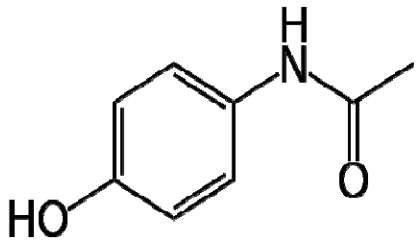

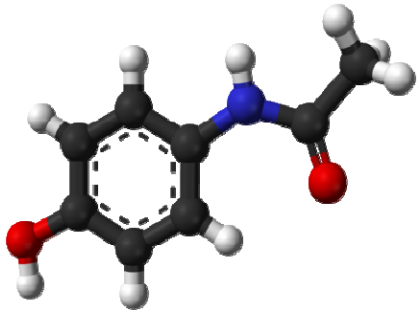

- Two well-known polymorphs: monoclinic and orthorhombic.
- Surface chemistries presented on crystal faces differ between the two polymorphs.
- Popular use in medication and readily available.
- Monoclinic polymorph is the thermodynamically preferred and commercially produced form.
- However, the orthorhombic form is desirable for easier commercial processing due to its flat cleavage planes.

https://en.wikipedia.org/wiki/Paracetamol

Two well-known polymorphs

Monoclinic (Form I)

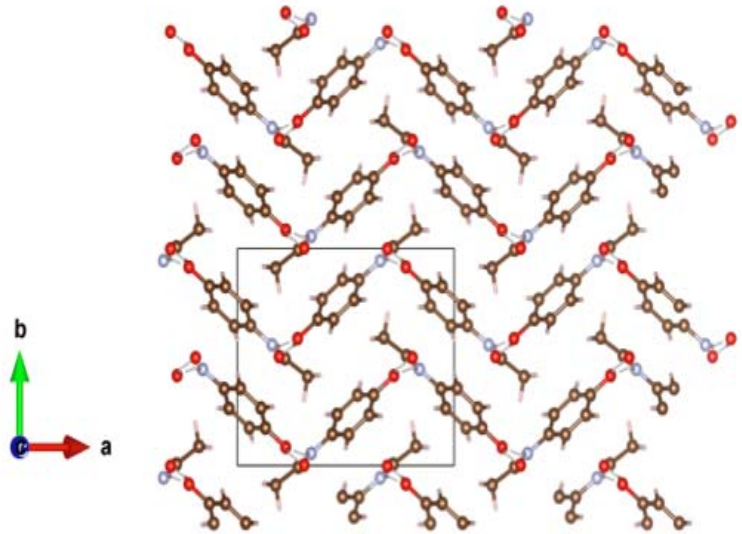

(001) face shown

Example solution grown crystals:

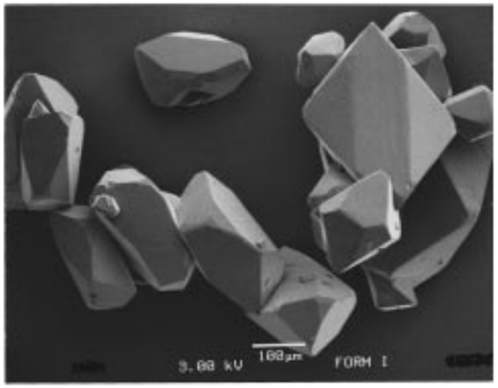

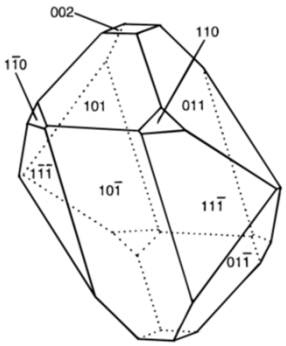

G. Nichols and C.S. Frampton. *J. Pharm. Sci.* 1998, **87**, 684.

Orthorhombic (Form II)

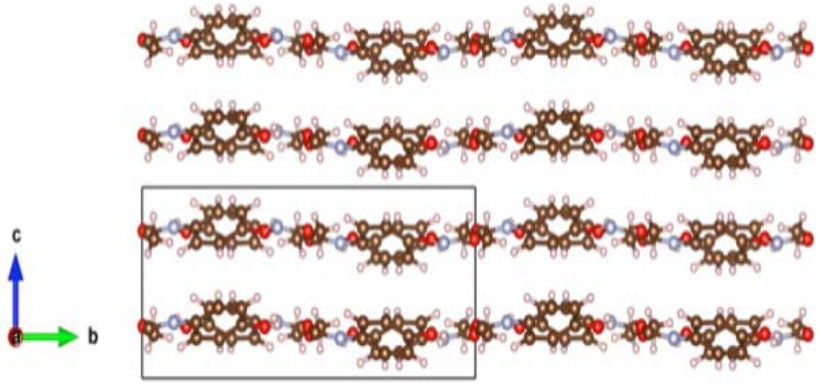

(200) face shown

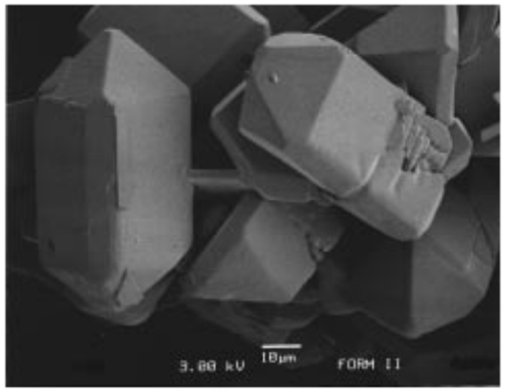

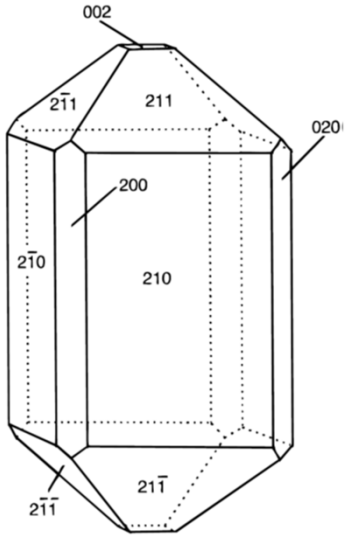

Note: indices h and k are switched from our convention in this schematic

Expanding the variety of substrates and chemistries

Moving from gold to silica based surfaces:

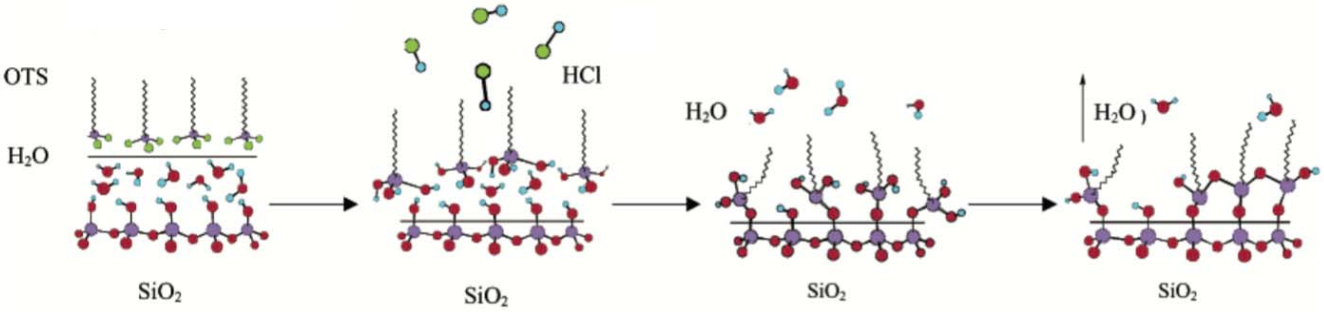

Y. Wang et al., *Langmuir* 2003, **19**, 1159

Advantages:

- Less expensive and wider range of substrates and chemicals
- Transparency of glass allows for in-situ observation of crystallization under optical microscopy
- SAMs on silica are more stable (up to 12 months)

Disadvantages:

- Surfaces are less well-ordered
- Potential for multilayer formation

Solvent Effects on the polymorph control: hydrophobic surfaces

Solvent	*SAM chemistry*	*n*	*Form I*	*Form II*
Ethanol 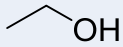	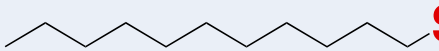	20	**80%**	20%
	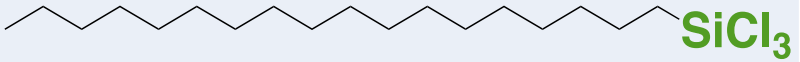	18	**94%**	6%
	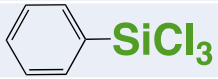	14	**93%**	7%
Deionized water	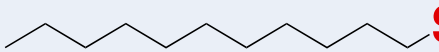	9	**93%**	7%
	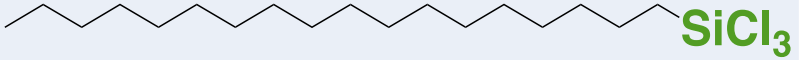	18	**89%**	11%
	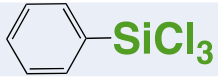	10	**90%**	10%
1,4-dioxane 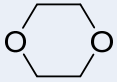	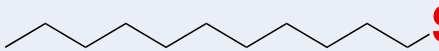	12	**100%**	0
	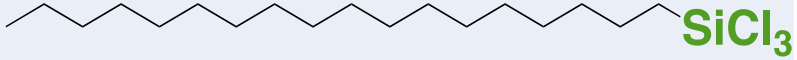	10	**90%**	10%
	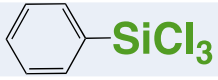	10	**70%**	30%
DI water/dioxane 20:80	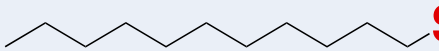	11	9%	**91%**
	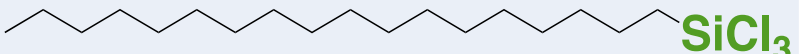	11	0	**100%**
	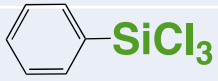	9	0	**100%**

Form II, the less thermodynamically preferred form, is formed on all hydrophobic surfaces using a water/dioxane solvent mixture, where as Form I is formed when using only pure water or pure dioxane. Even small amounts of water in dioxane will yield a greater fraction of Form II.

Both solvent and substrate work together to control crystal polymorph

Solvent \ Substrate	$-CH_3$ on gold (hydrophobic)			-OH on gold (hydrophilic)		
	n	Form I	Form II	n	Form I	Form II
DI water	9	**93%**	7%	17	**100%**	0
DI water/ dioxane 20:80	11	9%	**91%**	10	0	**100%**
1,4-dioxane	11	**100%**	0	10	20%	**80%**
Ethanol	20	**80%**	20%	11	9%	**91%**

- In water containing systems, polymorph selection is independent of substrate chemistry, whether hydrophobic or hydrophilic.
- However, for pure organic solvents, polymorph switches from Form I to Form II when surface chemistry is changed from hydrophobic to hydrophilic.
- Therefore, solvent and surface chemistry must be considered in concert when predicting or designing crystallization process.

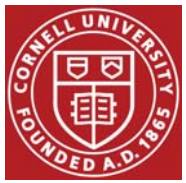

Substrate can dictate crystallographic orientation

Solvent	*SAM chemistry*	*n*	*Form I*	*Form II*
DI water/dioxane 20:80	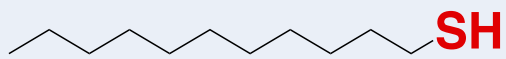	11	9%	**91%**
	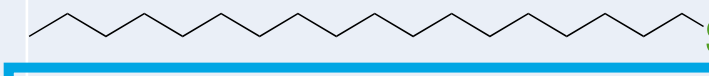	11	0	**100%**
	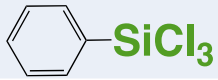	9	0	**100%**
	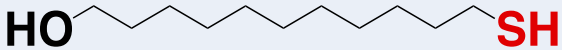	10	0	**100%**

X-ray diffraction ACM on PTS and –OH:

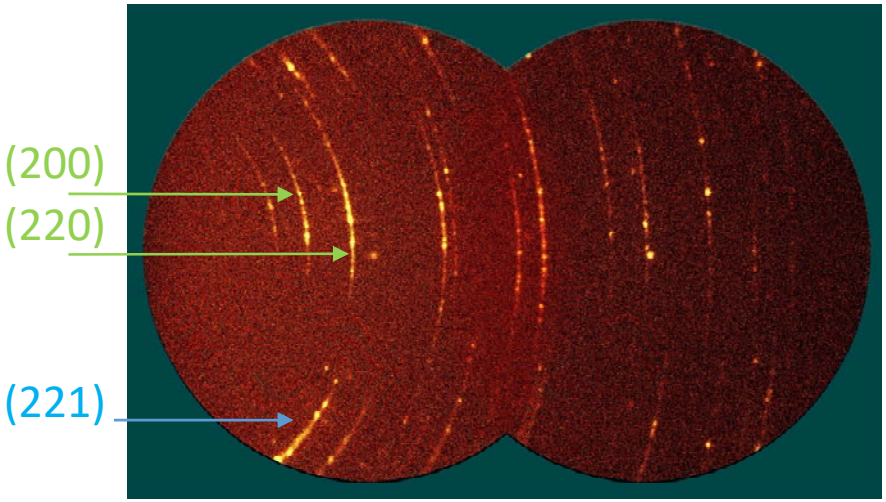

PTS:

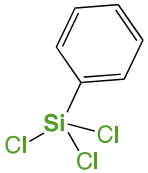

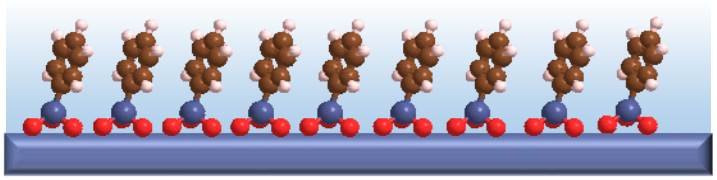

Substrate can dictate crystallographic orientation

Solvent	*SAM chemistry*	*n*	*Form I*	*Form II*
DI water/dioxane 20:80	SH	11	9%	**91%**
	$SiCl_3$	11	0	**100%**
	$SiCl_3$	9	0	**100%**
	HO SH	10	0	**100%**

X-ray diffraction ACM on PTS and –OH:

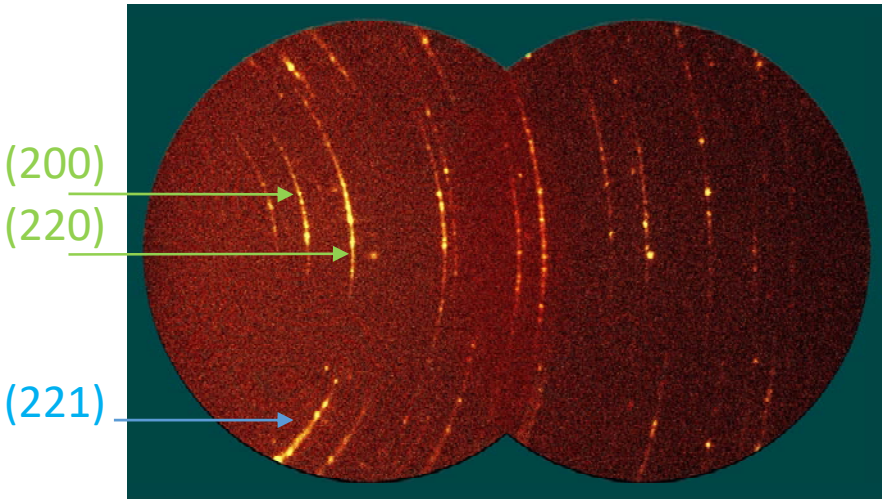

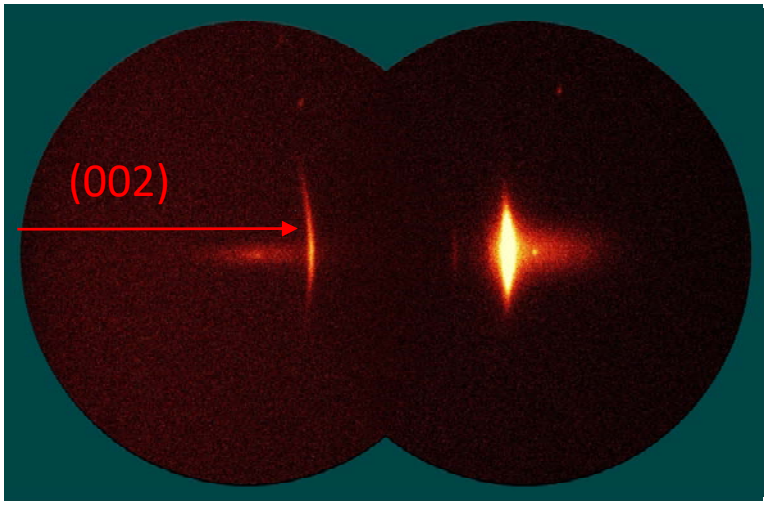

PTS:

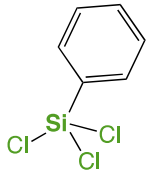

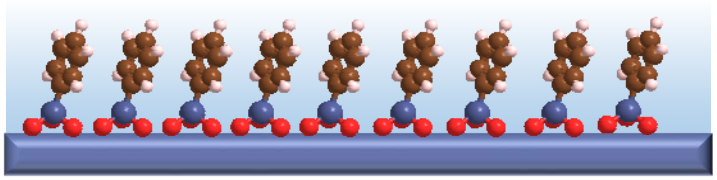

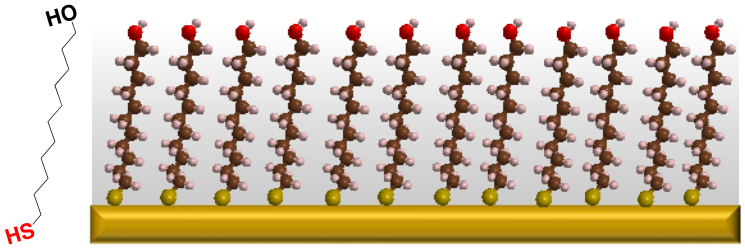

Substrate can dictate crystallographic orientation

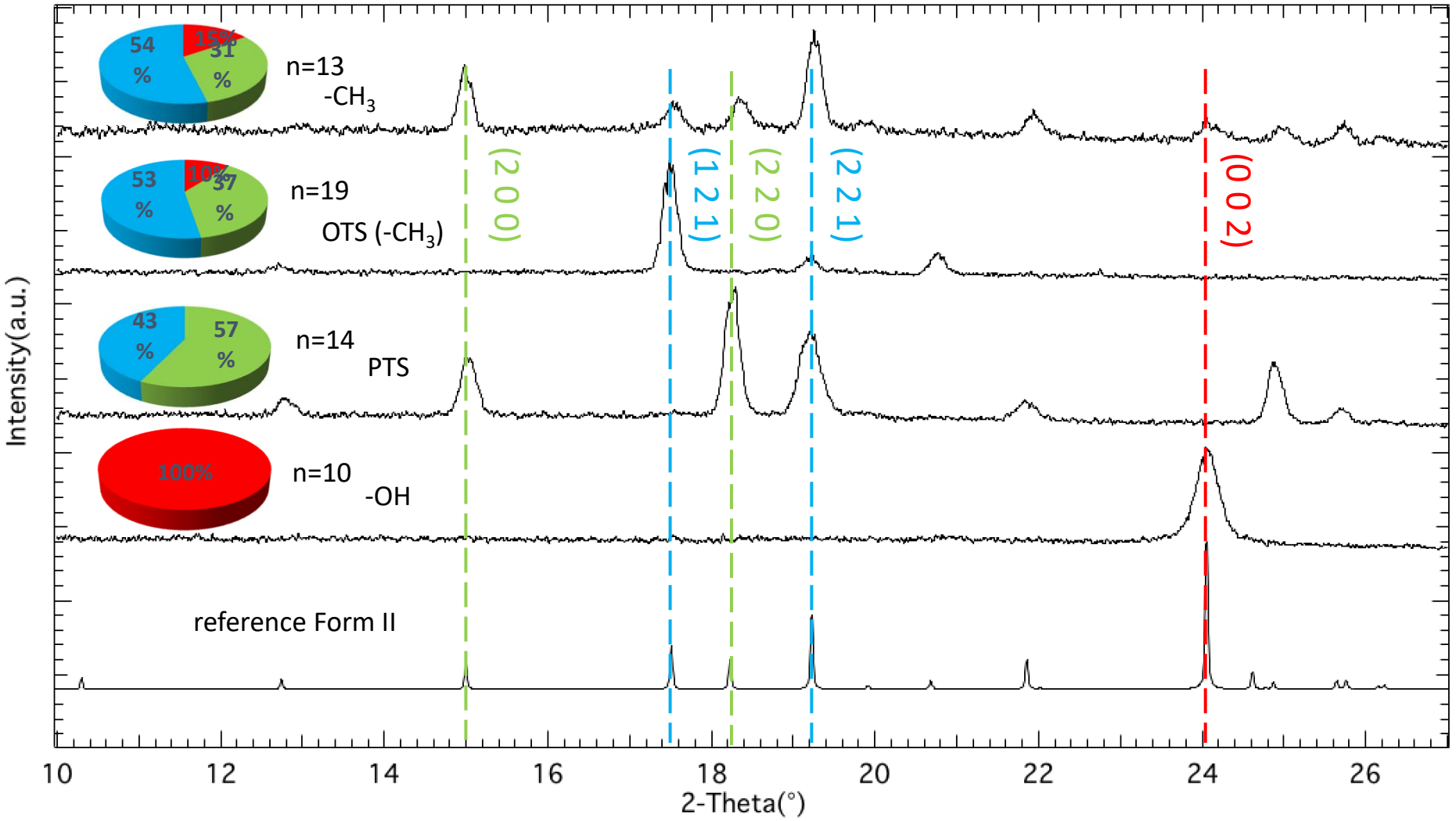

■ (0 0 2) or parallel ■ Non-orthogonal angles ■ Perpendicular to (0 0 2)

Circle charts indicate the observed % of each class of relflections in the 2D XRD patterns

Substrate can dictate crystallographic orientation

- The phenyl terminated surface promotes the crystals to nucleate with the phenyl rings oriented approximately perpendicularly to the substrate (e.g. (200), (211) and (210) reflections lie parallel to the substrate).
- Powder-like arcs and high angle planes are also observed, indicating some rotational variation around the (200) and similar planes
- The (002) plane is never observed. i.e. the cleavage planes (red) are always perpendicular to the substrate

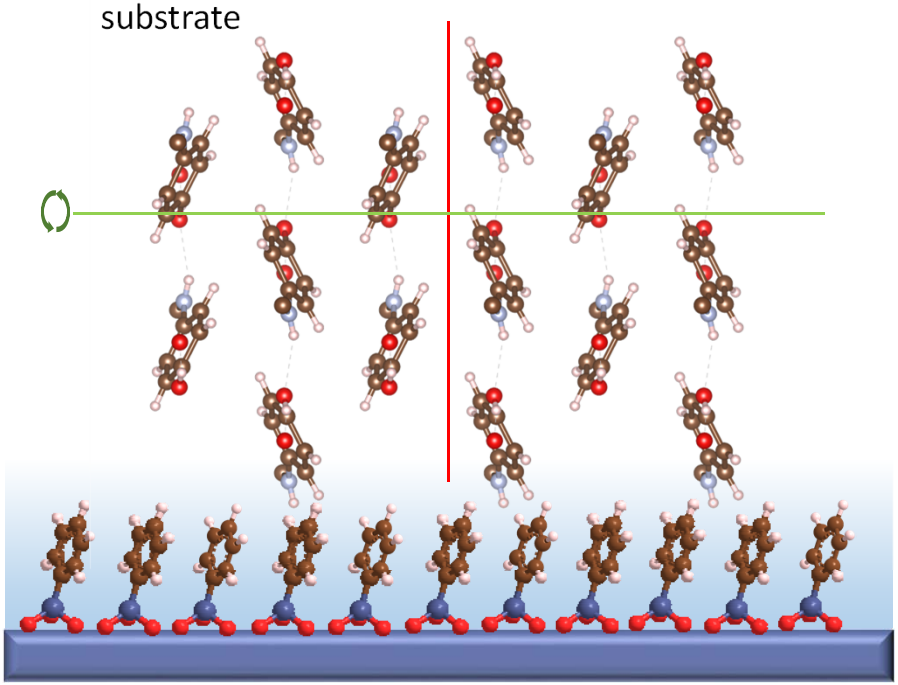

- The alcohol terminated surface promotes crystallization with the (002) cleavage plane stacked parallel to the substrate
- Some azimuthal spread of the (002) indicates that there is some tilt in the orientation – not all cleavage planes are perfectly parallel to the substrate
- The absence of all other reflections suggests that there is a strong preference for the phenyl rings to lie parallel to the substrate

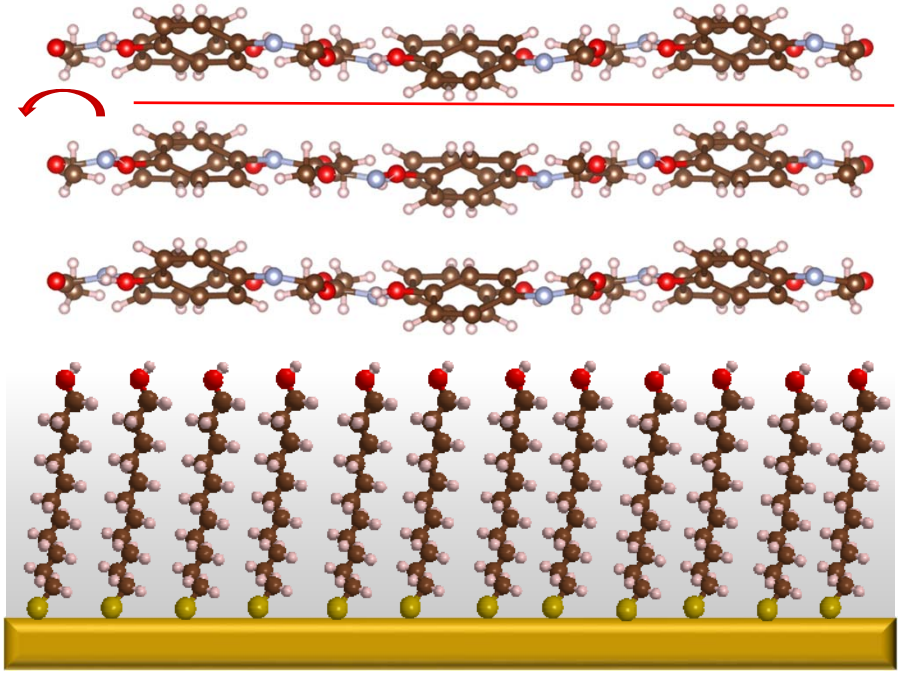

Influence of surface on orientation – from nanoscale to microscale

Orthorhombic (Form II) ACM on **PTS:**

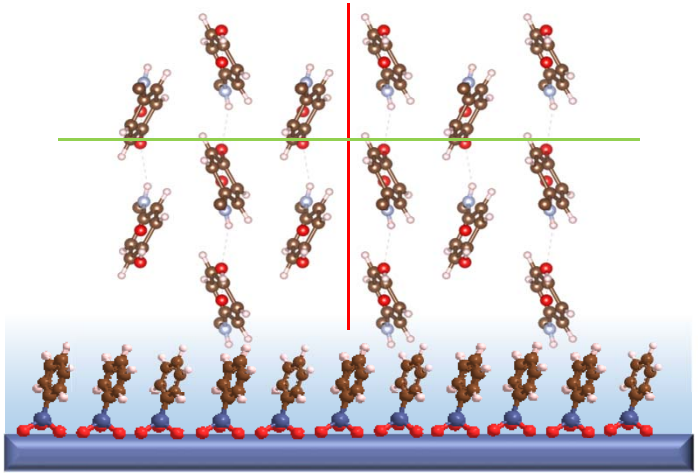

Molecular interpretation

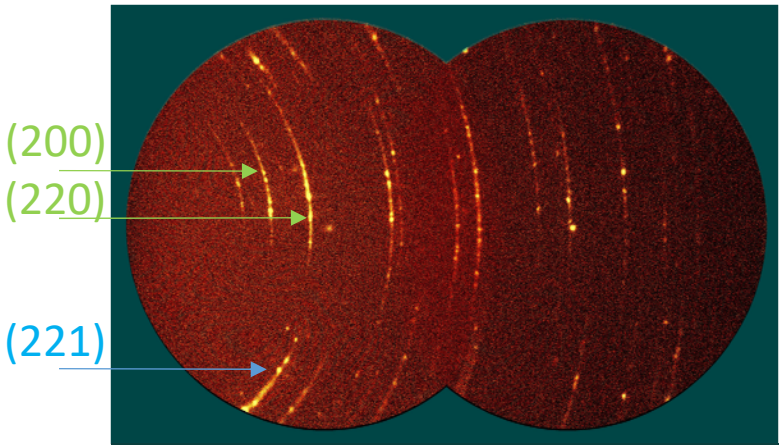

X-ray diffraction (XRD)

Nucleation often occurs near the edge of the droplet

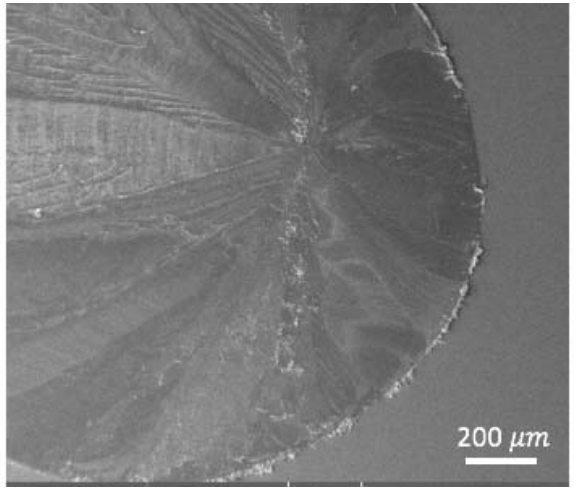

Large, flat crystallites form

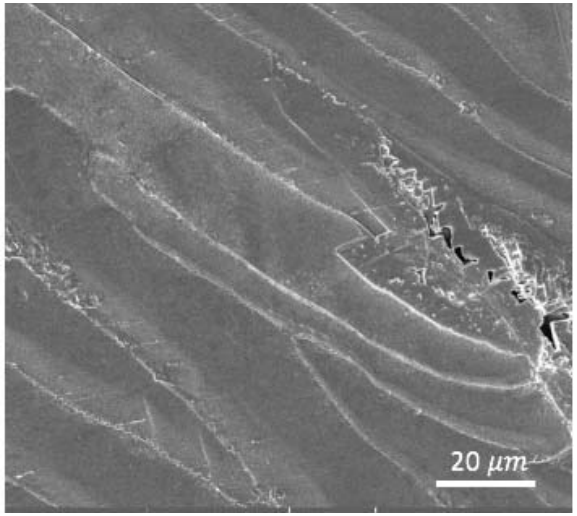

Scanning electron microscopy (SEM)

Influence of surface on orientation – from nanoscale to microscale

Orthorhombic (Form II) ACM on **–OH:**

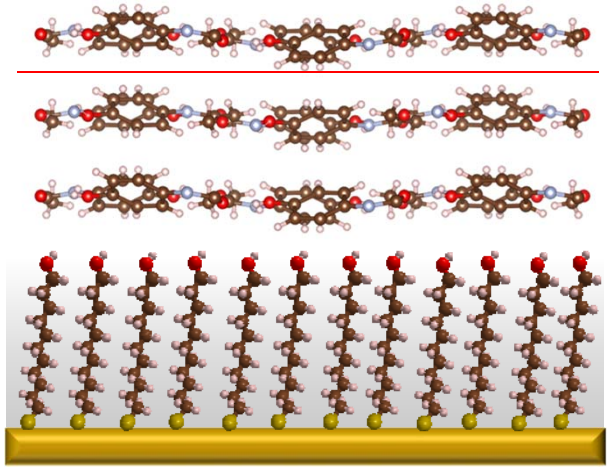

Molecular interpretation

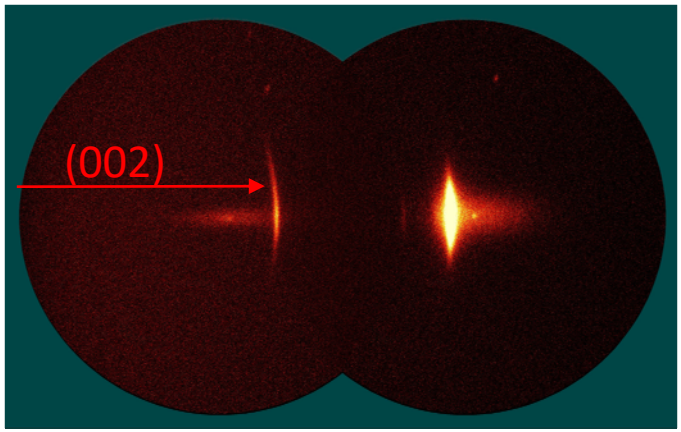

X-ray Diffraction (XRD)

Nucleation often occurs near center of the droplet

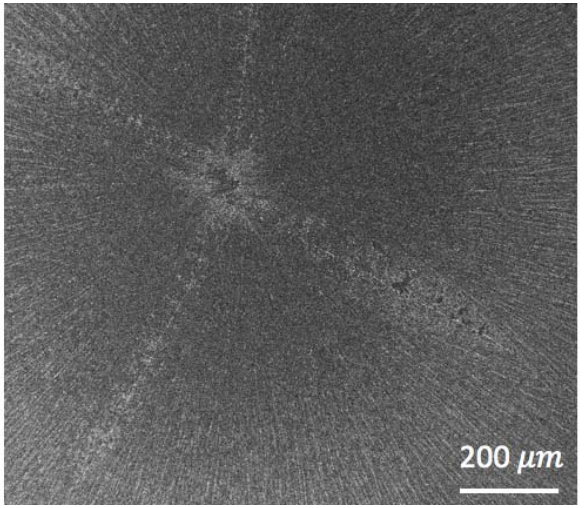

Small, rough crystallites form

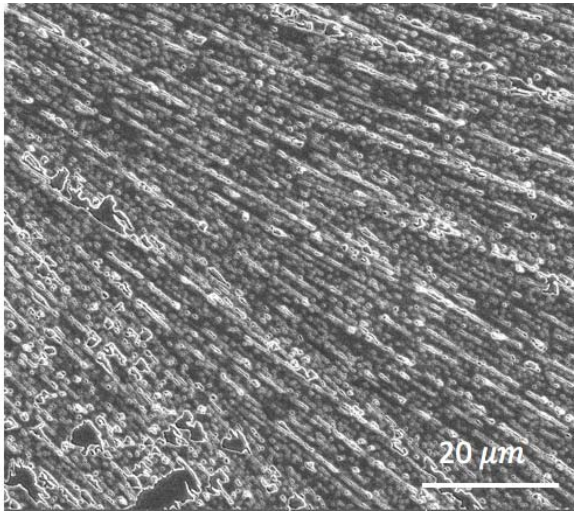

Scanning electron microscopy (SEM)

Future directions: Blade coating and in-situ WAXS

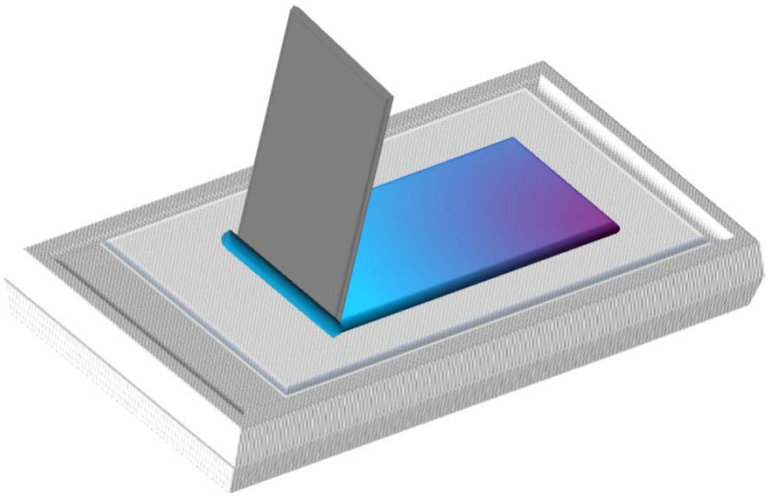

Blade coating ACM solution on silane functionalized glass or silicon wafer

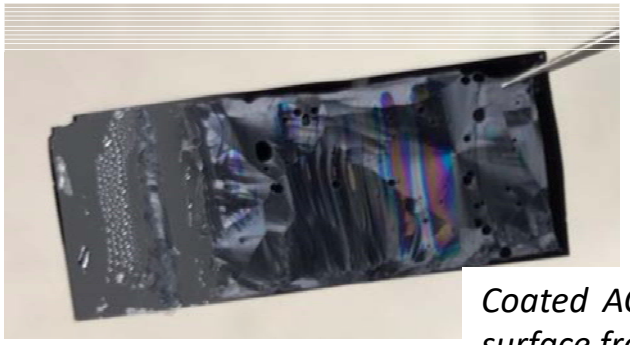

Coated ACM crystals on PTS surface from 1,4-dioxane

	1,4-dioxane	Ethanol
PTS	Form I	Form II
-OH	Form II	Form II

preliminary results

In-situ grazing incidence x-ray scattering (GIXS), performed at CHESS:

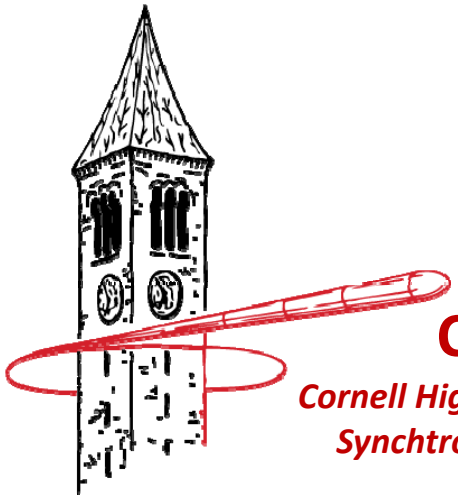

CHESS

Cornell High Energy Synchtron Source

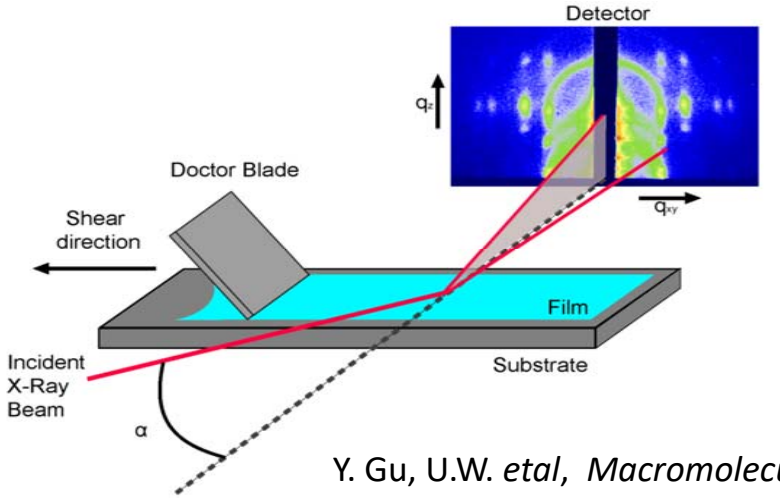

Y. Gu, U.W. *etal*, *Macromolecules 2016,* **49,** 4195.

Conclusions

- A more reproducible and inexpensive SAMs system on silicon wafers was introduced, the results of which are consistent with our earlier studies on gold-thiol based SAMS;

- On hydrophobic surfaces, use of pure solvents resulted in ACM Form I, while a mixture of water and dioxane produces Form II

- In general, both the solvent and SAM surface chemistry act in concert to control polymorph selection

- The SAM detailed surface chemistry further influences crystal orientation

Outlook/Future Work (Year 3)

- In-depth studies of earliest stages of nucleation and crystal formation processes identified in year two by means of *in-situ* techniques including *in-situ* X ray scattering at Cornell's High Energy Synchrotron Source (CHESS).

- Work with industry to identify (i) other organic compounds for in-depth polymorph studies, and (ii) modeling capabilities to enhance molecular understanding.

Die Filling of Aerated Powders

- Renewed in 2016
- Joey El Hebieshy (2014.9-2017.8)
- Kevin Zhong (2017.5 -)

IFPRI 39th AGM, Philadelphia, Pennsylvania, USA, June 18-22, 2017

Charley Wu
Chemical and Process Engineering
University of Surrey,
Guildford, GU2 7XH
@charleywu
C.Y.WU@surrey.ac.uk

UNIVERSITY OF SURREY

Objectives & Tasks

UNIVERSITY OF SURREY

- *The goal is to understand the die filling behaviour of aerated powder blends.*
- *The objectives are*
  1) *to explore fine powder mixtures during die filling processes;*
  2) *to identify the critical material attributes and critical process variables*
  3) *to develop a design space for fine powder mixtures to achieve controlled/specified properties during die filling (such as mass variation, content uniformity, mass flow rate).*

Task 1 – Rotary die filling
(Month 1-Month 12).

Task 2 – Assisted die filling
(Month 13 - Month 24).

Task 3 – Segregation during die filling
(Month 24 - Month 36).

CONTENTS

UNIVERSITY OF SURREY

(1)

Rotary die filling

(2)

Segregation

(3)

Air-pressure build up during die filling

(4)

CMA identification

(5)

Conclusions & Future work

Rotary Die Filling

Speeds: from 5 mm/s to 1,500 mm/s

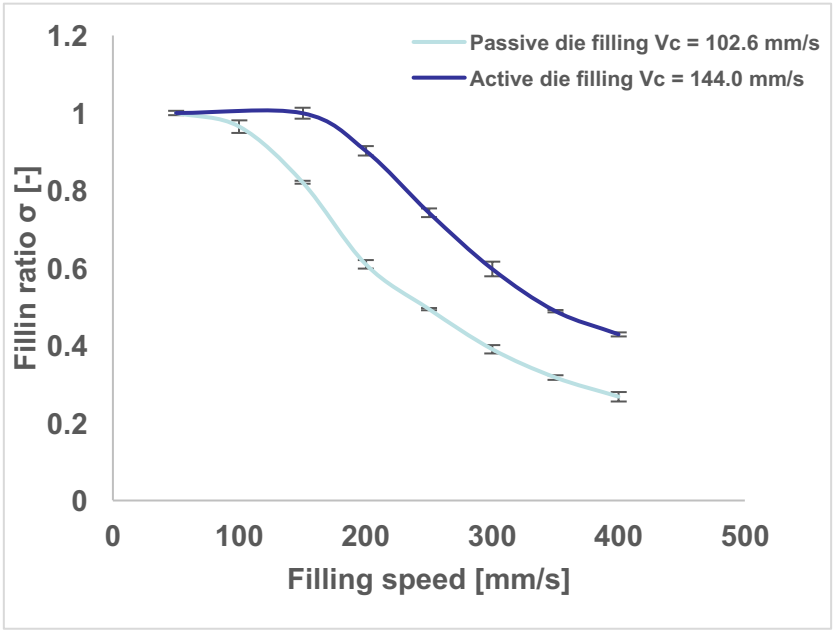

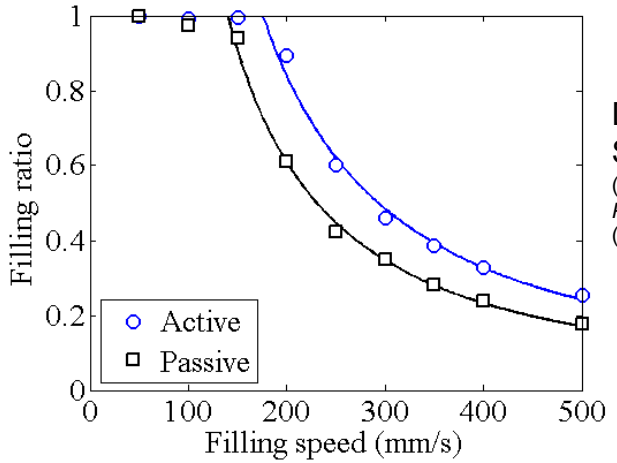

DEM Simulation
(Wu, 2008, *PARTICUOLOGY*, 6 (6), pp. 412-418.)

Rotary Die Filling

Shoe lengths:

1. 30 mm
2. 60 mm
3. 90 mm
4. 120 mm
5. 150 mm

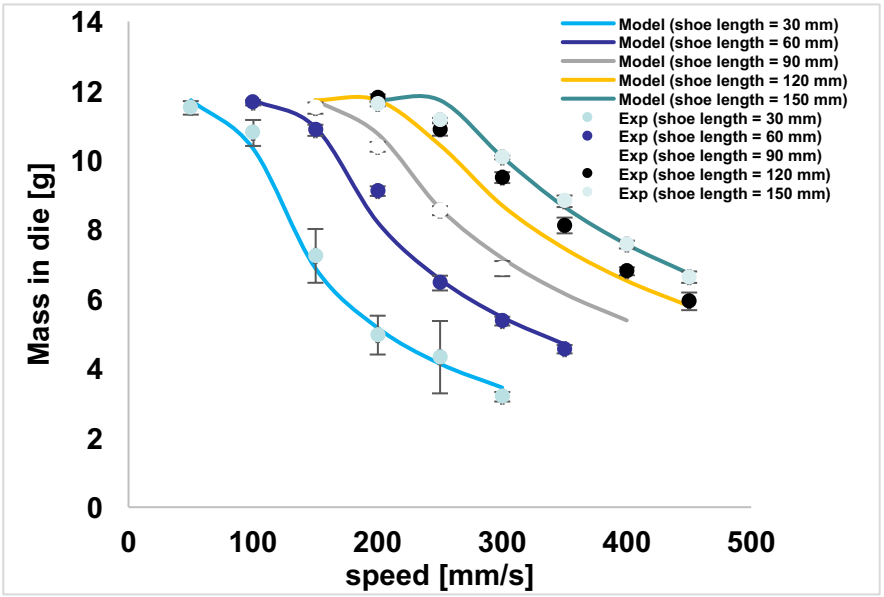

Material: Cenopheres 500

Density induced segregation

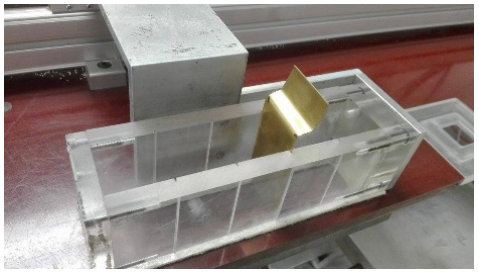

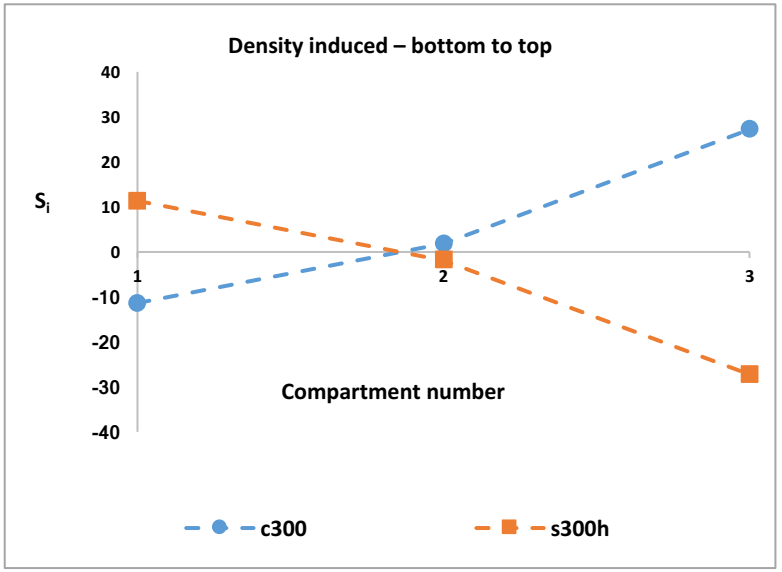

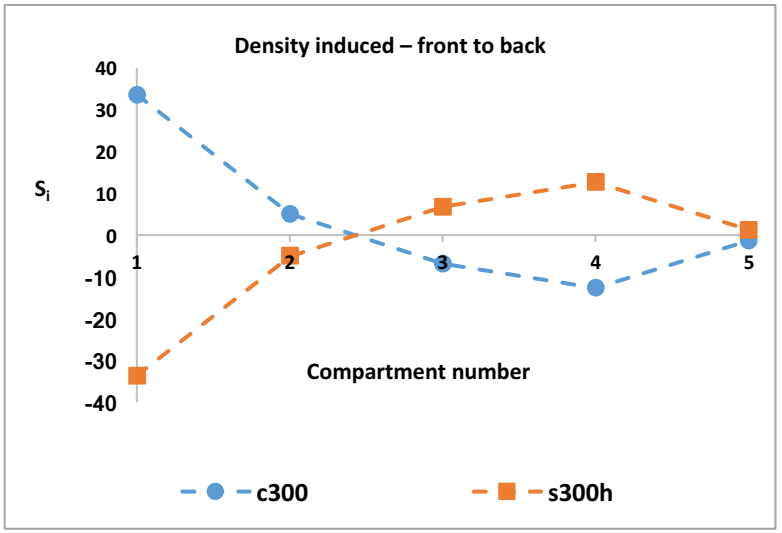

Air pressure build-up during die filling

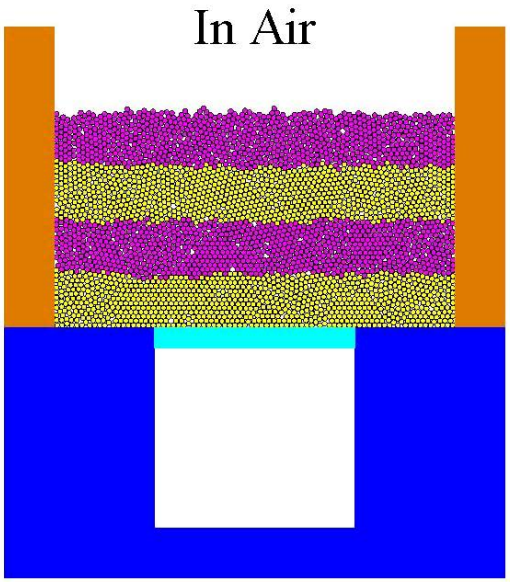

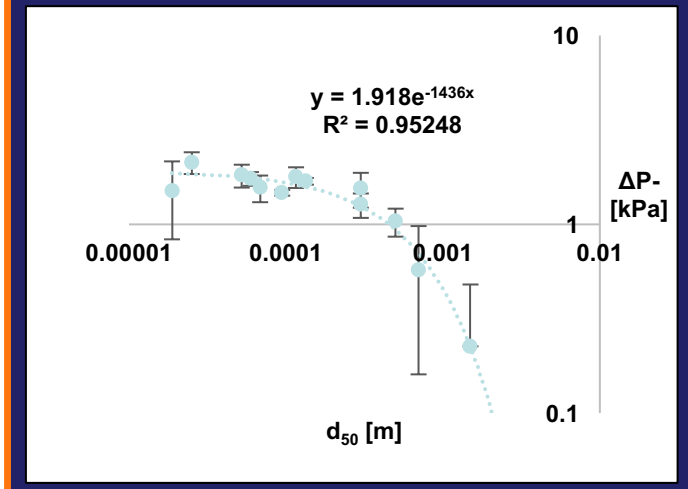

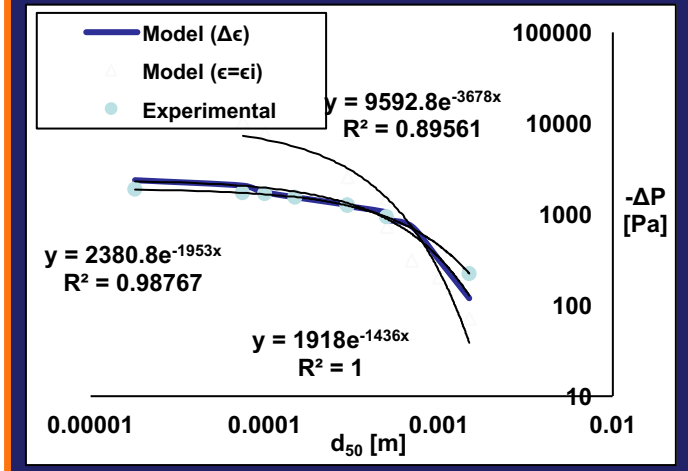

CMA identification

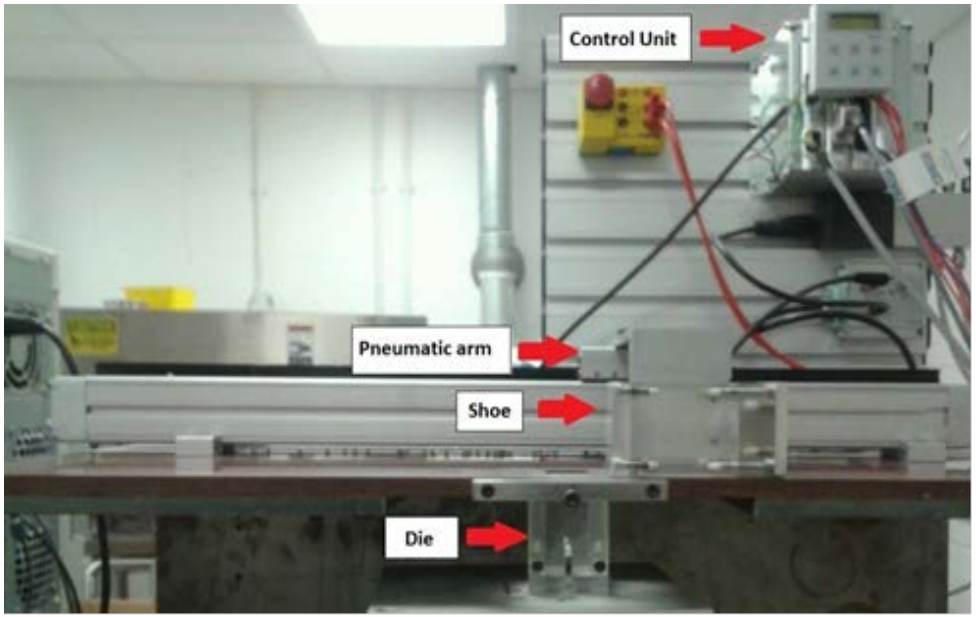

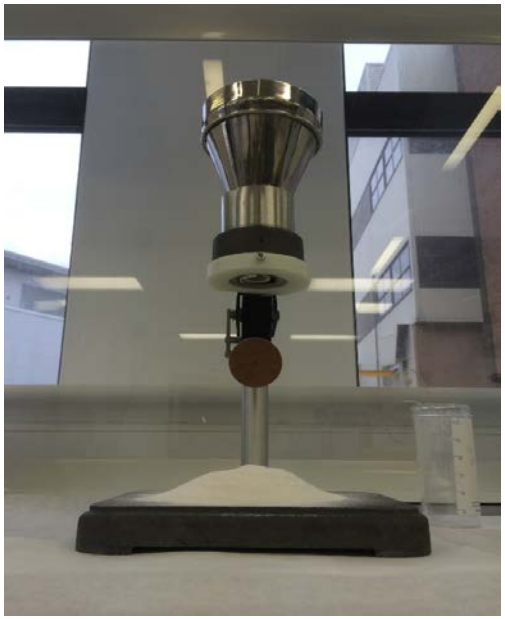

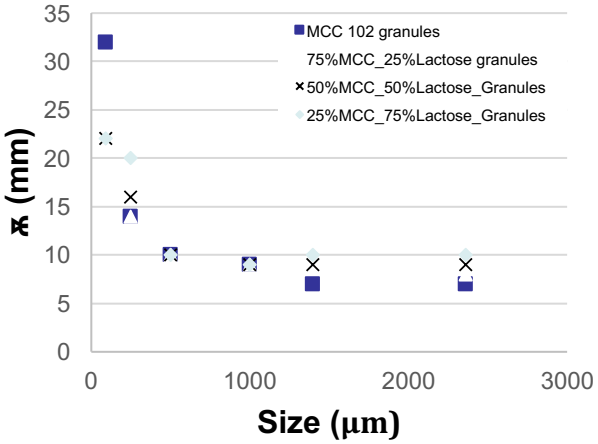

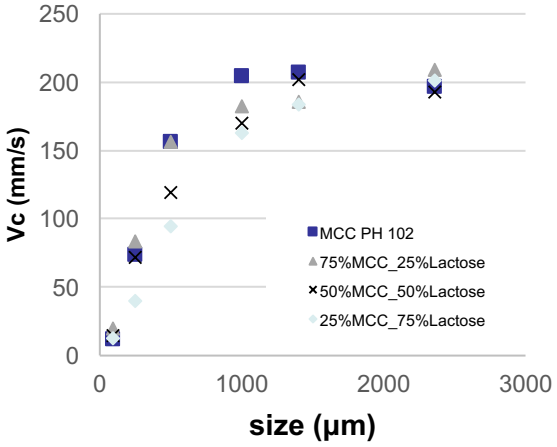

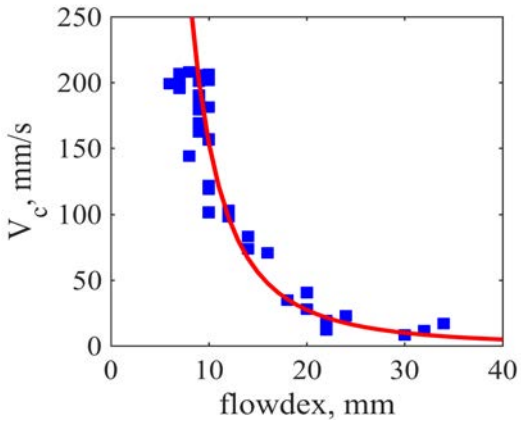

Summary and Future Work

UNIVERSITY OF SURREY

- *Active (rotary) die filling can lead to higher filling efficiency than passive (linear) filling.*
- *Significant density induced segregation can be induced die filling.*
- *A theoretical framework was developed to predict the air pressure build up during die filling. Its accuracy relies on the precise determination of porosity.*
- *Critical filling speed has a strong correlation with the Flodex measurements*

Task 2 – Assisted die filling
(Month 13 - Month 24).

Task 2.1 – Suction filling: system development and detailed experimental investigation

Task 2.2 – Paddled hopper/shoe: system development and preliminary investigation

Further CMA study –correlation with other flow measurements;

Further Rotary die filling study – Moist/cohesive powders

Relating Compaction Performance to Process Conditions with Emphasis on Powder Mixtures

Antonios Zavaliangos
Department of Materials Science and Engineering
Drexel University

IFPRI
International Fine Particle Research Institute

Annual General Meeting 2017

Drexel UNIVERSITY

Strength of mixtures

INDUSTRIAL IMPORTANCE

- **Knowledge of mixture rules can reduce dramatically the complexity of multicomponent formulations**

CONNECTION TO FUNDAMENTALS

- **To address strength of binary mixtures compacted at high relative density, we must also understand basic concepts of strength for simple materials and find ways to connect individual granule parameters with the compact properties**

PERSONAL INTEREST

- **Explore the possibilities of Discrete Element Method for compaction as a natural platform to address strength despite the inherent shortcomings of the method**

Goals for this period

1. Model parameter identification procedures that extract material properties from experimental measurements
2. Work towards the validation of the models developed
3. Parametric studies using DEM that elucidate the physics of the problem

Appropriate (for high density) force-displacement laws

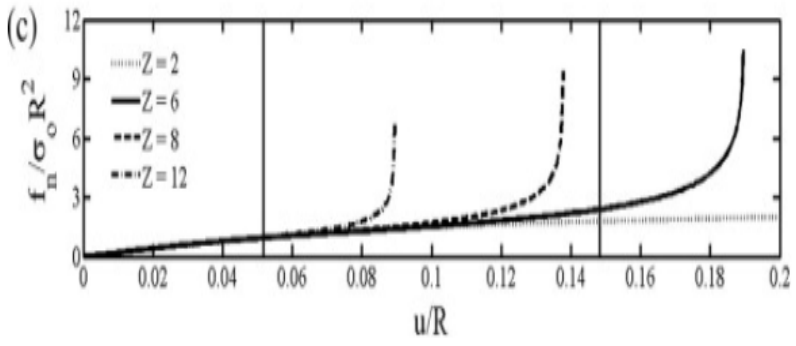

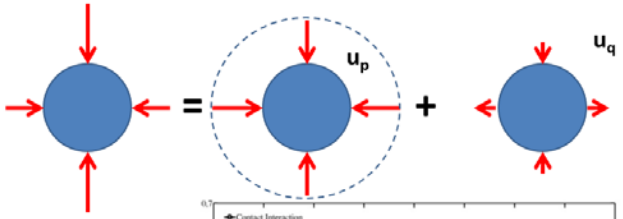

Force displacement law depends on

1. mode of loading
2. deformation of all contacts on the particle

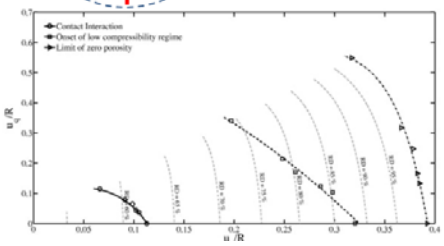

International Journal of Solids and Structures

Volumes 60–61, 15 May 2015, Pages 17–27

Detailed, complex
and computationally expensive

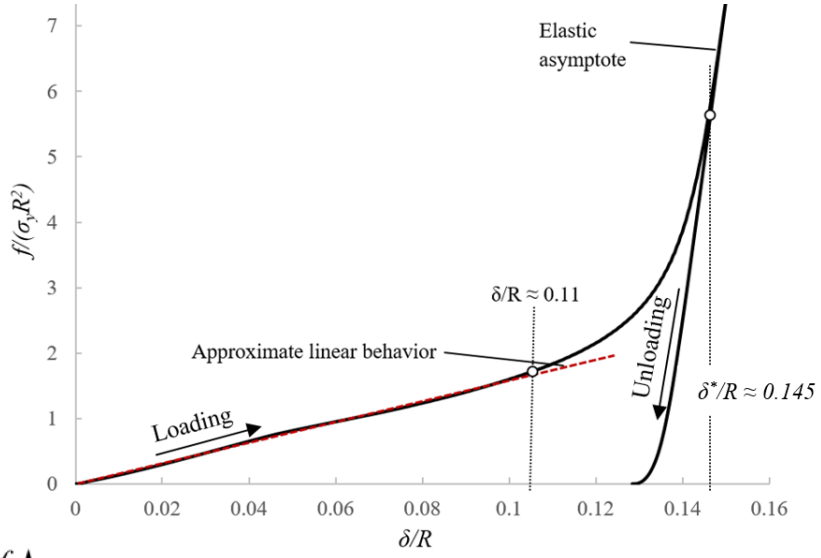

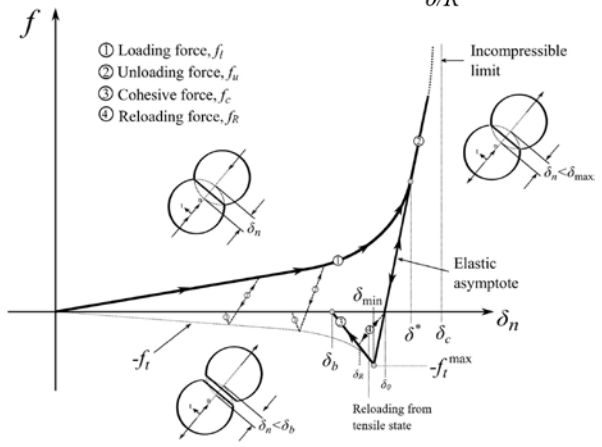

INCLUDES COHESION → STRENGTH

1) **Small deformation regime** - contacts are independent from others
2) **Contact interaction regime** – each contact "feels" the presence of its neighbors
3) **Low compressibility regime** – where the porosity closing locally and elasticity dominates

$$y_n = \beta_0 + \sum_{i=1}^{m} \beta_i x_i + \sum_{i=1}^{m} \beta_i^2 x_i^2 + \sum_{i<j} \sum \beta_{ij} x_i x_j$$

F-δ law – Model parameter identification

x_m, $m=1..M$ model parameters that needs to be identified,

$y_n(x_m)$, $n=1..N$ model response variables that we are interested in and

$y_n^*, n = 1..N$ experimental observations.

In traditional non numerical models we choose x_m so that $|y_n(x_m)-y_n^*|$ is minimum

DEM: $y_n(x_m)$ is the output of the DEM simulations
Numerous DEM simulations are needed in a problem where M is LARGE!

Instead approximate the DEM response $y_n = \beta_0 + \sum_{i=1}^{m} \beta_i x_i + \sum_{i=1}^{m} \beta_i^2 x_i^2 + \sum_{i<j} \sum \beta_{ij} x_i x_j$

By identifying β's with a limited number of simulations and then extract the model parameters using the analytical expression for y_n

Example: single material

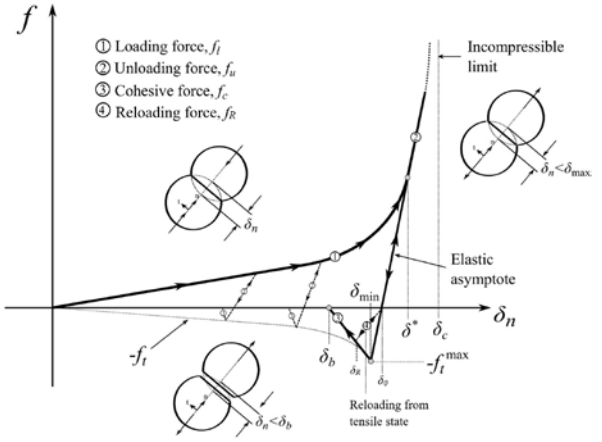

EXPERIMENT 1: Compaction in instrumented die

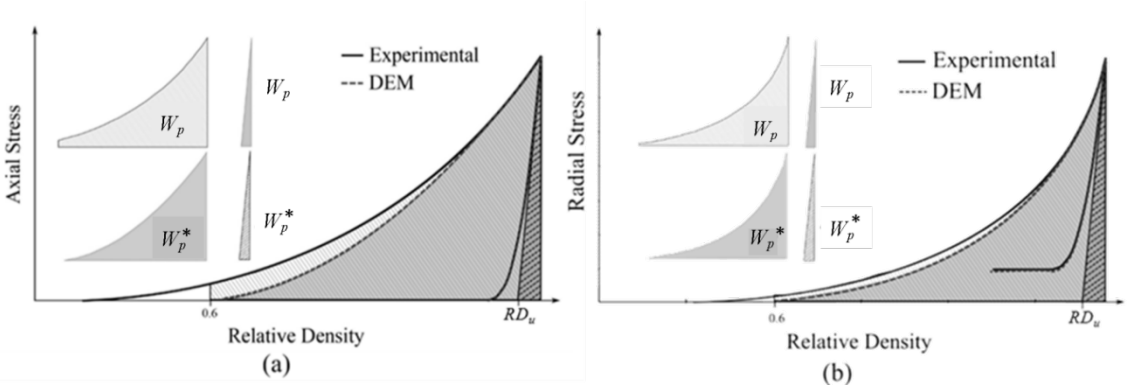

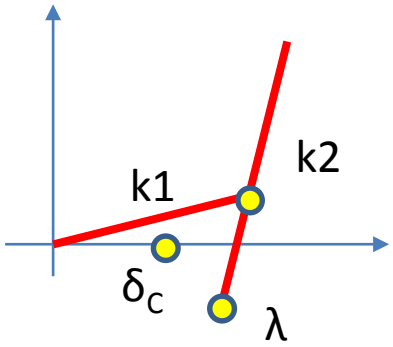

\+ μ

EXPERIMENTS 2: Diametrical tension test – 3 Densities

Material A

k_1 [kN/m]	$\hat{k}_2/k_1$	θ	μ	λ	δ_C
35.1	37.1	0.323	0.21	0.187	0.895

Material A+ 0.5% MgSt

k_1 [kN/m]	$\hat{k}_2/k_1$	θ	μ	λ	δ_C
33.5	31.7	0.301	0.094	0.061	0.930

Predictions well: Radial stresses to be lower with lubricant
Axial expansion to be higher with lubricant

Underestimates: Axial expansion in magnitude.

WHAT DETERMINES THE STRENGTH OF COMPACTS

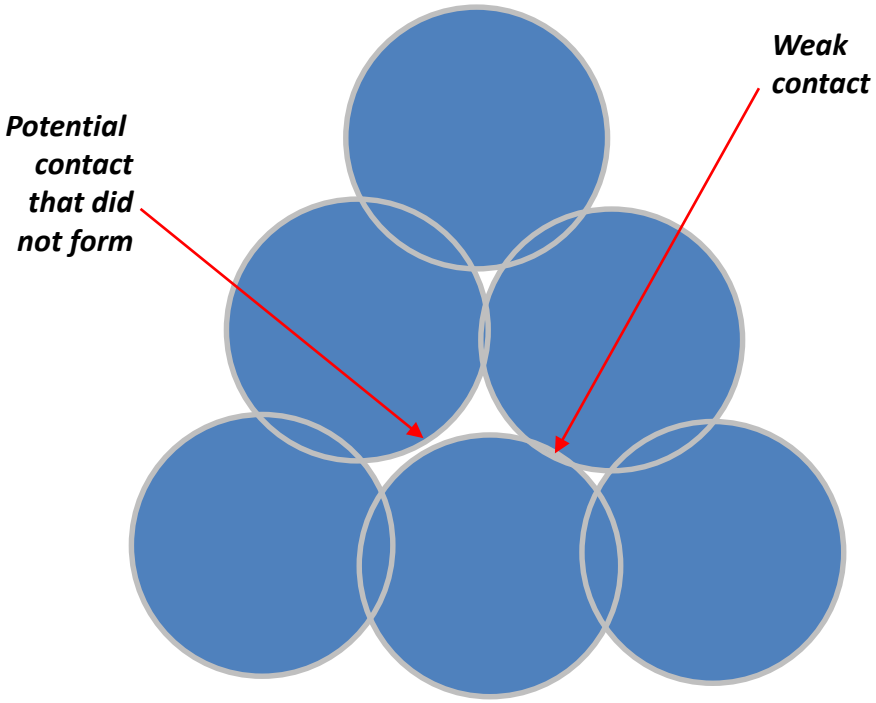

- Contacts that did not form
- Weak contacts pressed at F << average force
- Broken contacts (during unloading)

5% Cohesion Damage Visualization

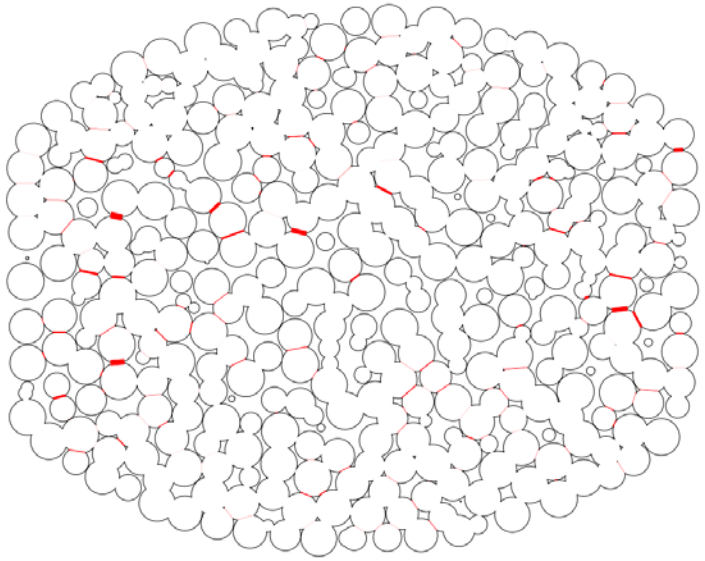

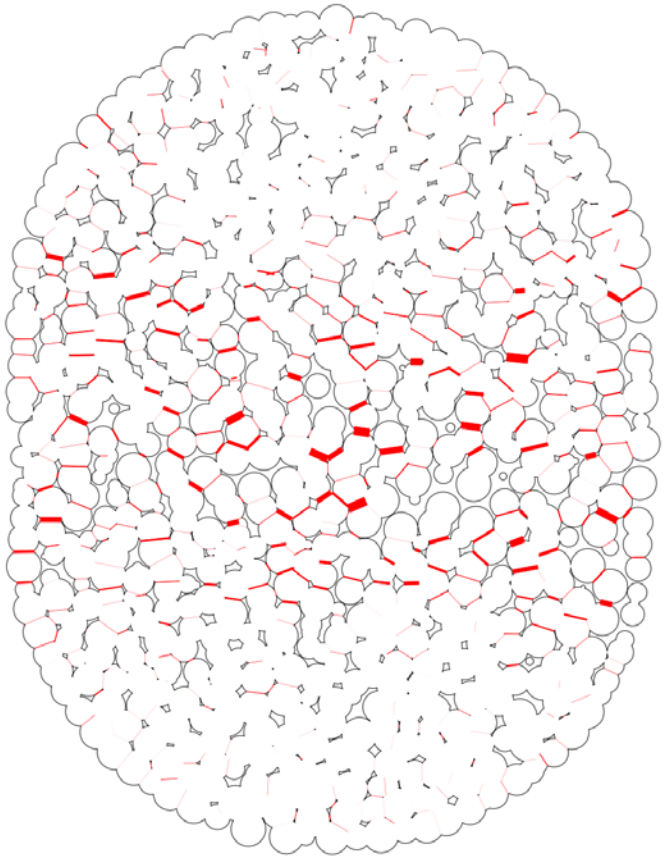

“Connected damage”

Mixtures

Material A

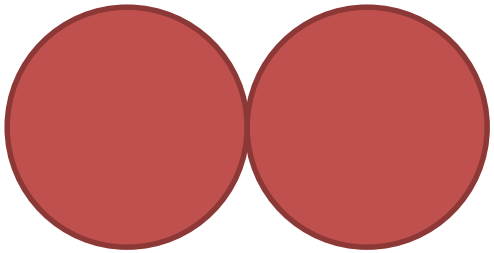

Property AA

Material B

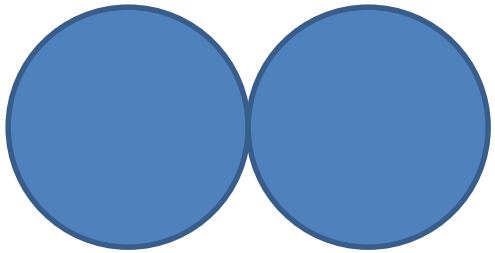

Property BB

Mixture A+B

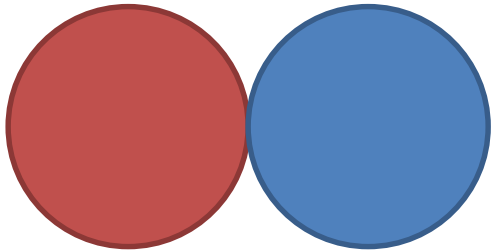

Property AB = ?

Properties AA and BB from individual materials

Properties AB:

- compaction – from model (heavily dominated by softer material, most of the times)
- unloading – from model (dominated by softer material)
- interparticle friction and strength → unknown

Mixtures of particles with different elastic moduli

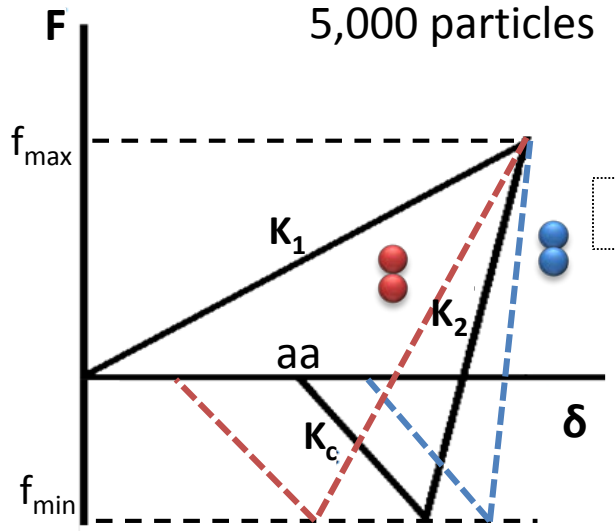

5,000 particles

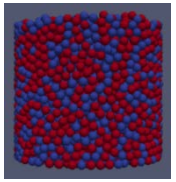

$$E^* = f_A E_A + f_B E_B$$

f_A – fraction of material A
E_A – Elastic modulus of A
f_B – fraction of material B
E_B – Elastic modulus of B

k_c/k_1 = 0.1 → Elastic modulus, E = 2 GPa

E* **was kept constant**

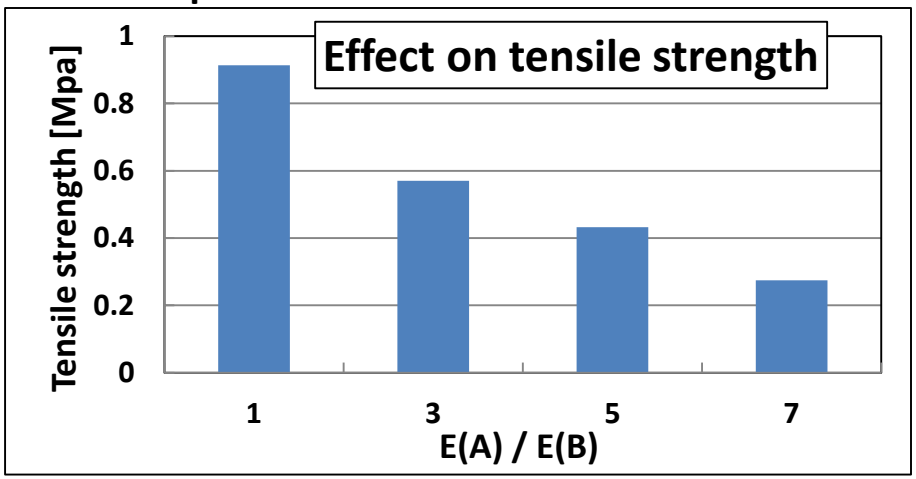

Property	Material A	Material B
Yield Strength [MPa]	25	25
	Changing	
Ratio of loading to unloading stiffness, k_2/k_1	75	25
Ratio of loading to cohesion stiffness, k_c/k_1	0.1	0.1
$\Lambda = f_{min}/f_{max}$	0.035	0.035
Adhesion factor, aa	0.6	0.6

- **After ejection, the stiffer phase will experience tensile residual stresses, which scale with increase in moduli difference**

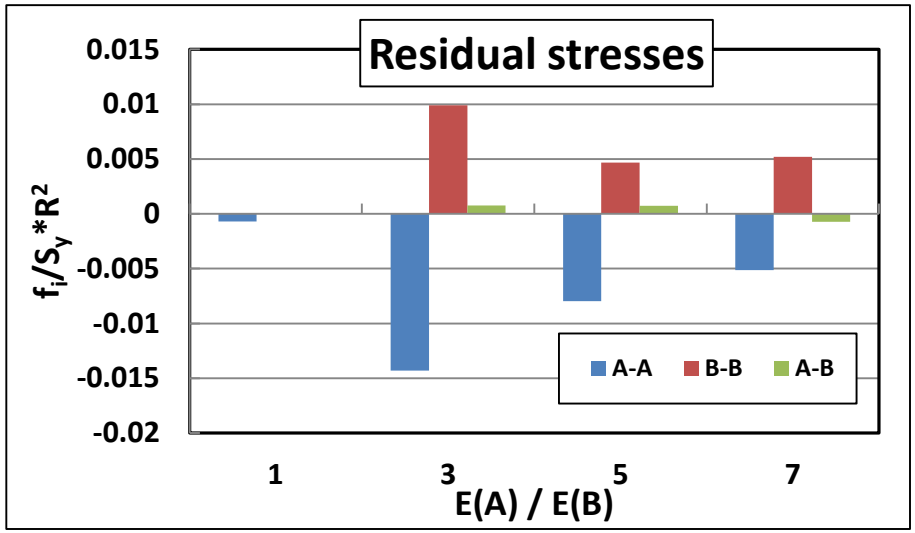

Current Status

- Damage definition and visualization
- We have explored the predictions of the single material model with an without lubricant
- Developed a setup for calibration of the two-material model
- Parametric studies have shown the importance of residual stresses

Work Ahead

- Model parameter identification for mixtures
- Residual stresses experimental work
- Damage assessment and propensity for failure
- Identify weaknesses of the current model/approach

IFPRI AGM 2017

From powders to solids

Antonios Zavaliangos
Department of Materials Science and Engineering
Drexel Univer

Outline

- Few words about Drexel University
  (if you don’t praise your house it will fall on your head)
- Some titbits from the history of powder technology at Drexel
- Recent work on powder consolidation
- Some ideas for the future

Drexel?

Anthony Joseph Drexel, Sr. (1826-1893)

- Son of Austrian immigrant
- An banker
- Played a major role in the rise of modern global finance.
- Founded Drexel, Morgan & Co (later J.P. Morgan & Co.) in New York in 1871 with J.P. Morgan as his junior partner.
- Founded Drexel University in 1891

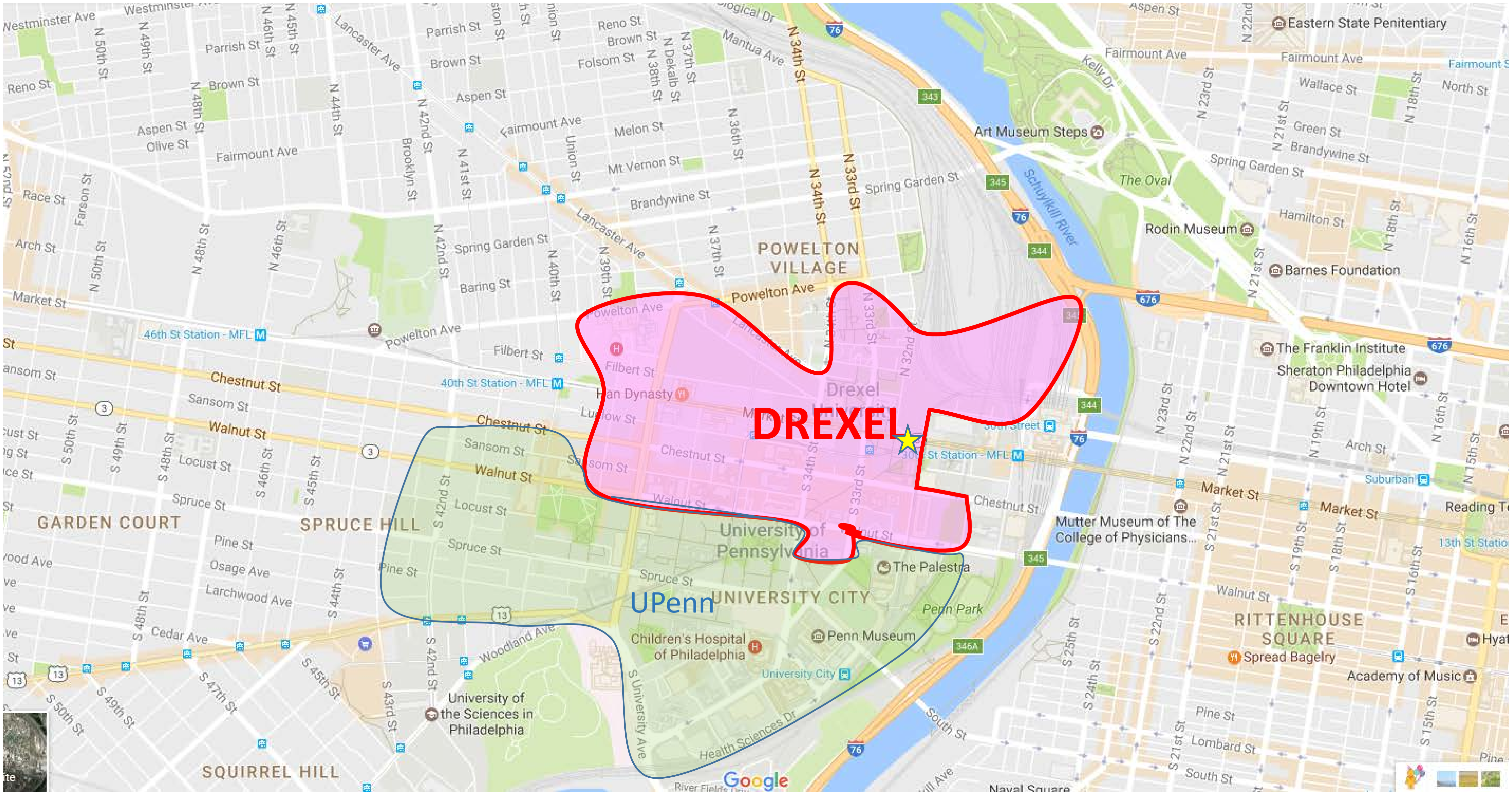
DREXEL
UPenn
Drexel
University of Pennsylvania
POWELTON VILLAGE
UNIVERSITY CITY
GARDEN COURT
SPRUCE HILL
SQUIRREL HILL
RITTENHOUSE SQUARE
Schuylkill River
Eastern State Penitentiary
Art Museum Steps
The Oval
Rodin Museum
Barnes Foundation
The Franklin Institute
Sheraton Philadelphia Downtown Hotel
Mutter Museum of The College of Physicians...
The Palestra
Penn Park
Penn Museum
Children's Hospital of Philadelphia
University of the Sciences in Philadelphia
Spread Bagelry
Academy of Music
Han Dynasty
46th St Station - MFL
40th St Station - MFL
30th St Station - MFL
30th Street
Suburban
13th St Station
University City
Market St
Chestnut St
Walnut St
Sansom St
Spruce St
Locust St
Pine St
Powelton Ave
Lancaster Ave
Spring Garden St
Fairmount Ave
Baltimore Ave
Woodland Ave
South St
Health Sciences Dr
Google

- 1891 Drexel Institute of Art, Science and Industry
  - Department of Domestic Economy (Now Westphal College of Media Arts and Design)
  - Business Department (now LeBow College of Business)
  - Business Department (now College of Computing and Informatics)
  - Scientific Department and Department of Mechanic Arts (now College of Engineering)
  - Department of Lectures and Evening Classes (now Goodwin College of Professional Studies)
  - Art Department
- 1931 Renamed to Drexel Institute of Technology
- 1970 Drexel University - Humanities and Technology Program (now College of Arts and Sciences)
- 2002 Drexel acquired/merged with MCP Hahnemann University (founded in 1850 as **Woman's Medical College of Pennsylvania**) to create the **Drexel University College of Medicine**
- 2006, Established the Thomas R. Kline School of Law
- 2011 Drexel acquired The Academy of Natural Sciences.

Academy of Natural Sciences of Drexel University

- **Founded in 1812, it is the oldest natural science research institution and museum in the New World.**
- **Biological taxonomy & Biological systematics**
- **Patrick Center for Environmental Research**
- **17 million biological specimens**
- **Including the** Lewis and Clark Herbarium, (all the botanical specimens the Lewis and Clark Expedition)

Fast Facts

Enrollment

- **24,232** total students
- 15,499 undergraduate students
- 8,733 graduate and professional students
- 4,868 online students

Academic Offerings

- Over 200 degree programs
- 15 colleges and schools

Drexel Co-op

- One of the nation's oldest, largest, and best-known cooperative education programs

Test drive your career with cooperative education

Three Co-op Option (Five Years)

	fall	winter	spring	summer
Year one	●	●	●	♦
Year two	●	●	■	■
Year three	●	●	■	■
Year four	●	●	■	■
Year five	●	●	●	

10,000 students are placed in co-op jobs per year in 2x6-month cycles (Fall/Winter-Spring Summer)

Engineering placement is 97% (92-95% paid 2007-2012 data)

Drexel Materials Coop Employers

The irrelevant fact of the day: GPA vs Coop Salary

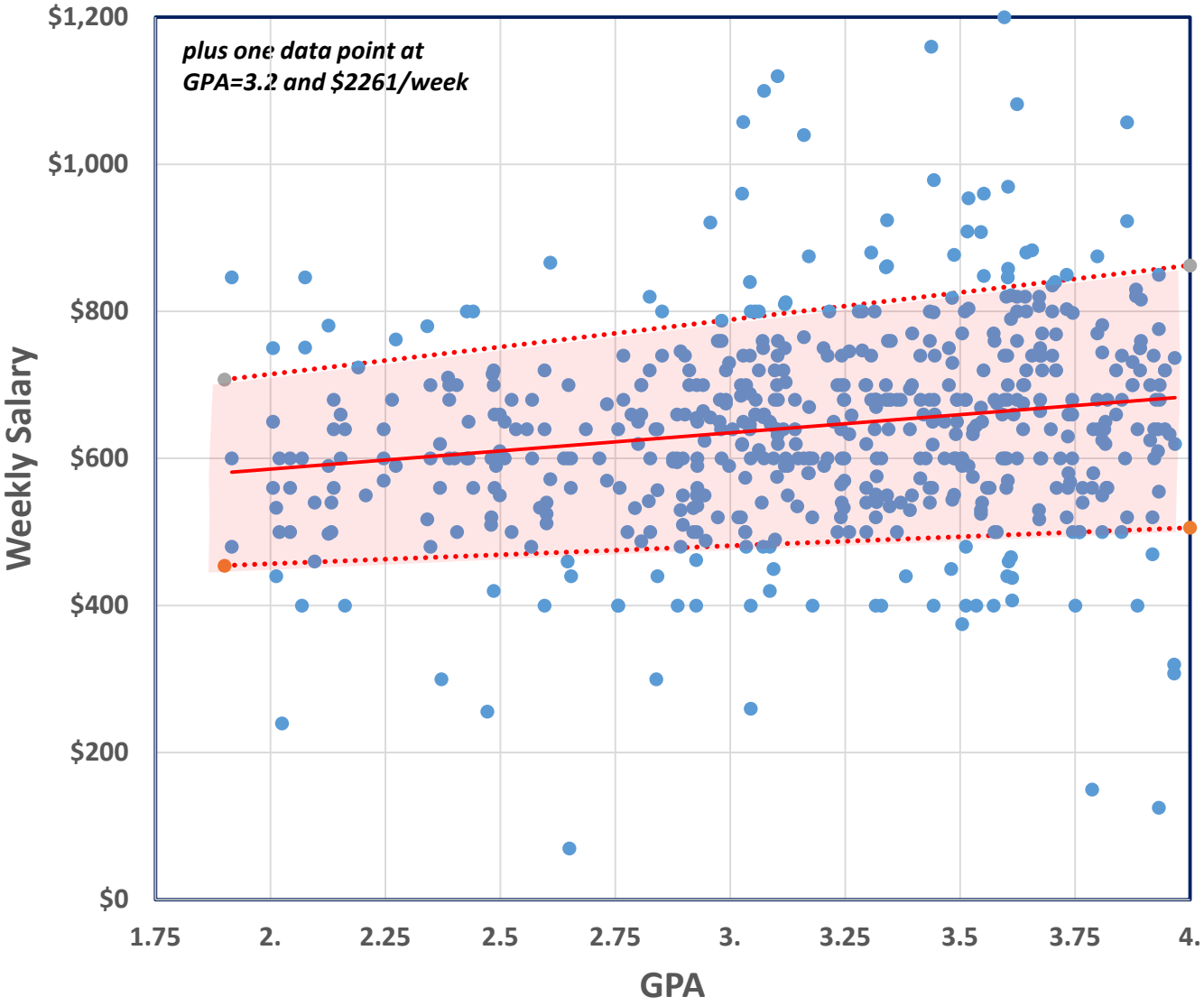

There is a weak correlation

Significant variability (95% CI shown)

Highest values for those with
GPA 3-3.8

Some very low compensation for people across the GPA range (Communications skills? Overall personality?)

Average annual increase 1.2%

Data from 2000-2013 Materials Science and Engineering

A “historical” connection with fine powder at (or actually near) Drexel

What is Combustible Dust?

Agricultural Products			Chemical Dusts	
Egg white	Cottonseed	Soybean dust	Adipic acid	Epoxy resin
Milk, powdered	Garlic powder	Spice dust	Anthraquinone	Melamine resin
Milk, nonfat, dry	Gluten	Spice [illegible]	Ascorbic acid	Melamine, molded (phenol-cellulose)
Soy flour	[illegible] dust	Sugar	[illegible]	Melamine, molded [illegible] flour and [illegible] filled phenol-formaldehyde]
Starch, corn	[illegible]	[illegible]	[illegible]	[illegible]
Starch, rice	[illegible]	[illegible]	[illegible]	[illegible]
Starch, wheat	[illegible]	[illegible]	[illegible]	[illegible]
Sugar, [illegible]	[illegible]	[illegible]	[illegible]	[illegible] acrylate, [illegible]
Wheat [illegible]	[illegible]	[illegible]	[illegible]	[illegible]
[illegible]	[illegible]	[illegible]	[illegible]	[illegible]
Apple	[illegible]	[illegible]	[illegible]	[illegible] copolymer
Beet [illegible]	[illegible]	[illegible]	[illegible]	[illegible] alcohol
[illegible]	[illegible]	[illegible]	[illegible]	[illegible]
Carrot	[illegible]	[illegible]	[illegible]	[illegible] vinyl chloride/ [illegible]ene/vinyl acetylene suspension copolymer
Cocoa bean [illegible]	[illegible]	[illegible]	[illegible]	[illegible]
Cocoa powder	[illegible]	[illegible]	[illegible]	[illegible]
Coconut shell dust	[illegible]	[illegible]	[illegible]	[illegible]
Coffee dust	Rice flour	Cellulose [illegible]	[illegible]lyl) Acrylamide	(poly) Vinyl chloride/ vinyl acetylene emulsion copolymer
Corn meal	Rice starch	Cellulose [illegible]	[illegible]lyl) Acrylonitrile	
Cornstarch	Rye flour	Cork	(poly) Ethylene (low-pressure process)	
Cotton	Semolina	Corn		

Combustible dusts are fine particles that present an explosion hazard when suspended in air in certain conditions.

Source: OSHA Fact Sheet.

Combustible Dust Webinar
March 2015 - Woodworkingnetwork.com

Woodworking Network

GreCon

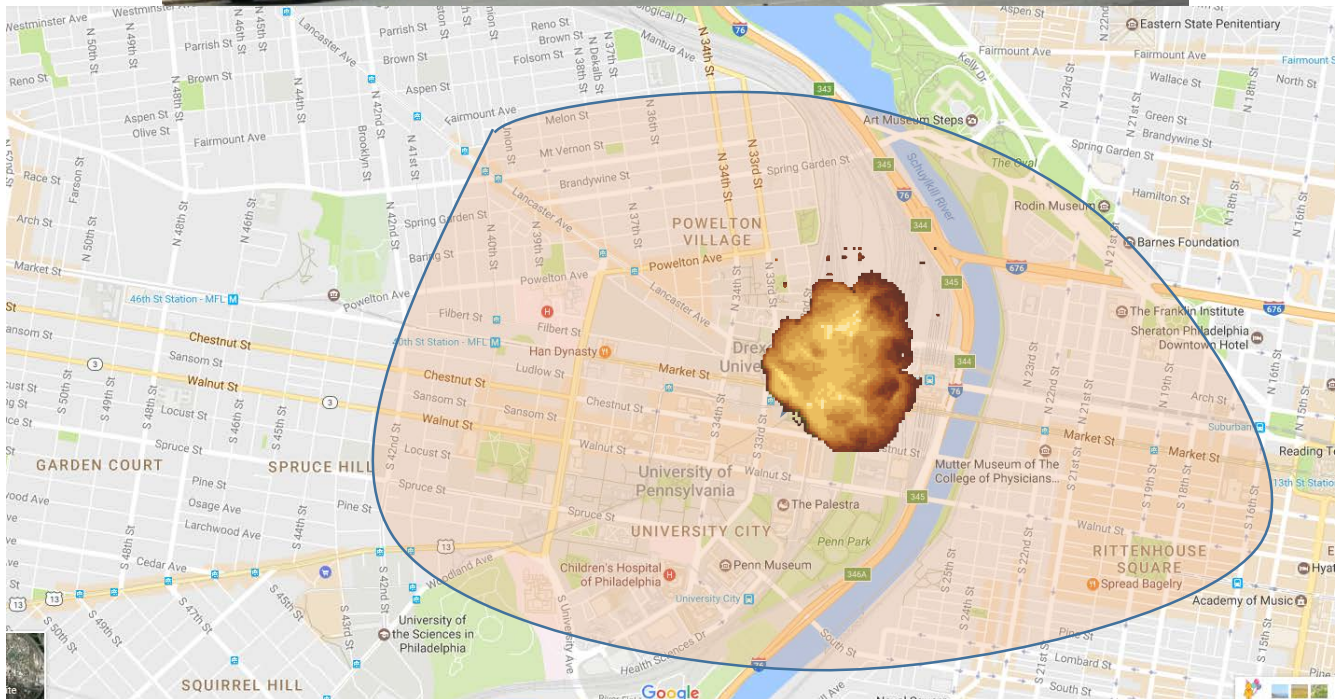

Powder explosion:
Tidewater corn elevator (1956)

- Tidewater Grain Company: Mill and Grain Elevator complex.
- On the east side of the Pennsylvania Railroad High Line
- 6 5-story corrugated iron, brick and concrete grain elevators built in 1860.
- 8 PM, 3/28/1956, an explosion ripped one of the grain silos → a major fire and collapse.
- 2 employees killed
- Severe damage to
  - Philadelphia Bulletin building
  - Railway Express Agency building
  - Drexel Institute of Technology (now Drexel University),
  - United States Post Office Building,
  - Pennsylvania Railroad 30th Street Station, and Abbotts Dairies.
  - Damage from 15th to 43rd Streets, and from Aspen to South
- initial estimate of the damage was several million dollars

Research in Powder Technology at Drexel University: Early 1960s

THE HECKEL PLOT

- A relation between relative density and applied axial stress in die compaction. Slope “correlates” to material yield strength
- R.W. Heckel, *Trans. AIME,* Vol 221, 1961, p 1001-1008
- Dick Heckel 1960-71: Professor,
  Drexel U., Materials Eng. (passed away in 2010)

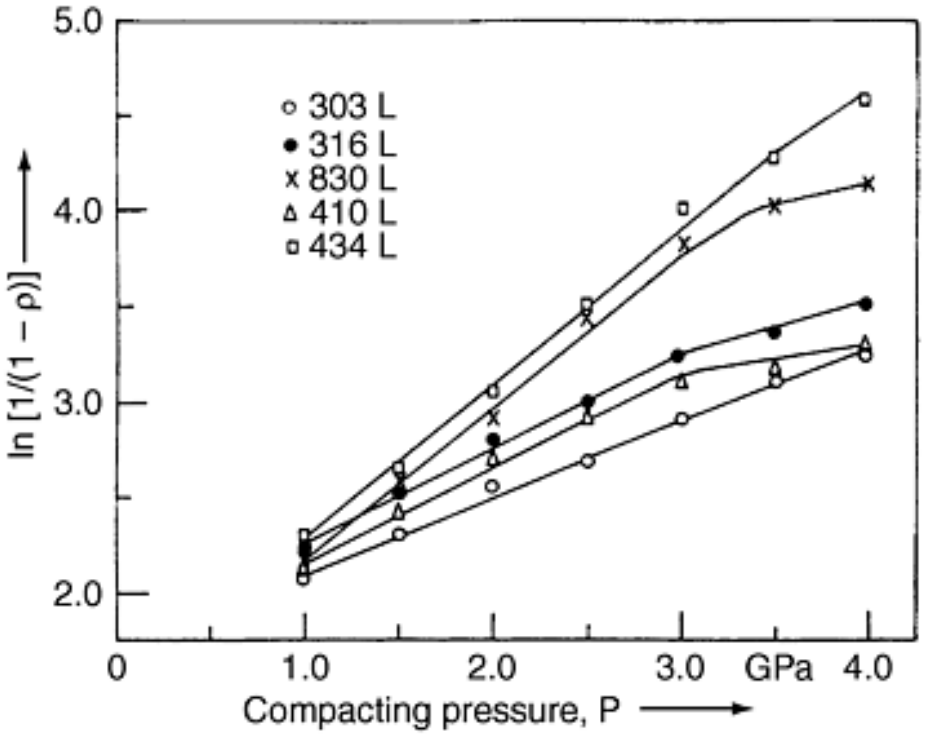

Various types of behavior, not clear association with material behavior

From powder to solids at Drexel 1970-1980

- DoD funded work in explosives (Project Themis) sparked interest in powder metallurgy
- Components from implantable devices (1970)
- Powder Forging (1972)
- One of the first model for porous material (Kuhn and Downey) (1973)
- Metal Matrix Composites by powder compaction and sintering (1978)
- Elemental Power Metallurgy (A+B mixed and pressed before sintering rather than A-B alloy which is usually harder)

Path Dependence

Density does not correspond 1-to-1 to properties

- **Density alone does not determine strength**
- **The mode of compaction affects compact microstructure**

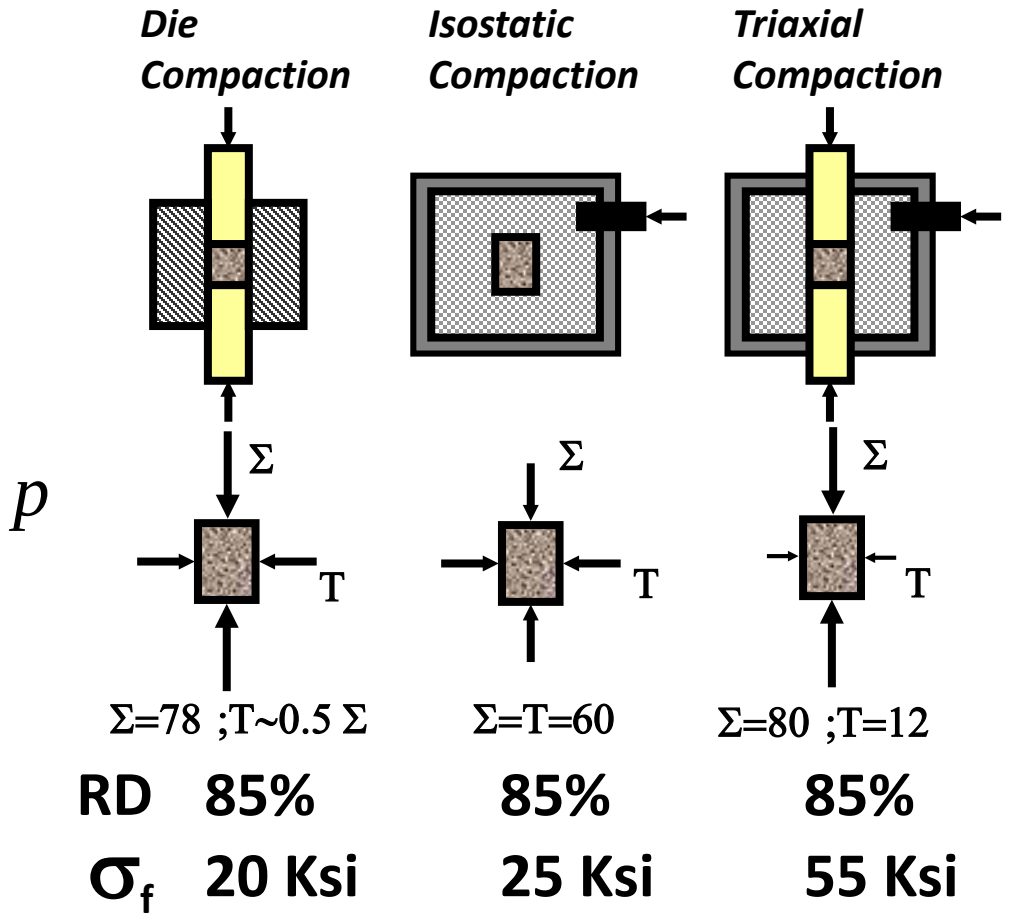

(R. KOERNER Drexel University 1972)

Strength in Die ≠ Isostatic ≠ Triaxial Compaction

Path Dependence
Triaxial Testing

- **A triaxial testing machine was designed at Merck**
  - **400 MPa** maximum cell pressure
  - **50 kN** maximum axial force
    - Compressive only
  - **50 mm** axial travel
  - Cell dimensions
    - 37.5 mm bore

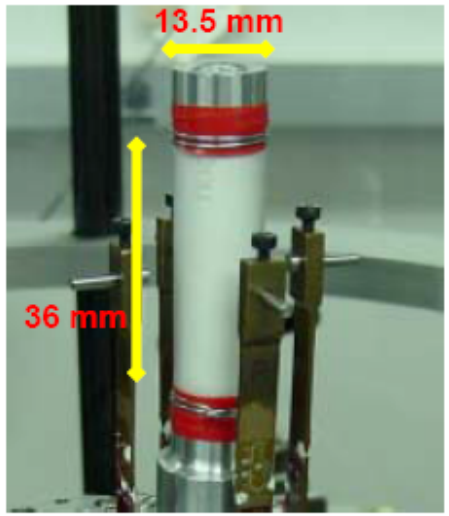

- **0.5 mm rubber sleeve**
- **Contact extensometer**
  - Travels with specimen
  - 32 mm across with pins

- **A-Tab**, **a ceramic, was selected as a model material**

A-Tab
Dibasic Calcium Phosphate
Av. Part. Size 180 microns

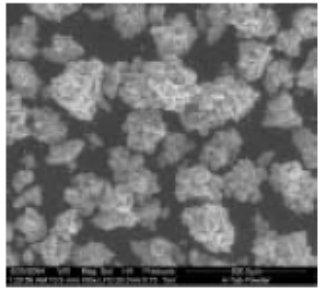

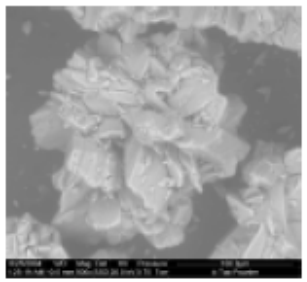

Dibasic Calcium Phosphate (A-Tab)
Av. Part. Size 180 microns

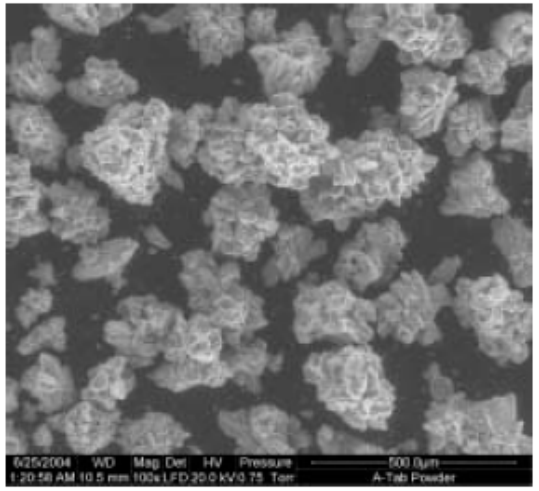

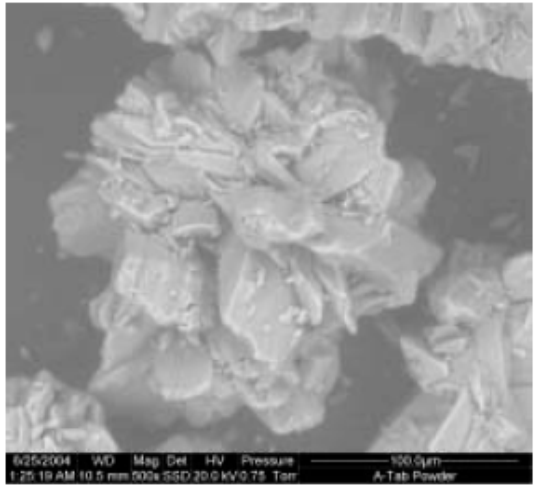

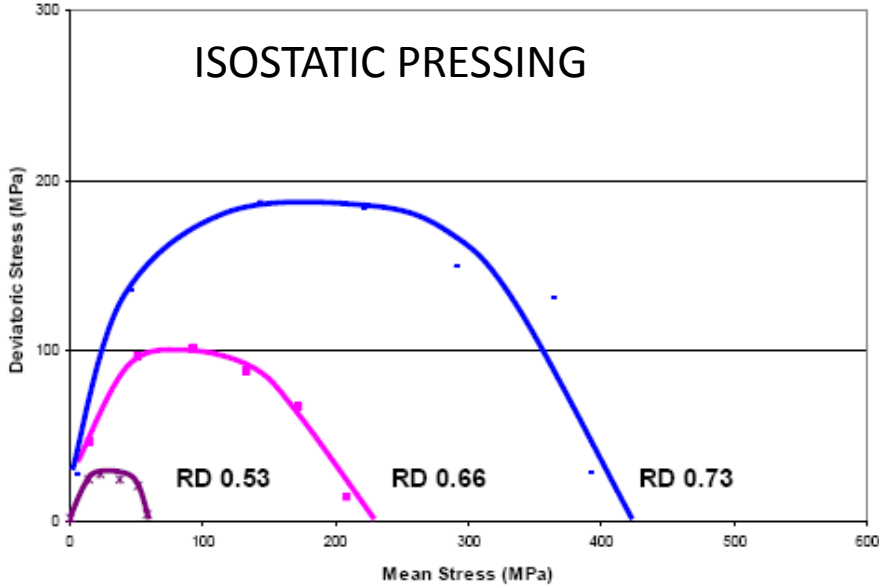

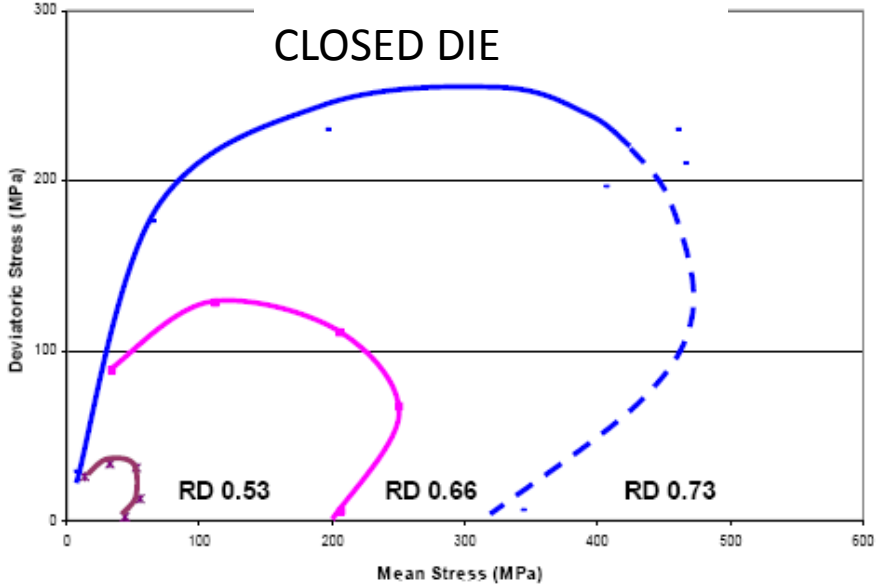

Yield locus depends on the stress path that produces the specific relative density

Path dependence RD=0.66

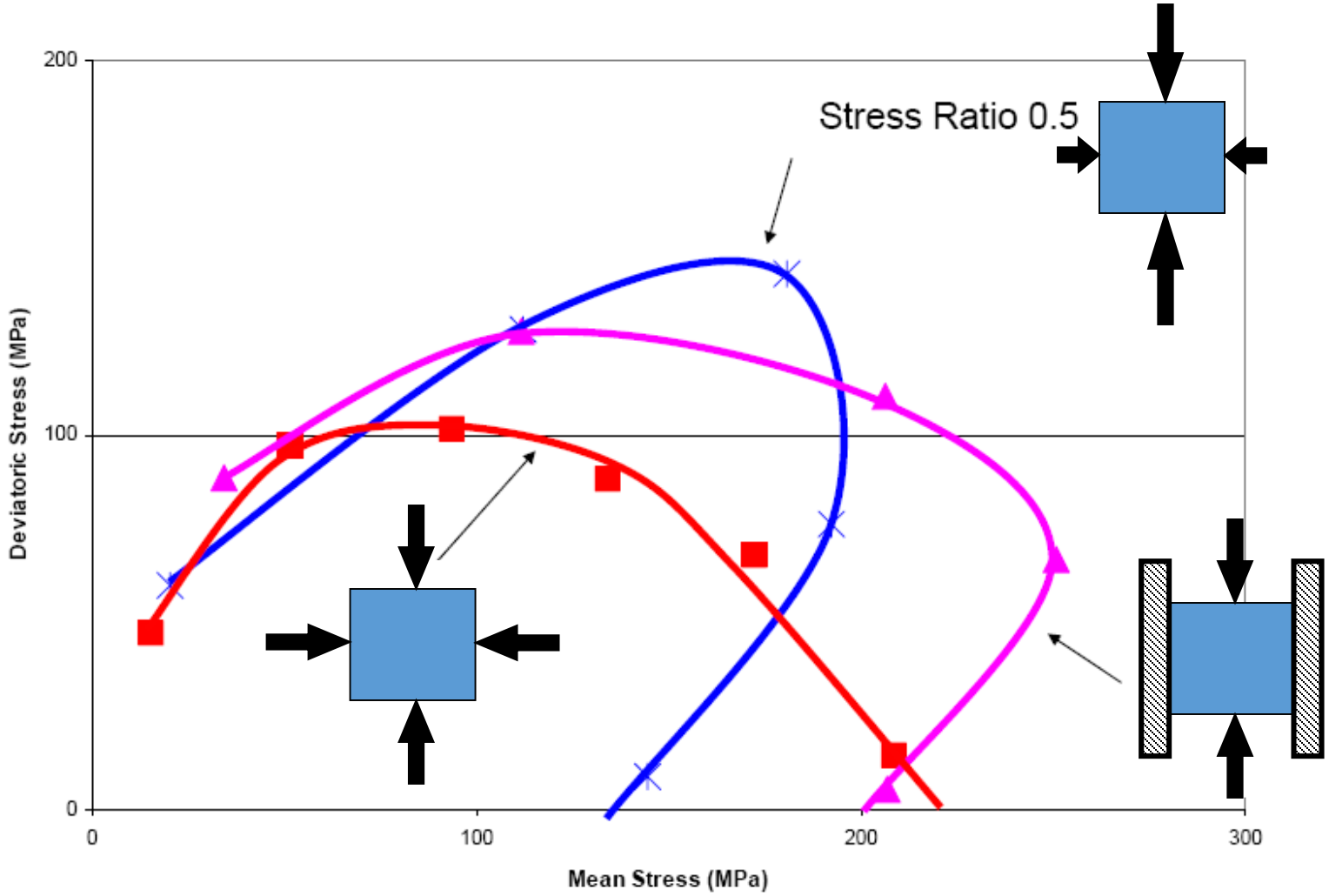

Post Compaction Strength

EXPERIMENTAL

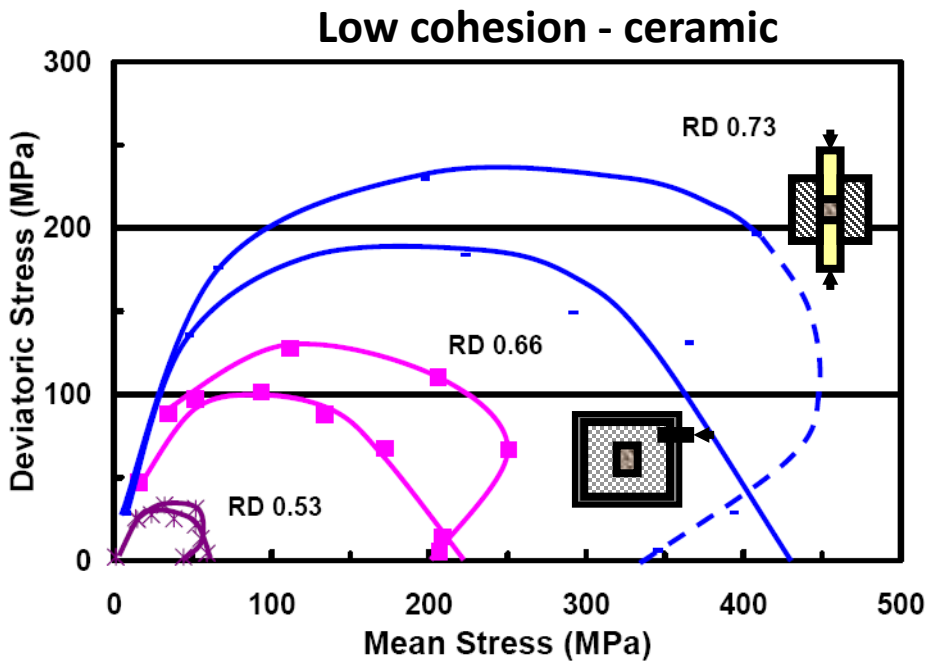

MPFEM

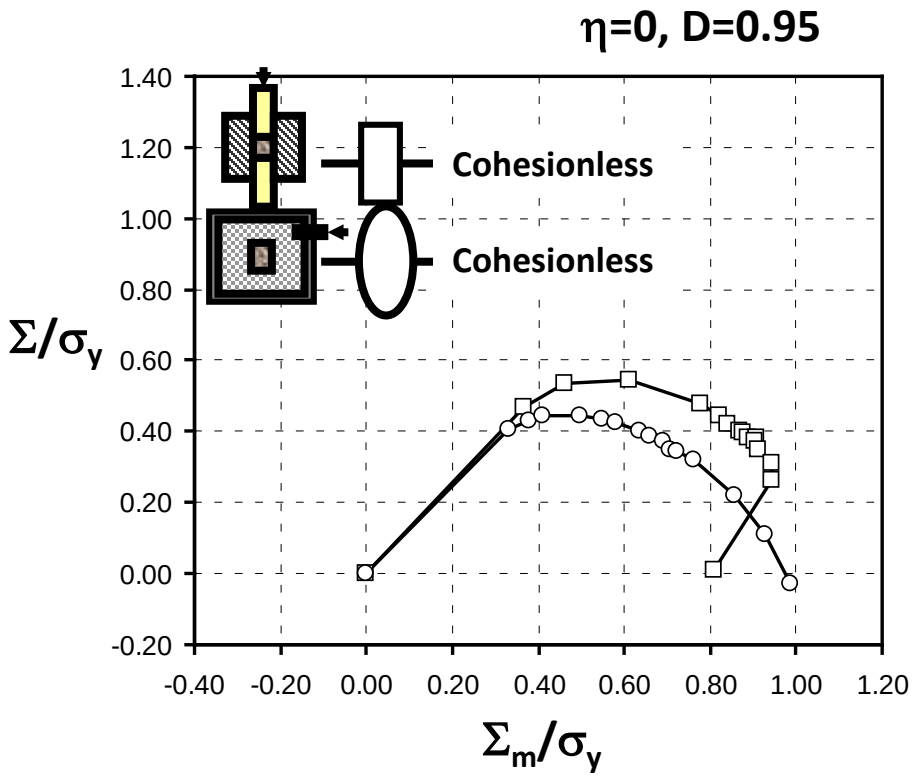

Steve Galen PhD 2004 (Drexel University)

Path dependence is an open topic

Model based optimization of processing 1980-90

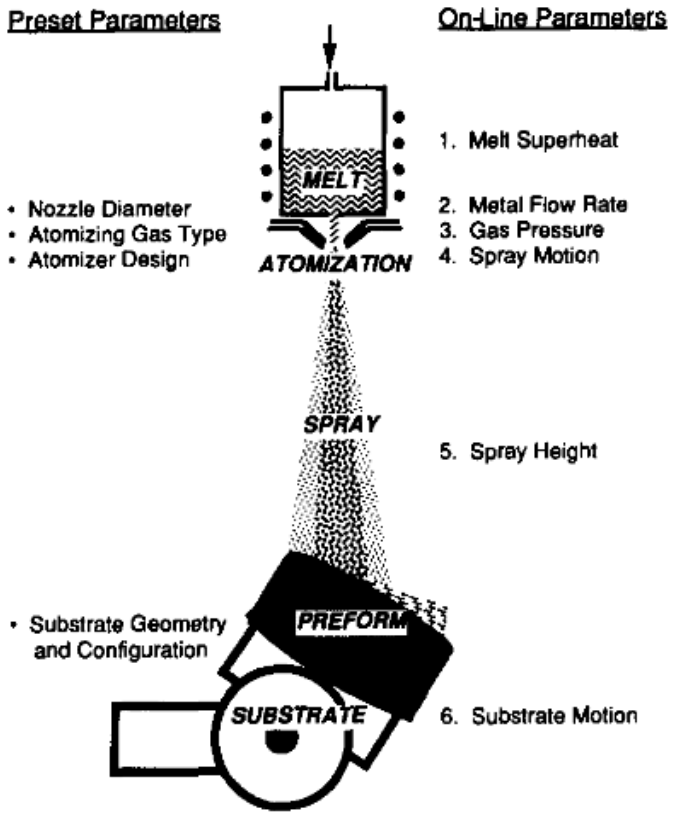

Fig. 1. Schematic diagram of the Osprey™ spray-casting process showing the formation of a disk or billet, and the process parameters which can be manipulated to optimize preform shape, structure and yield.

several independent process parameters on preform integrity, namely (i) melt superheat (typical range 10–200 °C) (ii) metal flow rate

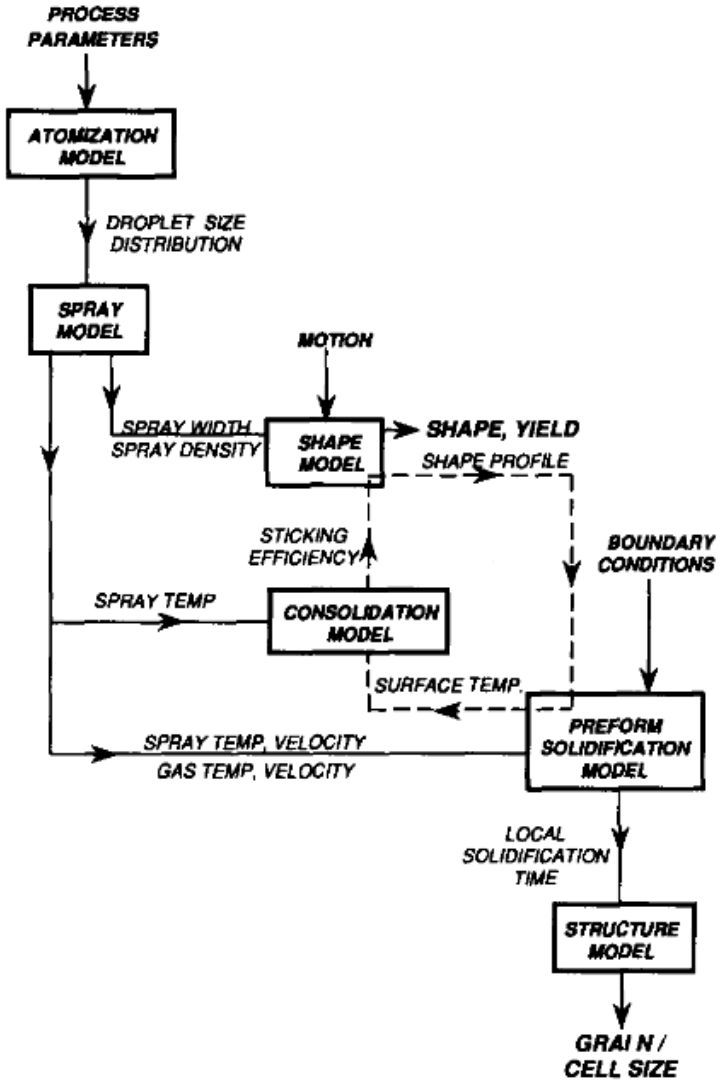

Fig. 2. Flow chart of the integral model for spray deposition.

Mix of fundamental and semiempirical components in the model allows for the optimization of

- **Shape**
- **Microstructure &**
- **Properties**

of the final product

SEMISOLID PROCESSING

Alloys with a dendrite-free microstructure exhibit thixotropy and low viscosity upon shearing in the semisolid range and are formable to complex shapes

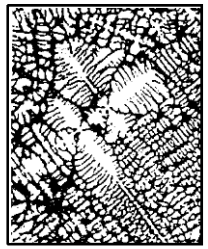

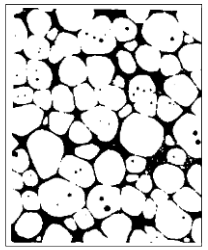

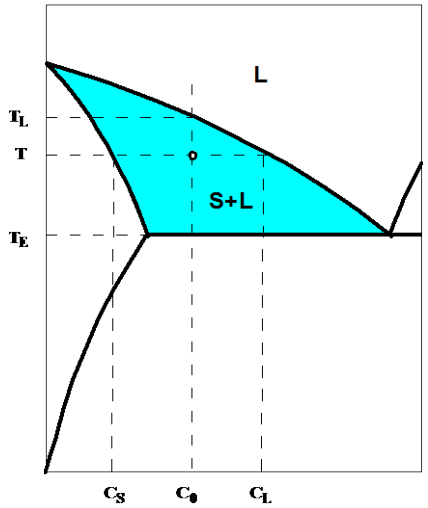

GEOMETRY

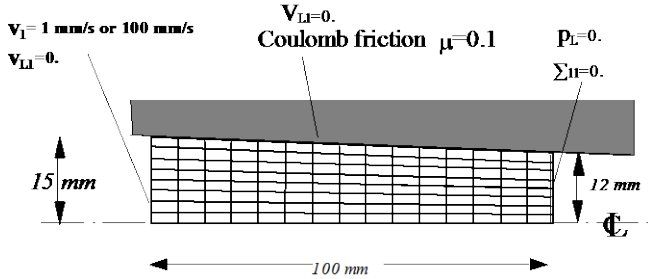

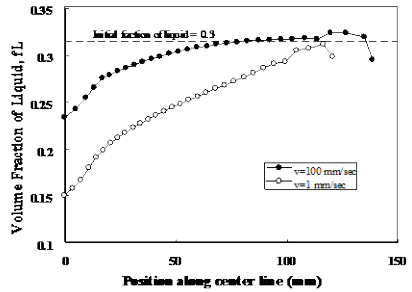

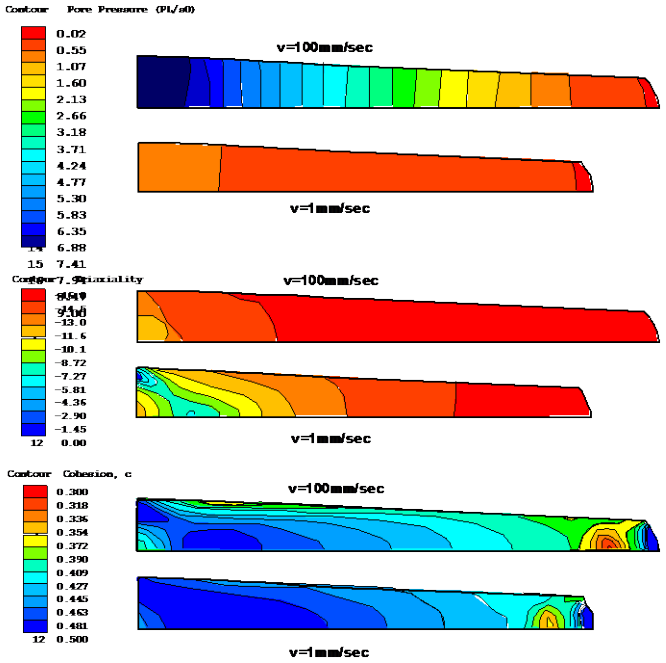

Zavaliangos A., "Modeling of the Mechanical Behavior of Semisolid Metallic Alloys at High Volume Fractions of Solid", *Int. J. Mechanical Science,* **40**, 10, pp. 1029-1041, 1999

Tzimas E., & **Zavaliangos A.**, **"**The Mechanical Behavior of Semisolid Alloys with Equiaxed Microstructure at High Volume Fraction of Solid", *Acta Met.& Materialia,* **47**, 2, pp. 517-528, 1999.

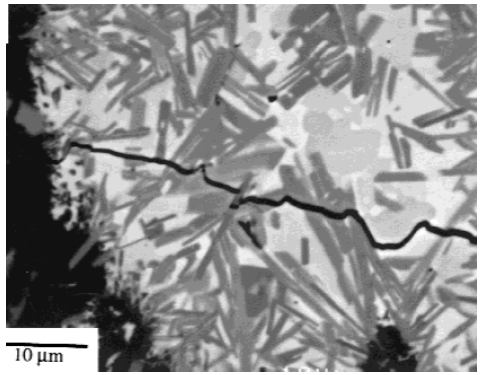

REACTIVE SINTERING

Transient Plastic Phase Sintering is a reactive sintering technique that uses a transient "soft" phase to densify a powder mixture and create in-situ monolithic of composite materials that are difficult to process directly

(effort led by Prof M. Barsoum - contributions in particulate processing and mechanical properties)

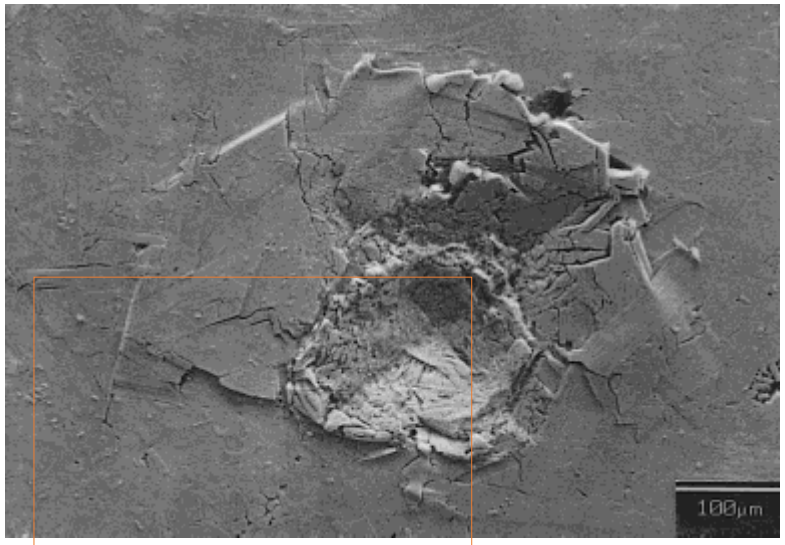

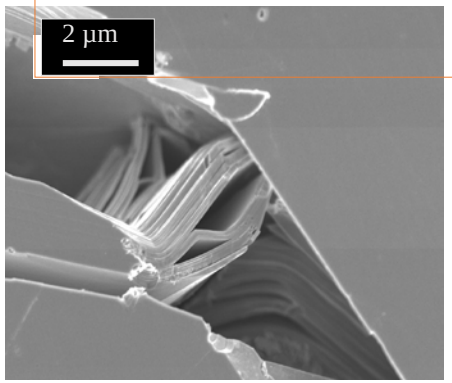

El-Raghy T., Barsoum M., **Zavaliangos A.**, and Kalidindi S., "The Mechanical Properties of Ti3SiC2: Effect of Grain Size and Temperature", *Journal of the American Ceramic Society*, **82**, 3, pp. 665-72, March 1999

El-Raghy T., **Zavaliangos A.**, Barsoum M., Kalidindi S., "Observations of Damage Mechanisms Around Indentations on Ti3SiC2", *Journal of the American Ceramics Society*, **80**, pp. 513-516, 1997.

Sintering under Electrical Current

Fully Coupled modeling of thermal, electrical and sintering problems in this promising technology that is capable of densifying nanocrystalline materials and maintain the nanosize of the microstructure

(Collaborative effort: Joanna Groza UCDavis – Experiments)

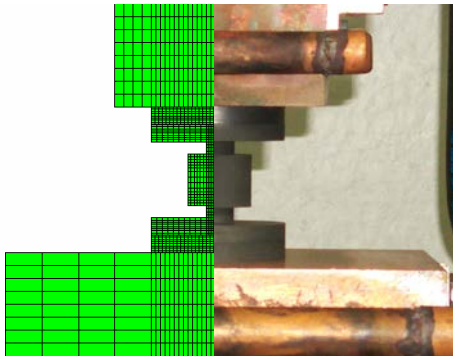

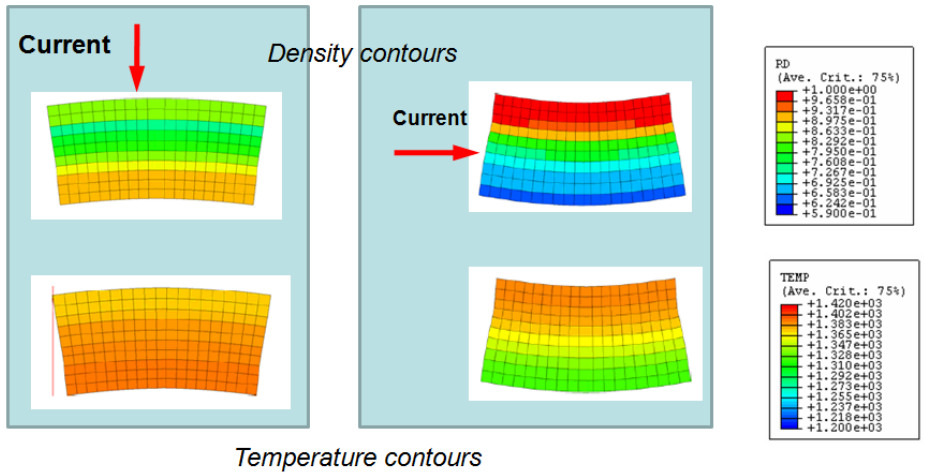

Temperature contours

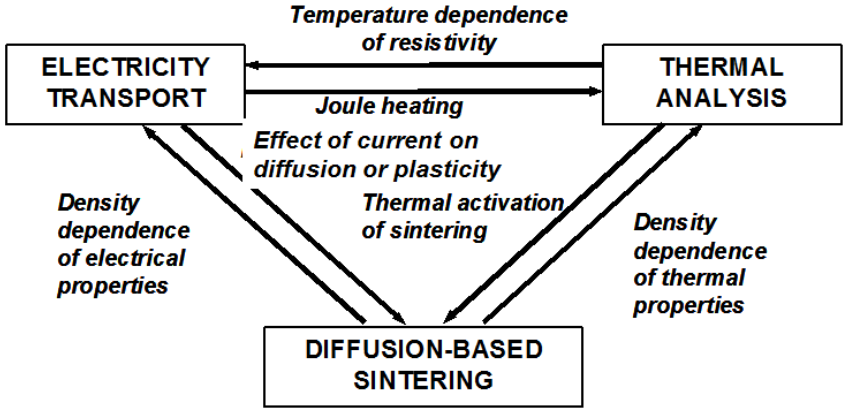

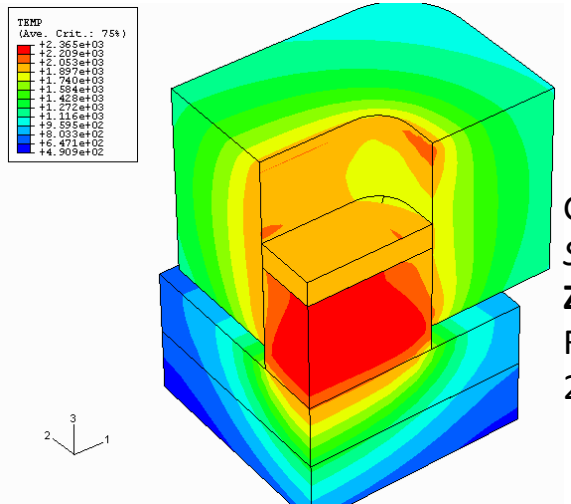

Groza J., and **Zavaliangos A.**, **"**Sintering Activation by External Electrical Field", *Materials Science and Engineering A,* **287**, 2, pp. 171-177, 2000

Zavaliangos A., Zhang J., Martin Kramer, and Groza J. "Temperature Evolution during Field Activated Sintering", *Materials Science and Engineering A,* Vol 379/1-2 pp 218-228., 2004

EXAMPLE 1

- The effect of tools/tablet friction on the distribution of density of tablets and its implications for post compaction properties

Show the differences between two
tablets of identical geometry and average density
under two extreme conditions:

1) **High tool lubrication by precompacting a MgSt "tablet" before the actual compaction**
2) **High friction – clean tools with solvent before compaction**

Cunningham J., C. I. Sinka, and Zavaliangos A. "Analysis of Tablet Compaction. Part 1 – Characterization of Mechanical Behavior of Powder and Powder/Tooling Friction", Journal of Pharmaceutical Sciences, Vol. 93, No 8, Date: August 2004, Pages: 2022-2039

C. I. Sinka, Cunningham J., and Zavaliangos A. "Analysis of tablet compaction. Part 2 – Finite element analysis of density distributions in convex tablets", *Journal of Pharmaceutical Sciences*, Vol. 93, No 8, Date: August 2004, Pages: 2040-2053

VALIDATION

“High” friction
die cleaned by alcohol
before experiment

“Low” friction
MgSt “tablet” compacted
before experiment

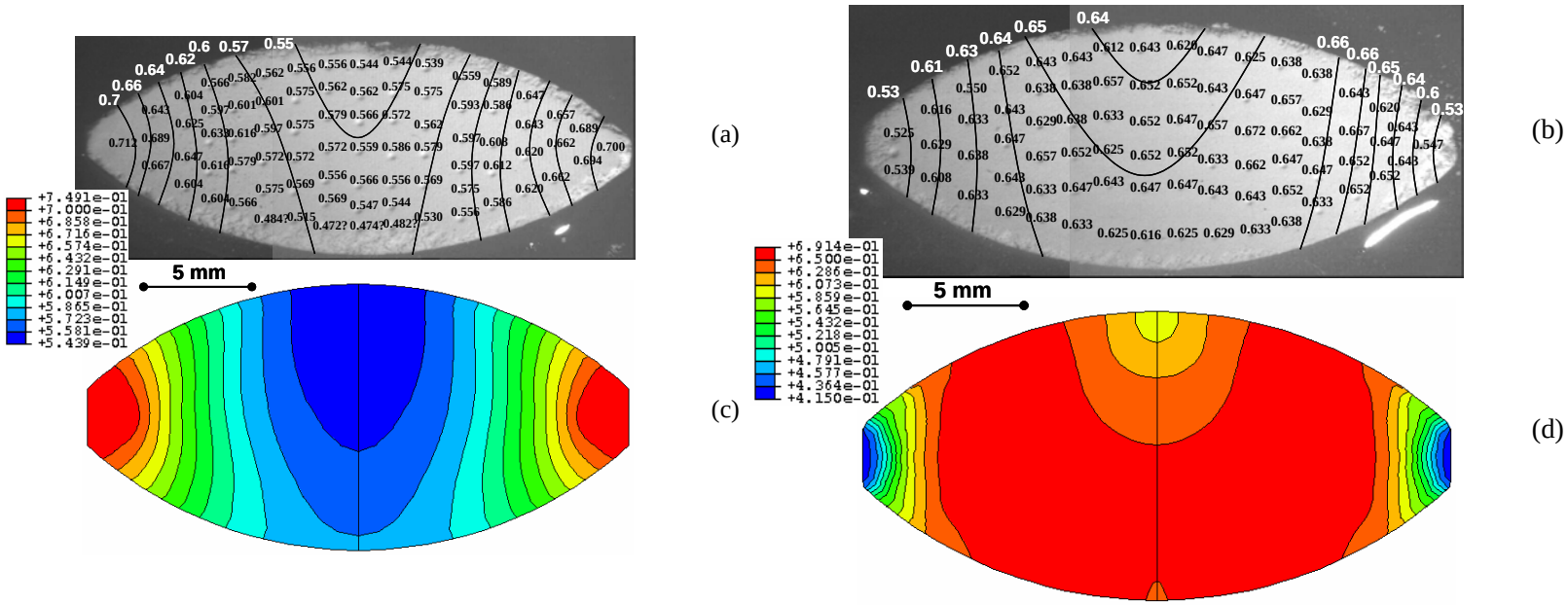

Radial distribution of porosity is completely inverted simply by changing the wall friction conditions

Important implications for strength, dissolution and drug availability

C. I. Sinka, Cunningham J., and Zavaliangos A. “Analysis of tablet compaction. Part 2 – Finite element analysis of density distributions in convex tablets”, *Journal of Pharmaceutical Sciences*, Volume 93, Issue 8, Date: August 2004, Pages: 2040-2053

Friability and Abrasion test

1000 rev

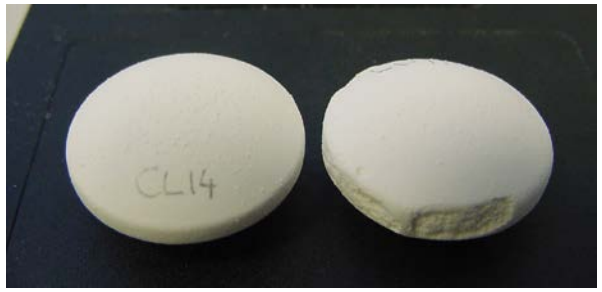

2000 rev

Friability

Abrasion

While results cannot be quantitatively predicted, they can be rationalized by the model

C. I. Sinka, Cunningham J., Zavaliangos A. "Analysis of tablet compaction. Part 2 – Finite element analysis of density distributions in convex tablets", *Journal of Pharmaceutical Sciences*, 2004

EXAMPLE 2

- Temperature increase during tableting

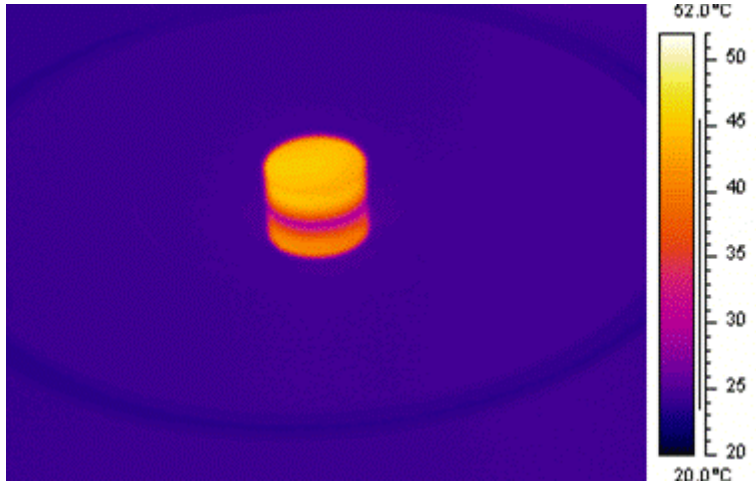

Tablets after compaction are "warm". What is the maximum temperature that the tablet reaches during compaction?

Klinzing G.R., Zavaliangos, A., Cunningham J. C., Mascaro T. and Winstead D. A., "Temperature and density evolution during compaction of a capsule shaped tablet", accepted for publication in Computers in Chemical Engineering, Volume 34, 2010, pp. 1082–1091

Zavaliangos, A., Galen S., Cunningham J. C., and Winstead D. A., "Temperature Evolution During Compaction of Pharmaceutical Powders", Journal of Pharmaceutical Science, Volume 97, Issue 8, 2008, pp. 3291-3304

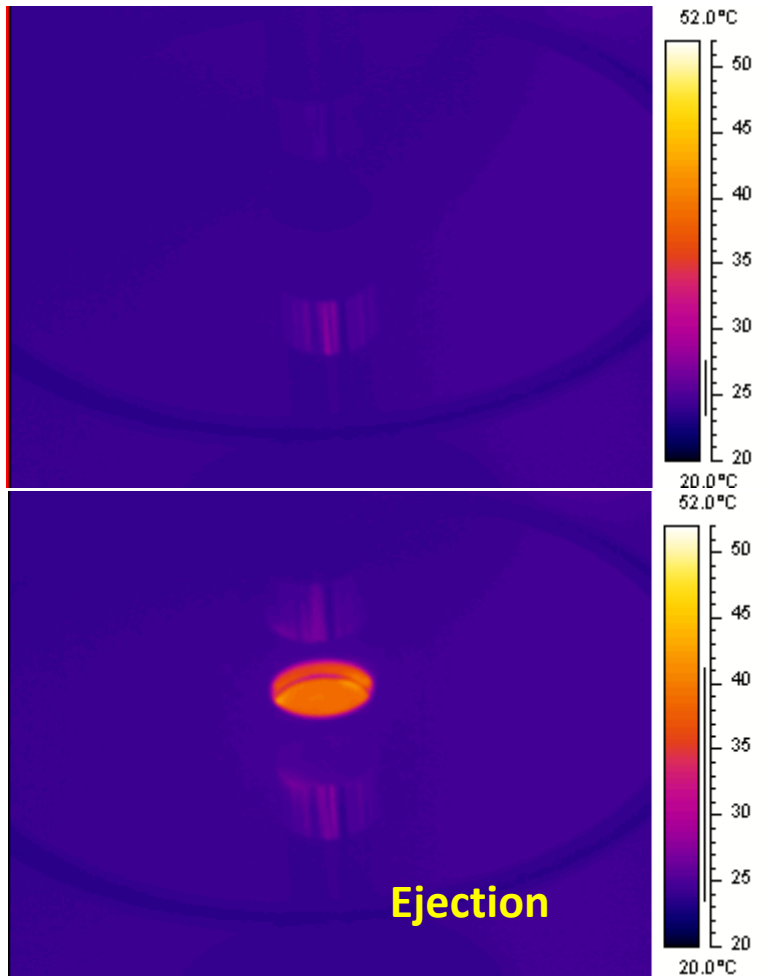
52.0°C
50
45
40
35
30
25
20
20.0°C
Ejection

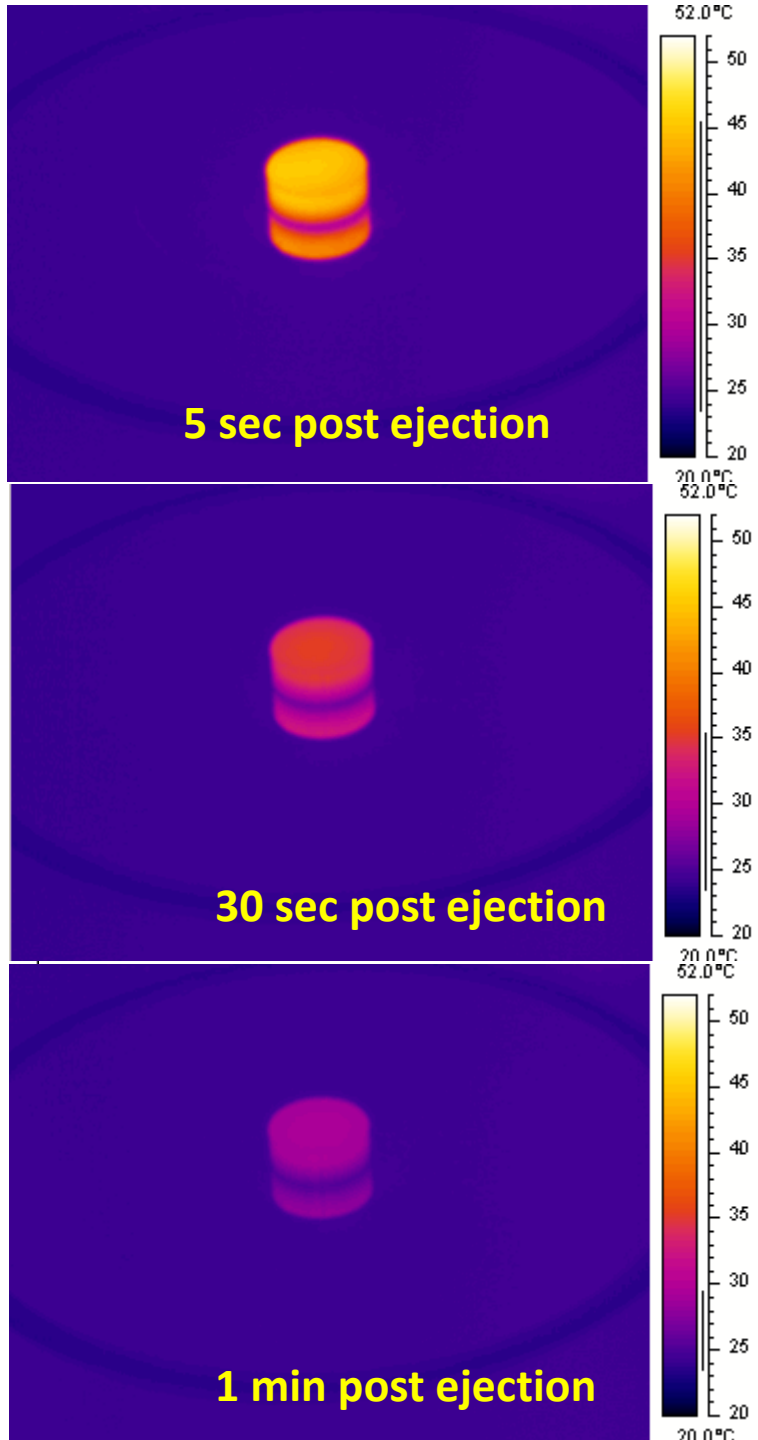
52.0°C
50
45
40
35
30
25
20
20.0°C
5 sec post ejection
30 sec post ejection
1 min post ejection

Pharmaceutical Research, Vol. 9, No. 4, 1992

Infrared Imaging of Pharmaceutical Materials Undergoing Compaction

Simon R. Bechard[1,2] and G. R. B. Down[1]

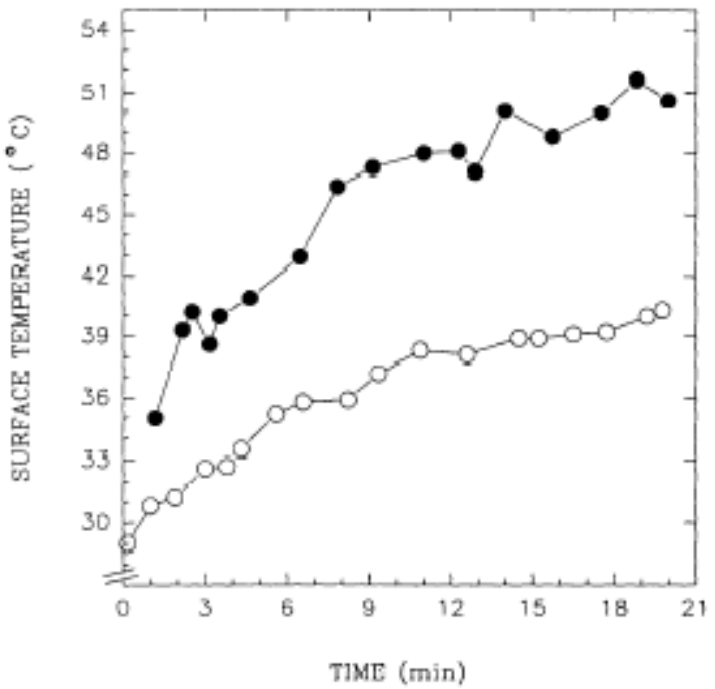

Fig. 8. Tablet surface temperatures as a function of run time for granulations lubricated with 0.5% (●) and 1.0% (○) magnesium stearate.

INTERESTING LONG TERM, TRANSIENT

Drexel UNIVERSITY

Johnson & Johnson PHARMACEUTICAL RESEARCH & DEVELOPMENT, L.L.C.

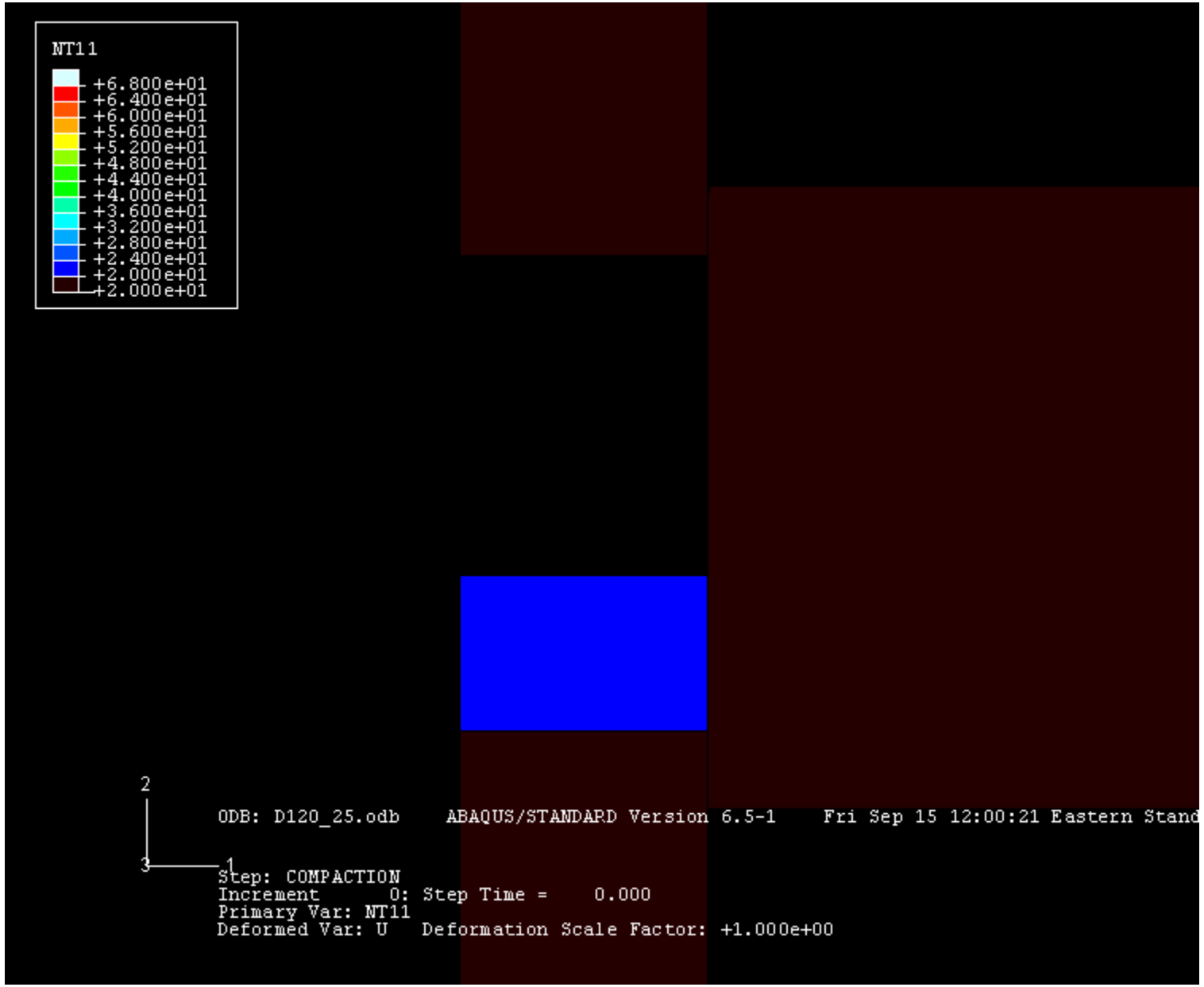

Drexel UNIVERSITY

Temperature evolution in tableting

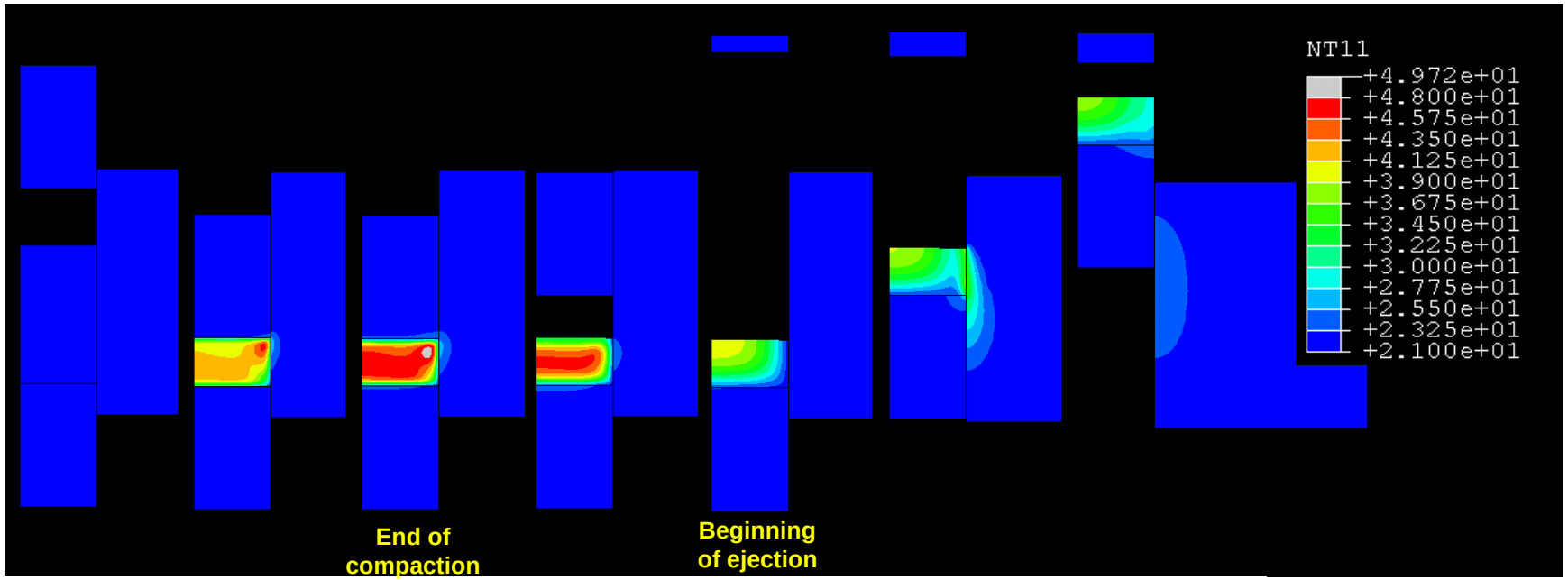

More Details:

1. Zavaliangos, A., Galen, S., Cunningham, J., and Winstead, D. 2008. *Temperature Evolution during Compaction of Pharmaceutical Powders*. J. Pharm. Sci. 97, 3291-3304.
2. Klinzing, G., Zavaliangos, A., Cunningham, J., Mascaro, T., and Winstead, D. *Temperature and density evolution during compaction of a capsule shaped tablet*. Computers in Chemical Engineering (2010)

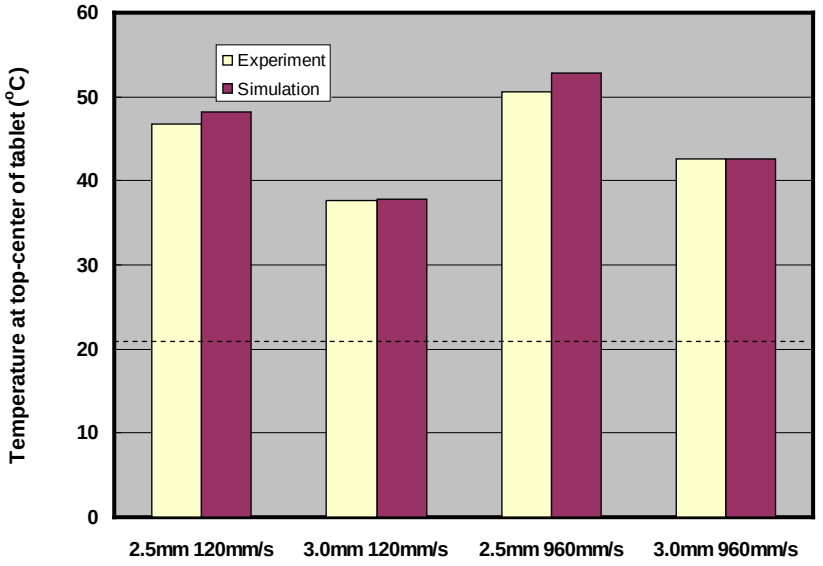

EXAMPLE 3

- **Effect of granule size on moisture absorption by hygroscopic tablets**

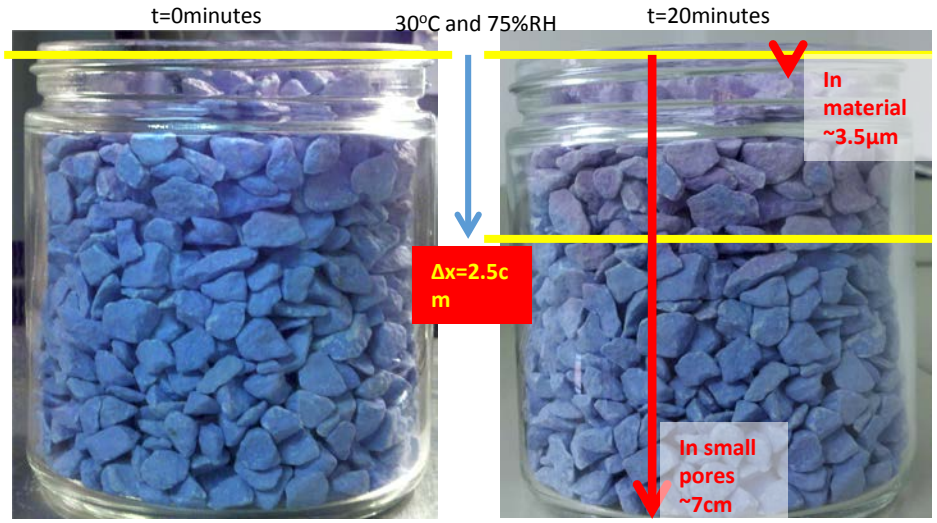

Can we change the moisture absorption rate by changing the granule size ?

Klinzing G.R, PhD Thesis Drexel U., 2012

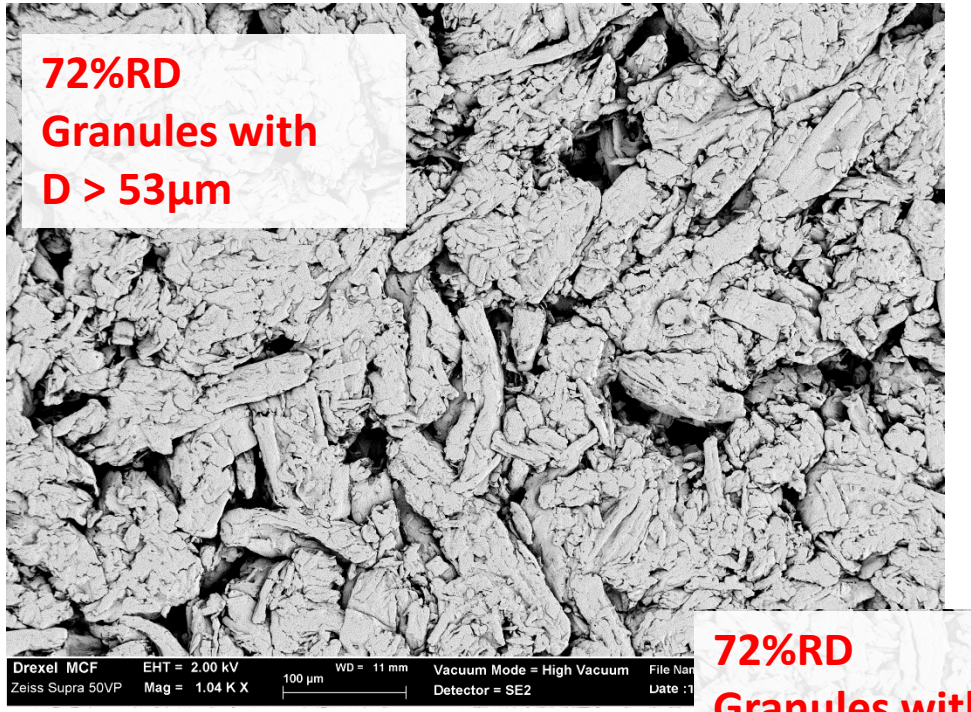
72%RD
Granules with
D > 53µm
Drexel MCF
Zeiss Supra 50VP
EHT = 2.00 kV
Mag = 1.04 K X
100 µm
WD = 11 mm
Vacuum Mode = High Vacuum
Detector = SE2

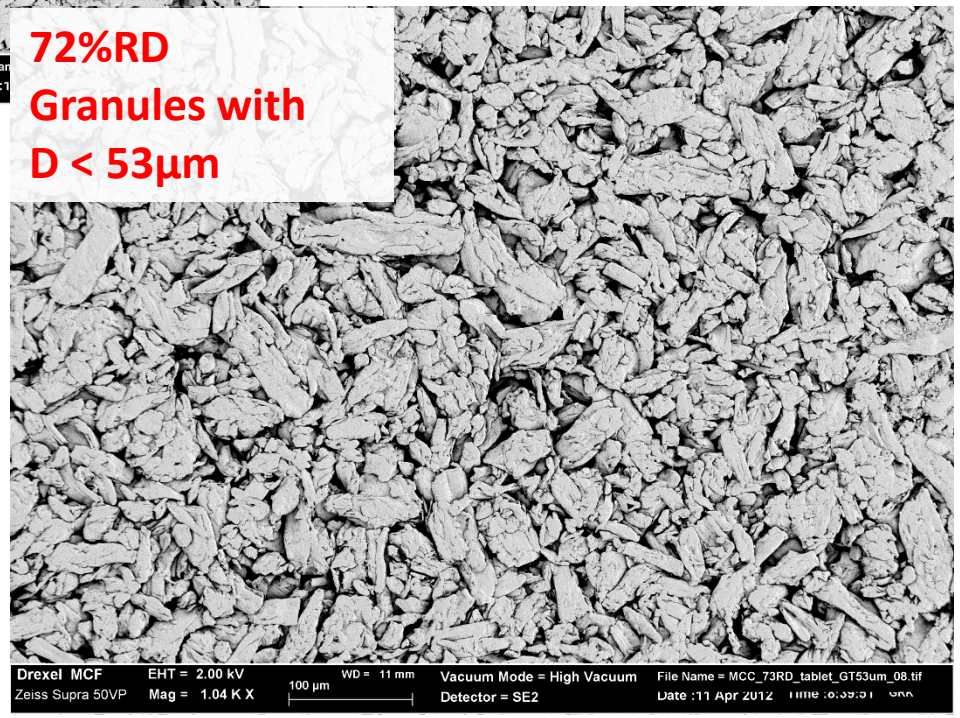
72%RD
Granules with
D < 53µm
Drexel MCF
Zeiss Supra 50VP
EHT = 2.00 kV
Mag = 1.04 K X
100 µm
WD = 11 mm
Vacuum Mode = High Vacuum
Detector = SE2
File Name = MCC_73RD_tablet_GT53um_08.tif

Pharmaceutical tablets contain a wide range or pore sizes

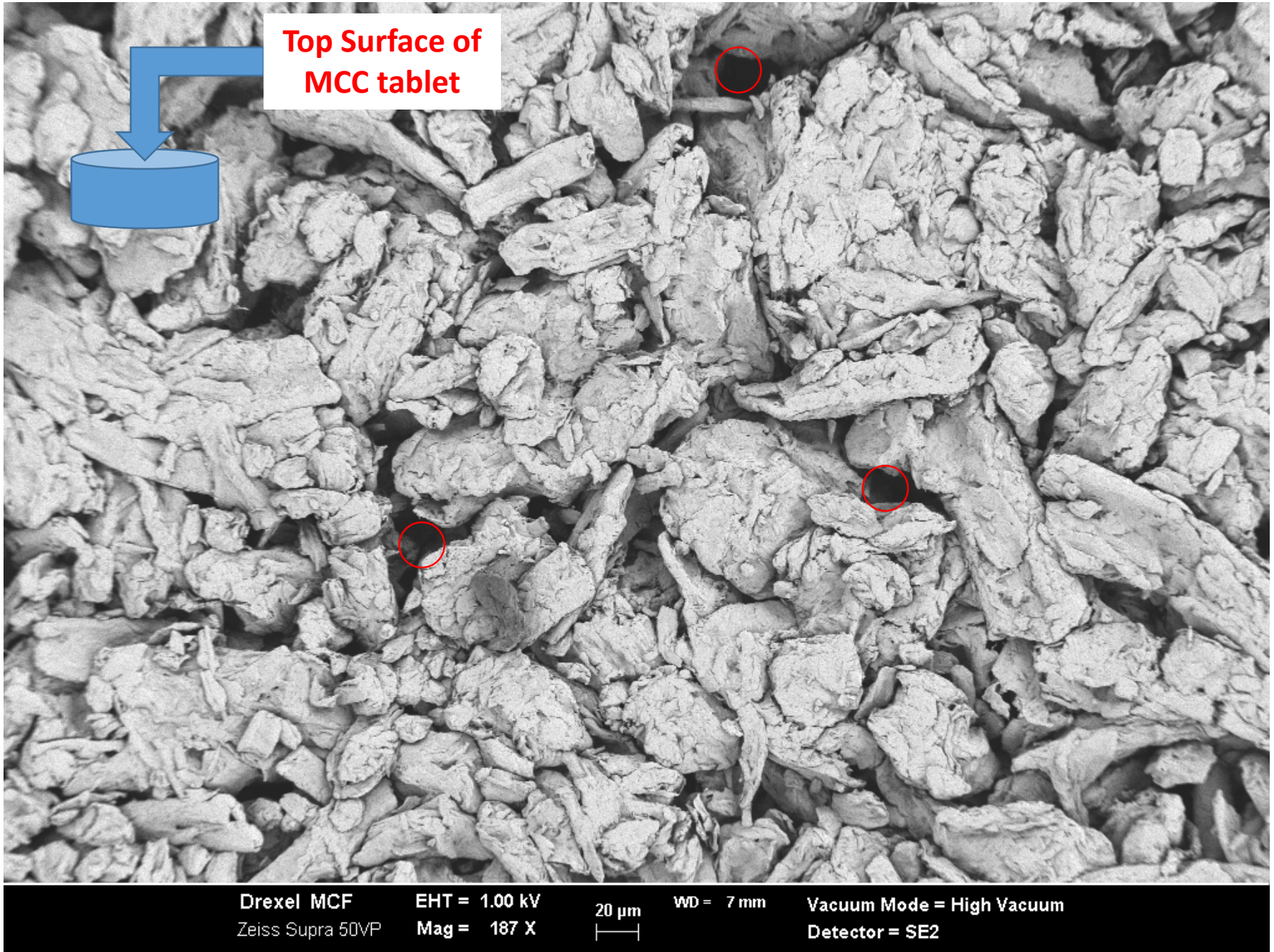

Pharmaceutical tablets contain a wide range of pore sizes

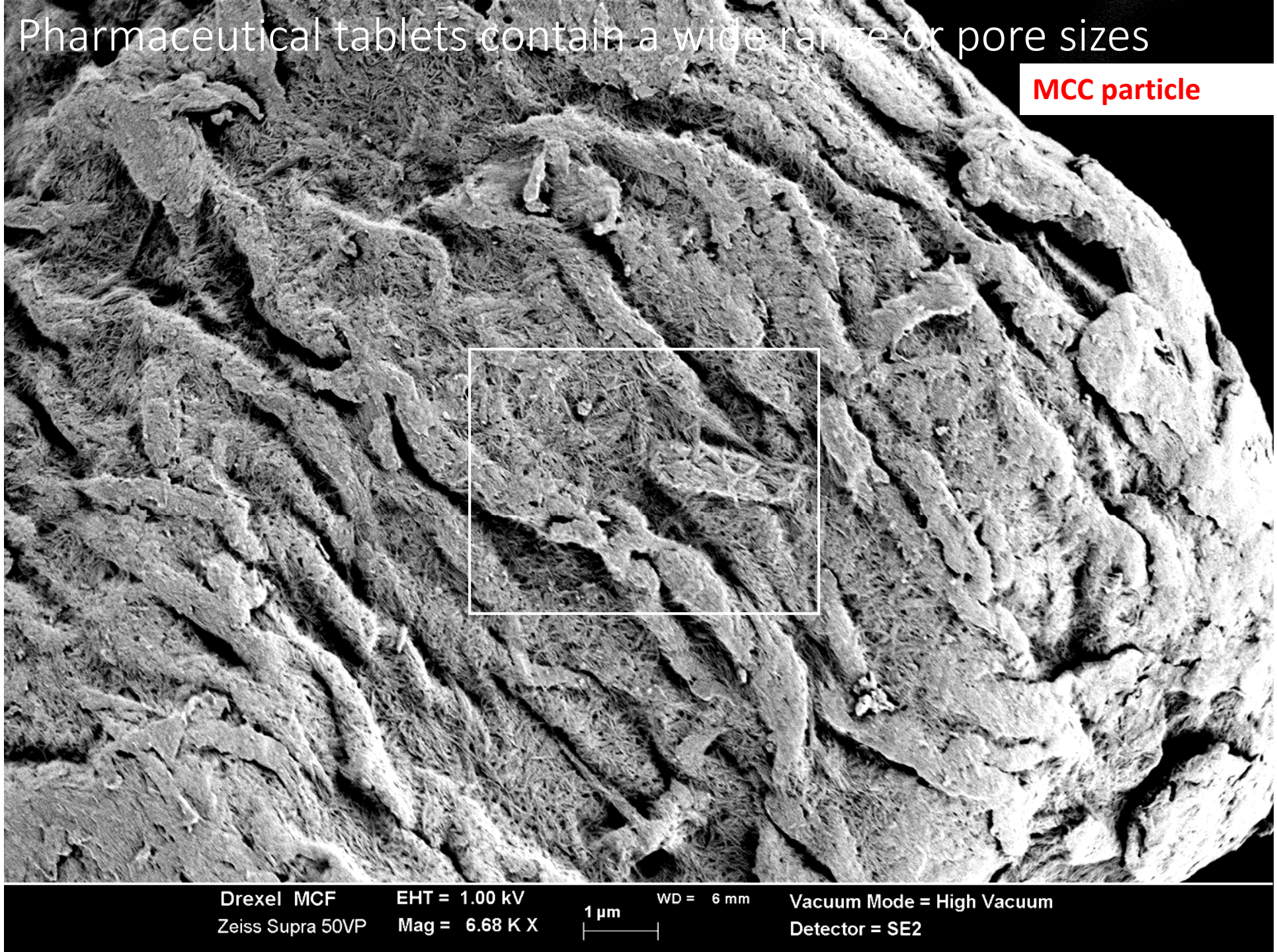

Pharmaceutical tablets contain a wide range or pore sizes

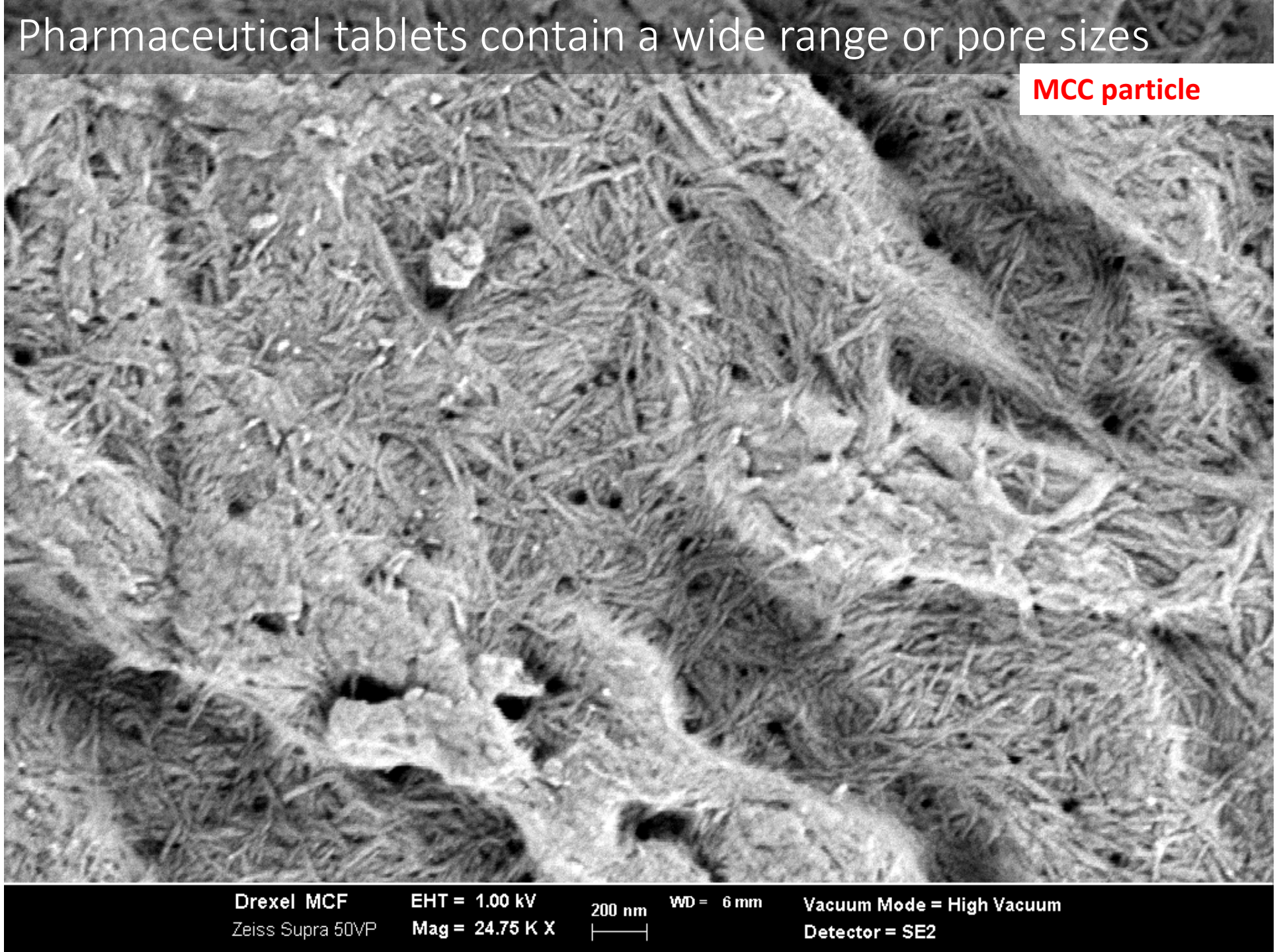

In this case, without even solving the problem we can get the time constant.

$$T = \frac{4\tau L^2}{D_{mp}^{H_2O} n^2 \pi^2}\left(1 + \frac{RD}{\beta(1-RD)}\right)$$

$$\beta = \frac{C_{H_2O,air}^{eq}}{C_{H_2O,solid}^{eq}}$$

τ_{NAB} Non-absorbing

τ_{AB} Absorbing

Not curve fit but predictions

25.4mm dia X 4mm thick

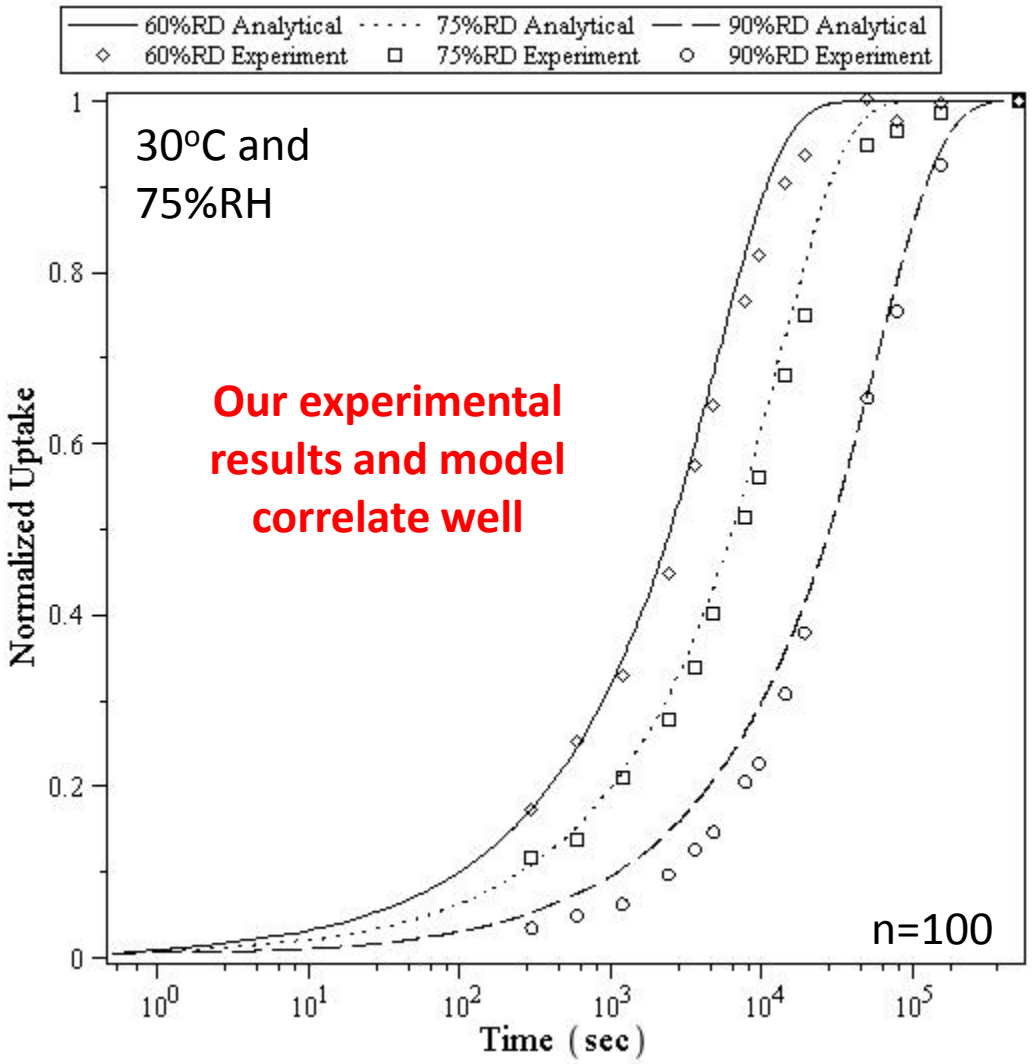

72%RD
Greater than
53µm particles

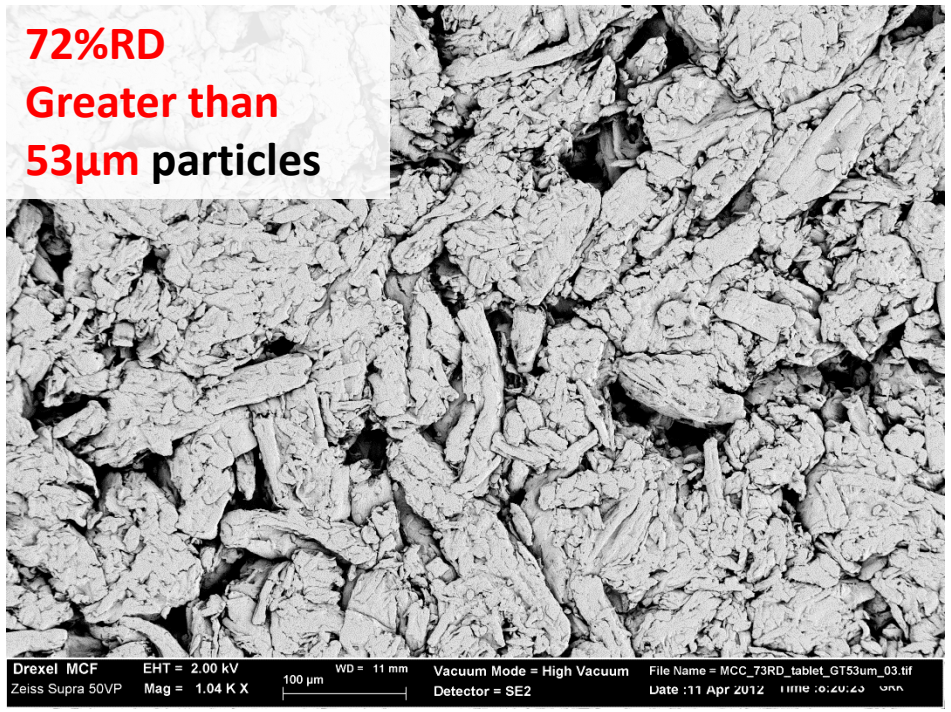

72%RD
Less than
53µm particles

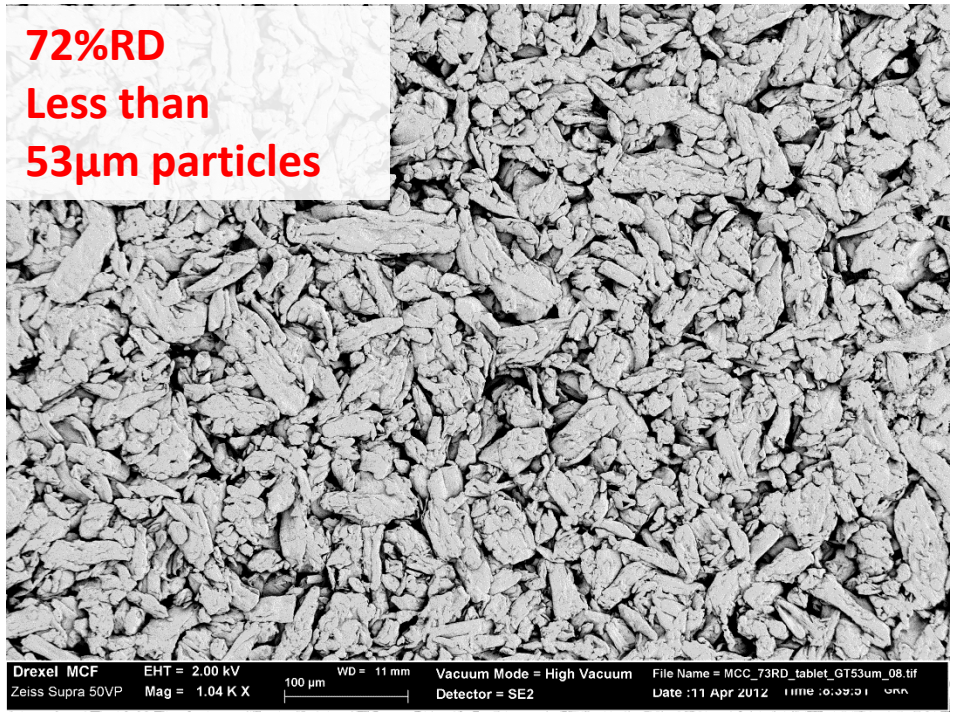

Analytical solution predicts particle size independence for the uptake process.

$$T = \frac{4\tau L^2}{D_{mp}^{H_2O} n^2 \pi^2}\left(1 + \frac{RD}{\beta(1-RD)}\right)$$

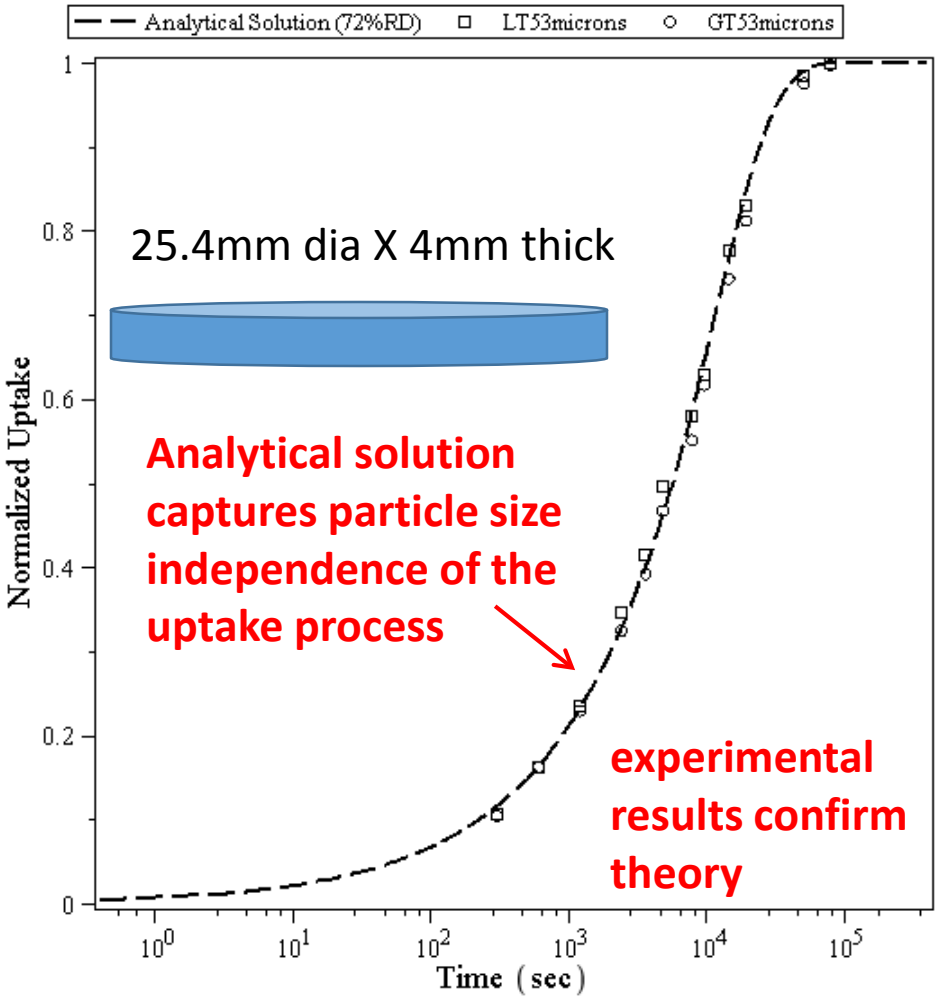

EXAMPLE 4

(work in progress)

- **What determines the long term mechanical integrity of bilayer tablets in a humid environment?**

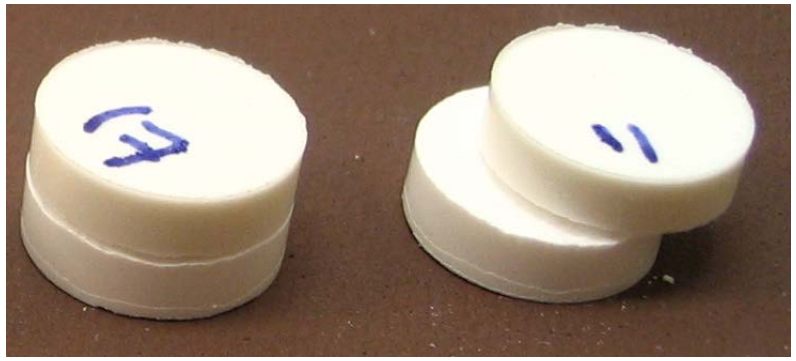

Bilayer tablets have residual stresses across the interface

State of the tablet after production

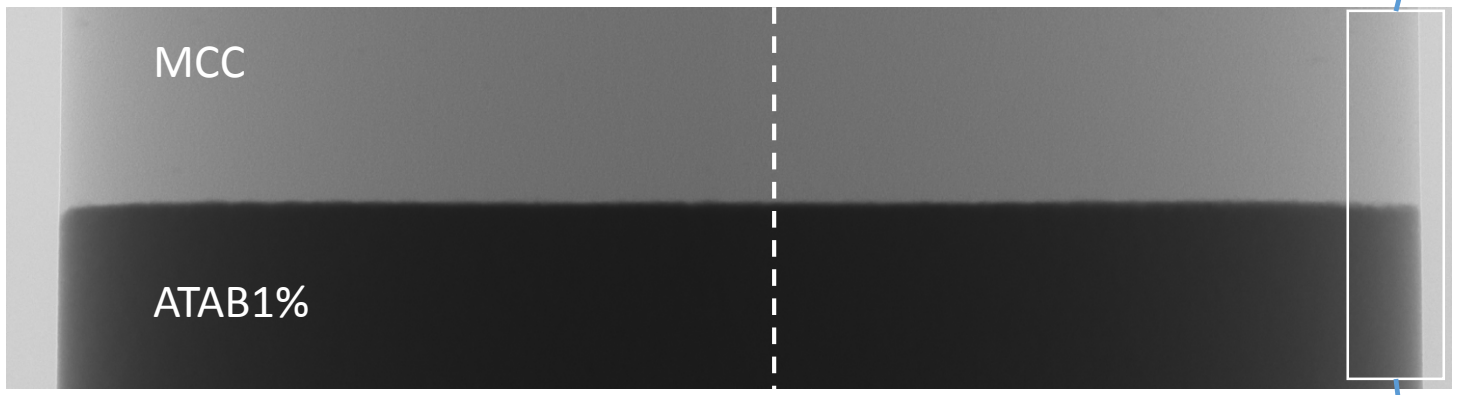

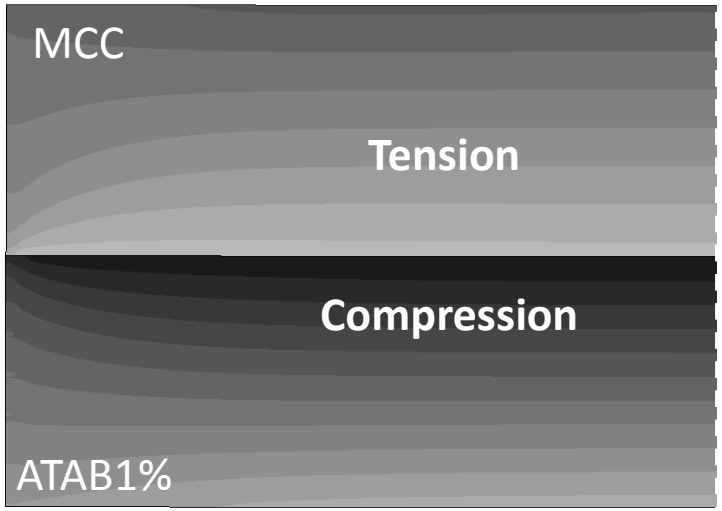

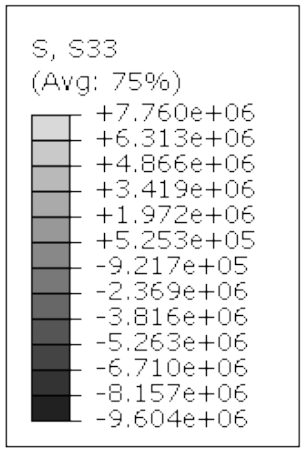

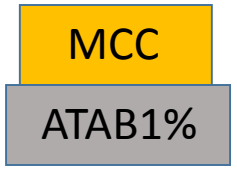

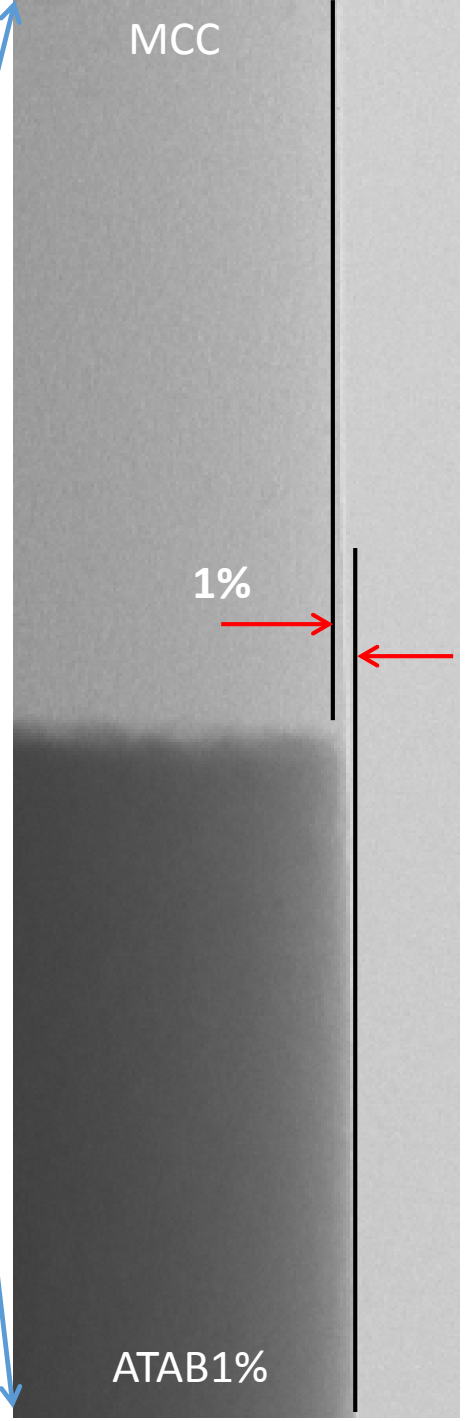

Residual stresses remain within each layer:

- MCC is in tension
- ATAB1% is in compression

Reducing the diametrical strain differential should alleviate the stress at the interface

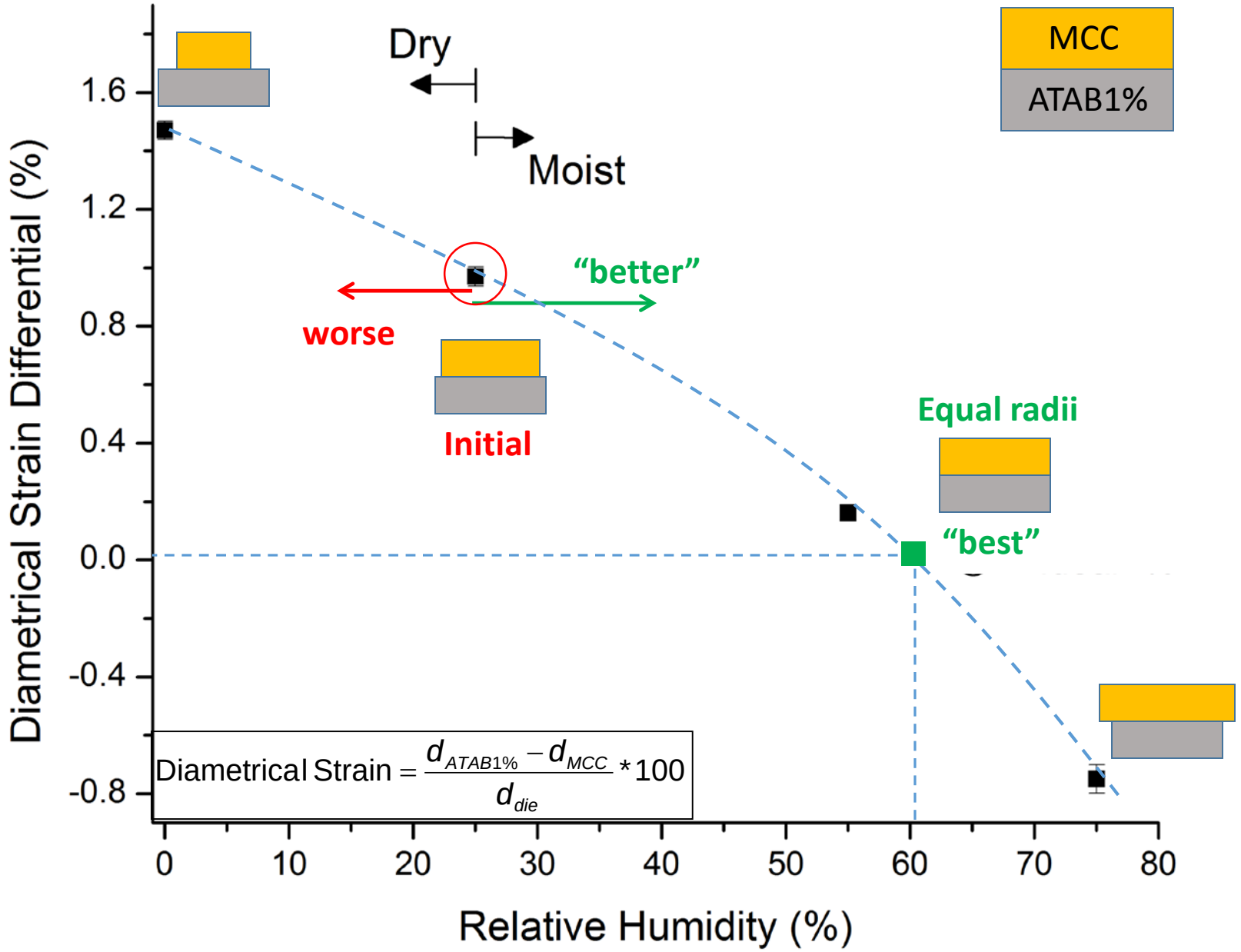

Changes in external humidity alters the interfacial strength dramatically

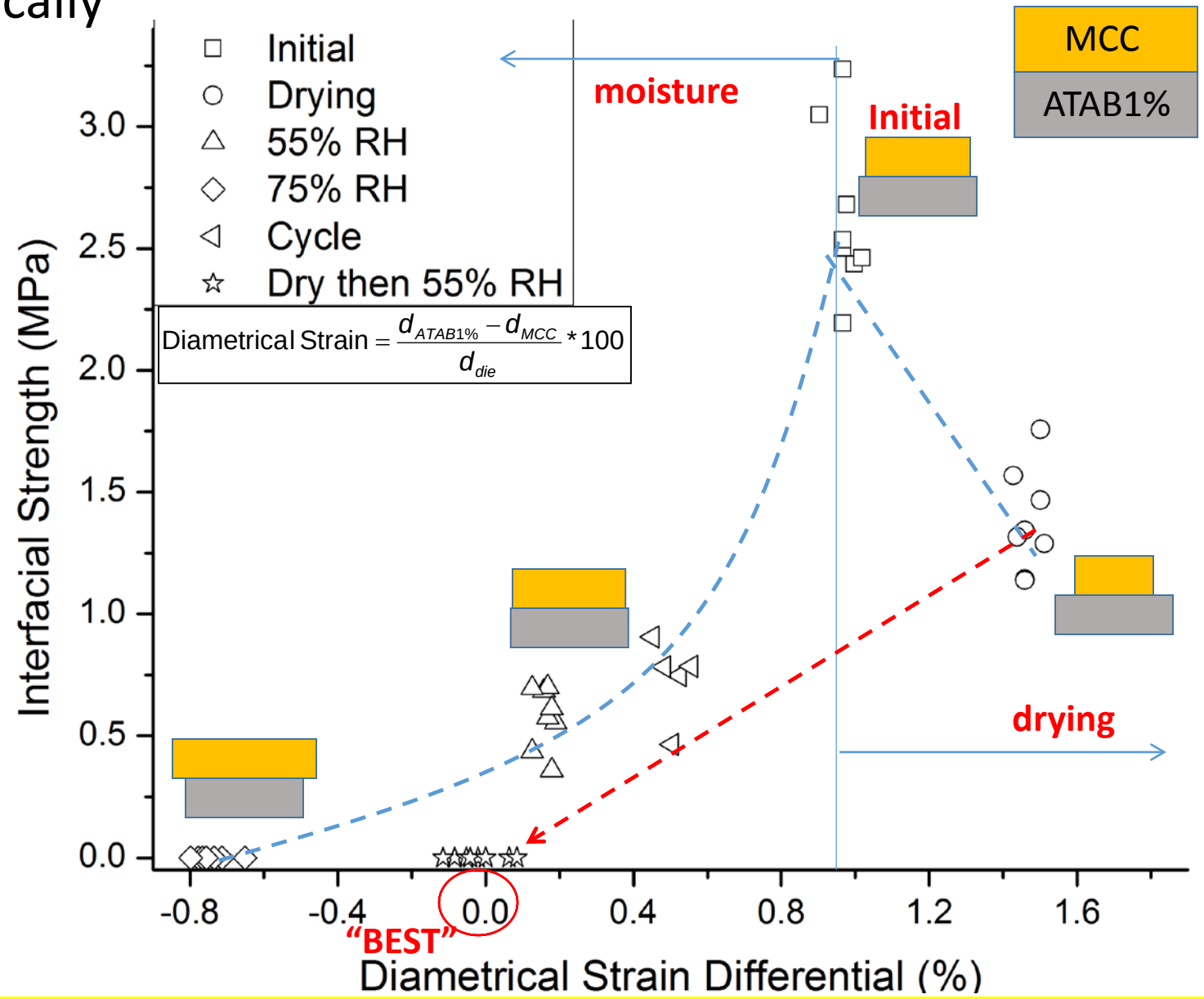

What is the mechanism of interfacial strength reduction?

Simulation of moisture diffusion

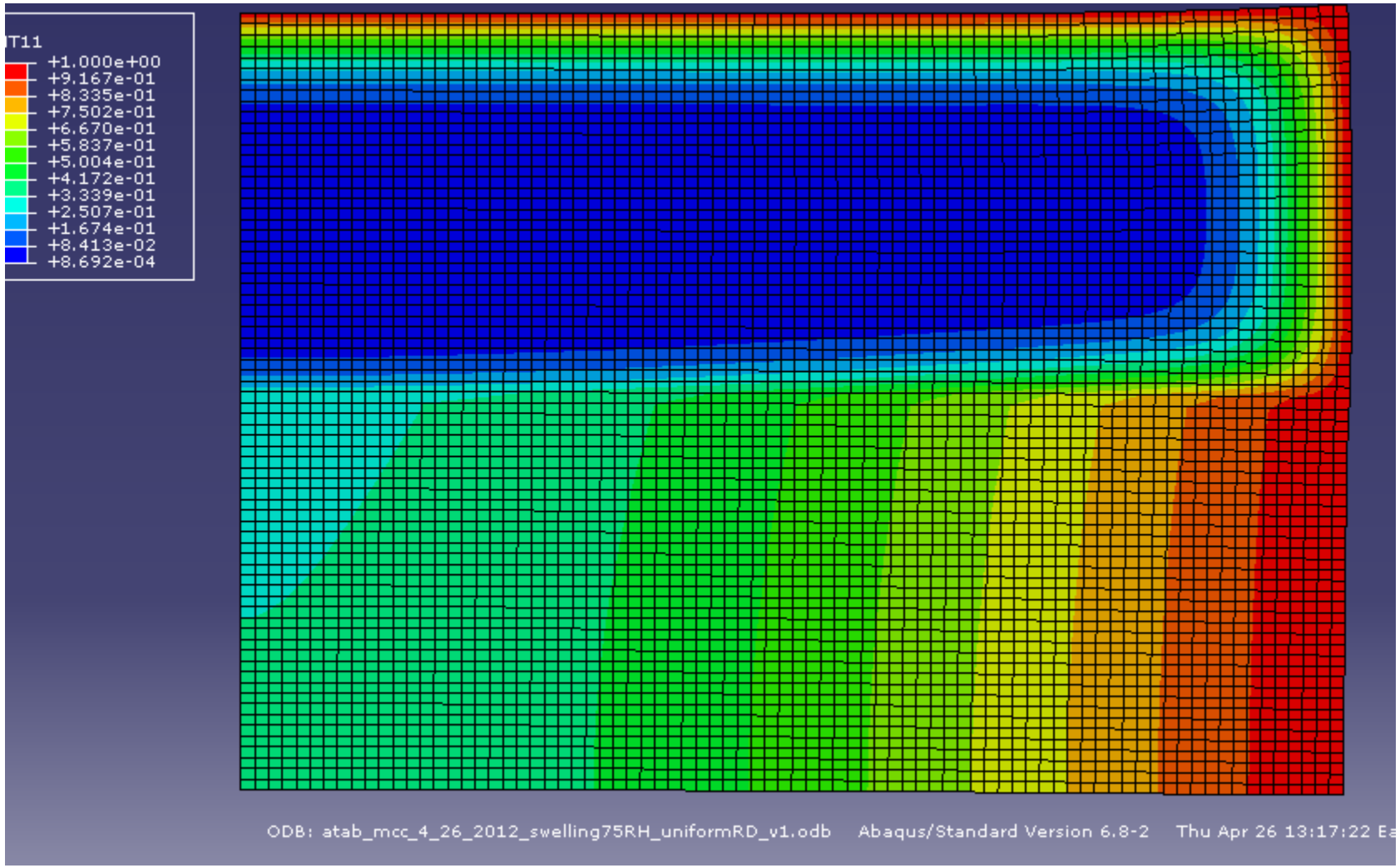

Swelling and drying results in cracking along the interface

Swelling Transient

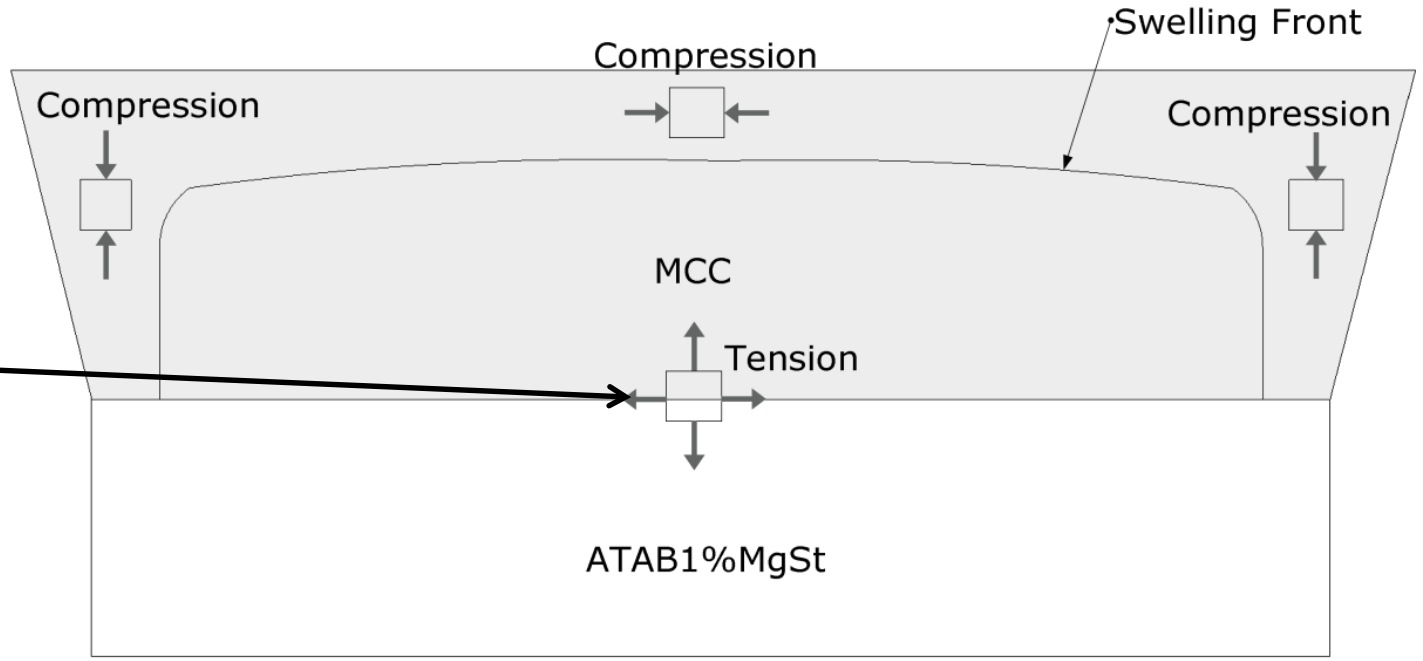

Region where crack will form

Drying Transient

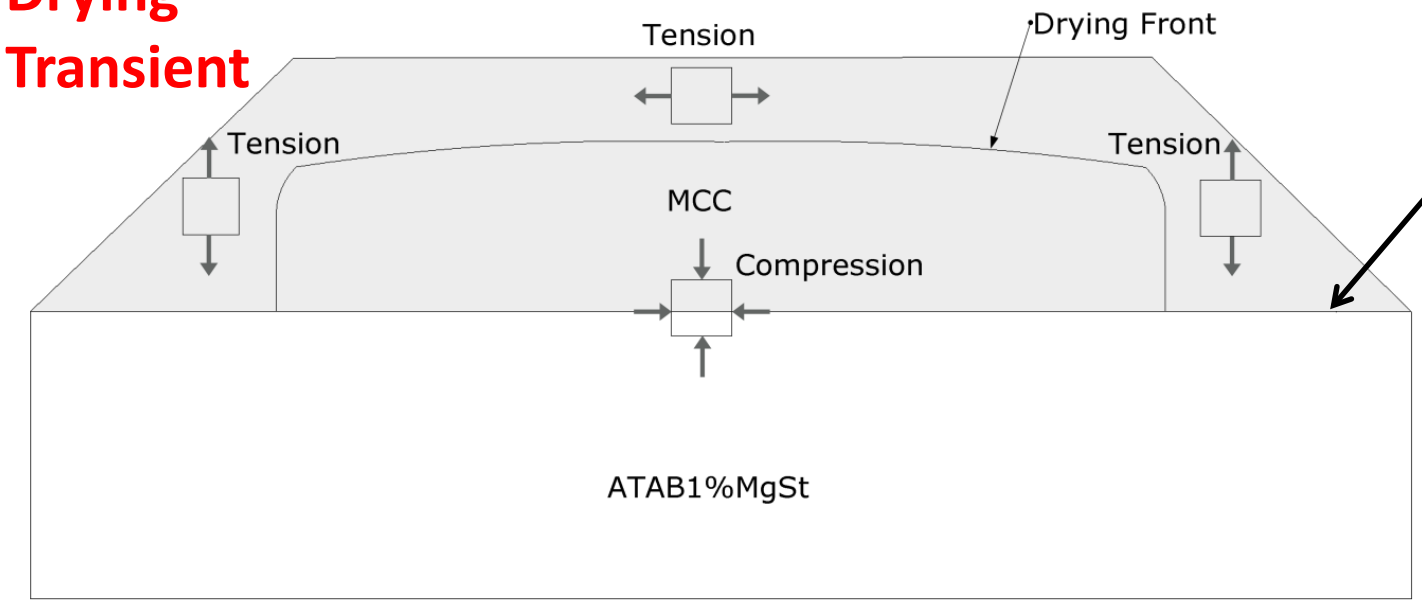

Region where crack will form

20MPa tamped/200MPa main at 75%RH within the microCT

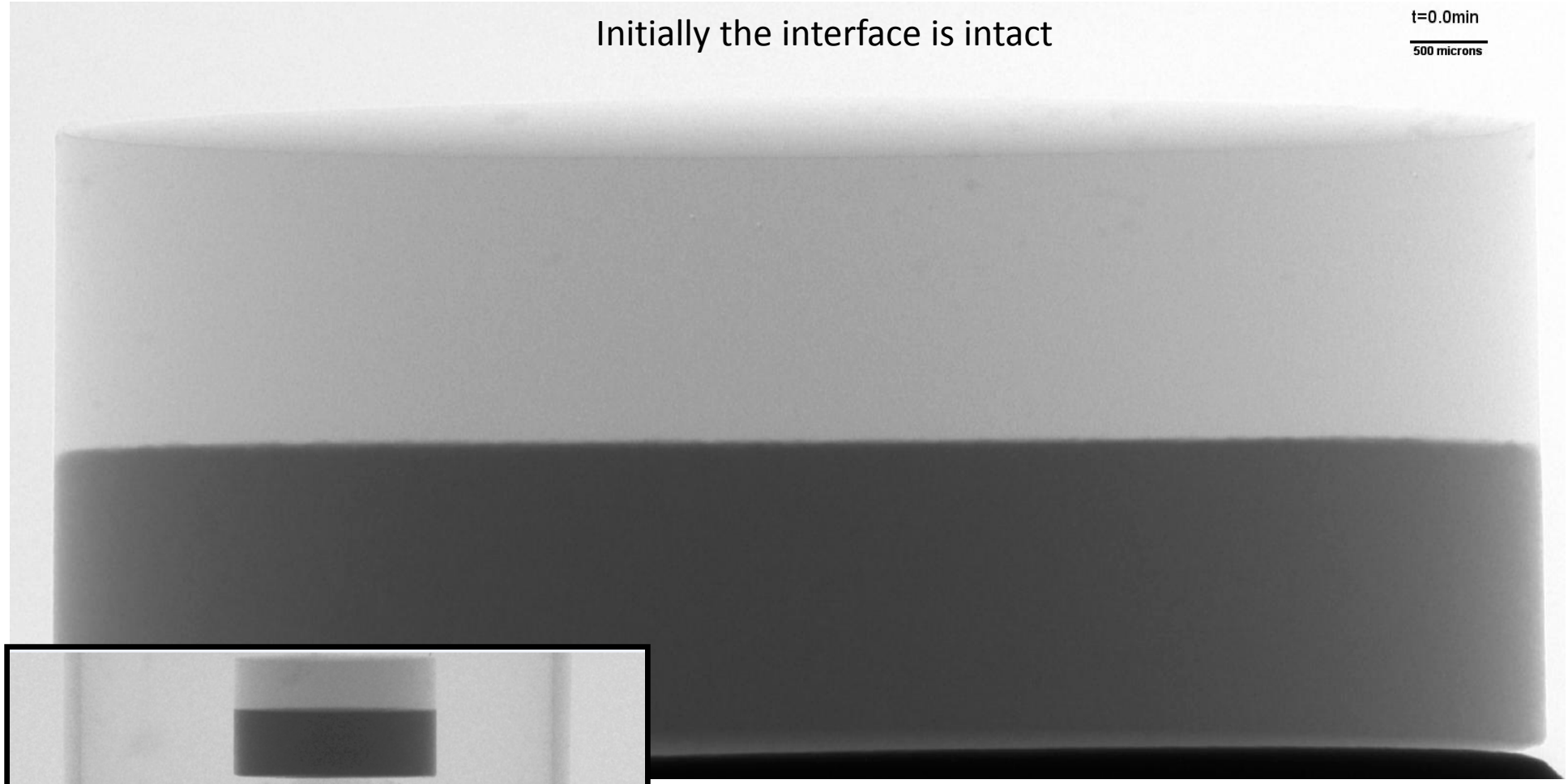

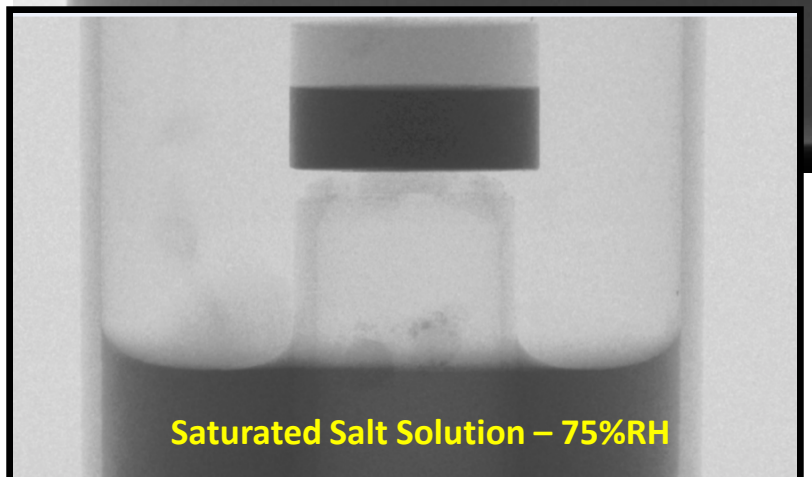

Experimental setup: HDPE vial filled with salt solution and tablet elevated above on stub.

Swelling video

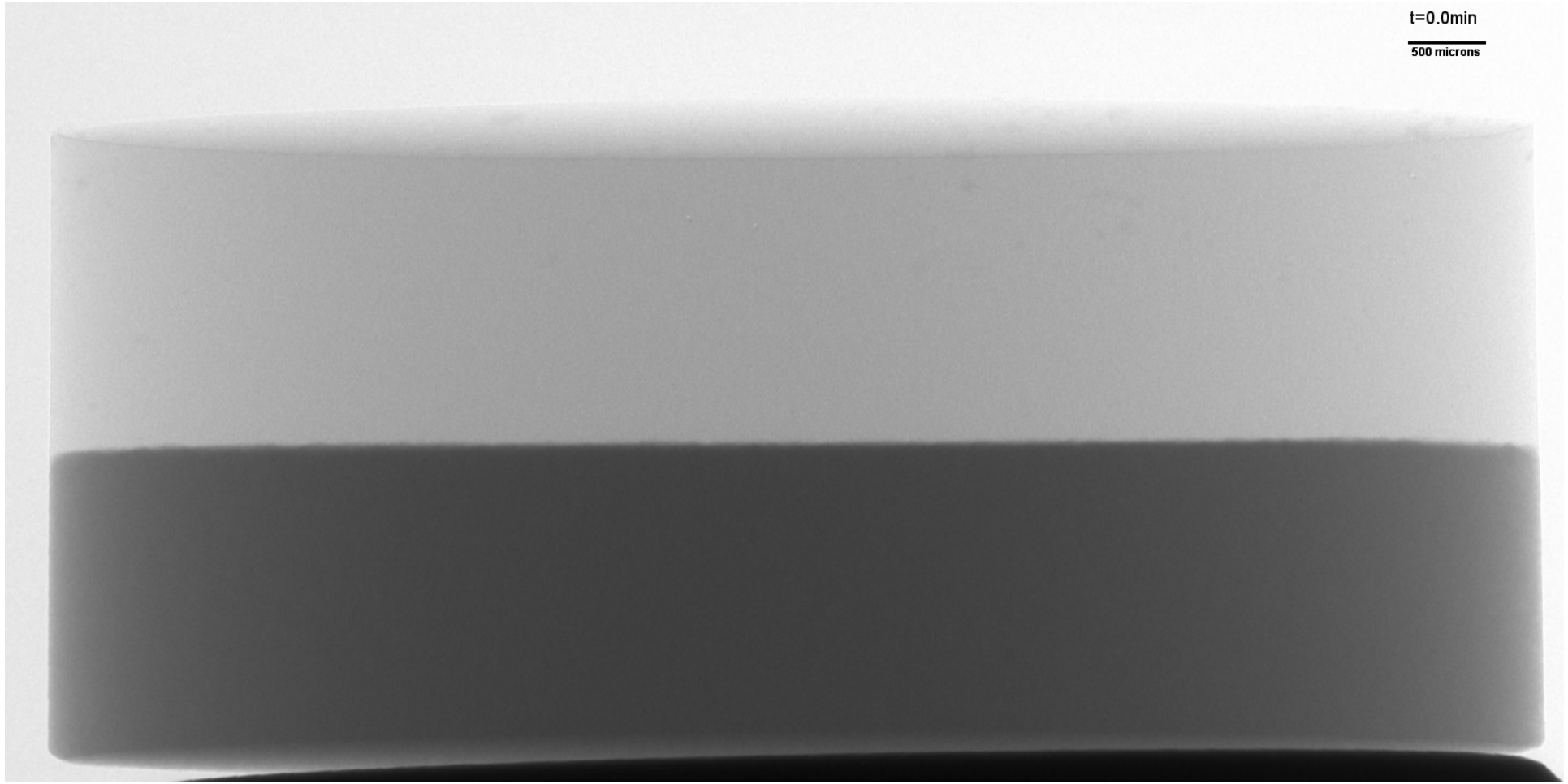

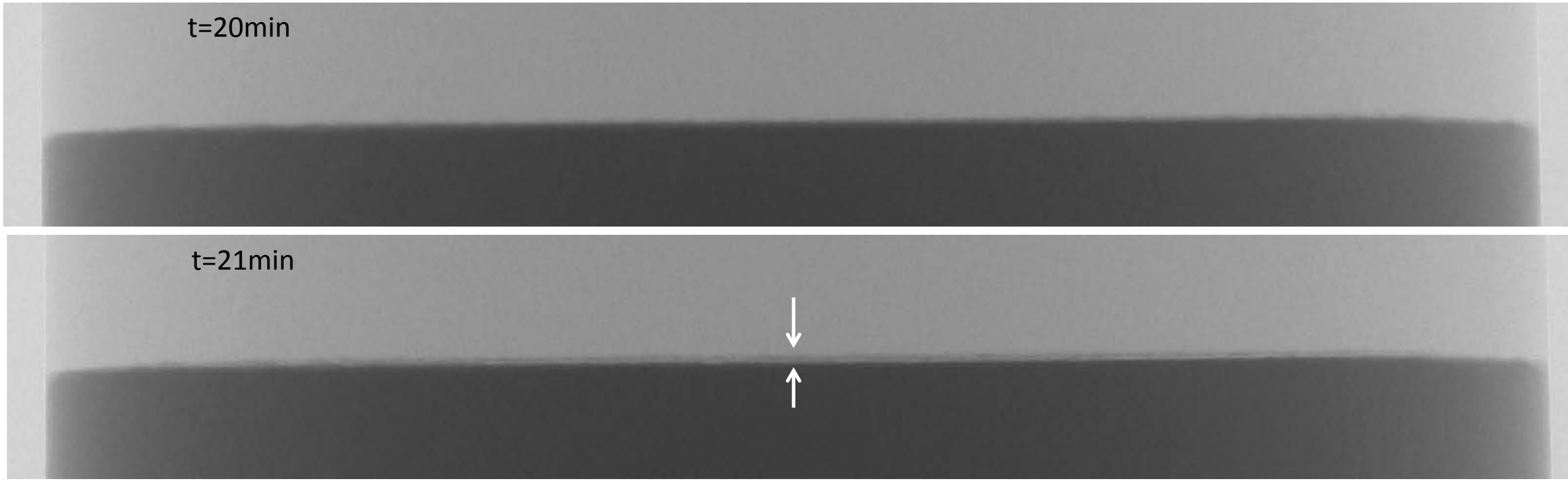

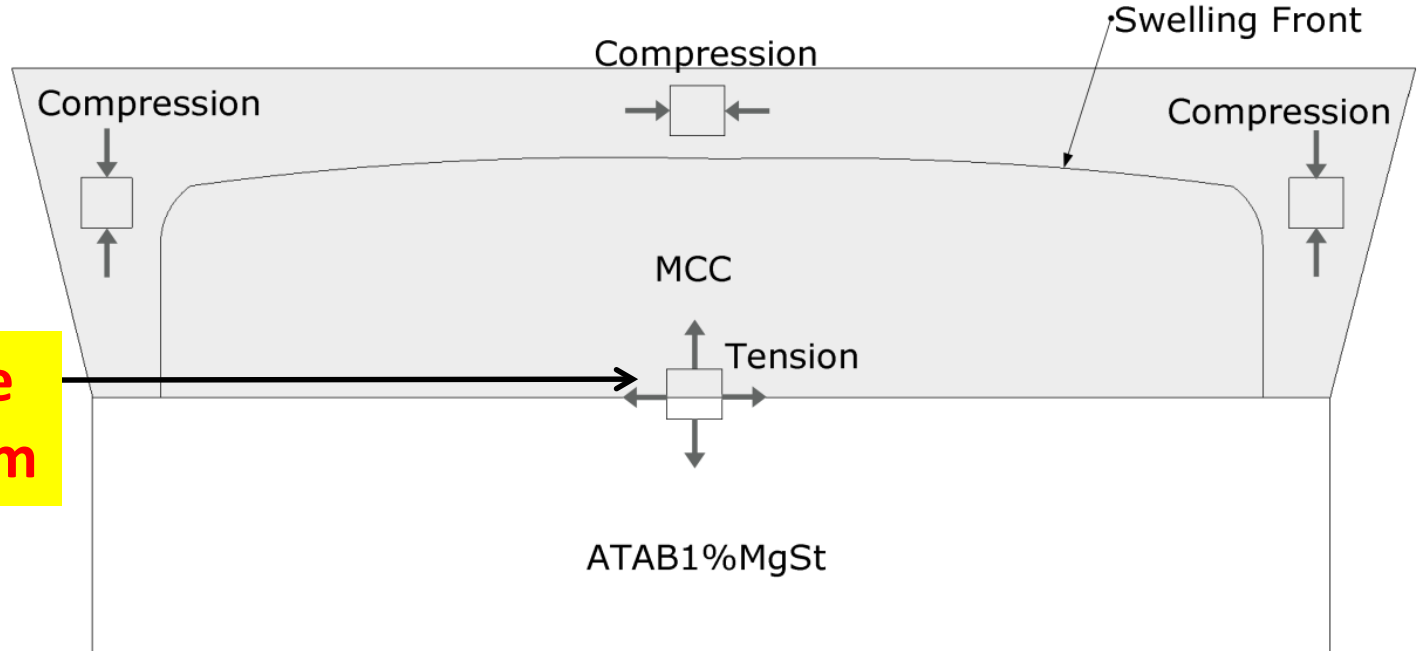

Region where crack will form

Drying video

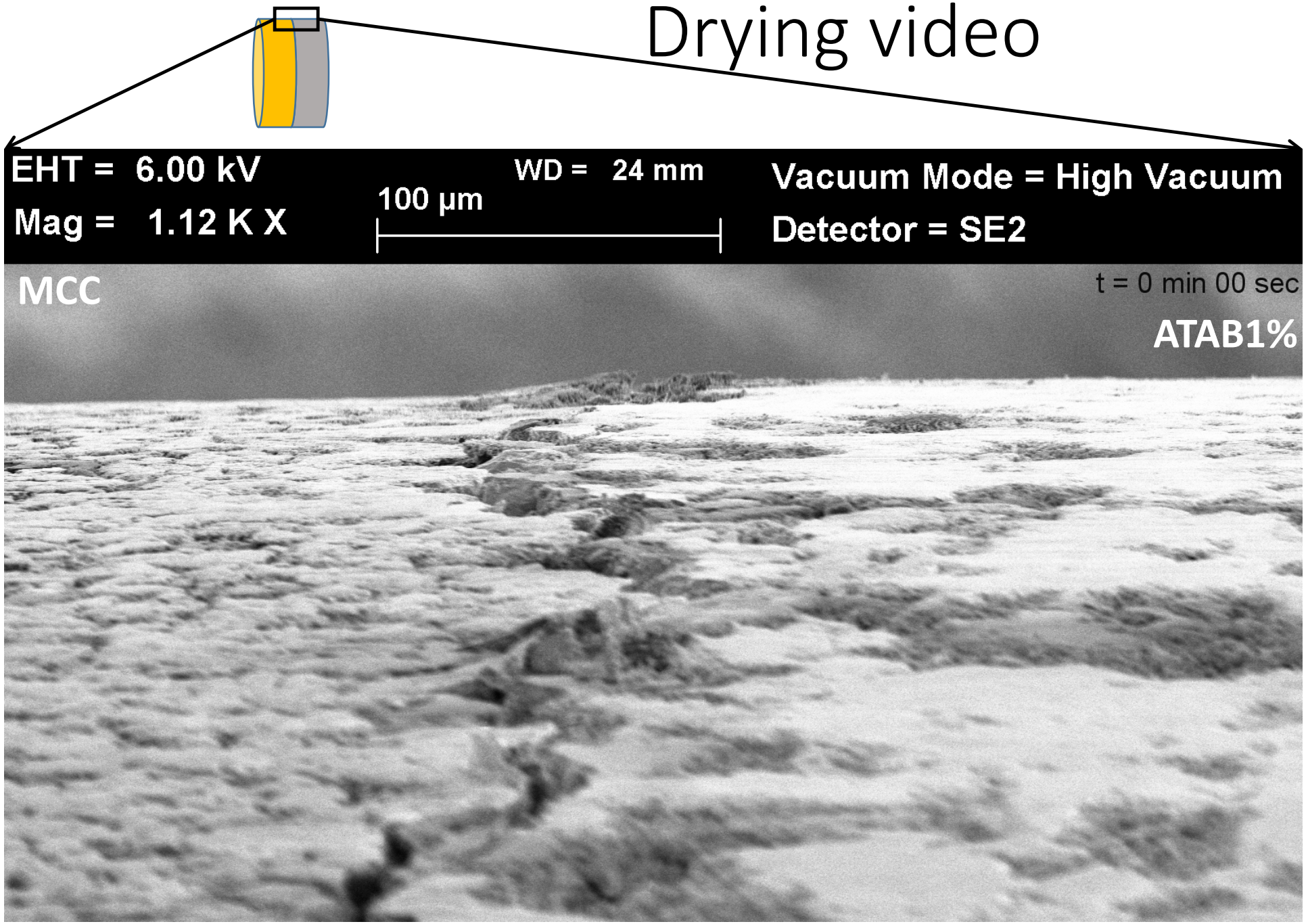

Modeling of Strength

The Discrete Element Method for Powder Compaction

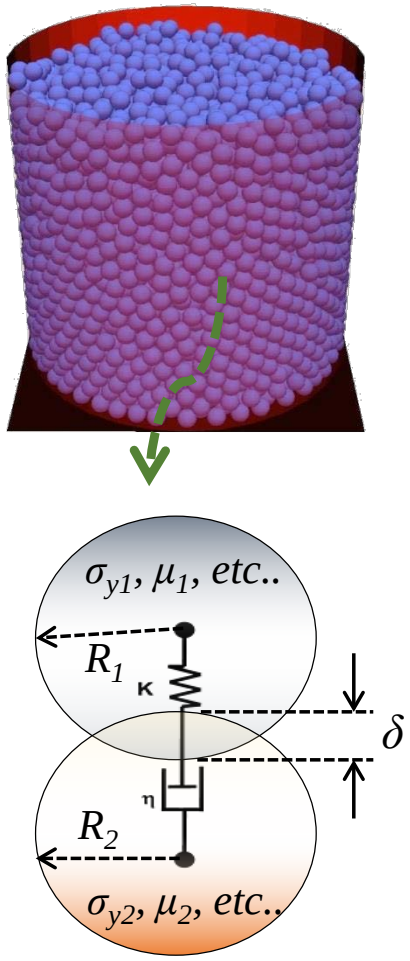

Method

- Newton's equations of motion to compute positions, velocities, and forces
- Particle interactions described by contact constitutive models
- Contact forces typically defined by spring-slider-dashpot models
- Strength at contact level by incorporating cohesion
- Spherical particles – contact detection

Current implemented DEM models are lacking in ability to describe compaction to high density and the associated strength or damage

Current DEM Model Relevant to this Work: Martin et al.

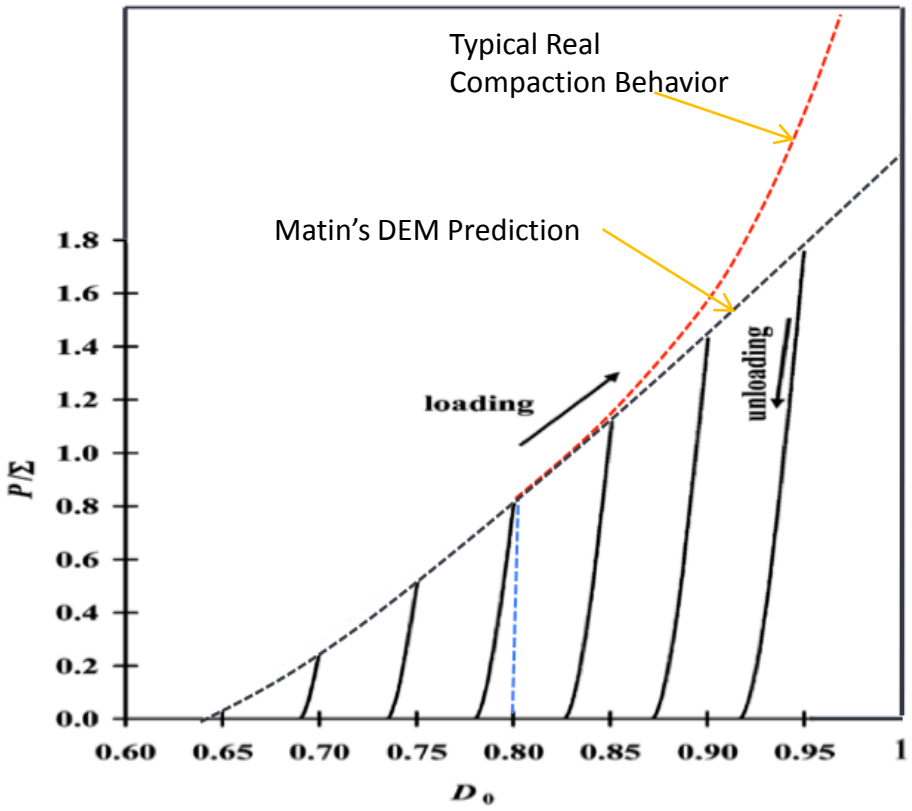

- DEM implementation does not work at high densities
  - Improper *F-δ* law
  - Produces linear dependence on strength
- Die walls and punches are excluded from simulations
- Does not consider die compaction (only isostatic compaction)
- Uses proprietary software
- Does not consider ejection or strength of ejected compacts

Martin, C.L., Acta Materialia, 2003. **51**: p. 4589-4602.

Multi-Particle FEM (MPFEM)

Implemented to overcome some of the concerns pertaining to DEM

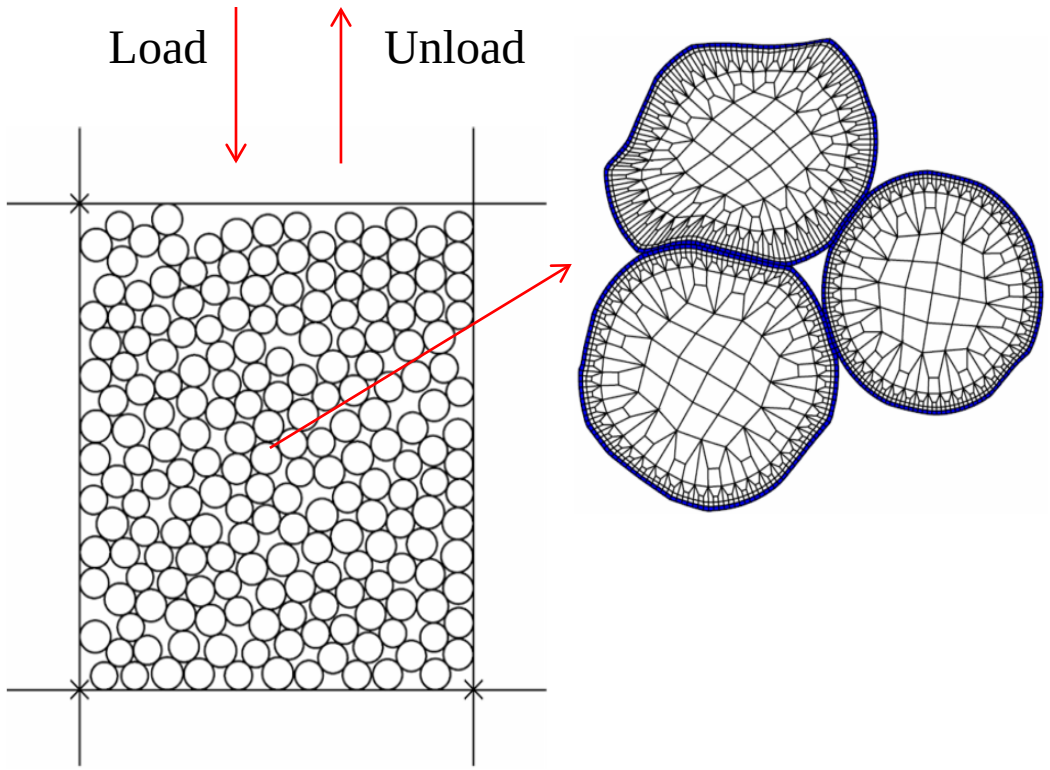

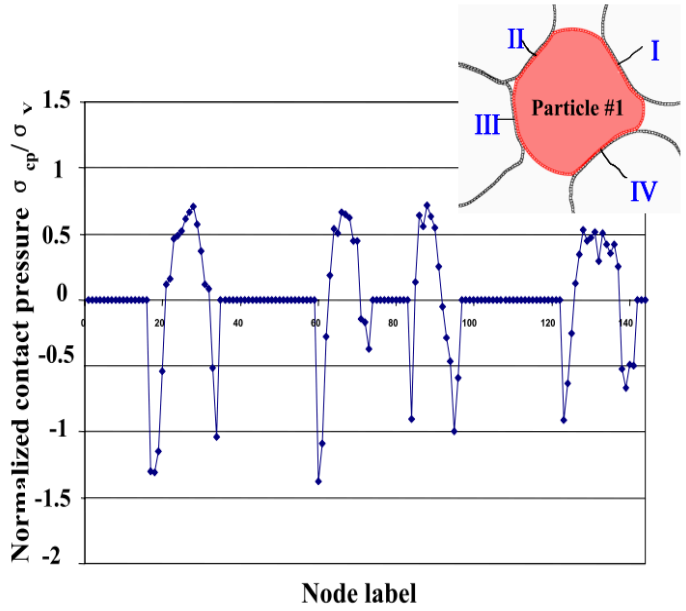

Restricted to either 2-D problems or 3-D problems involving a small number of particles

Wang, W., *Towards an improved understanding of strength and anisotropy of cold compacted powder*, 2007. p. 1-145.

Towards a predictive model for strength and damage in compacts

- **Use of DEM for micromechanical understanding of macroscopic particulate behavior in terms of the damage and strength**
- **Implement elasto-plastic cohesive contact model for powder compaction that will capture basic physics and provide correct macroscopic behavior**
- **Model should be able to be calibrated from experiments**

Appropriate (for high density) force-displacement laws

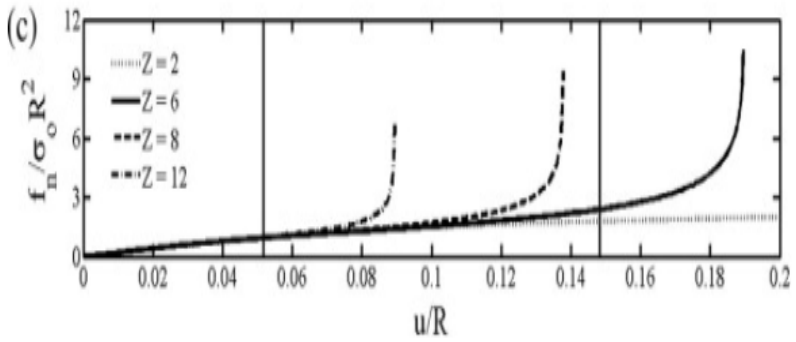

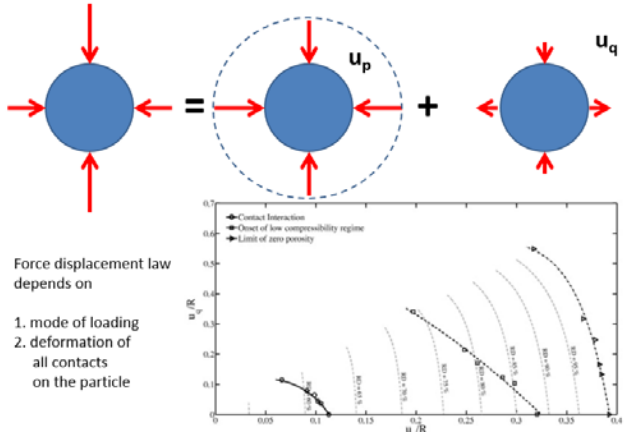

Force displacement law depends on

1. mode of loading
2. deformation of all contacts on the particle

International Journal of Solids and Structures

Volumes 60–61, 15 May 2015, Pages 17–27

Detailed, complex
and computationally expensive

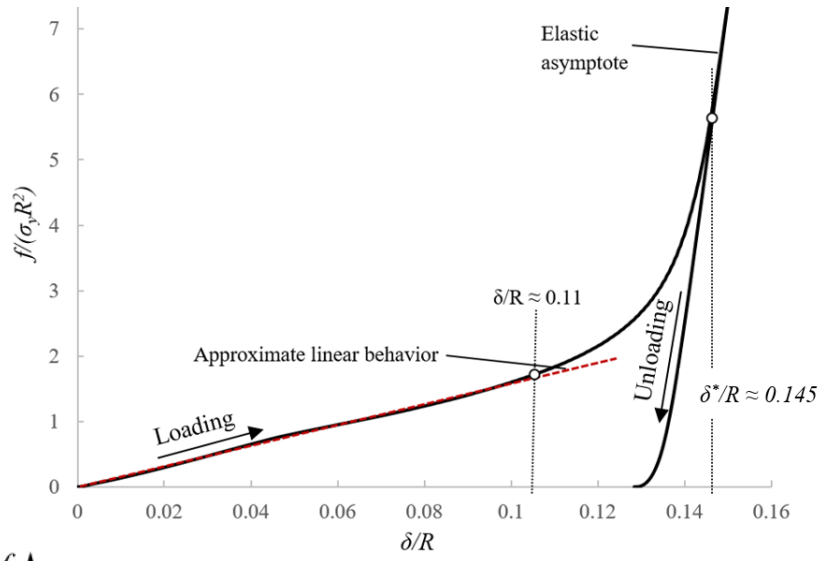

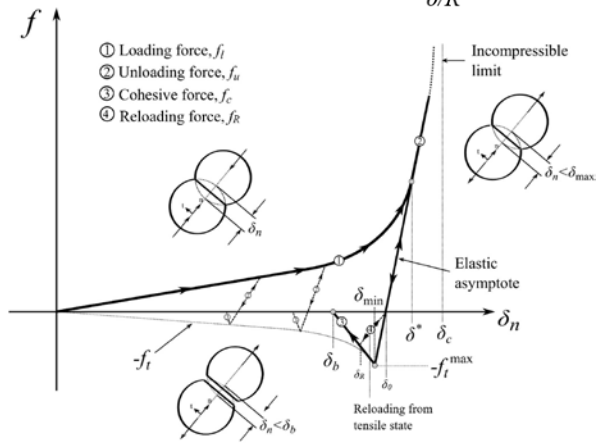

INCLUDES COHESION → STRENGTH

1) **Small deformation regime** - contacts are independent from others
2) **Contact interaction regime** – each contact "feels" the presence of its neighbors
3) **Low compressibility regime** – where the porosity closing locally and elasticity dominates

Model Parameter Calibration Procedure

- Model parameters are calibrated from bulk scale experiments, rather than from microscale experiments

  - Only two bulk scale experiments needed for calibration:
    1. Die compaction experiment → loading and unloading branches
    2. Axial tension test → cohesive branch

- Extraction of parameters achieved using statistical design-of-experiments (DOE) methods and regression analysis

  - Three-level 2^3 Central Composite Design (CCD) → loading curve
  - Regression analysis → unloading and cohesive curves

DEM Simulation Setup for Parametric Studies

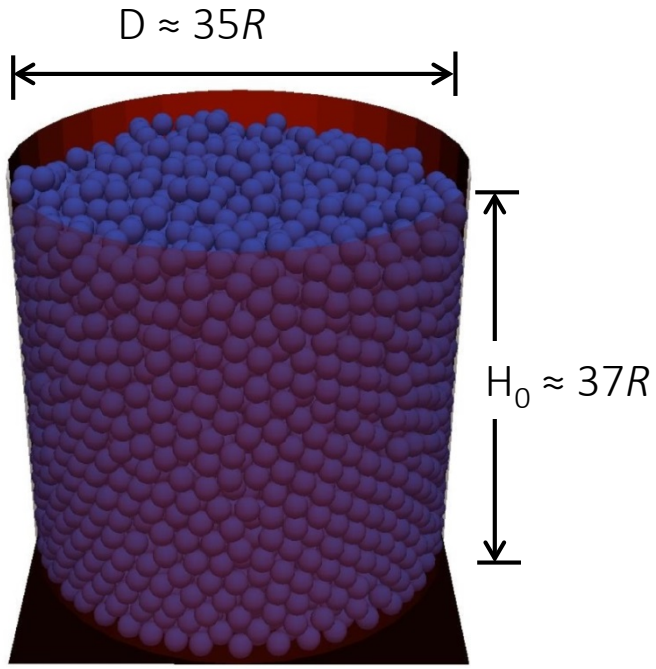

5000 Particles

Particle Radii = *R*

Calibration Material

Extruded Copovidone

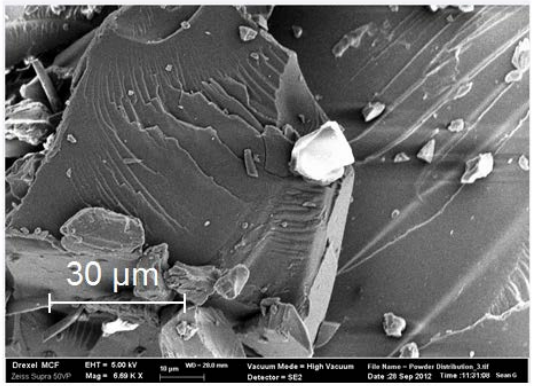

- Calibration of parameters made from 98% relative density compaction
- DEM simulations performed using open source DEM code (LIGGGHTS)
  - Code is extension of the widely used molecular dynamics code LAMMPS

Fully Calibrated Model Compared to Experiments

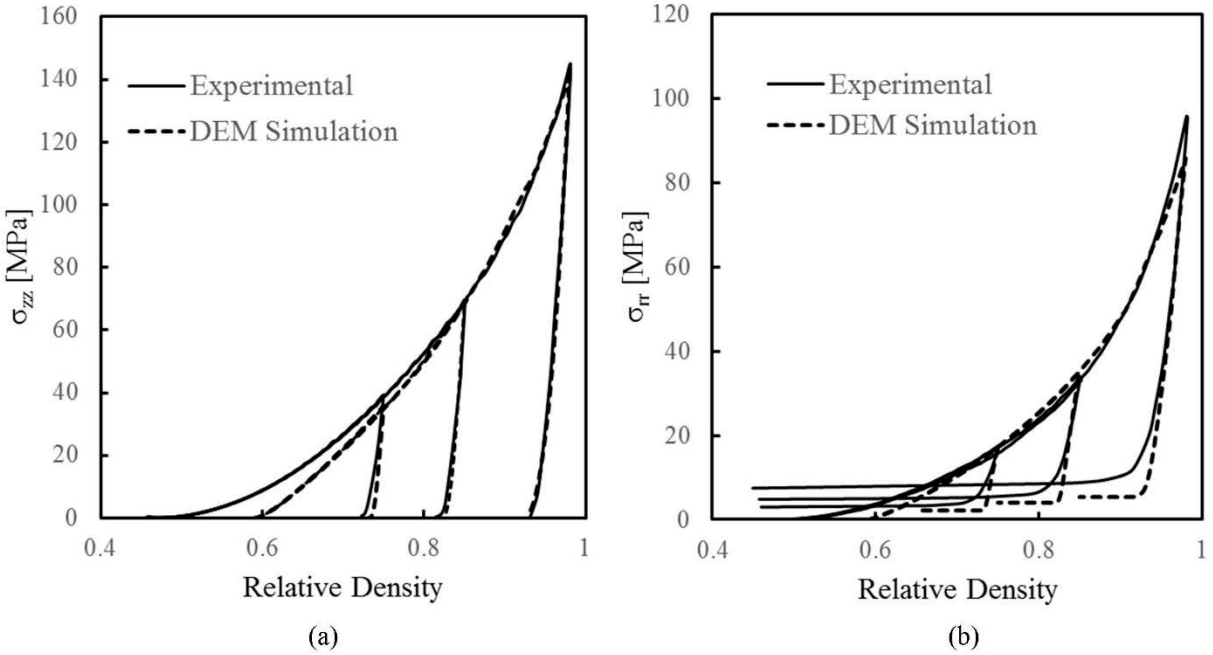

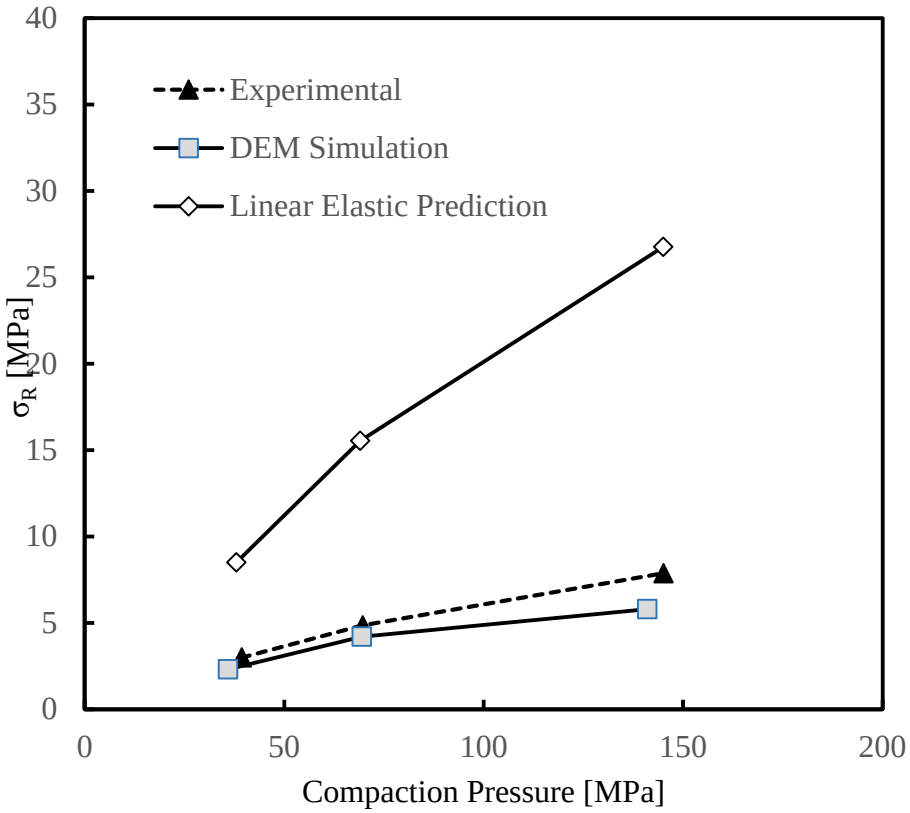

- Calibrated simple cohesive elasto-plastic contact model shows good agreement with axial stress experimental results
- Residual wall stress is under predicted for each RD→ more damage at end of loading for DEM tests compared to experiment

Effect of Cohesion on Residual Wall Stress σ_R

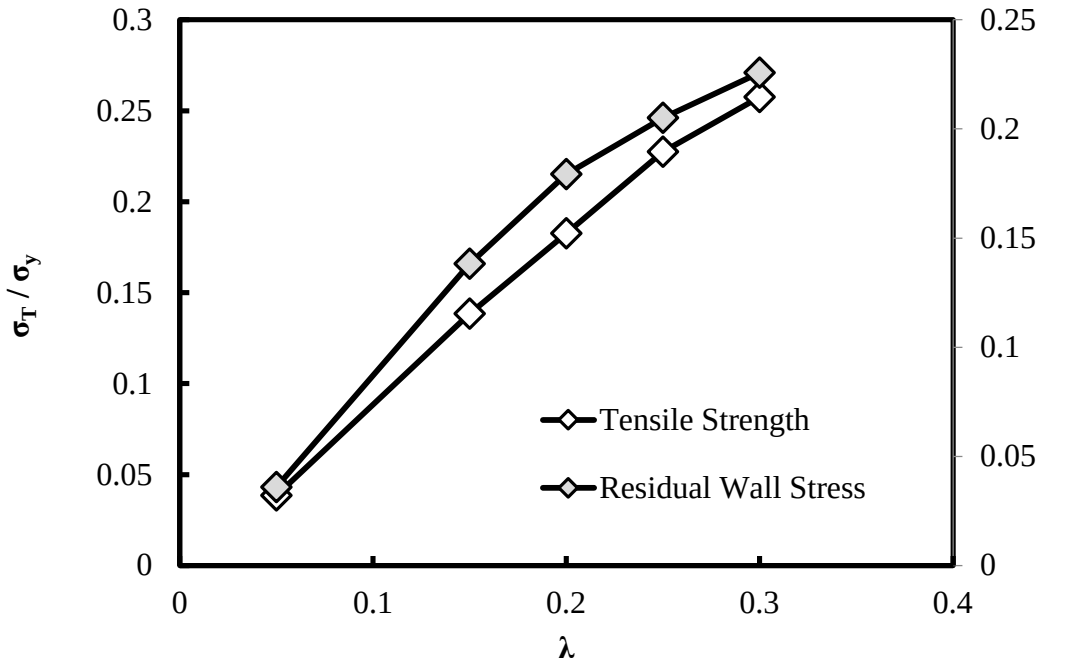

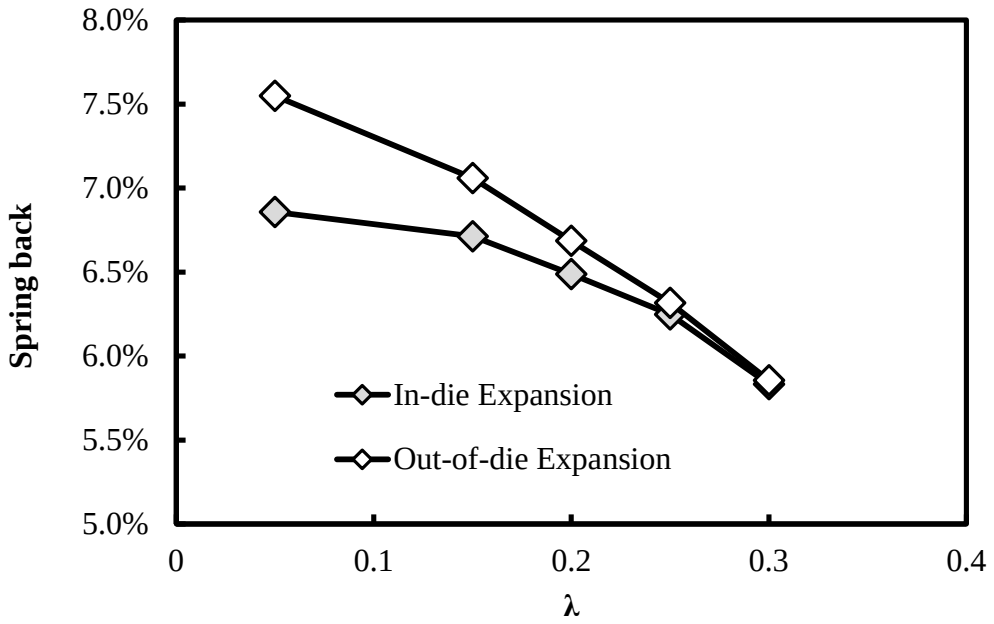

- **A weaker material (*λ* low) should exhibit a lower residual wall stress**
- **Interplay between in die microcracking and reduction of the elastic energy due to the residual wall stress**

Validation

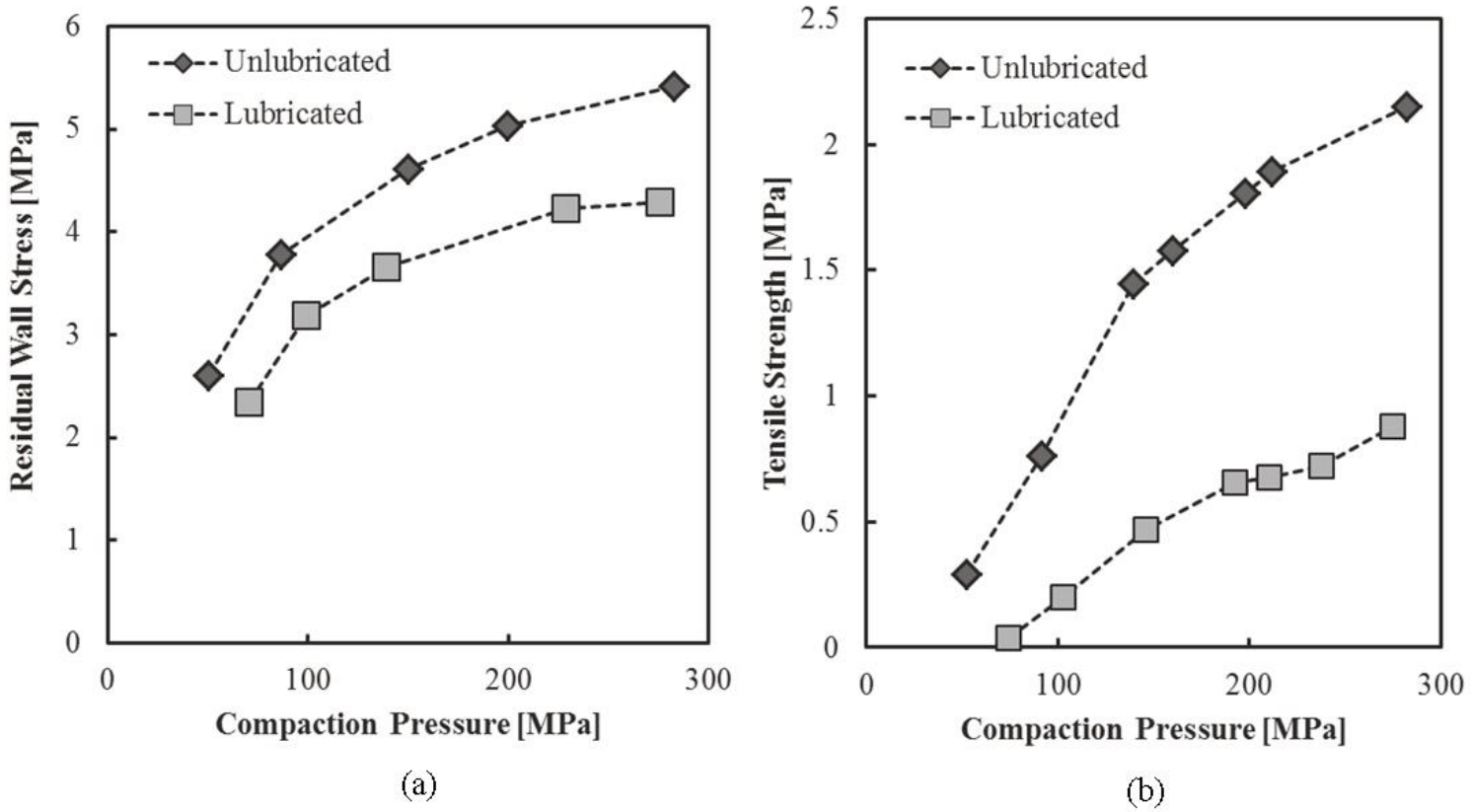

Copovidone versus Copovidone + 0.2%MgSt

Evolution of Damage During Unloading and Ejection

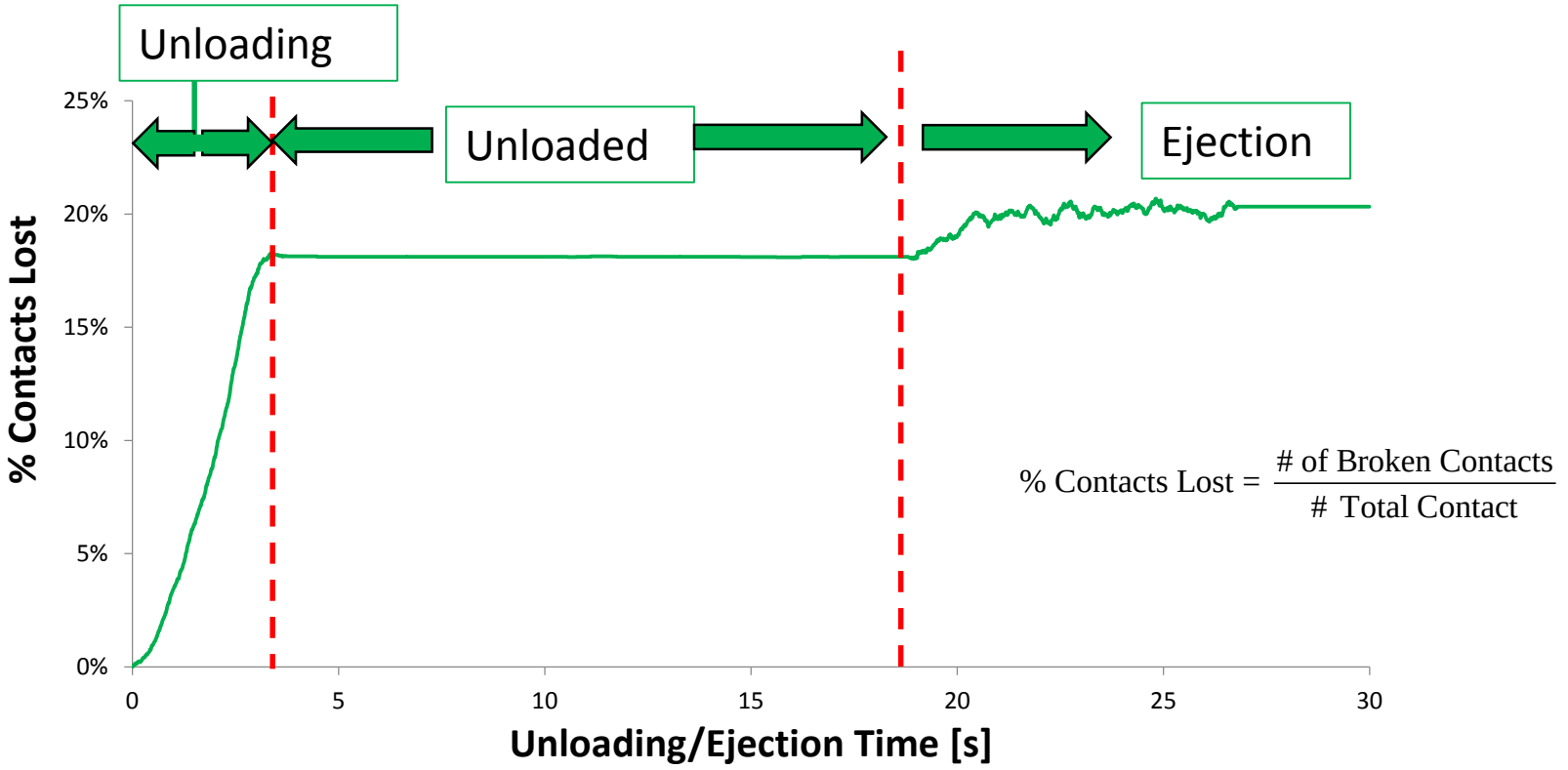

- DAMAGE BEGINS WITH UNLOADING
- EJECTION INCREASES THE DAMAGE
- FINAL STRENGTH IS A RESULT OF THE TOTAL DAMAGE

Damage as a Function of RD

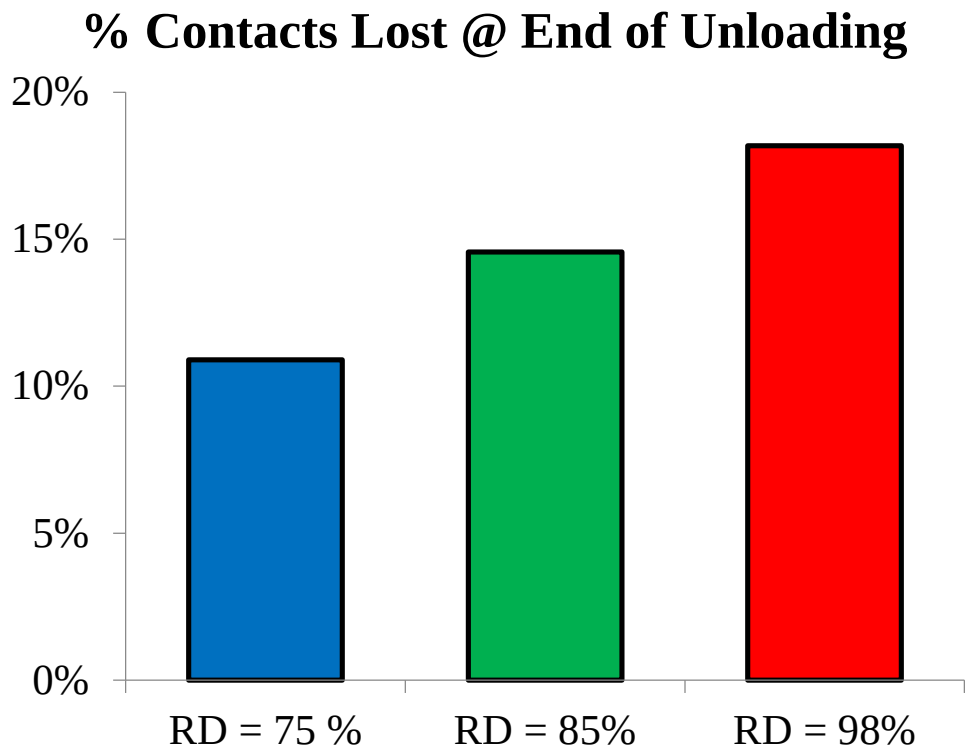

$$\% \text{ Contacts Lost} = \frac{\#\text{ of Broken Contacts}}{\#\text{ Total Contact}}$$

- While compacts with lower RD exhibit lower strength, it is experimentally observed that a decrease in damage (i.e. microcracks) occurs for decreasing RD
- Simulations show this decrease in damage

Example of increasing damage with increasing RD for MCC

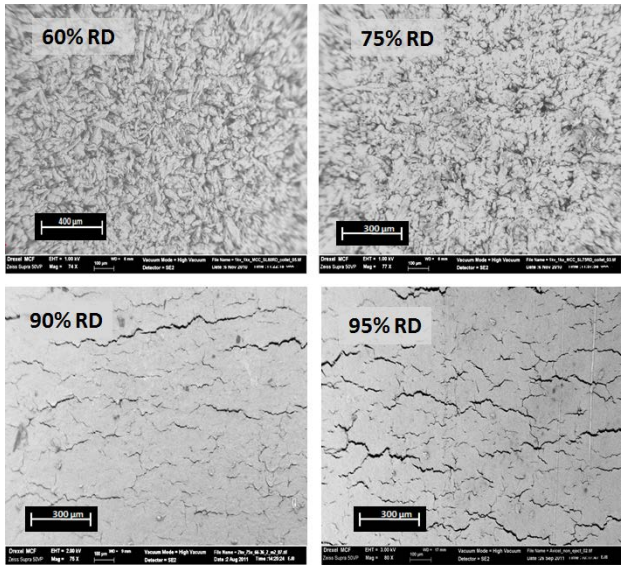

Straight vs. Tapered Die Ejection: DEM Simulation

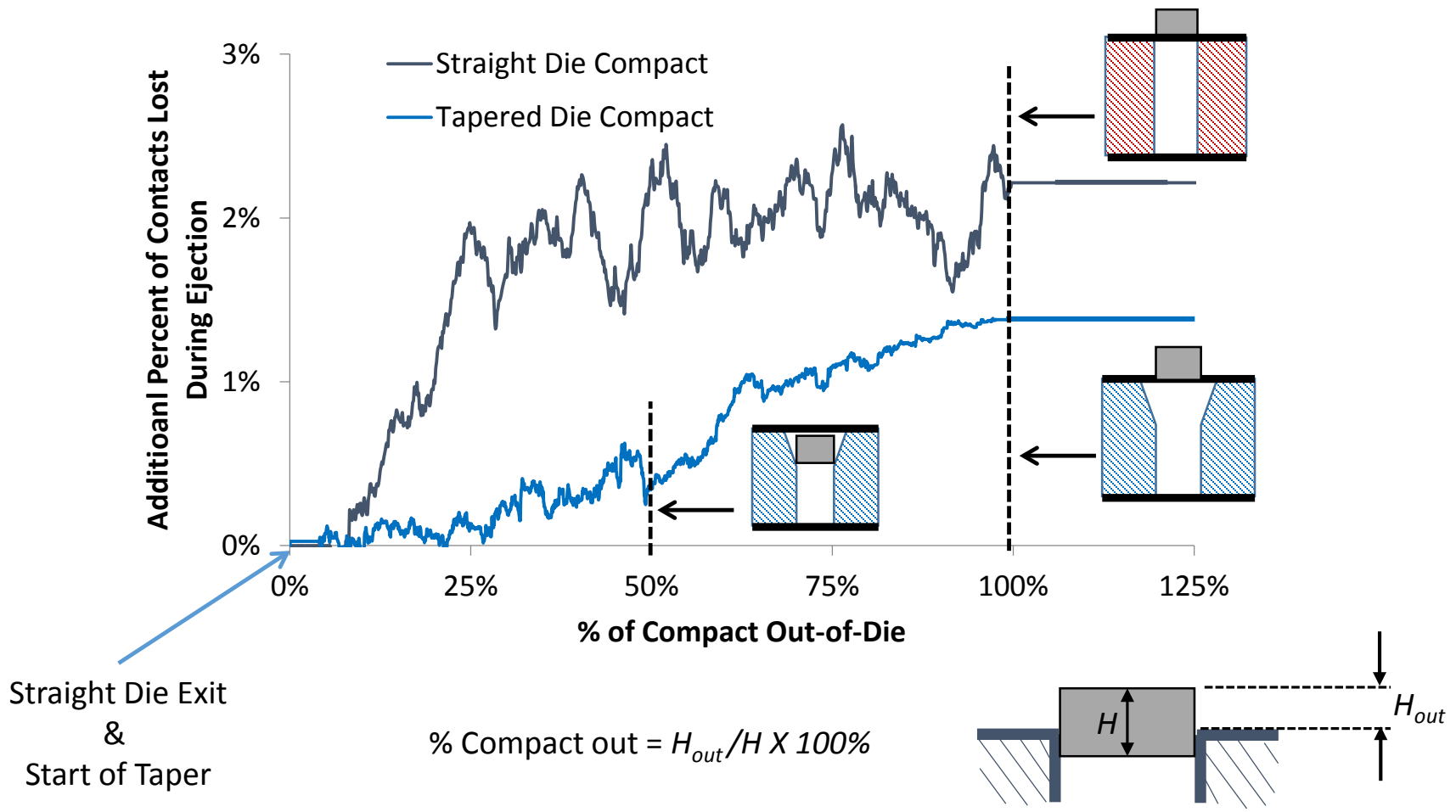

- More contacts lost during ejection of straight die compact—contacts lost more rapidly
- Gradual loss of contacts in tapered die compact -- approximately 1.0% less contacts lost than in straight die compact

Axial Tension Test Simulations

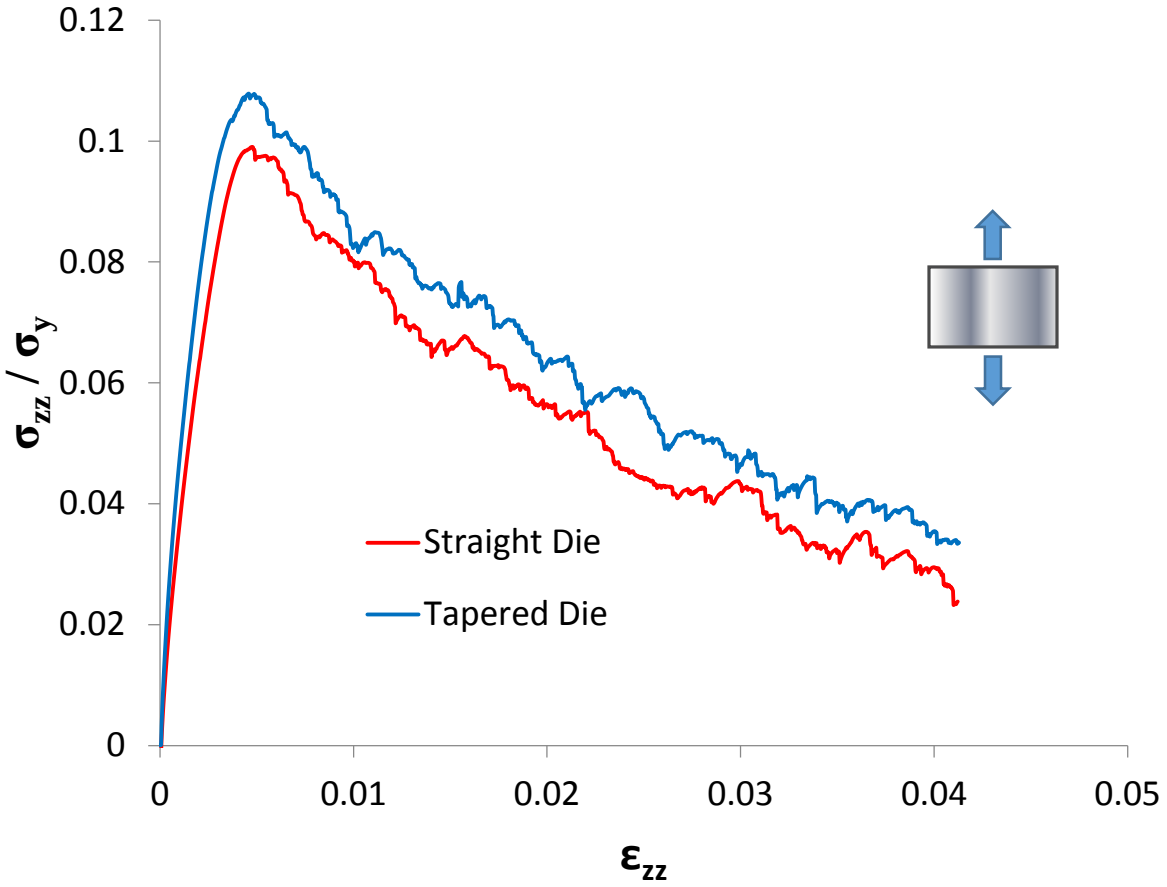

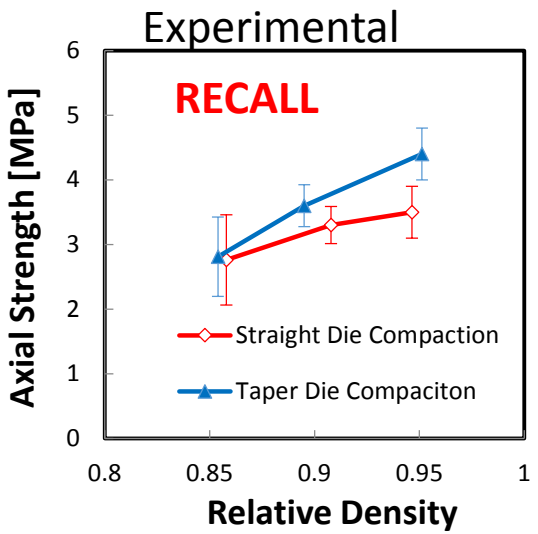

DEM result confirms experimental observation

Contacts Lost as a Function of Compact Radius

98 RD compaction of 5000 particles

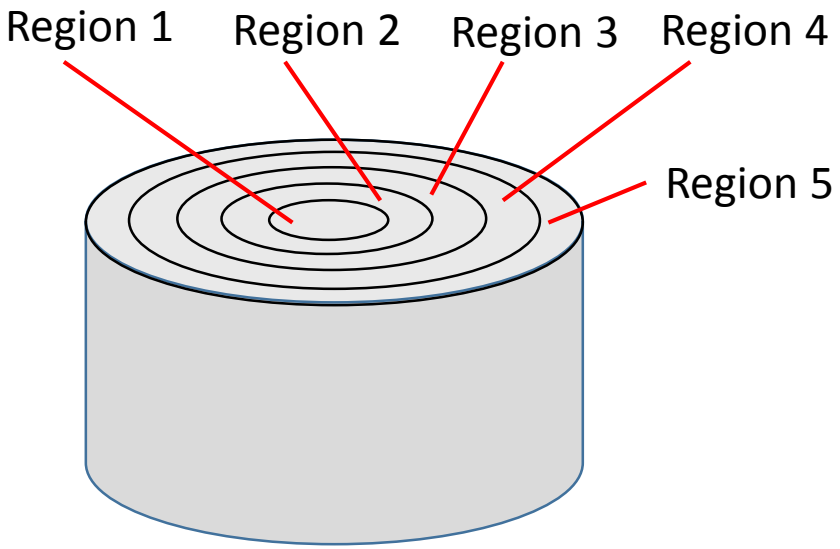

Equivalent volume per region

- Straight die shows progressively more contact loss as diameter is approached than tapered die –In-line with experimental study

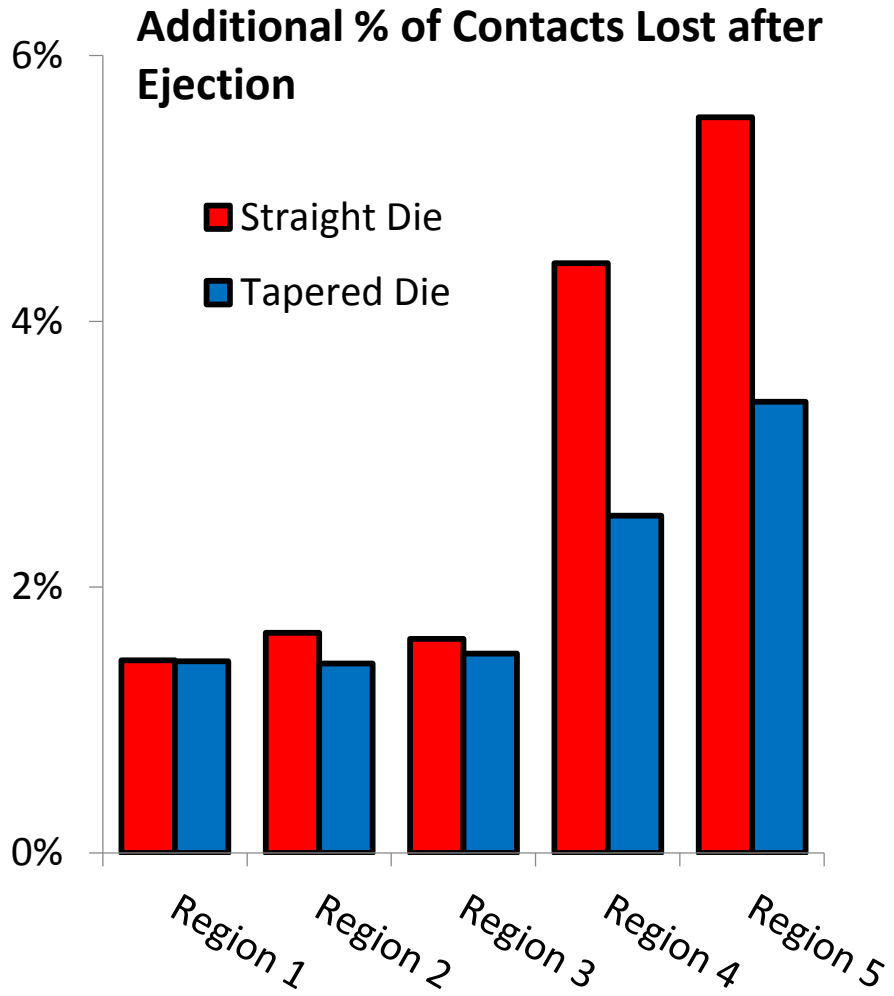

TODAY
Compaction design and optimization

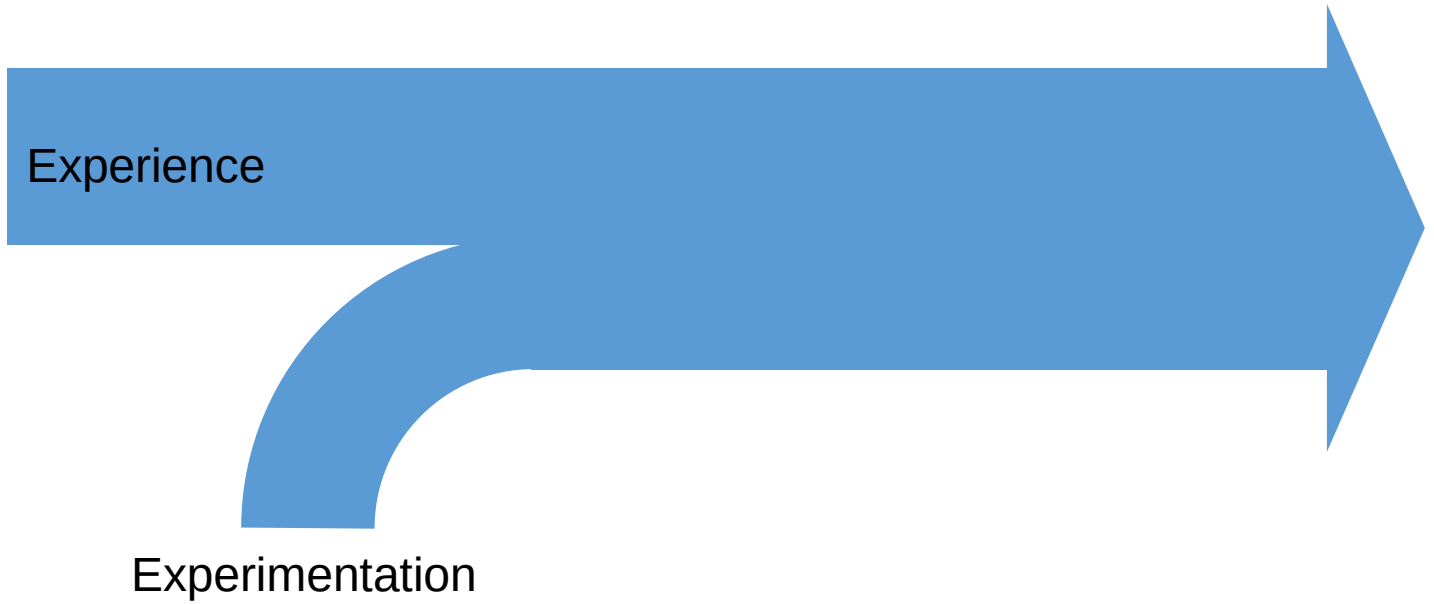

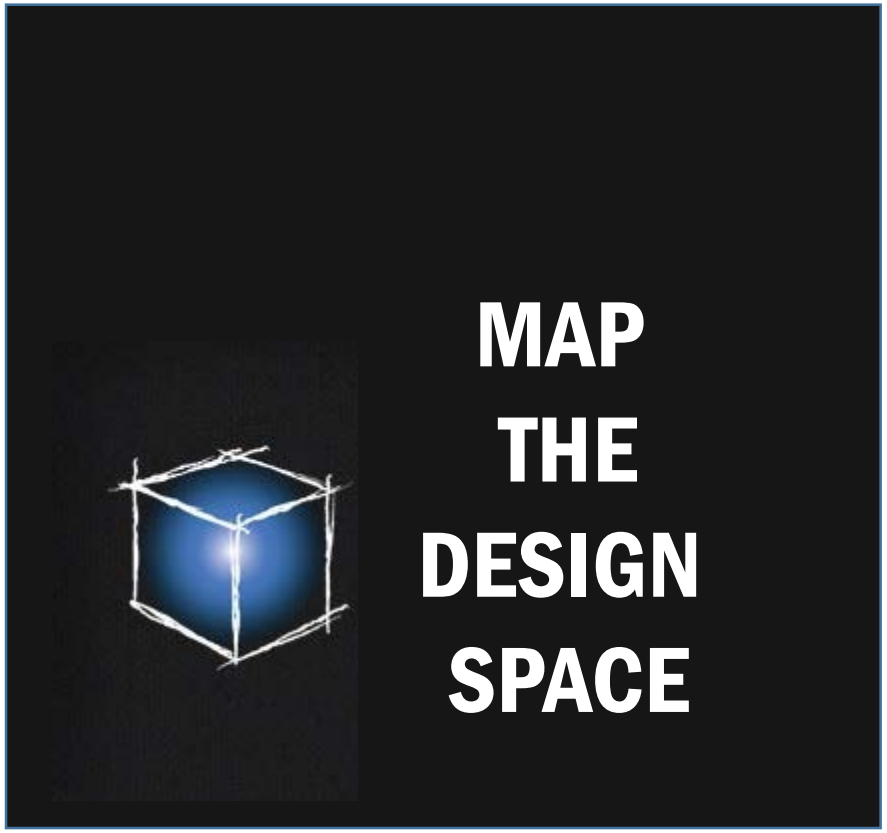

≠

Spray and pray

From Wikipedia, the free encyclopedia

“Spray and pray is a derisive term for firing an automatic firearm towards an enemy in long bursts, without making an effort to line up each shot or burst of shots. This is especially prevalent amongst those without benefit of proper training.”

THE FUTURE

To use a solid fundamental science basis to support tablet design and optimization

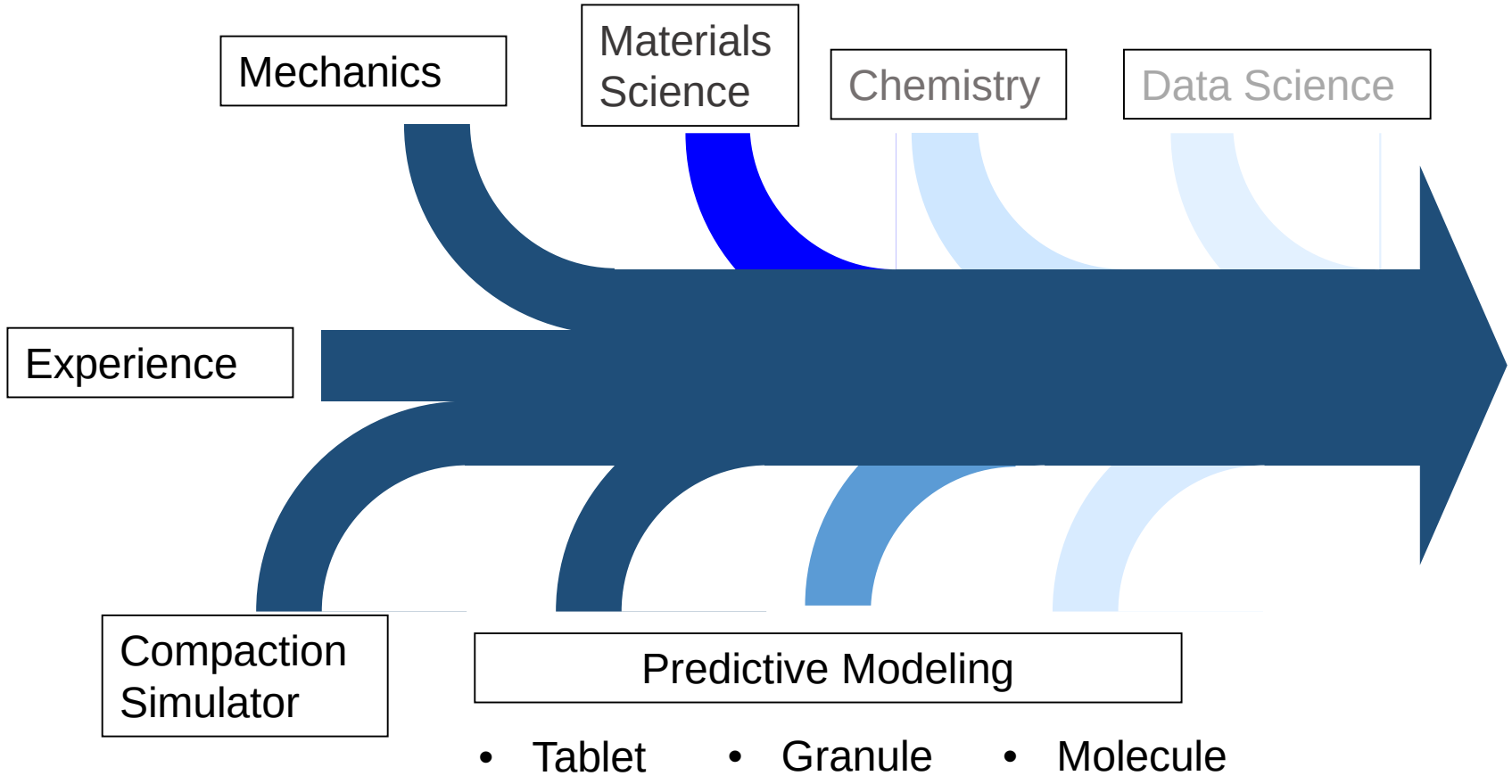

Where do we go from here

- There is plenty of work to be done on compaction (still)
- Coupled problems
  - Air flow + Consolidation
- Length scales and issues
- Structure characterization

ATOMIZATION OF VISCOUS FLUIDS

Nasser Ashgriz
Mechanical and Industrial Engineering
University of Toronto

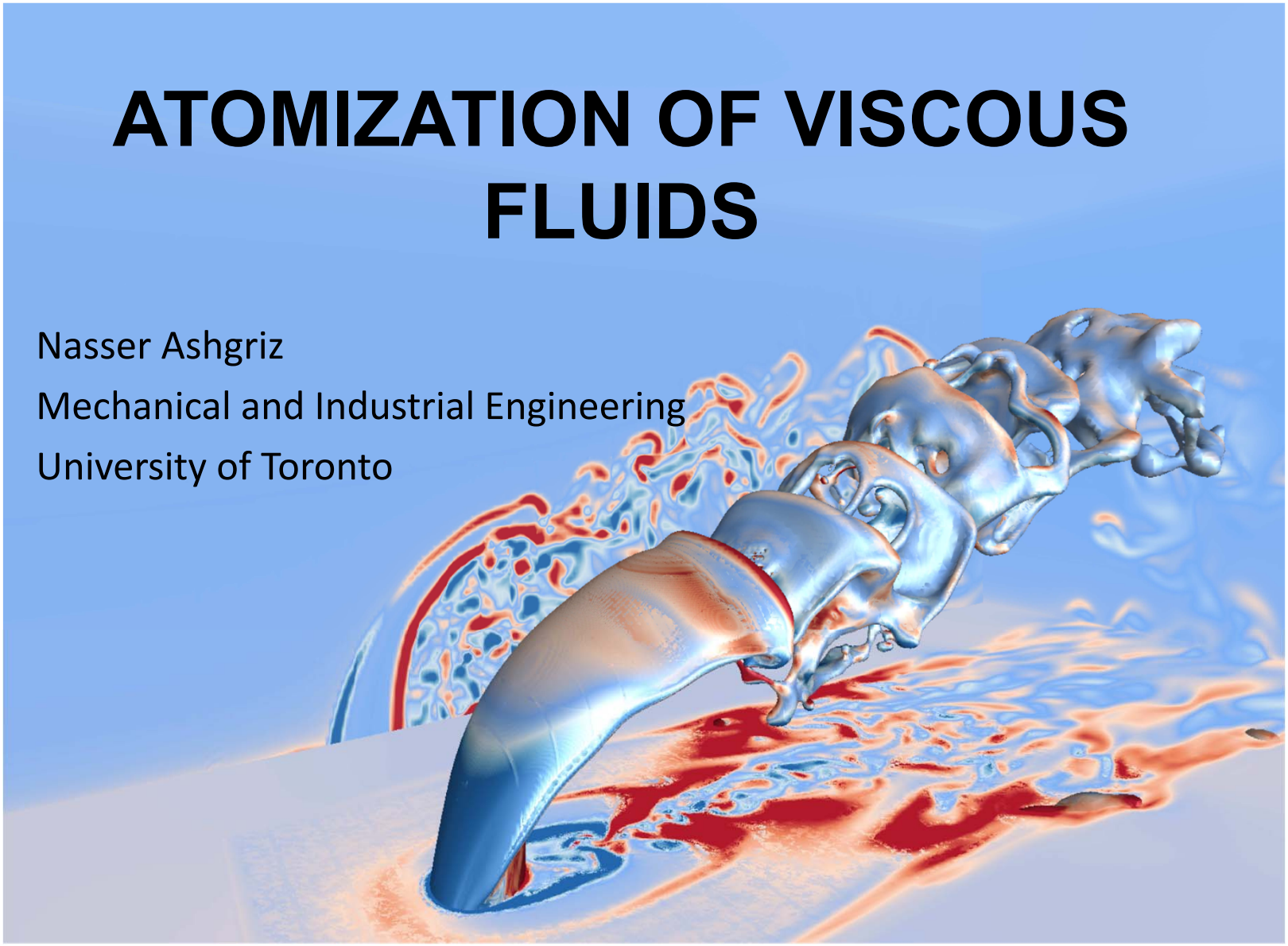

Outline

- Introduction: Spray nozzles used for high viscosity liquid
- How to choose a nozzle
- Performance of various spray nozzles for atomizing high viscosity liquids:
  - Single Fluid Nozzles
  - Twin Fluid Nozzles
- Prediction of Droplet Size Based on Nozzle Design

High Viscosity Liquids

- Numerous application areas, e.g., biofuels, petcoke, black liquor, powder production for pharma, polymers
- The application area dictates the required droplet size distribution, spray angle, flow rates, etc.

viscosity of 10s-1000s cp.

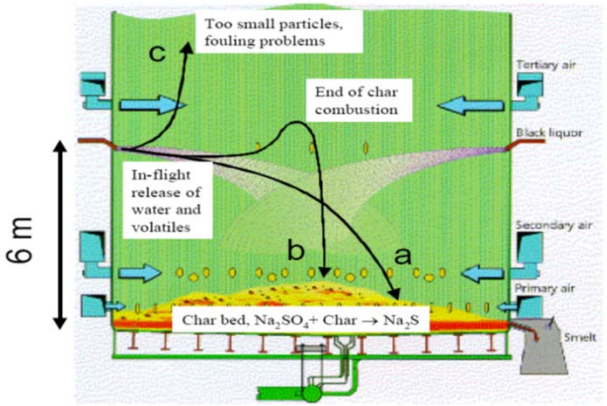

Black Liquor

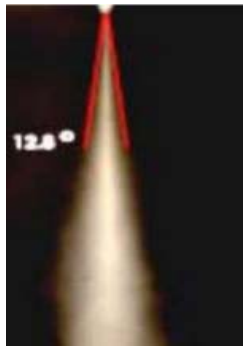

Biofuels

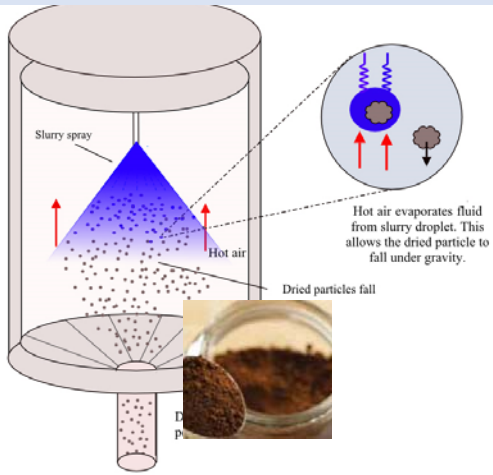

Spray Drying

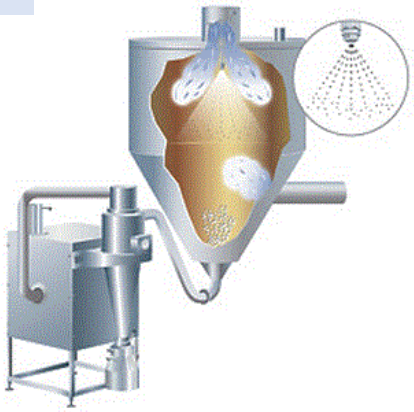

Chemical Processing

Spray Nozzles

Nozzle Types:

- Plain orifice - Diesel,
- Splash plate,
- Swirl,
- Twin fluid - effervescent
- ultrasonic,
- Rotary, and
- electrostatic.

Choose the nozzle based on:

- flow rate,
- spray angle,
- spray impact,
- droplet size,
- liquid distribution and
- spray pattern

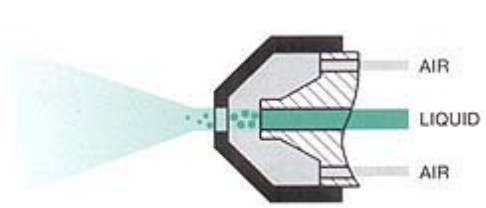

Internal Mix Twin Fluid

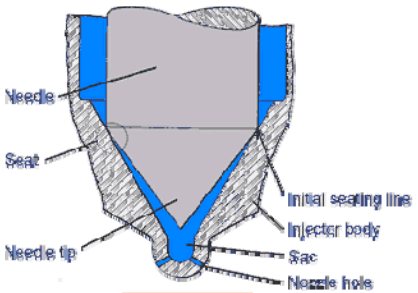

Diesel

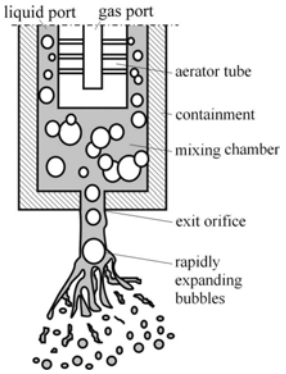

Effervescent

swirl

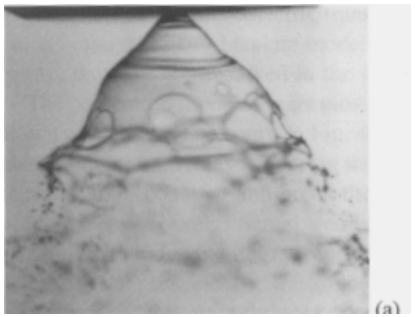

Splash Plate

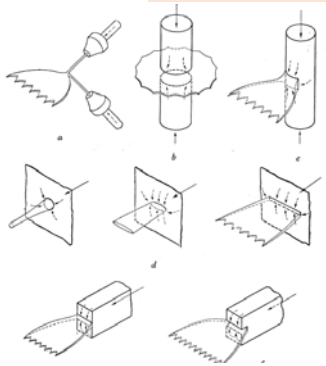

Flat fan

How to Choose a Nozzle

- The choice of an atomizing nozzle depends on the liquid properties and the application area.
- The liquid properties (density, viscosity, surface tension, as well as chemical composition) influence the atomization process in various ways.
  - High density liquids require more inertial input to accelerate them to high velocities;
  - high viscosity liquids dissipate the input energy, and
  - high surface tension liquids require more energy to form the required surface energy of the small drops.
- The higher the value of any of the three liquid properties, the more difficult it is to atomize the liquid and more energy is needed for its atomization.
- Liquids with solid suspensions have added complexity (e.g., coal slurries, black liquor):
  - Larger solid particles may separate from the liquid after atomization resulting in a bimodal droplet size distribution.

Single Liquid Nozzles: Diesel Nozzle

The Effect of Kinematic Viscosity on Sauter Mean Diameter, D_{32} - Pa=30 MPa

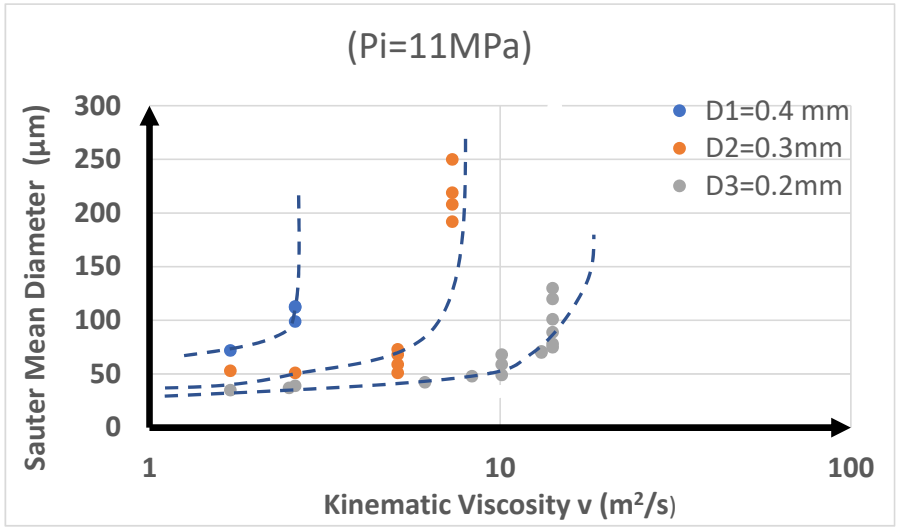

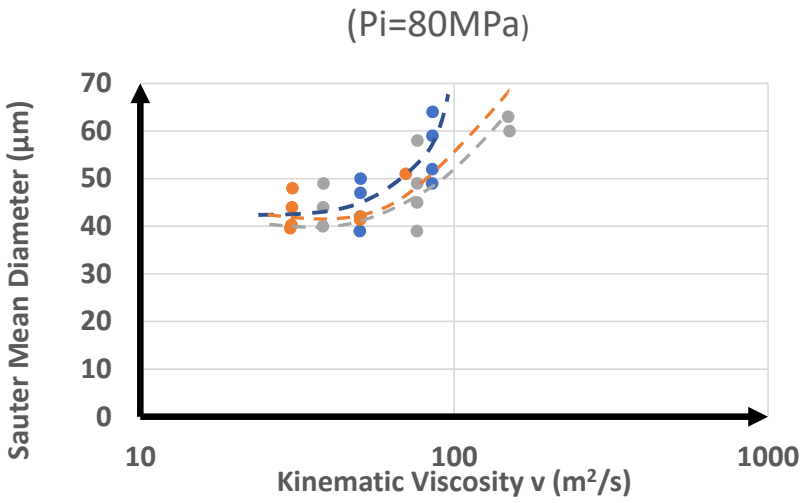

Tabata et al. (1986) for biofuels

✻Effect of viscosity diminishes as the injection pressure is increased.

Gas-Liquid Nozzles: Twin fluid nozzles

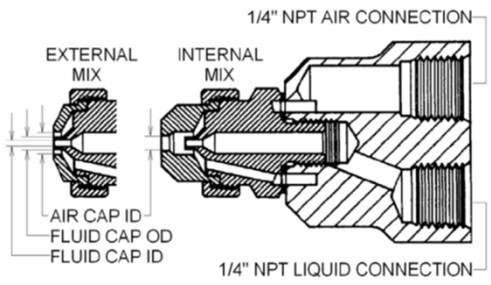

External mix

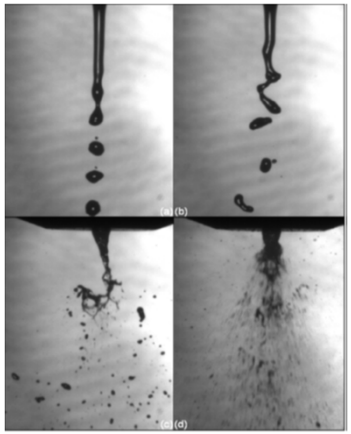

Increasing air flow

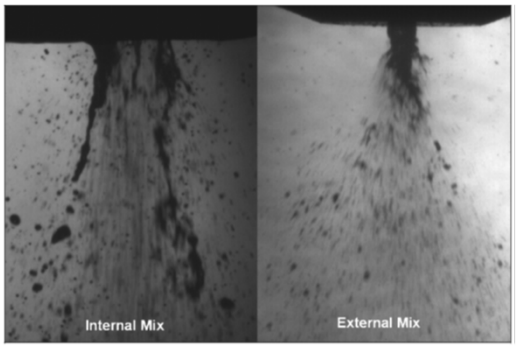

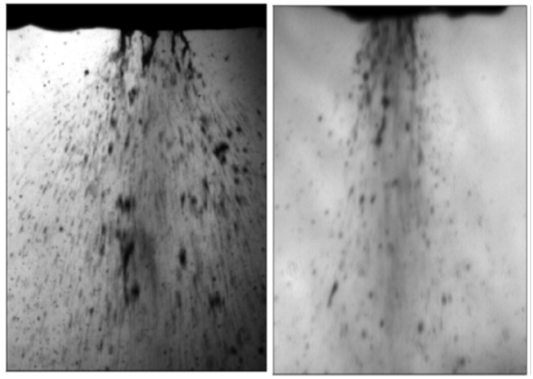

Mackrory, A.J., BYU, PhD., 2006

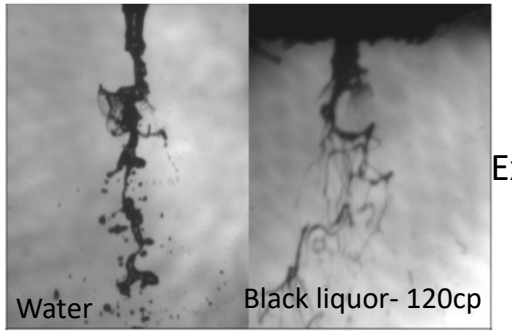

External mix

Aliseda et al., J. Multiphase flows, 2008

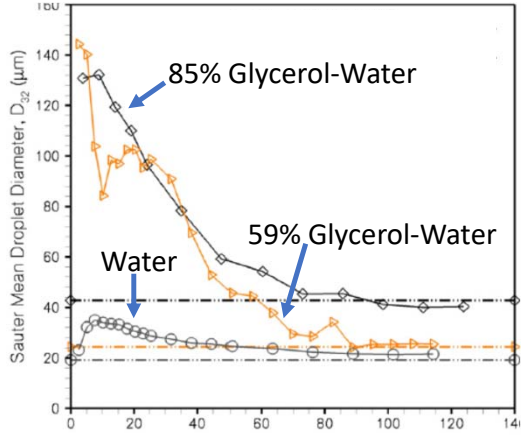

Z(mm) Distance for the nozzle

Y-jet & Effervescent Nozzles

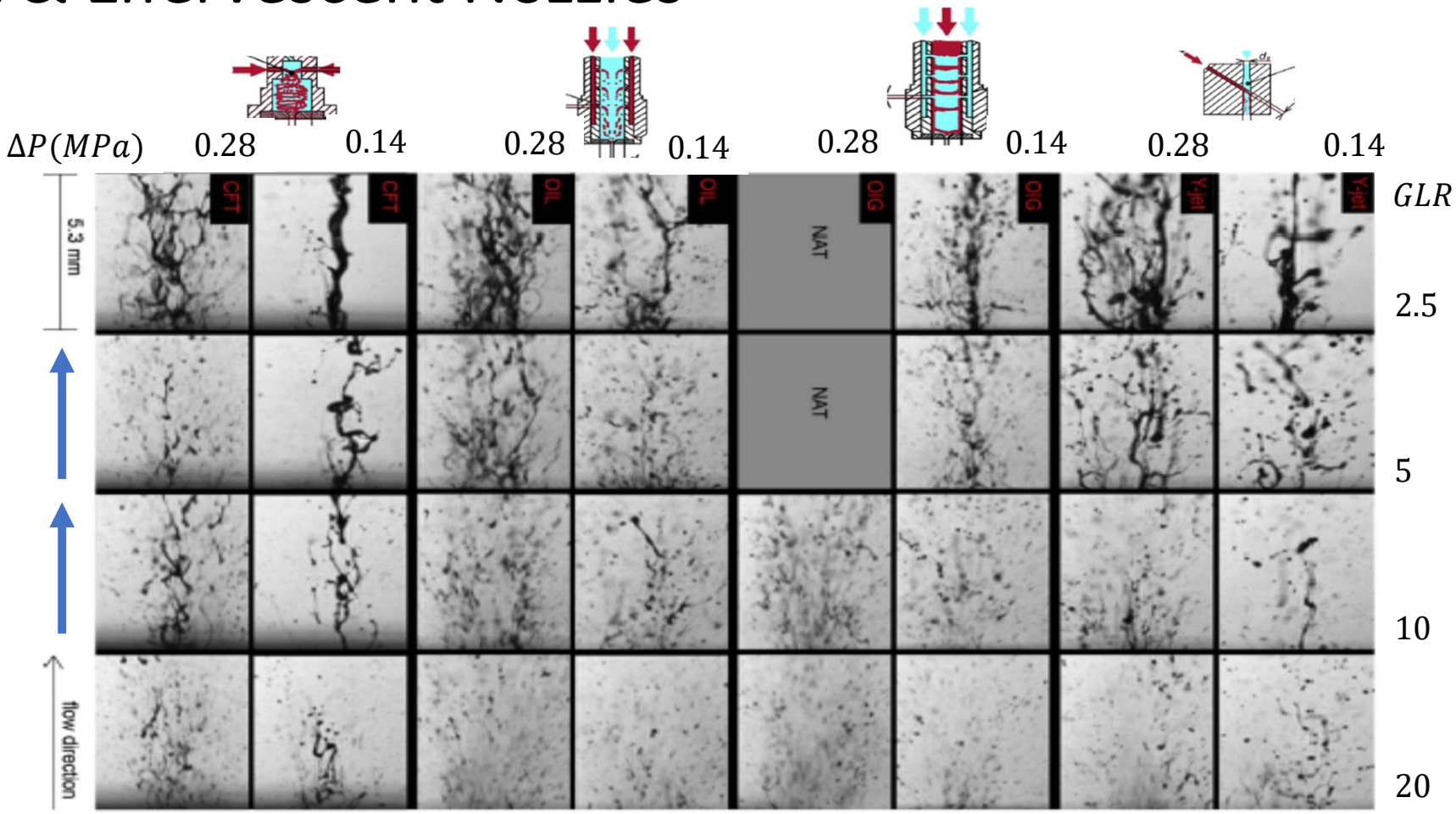

Mlkvik, et al., J. Multiphase flows, 77 (2015)

Effect of Viscosity on SMD - General Findings

- Although some studies show that SMD increases with viscosity, most studies show that SMD is not significantly affected by viscosity far downstream of a nozzle.
- SMD decreases with an increase in gas to liquid ratio (GLR), but the negative effects of viscosity become stronger as GLR increases.
- The negative influence of viscosity on SMD becomes obvious only at high operating pressures.

Single Liquid Nozzles: Splash Plate Nozzles

- Significant discrepancy in the reported result for this nozzle.

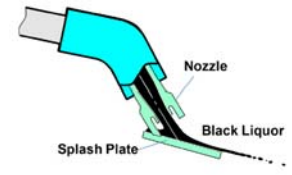

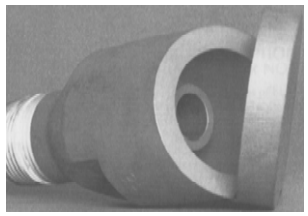

$$d_{MN} = C\mu^a V^b d_n^c \rho^d \sigma^e$$

	d_{MN}	C	μ^a	V^b	d_n^c	ρ^d	σ^e
Ashgriz et al.	d_{32}	8.6	0.06	-0.4	0.28		
Bennington & Kerekes	d_{32}	1600	0.18	-0.54	0.64	-0.36	0.18
Dombrowski & John	d_{mm}	1880	0.1	-0.55	0.65	-0.21	0.24
Empie et al.	d_{mm}	5.6	**0.026**	-0.39			
Helpio & Kankunen	d_{mm}	1350	**0.26**	-0.26	0.74	0.26	

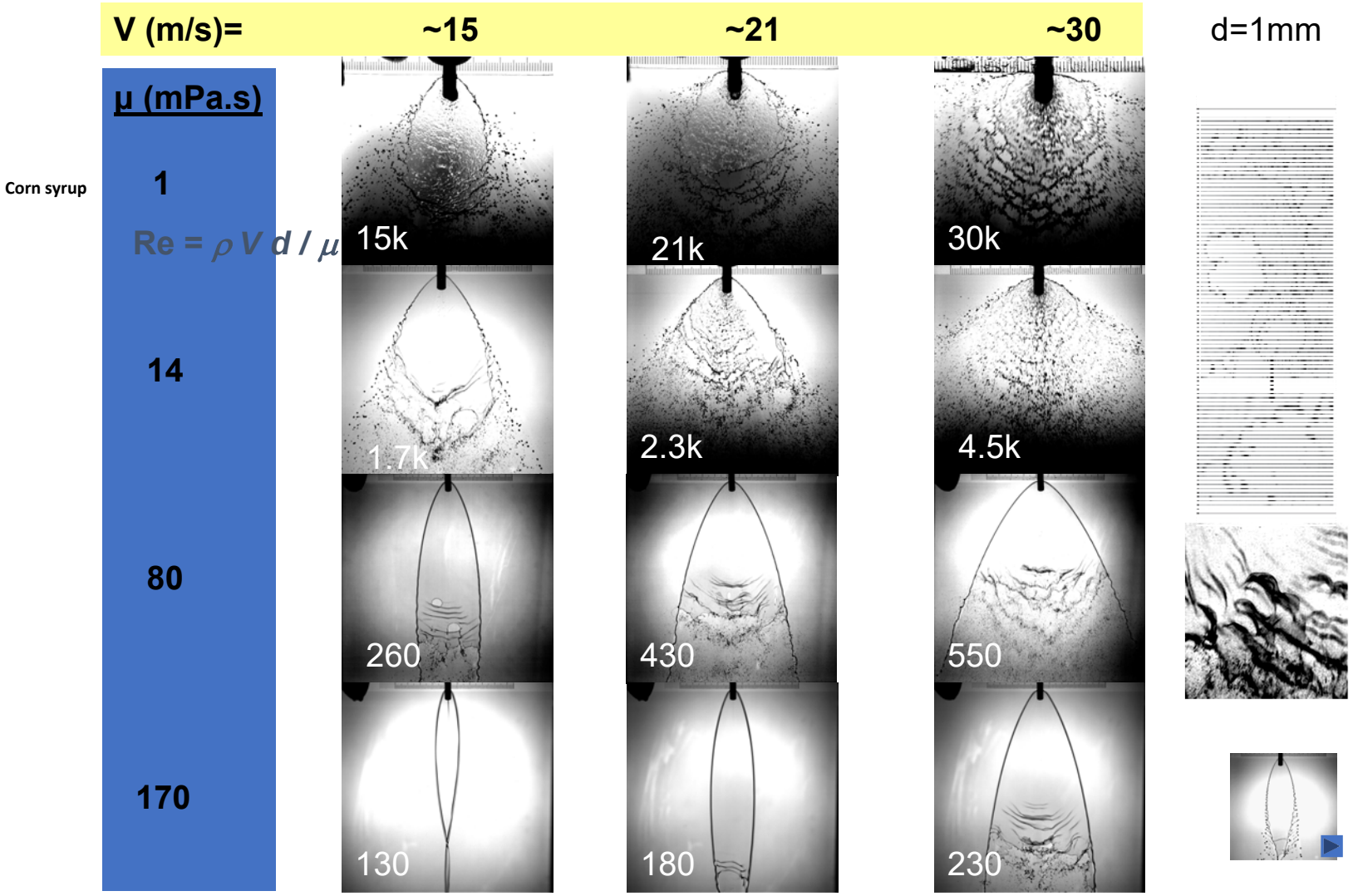
V (m/s)=
~15
~21
~30
d=1mm
μ (mPa.s)
Corn syrup
1
Re = ρ V d / μ
14
80
170
15k
21k
30k
1.7k
2.3k
4.5k
260
430
550
130
180
230

Mechanisms of droplet formation

- **Aerodynamic surface waves**

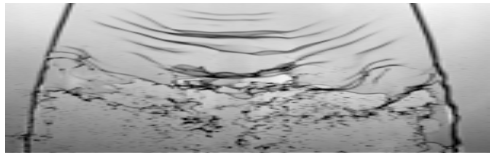

V	μ	d	Re
12	**12**	1	250

- **Laminar edge instability**

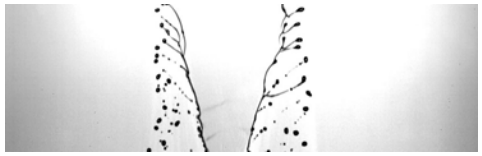

30	**170**	**1**	**1300**

- **Laminar tearing**

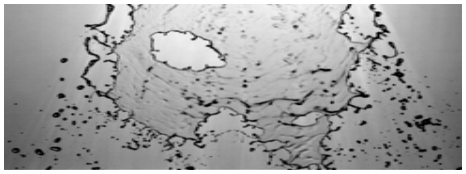

9	**12**	**2**	**1,700**

- **Turbulent edge instability**

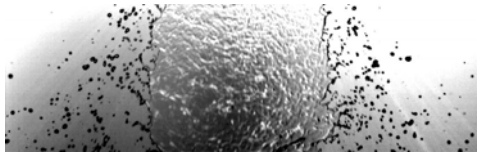

15	**1**	**1**	**15,000**

- **Turbulent Tearing & perforation**

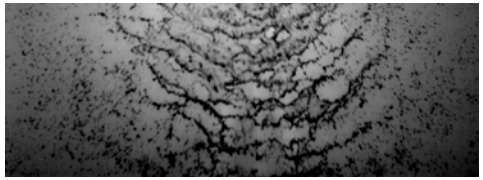

30	**1**	**1**	**30,000**

Different Breakup Regimes

$$Oh = \frac{\mu}{\sqrt{\rho \sigma d}}$$

$$\mathrm{Re} = \frac{\rho V d}{\mu}$$

A

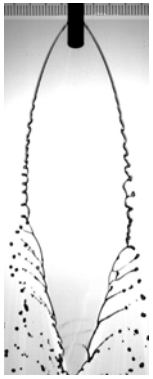

B

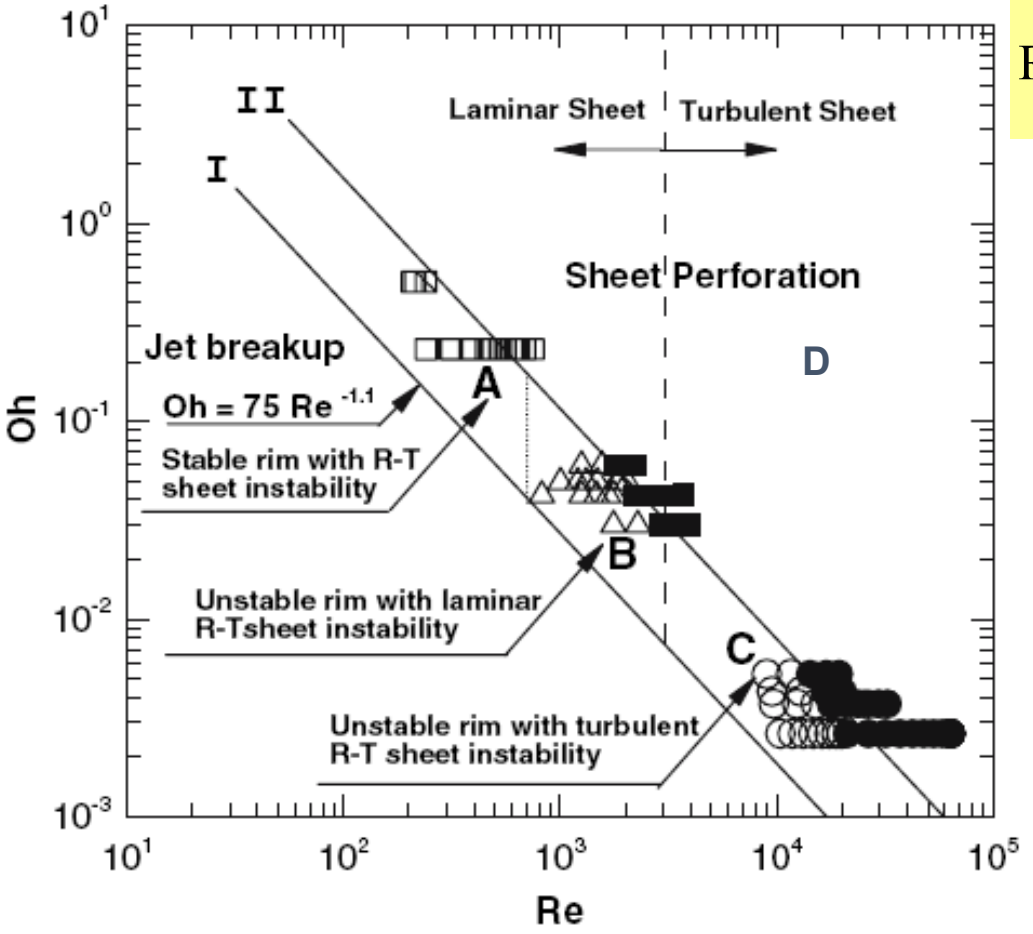

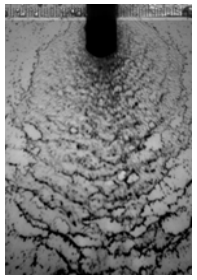

D

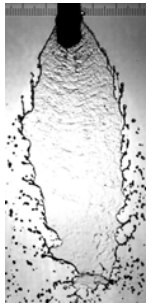

C

Comparison of various correlations

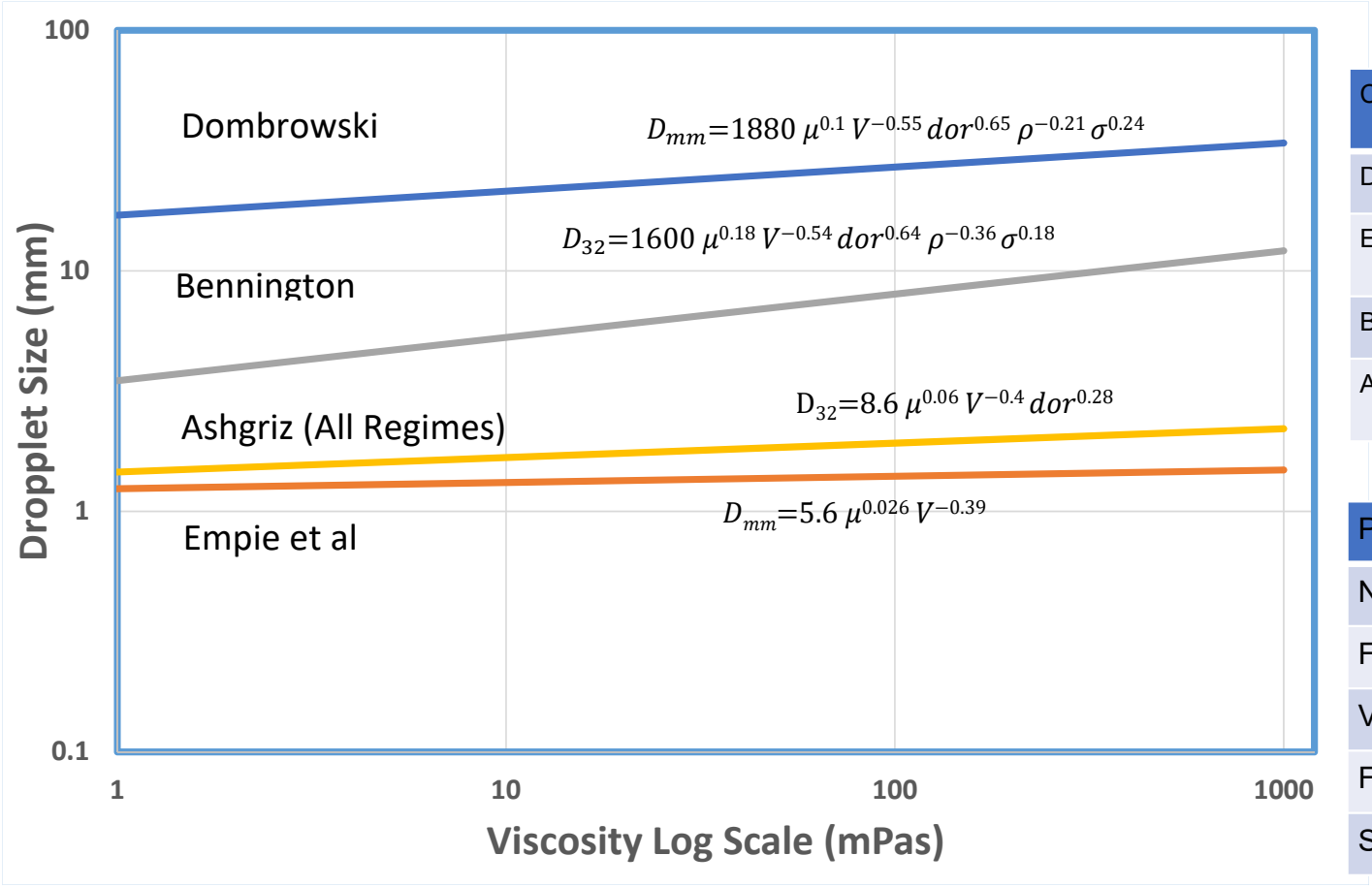

Correlation	Nozzle Di (mm)	Viscosity (mPas)	Fluid
Dombrowski	-	-	-
Empie et al	8.5 - 9.5	50 - 200	Black Liquor
Bennington	1.0	1 - 15	Glycerol/ Water
Ashgriz	0.5 - 1	65 - 140	Corn Syrup/ Water

Parameter Used	Value
Nozzle Diameter (mm)	1
Fluid Velocity V (m/s)	30
Viscosity Range (mPas)	1 - 1000
Fluid Density (kg/m3)	1225
Surface Tension (N/m)	0.067

Correlation for each breakup regime

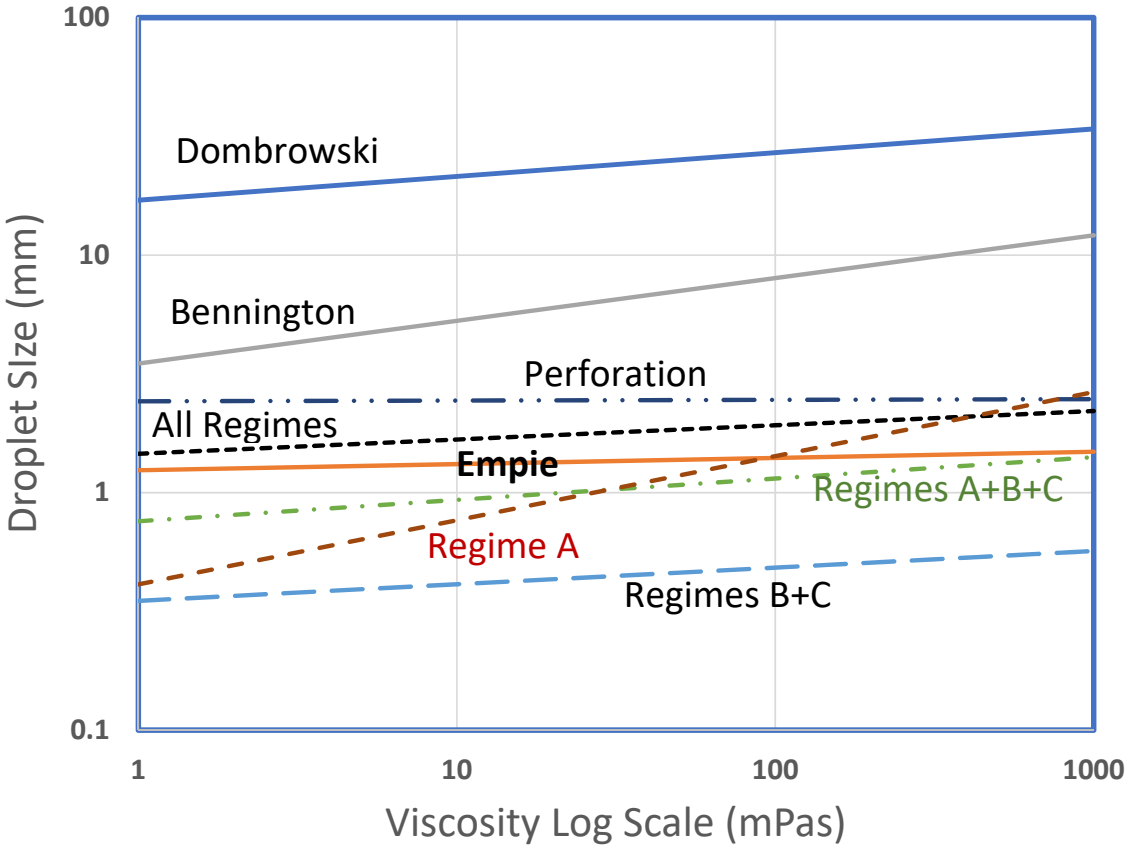

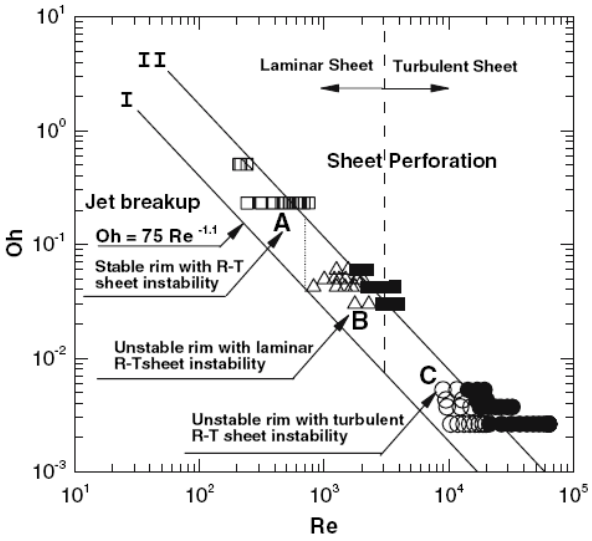

Splash Plate Nozzles – viscosity effect on SMD

- The theoretical predictions show that $d \propto \mu^{0.1}$.
- Experimental results on practical splash plate nozzles show a viscosity dependency of $d \propto \mu^{0.003}$ to $d \propto \mu^{0.26}$.
- Droplet size is strongly affected by the viscosity, $d \propto \mu^{0.26}$, at low Re, Re< 800, and high Oh, Oh> 0.22
- Droplet size is moderately dependent on viscosity, $d \propto \mu^{0.07}$, at moderate Re and Oh numbers, 800<Re< 3000, and 0.03<Oh< 0.22.
- Droplet size is weakly dependent on viscosity, $d \propto \mu^{0.003}$, at high Re, Re> 18000, and low Oh, Oh <0.003
- Therefore, the discrepancy between different correlations may be due to different breakup regimes that the nozzle was tested for.

How to Choose a Nozzle and Predict the Droplet Size

1. Determine the requirement from the spray application.
2. Determine a nozzle that may potentially provide the required droplet sizes, etc.
3. Determine Liquid Characteristics in Primary Atomization Region – Near the Nozzle.
4. Parametric study of the Nozzle design parameters to determine the optimum conditions.
5. Provide the Primary Atomization information to a spray code with a secondary atomization model, to determine the spray size distribution further downstream.
6. Parametric study of the flow conditions to obtain desired size distributions.

Theoretical Prediction of Droplet Sizes

1- Simulate the internal flow of the nozzle to determine the governing characteristic dimensions.

2- Use a model to determine the initial droplet sizes in the primary atomization region.

For example, droplet sizes can be obtained from the liquid sheet thicknesses close to the exit of the nozzle.

A Linearized Instability Sheet Atomization (LISA) model can be used to find droplet sizes. In LISA, droplet size is related to the wavelength belonging to the most unstable disturbance wave number on the surface of the liquid sheet.

3-Use a spray model for the secondary atomization and to calculate droplet sizes downstream of the nozzle.

Example 1: BL Gasifier -What constitutes a good nozzle?

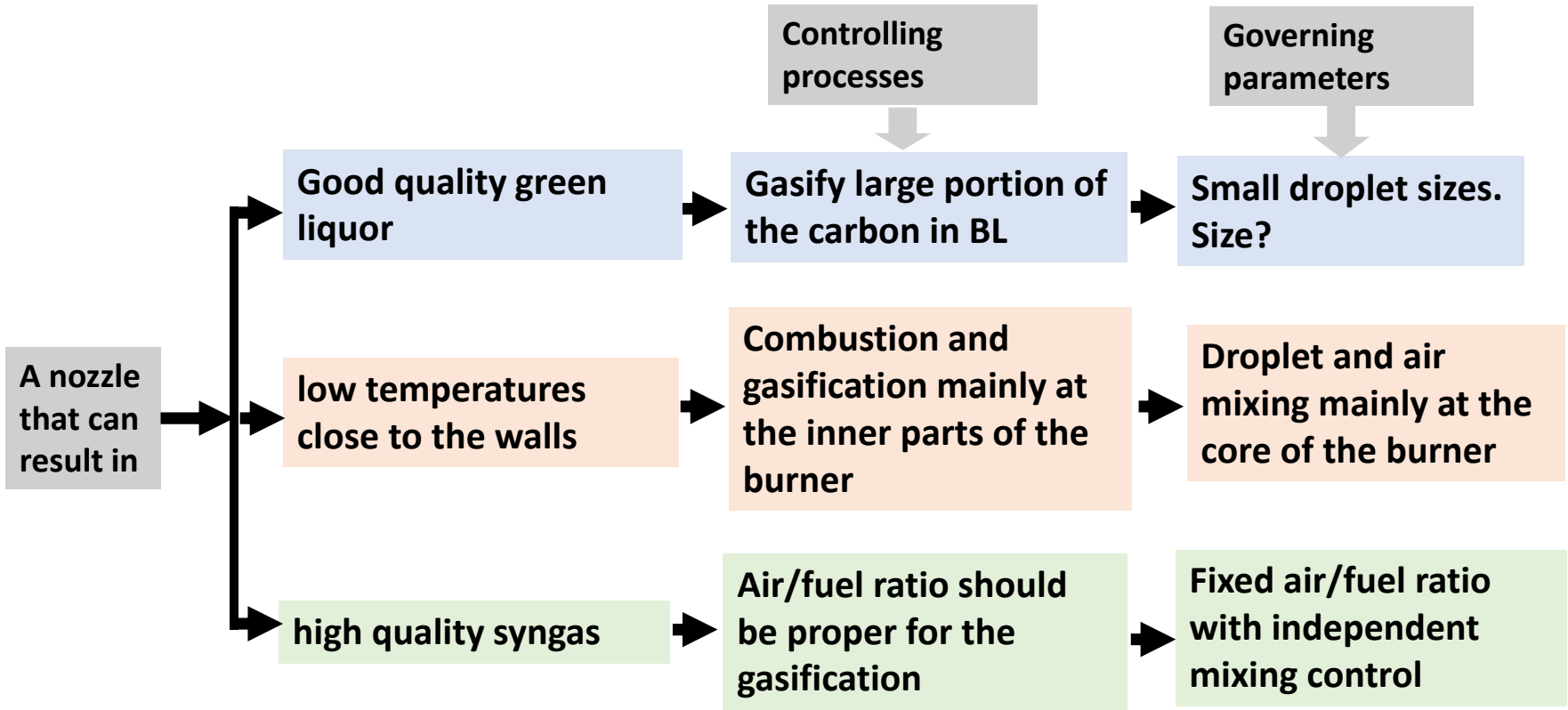

Example 1: Criteria for Selecting the Nozzle

The nozzle should be able to

- spray a liquid with high viscosity (typically 100 cP);
- handle liquids with particles and liquids which are corrosive;
- generate a spray with drop sizes of less than 300 microns;
- handle large mass flow rates, and
- operate at high temperatures.

Example 1: Potential Nozzles

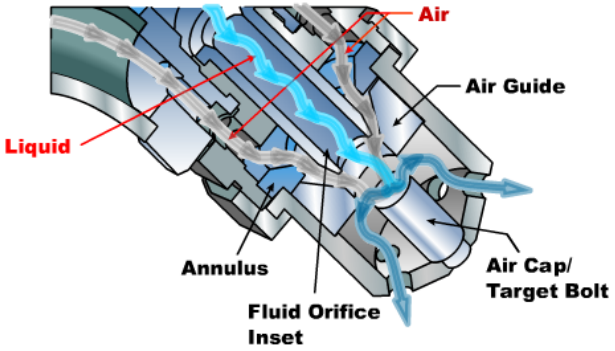

Y-jet: SMD=60µm, Q=20gpm with air

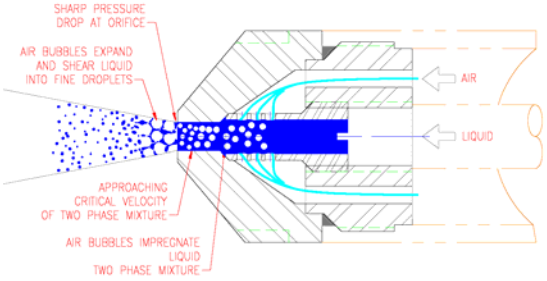

Effervescent: SMD=40µm, Q=20gpm with air

Operating Param.

P_s = 10 bars

T_s = 200 °C (400 F)

m = 5500-6000 lb/hr

= 207-218 m/s

M_{BL}= 30-50 GPM

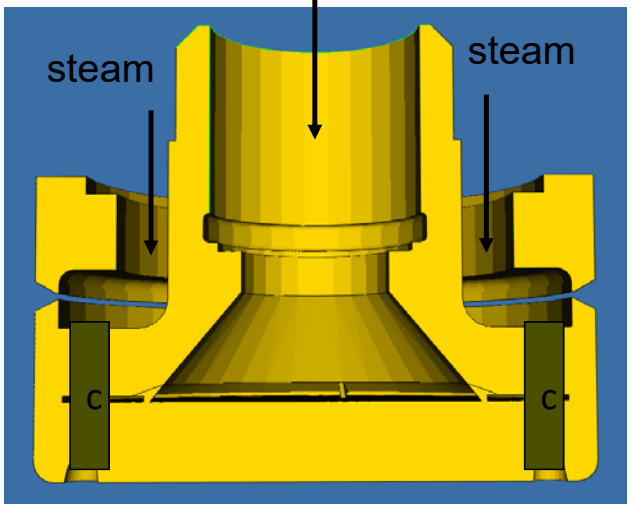

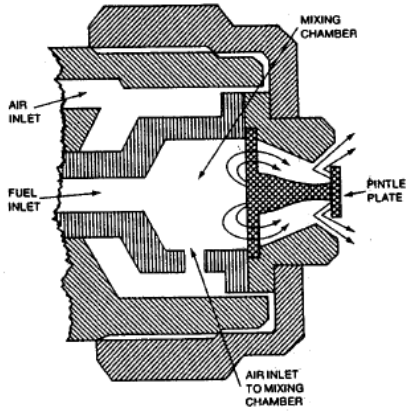

Swirl: SMD=100µm, Q=25gpm air at 50psi

Example 1: Primary Atomization Region – Near the Nozzle

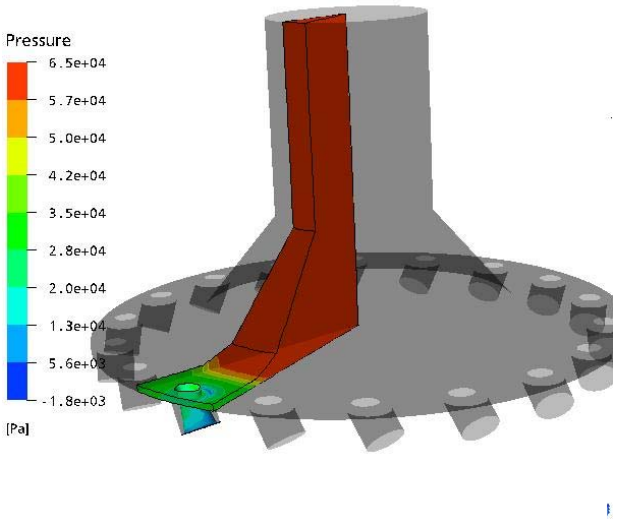

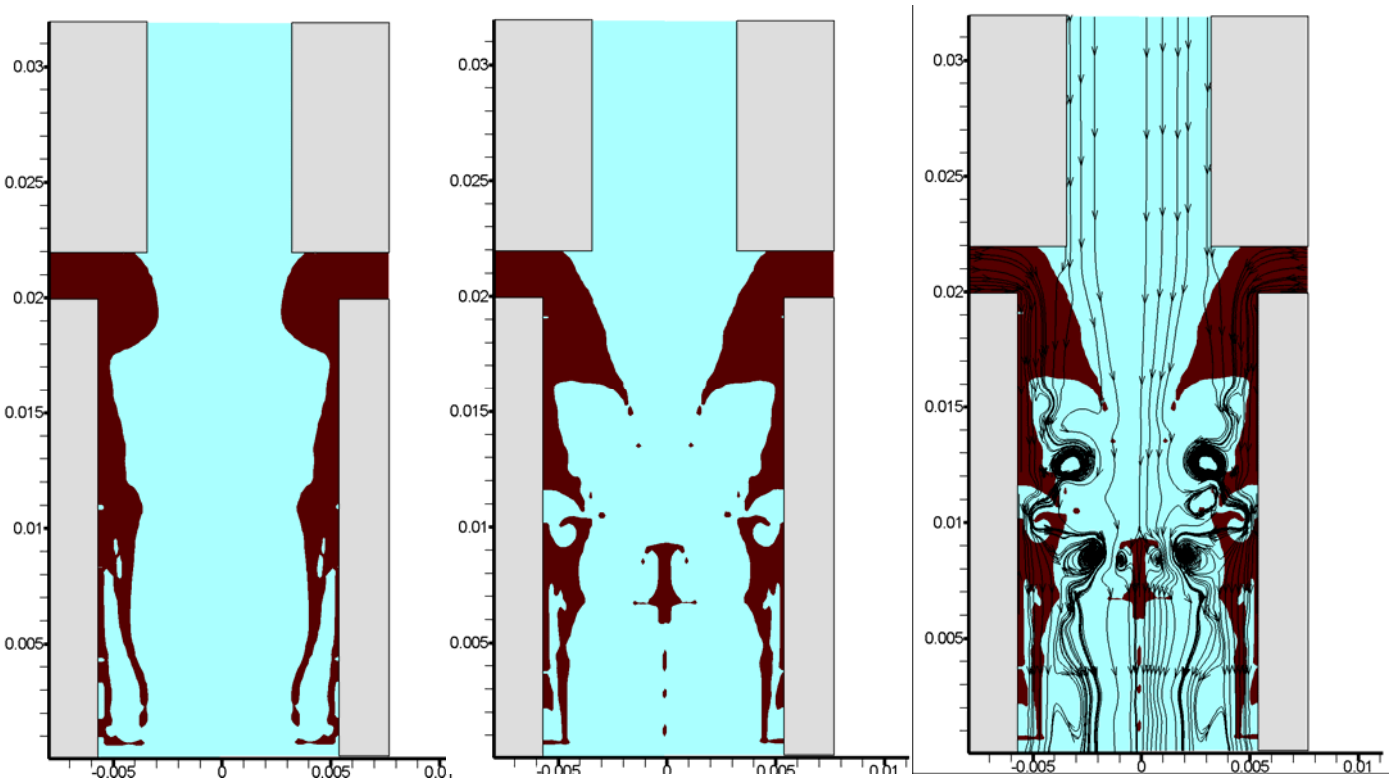

Example 1: Effect of Nozzle Parameters on Spray

	Steam Velocity (m/s)		
	100	200	300
Average(microns)	518.3	328.72	273.53
Max(microns)	1679.47	917.22	662.09
Min(microns)	5.611	0.827	2.759
Stdv(microns)	253.49	164.74	113.39
Variance(microns^2)	64258.976	27140.05	12856.77
Frequency	**800**	**1110**	**1110**

	BL Velocity (m/s)		
	1.5	2	2.5
Average(microns)	336.25	328.72	352.46
Max(microns)	1161.8	917.22	1156.09
Min(microns)	1.583	0.827	1.182
Stdv(microns)	169.37	164.74	190.39
Variance(microns^2)	28687.867	27140.05	36246.58
Frequency	790	1110	1220

	R1=3.5mm	R1=5.5mm
	Teta=30	Teta=30
Average(microns)	363.97	211.57
Max(microns)	1095.62	526.27
Min(microns)	0.602	1.045
Stdv(microns)	165.44	95.29
Variance(microns^2)	27369.088	9080.629
Frequency	1770	2400

Effect of Steam Velocity

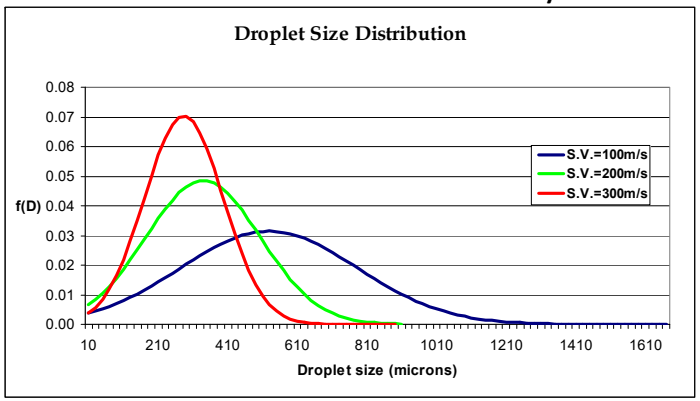

Effect of Liquid Velocity

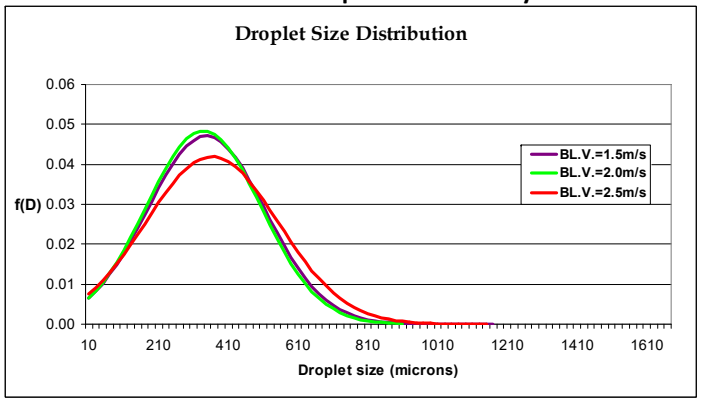

Effect of Inlet Nozzle Diameter

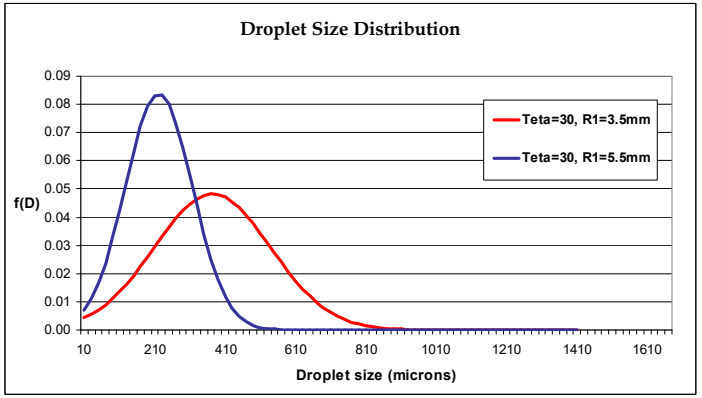

Example 1: Secondary Atomization

- Method to determine the size distribution:
  - Calculate the local mean size;
  - Determine the variation of the mean size across the nozzle;
  - Determine the local flow rate;
  - Determine the spray angle;
  - Determine both drop and steam velocities; and
  - Use the above information in a Spray Code to determine the spray characteristics downstream of the nozzle.

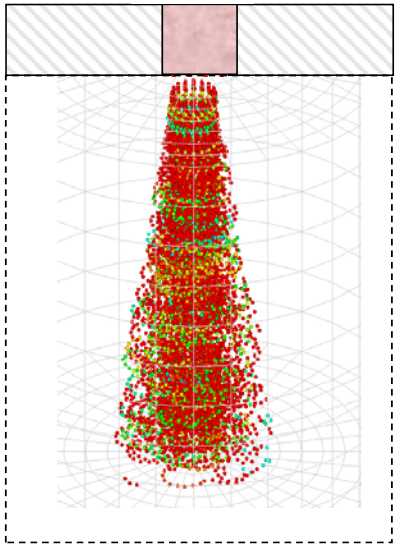

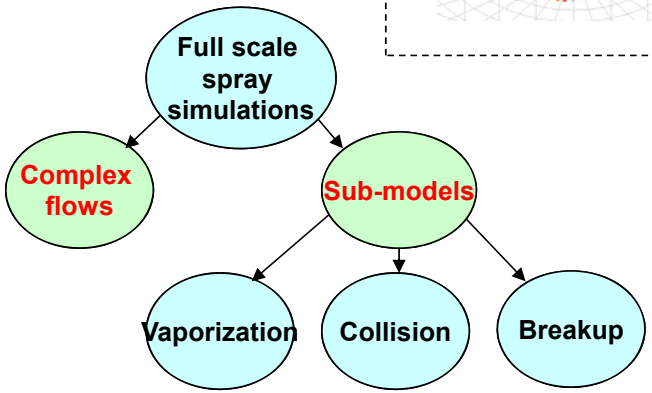

Example 1: A Black Liquor Burner

- 18 Spray nozzles tilted by 25^{o}, and mass flow rate of 65 GPM

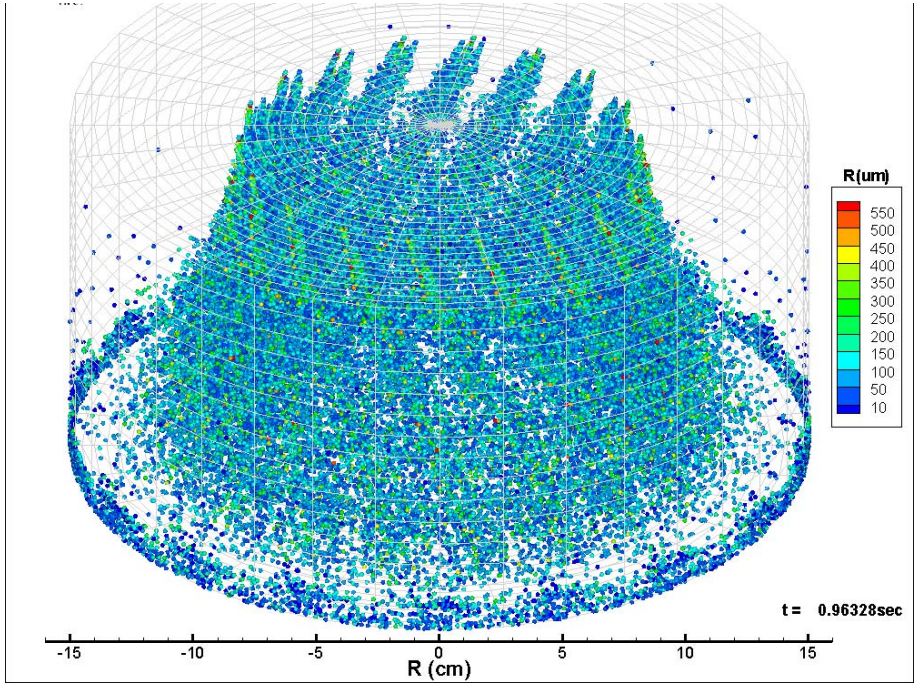

Example 1: Comparison with Experiment

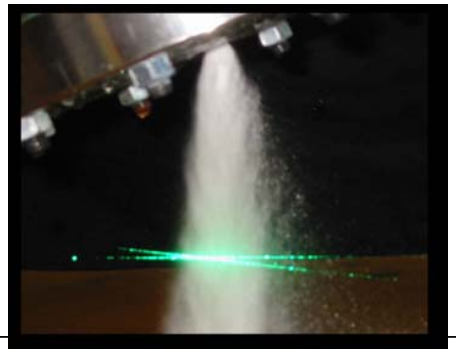

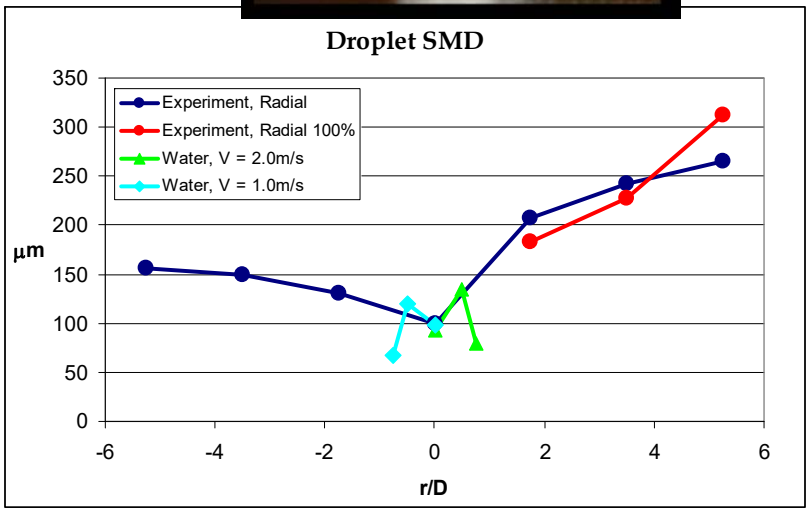

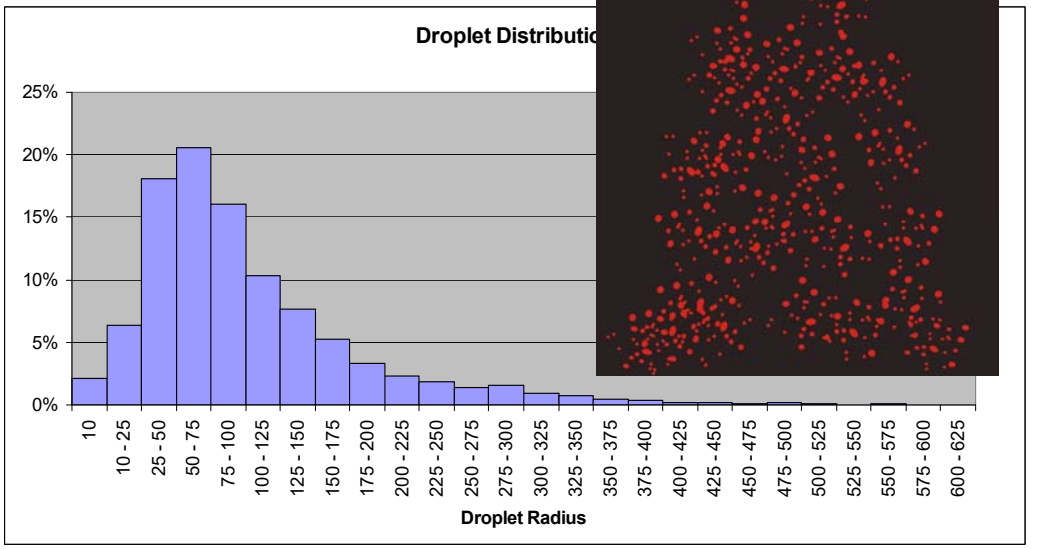

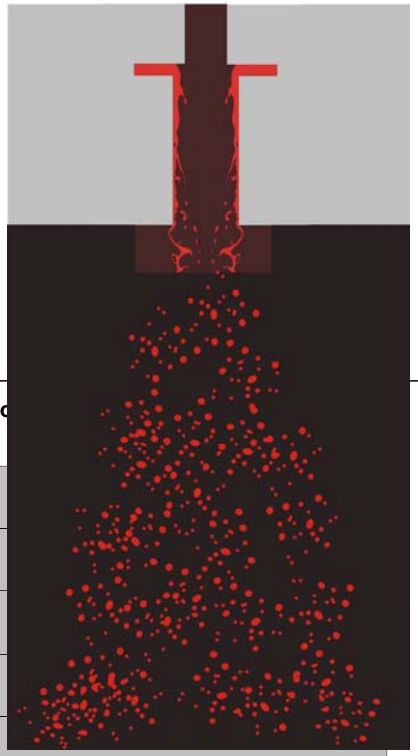

Example 2: Annular Nozzle for a coal Slurry Gasifier

- Passive division of oxygen into two outer and inner flows.

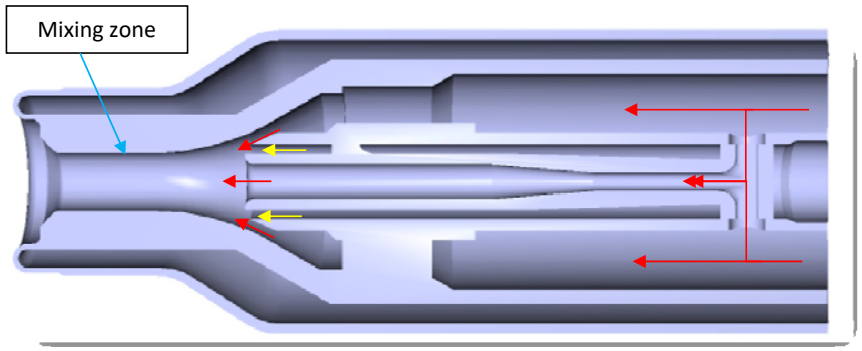

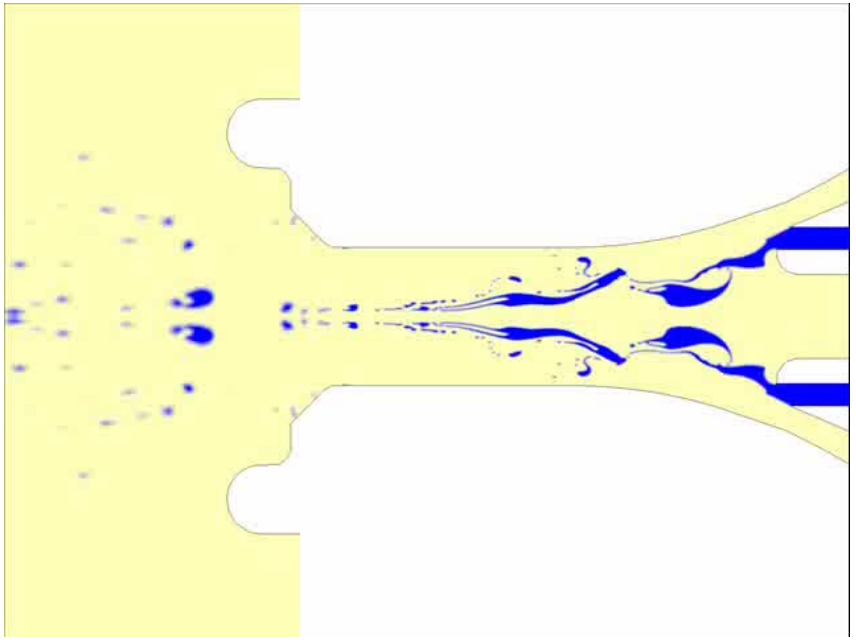

Example 2: Modeling the Primary Atomization

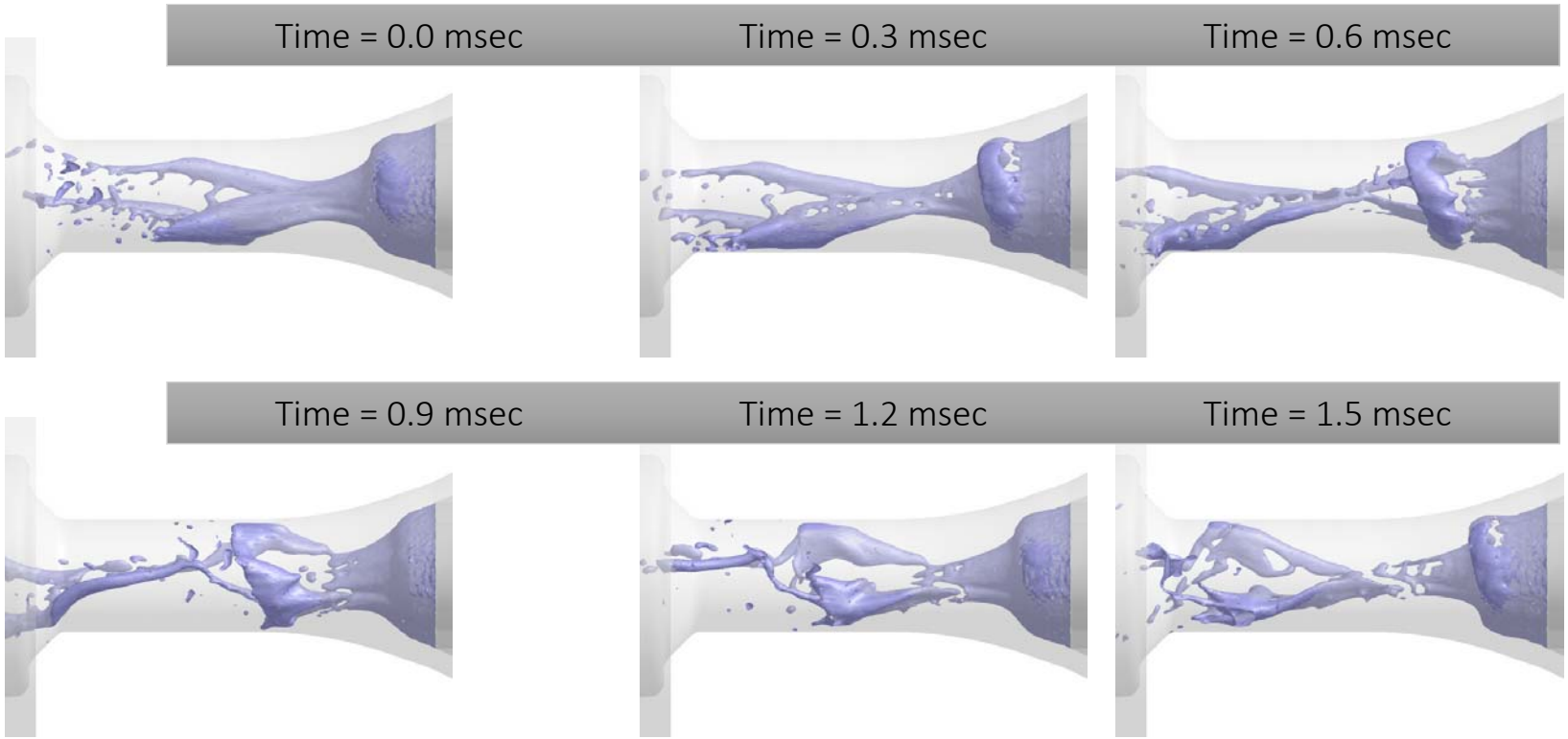

Secondary Atomization and SMD

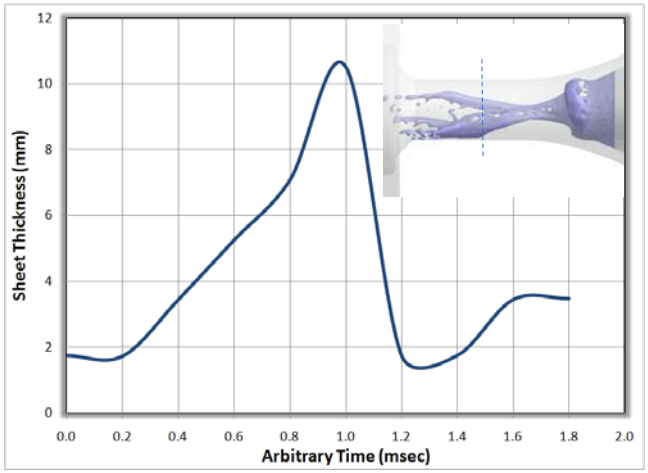

SMD= 26 microns

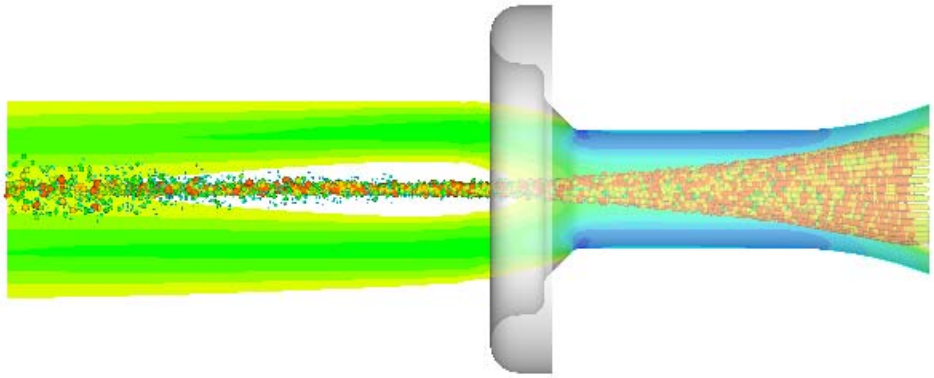

Mulhem et al. (coal slurry)

$$D_{32} = 0.21\, d_l\, (Oh)^{0.0622} \left(We_A \frac{\dot{m}_A}{\dot{m}_L} \right)^{-0.4}$$

Compares well with Mulhem correlations

Summary

- The liquid breakup process depends on the injection velocities, as well as fluid properties and ambient conditions.
- Generally, it is more difficult to atomize high viscosity liquids. However, by increasing the injection Reynolds number, the atomization improves, so much so that the effect of viscosity can become insignificant.
- High viscosity liquid result in large drops close to the nozzle, however, large drops eventually breakup into smaller drops further downstream through secondary atomization.
- A theoretical analysis can be used to determine the effect of different nozzle design parameters on the droplet size distribution downstream of the nozzle.

END

IFPRI meeting, Philadelphia, 18 June 2017

In-Line Sensors for Real-Time Analysis of Bulk Powders – A Review

Wuqiang Yang
University of Manchester, UK

Contents

1. Introduction

My qualification

- Professor of Electronic Instrumentation
- >28 year experience in instrumentation and measurement
- Research: electrical capacitance tomography (ECT) for multiphase process/flow measurement, including powder property/flow measurement
- Worked with companies, involving powder, such as
  - ✓ AstraZeneca, GEA – pharmaceutical
  - ✓ Dalian Inst. CP – methanol-to-olefins (MTO)
  - ✓ Inst Eng. Thermophysics – circulating fluidized bed (CFB) for clean coal combustion
  - ✓ Shanxi Coal Chemistry Inst. – coal-gasifying

- Organised a large EU consortium, working on powder flow/process

Powder is everywhere

- Power – pulverised coal in coal-fired power plants, CFB, coal-gasifying
- Pharmaceutical – fluidised bed for drying, granulation, coating
- Chemical – industrial chemicals, e.g. catalytic material for fluid catalytic cracking (FCC), MTO
- Food – flour, ground coffee, powder milk
- Others – cement, copy machine toner, gun-powder, cosmetic powder

The need

- In-Line Sensors for Real-Time Analysis of Bulk Powders are important for industries
- Very few in-line sensors available
- Examples of serious problem
  - ✓ >70% energy from direct burning of coal, PM2.5 in China
  - ✓ Explosion in Kunshan
- Challenges in powder flow measurement

2. In-line powder property sensors

Frequency range

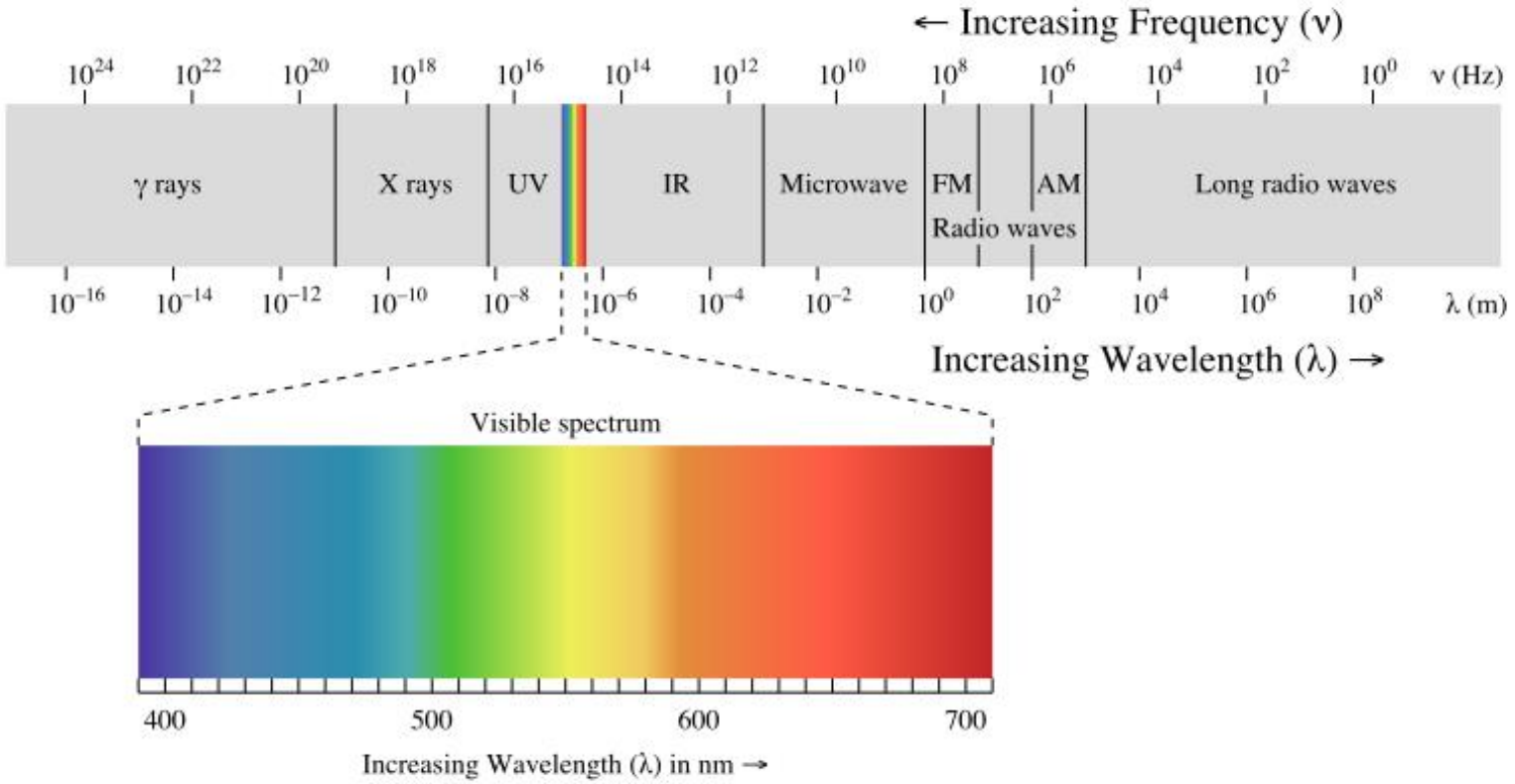

Powder property → sensor type / sensing modality

Powder properties (well known)

Property	Principle
Density	Radiation, ultrasonic
Moisture	Microwave, capacitance, infra-red
Particle size and distribution (shape)	Laser diffraction, PIV
Rheology and viscosity	Force

Other powder properties

- Surface texture, surface area
- Cohesion, adhesion
- Elasticity, plasticity
- Porosity

- Hygroscopicity
- Hardness / friability
- Amorphous content
- Potential for electrostatic charge

Examples of powder property sensor

1. Anton Paar density meter
2. ARTEC powder moisture meter
3. Malvern real-time in-line particle size analyser
4. Rheology Solutions in-line viscosity sensor
5. Lenterra Drag Force Flow Sensors (shear stress)

1. Anton Paar L-Dens 4X7 density meter

- Principle: unknown (ultrasonic?)
- Continuous density measurement
- 4-digit accuracy
- Used in petroleum, chemical and beverage industries

2. ARTEC MMA-9020 powder moisture meter

- Microwave (volumetric sub-THz microwave tomography)
- Look like mechanical movement for scanning
- Measure powder moisture
- PPM level

Problems

- Non-linearity
- Calibration
- Off-line?

3. Malvern Insitec real-time in-line particle size analyser

- Laser diffraction
- Range: 0.1 µm to 2.5 mm
- 4 measurements per second
- Application: dry, wet, spray
- Some ATEX
- Used in toners, pharmaceuticals, cement, minerals, powder coatings, pigments and metal powders

4. <u>Rheology Solutions</u> In-line viscosity sensor

- Measure viscosity, elasticity, processability and temperature of polymer powder

5. <u>Lenterra</u> Drag Force Flow (DFF) Sensors

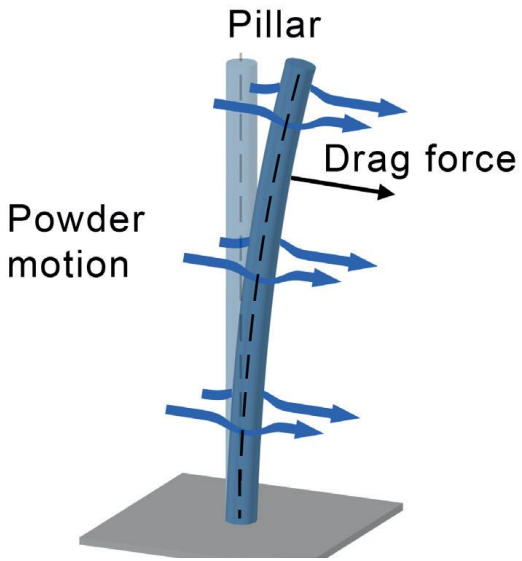

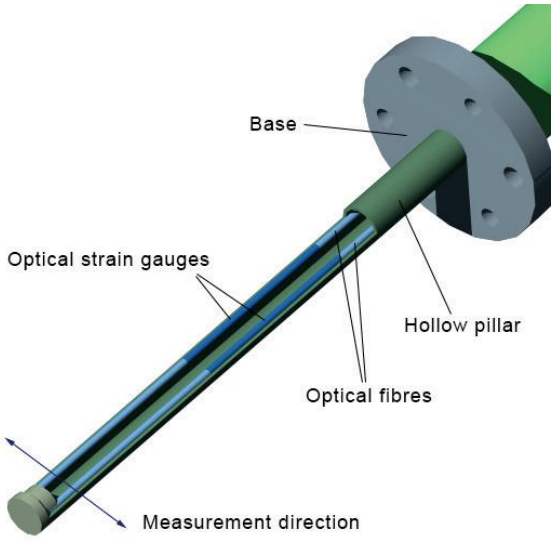

- Fiber Bragg Grating
- Measure drag force, and hence shear stress, in powder
- For pharmaceutical granulation

3. In-line powder flow sensors

Measured parameters

1. Concentration
2. Velocity

Sensing principles

1. Capacitance
2. Electromagnetic
3. Electrostatic/electrodynamic (triboelectric)
4. Optical
5. Microwave
6. Impact plate
7. Coriolis

1. Capacitance

- Principle: function of permittivity
- Non-intrusive and non-invasive
- Commonly used for concentration measurement, but non-linear and flow-regime-dependent
- Also used for velocity measurement by cross correlation, but measure superficial velocity only.

Thermofisher Scientific Ramsey Granucor Solids Flow Metre

- Endress+Hauser → Ramsey → Thermofisher Scientific
- DC13 capacitance sensors for concentration measurement
- DK13 capacitance sensors for flow velocity measurement by cross correlation

- For dense flow in pneumatic conveyor and loading

2. Electromagnetic (EM)

- Non-intrusive and non-invasive
- Limited to conductive flow (powder?)

SWR DensFlow

- For mass flowrate of dense flow in pneumatic conveyor
- No dead spots for residue to form
- Unlimited throughout
- Accuracy independent of flow speed, ±2 to 5%
- Velocity range: 1-10 m/s
- Maintenance-free
- Minimal distance to pipe bends and baffles required

SWR MaxxFlow HTC

- Measure high mass flowrate for bulk solids
- Particularly for free fall after belt conveyors and rotary valves
- Velocity measurement by correlation
- Diameter: 220-310 mm
- Velocity requirement: 1.7-3 m/s
- Accuracy: ±3%

3. Electrostatic/electrodynamic

- Passive sensing
- Simple, safe, non-hazardous operation
- Low maintenance
- Invasive (i.e. contact)
- Some non-intrusive, some intrusive
- Non-uniform sensitivity distribution
- Velocity measurement by cross-correlation
- Mass flowrate measurement based on assumption that signal strength is proportional to flowrate

ABB PfMaster Pulverized Fuel Flowmeter

- On-line measurement of pulverized-fuel (pf) distribution (pf split), absolute velocity and mass flowrate
- For lean flow, e.g. coal-fired power stations and blast furnaces to improve combustion efficiency and reduces emissions
- Not affected by changes in coal type and moisture content (?)
- No on-site calibration required?
- Velocity range: 0.3 to 60 m/s
- Pipe size: DN25 to DN600

Mütec Flowswitch FS600E

- For flow control, e.g. pneumatic conveyor, feeder or gravity chute
- Range of mass flow from g/h to T/h

4. Optical

MSE Meili Labasys 100

- Laser diode and optical fibre
- Intrusive and invasive
- Online measurement of concentration and velocity simultaneously

- For CFB, FCC, cyclone, mixing, granulation, pneumatic conveyor, drying
- Automatic cleaning

Mettler Toledo FBRM G400/G600

- Similar to MSE Meili Labasys 100
- Real-time online particle analysis

Dantec Dynamics Laser Doppler

- Online measurement of 1D to 3D particle velocity and concentration
- For particle dynamics analysis

Dantec Dynamics PIV (particle imaging velocity)

- Non-contact
- Measure 3D particle velocity

5. Microwave

- Non-intrusive and non-invasive
- No moving mechanical parts

SWR Microwave Solids Flow 2.0

- Microwave reflection
- Work in metal pipe for free fall and pneumatic conveyor
- Range: up to 20 T/h

- Accuracy: ± 2-5 %
- Feature: active roping compensation

SWR Microwave Radar FlowJam S Material flow monitoring

- Microwave Doppler
- Insensitive to material deposits
- No limit in diameter
- Signalling through relay switching with different sensitivity
- Detection through non-conductive wall
- Range: 0-2 m
- Min. velocity: 0.1 m/s

Endress and Hauser Microwave FTR20 Flow indicator for bulk solids

- Microwave Doppler
- Mass flowrate measurement
- For flow/no flow detection
- Adjustable sensitivity

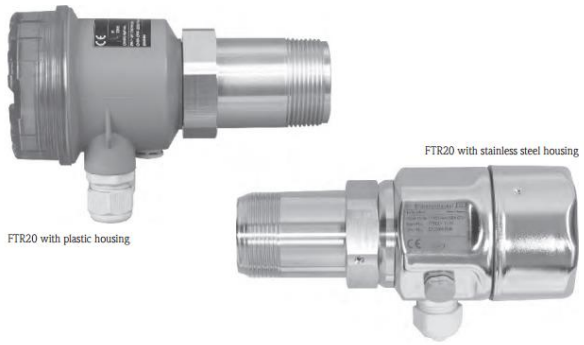

Thermofisher Scientific Granuflow DTR and GTR Non-Contact Flow Sensor

- Microwave Doppler
- Flow/no-flow detector

Promecon Microwave MECONTROL coal online measurement system for measuring fuel mass flow

- Microwave for concentration
- Cross-correlation for velocity
- Balance fuel flow to burners
- Manage mill heat balance and mill dynamics
- Reduce boiler load swings
- Mass-flow measurement of pulverised coal and biomass

- Independent measurement of velocity and density
- Calibration and maintenance free

Mütec MF3000 microwave mass flow meter

- Microwave Doppler
- Flow meas. in metallic pipe
- Range from kg/h to T/h
- Measure powder, dust, pellets, and granules from 1 nm - 2 cm
- Not affected by dust accumulation

Mütec: Microwave Flow Switch FS510

- Microwave Doppler
- Flow switch

Monitor Technologies LLT Microwave QuantiMass™ PrO

- Microwave Doppler
- Measure flow quantities in pneumatic conveyor and free-falling
- Accuracy: 1-3%
- Suitable for powders, dust, pellets, and granular up to 0.75 inch (2 cm)

6. Impact plate

- Impact force detected by load cell/strain gauges

Siemens SITRANS WF series

- Measure horizontal deflection
- For flowrate measurement of gravity feeding
- Max. rate: 1-900 T/h
- Applications: food, grain, milling, animal feed, plastics, glass, aggregates, grain, cement, mineral processing
- Accuracy: ±1% (33 to 100% of rate)

Thermofisher Scientific RamseyTM DE10 and DE20 Impact Weighers

- Measure mass flowrate and total mass of free-flowing dry solids and powders
- Ideal for vertical streams
- Range: D10: 4.54 to 726 T/h
  D20: 0.27 to 36 T/h

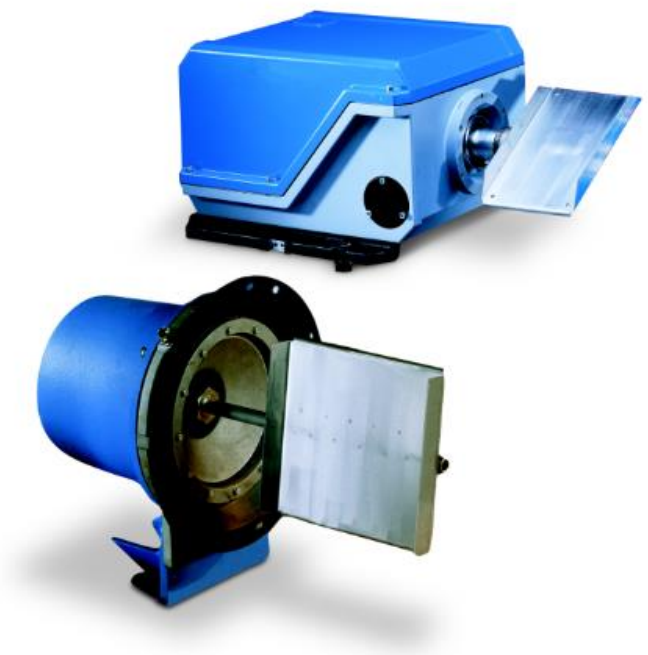

Schenck Multistream ® B

- In-line measurement of continuous flow rate and totalized amount
- Pulverized to granular materials with a grain size of up to 30 mm
- Range: 100 T/h, or max. 80 m^3/h
- Applications: flowrate and consumption measurement, totalization and batching
- Accuracy: ± 2% of nominal flowrate
- Turndown ratio: 1:5
- Bulk density: min. 0,4 T/m^3
- Grain size: max. 10 mm

Schenck DLM Solids Flow Meter

- Impact plate with curved guide chute
- Radial acceleration and chute deflection detected by load cell
- Measures high flowrate of free-flowing pulverized or granular materials
- Range: 30 to 600 T/h
- Accuracy: ± 2%
- Repeatability: 0.5%

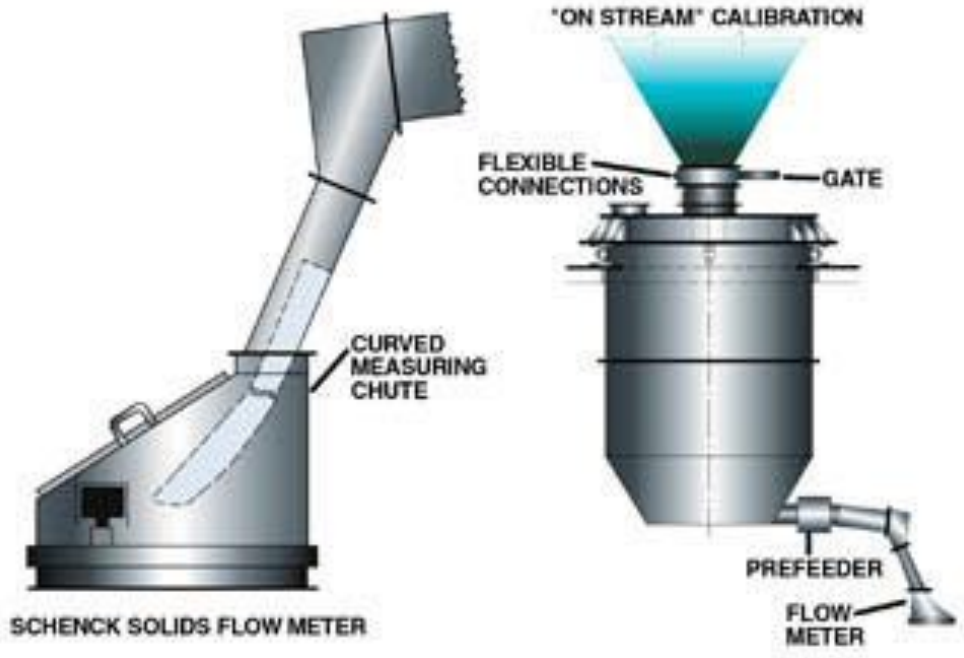

7. Coriolis

Schenck MULTICOR® S Coriolis particle flow meters

- Measure torque caused by Coriolis force on a wheel rotating at constant speed
- Torque is detected by strain-gauge load cell
- Provide flow rate
- Accuracy: ±0.5%
- Not affected by material density, friction or in-feed drop height

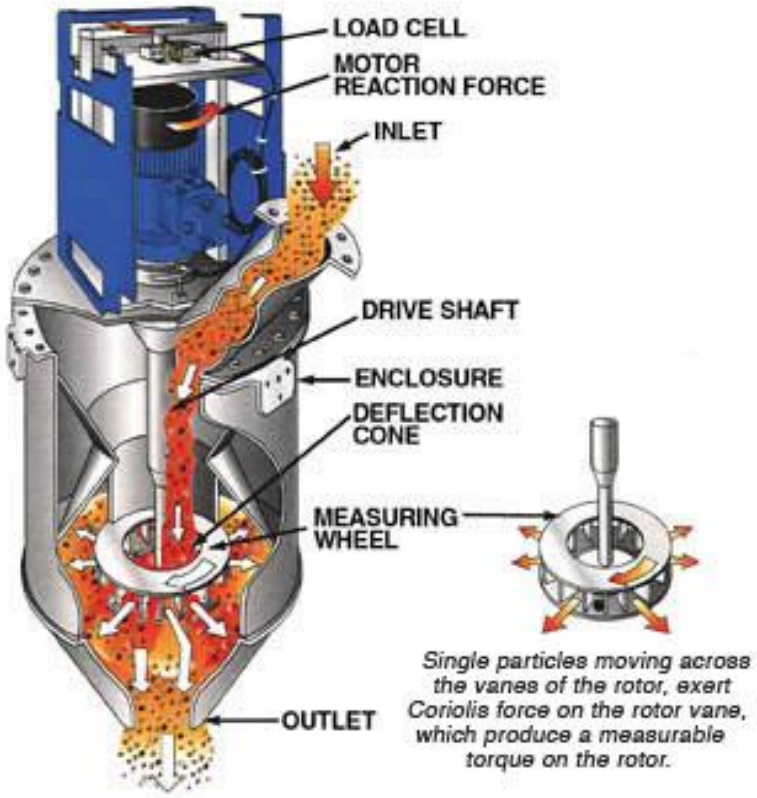

- Range: 0.5 to 150 T/h
- Simple calibration
- Suited for throughput and consumption measurement, totalizing batching of free to moderately flowing dry materials.

4. ECT and in-line measurement in pharmaceutical fluidized beds

- Based on capacitance measurement
- Interrogate a dielectric process from many angles
- Reconstruct ε distribution

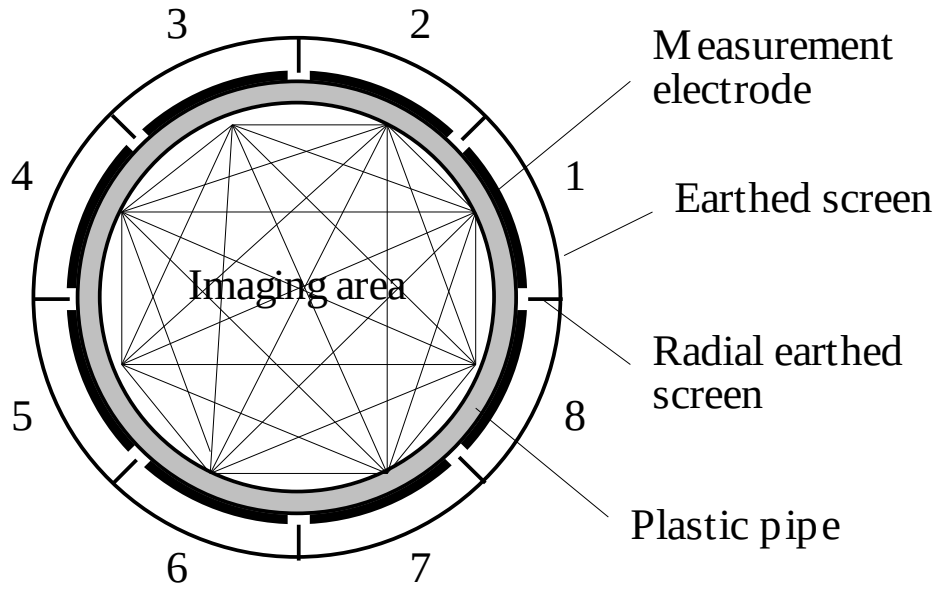

$$M = \frac{N(N-1)}{2}$$

Information from ECT images

- Powder distribution → flow regime
- Powder concentration, e.g. % of pulverised coal in nozzles or fluidized bed reactor
- Flow velocity profile by cross-correlation
- Non-measurable → measurable and hence controllable

Advantages of ECT over other tomography modalities

- No radioactive source
- Non-intrusive and non-invasive
- Fast (typically 100 frames per second)
- Robust & withstanding HTHP
- Low cost

Disadvantage

- Moderate image resolution

Key in hardware

- Small capacitance: 0.01 fF (1×10^{-5} pF)
- High speed: >100 frames/second
- High SNR: > 60 dB

Key in maths

- Non-linearity between C and ε
- Under-determined solution because of limited measurements
- Ill-posed ill-conditioned inverse problem

Key in engineering

- Scale-up (1 m) and scale-down (1 cm)
- Re-engineering ECT sensors (HP)
- Intrinsic safety, explosion-proof (tested) and ATEX

Image reconstruction

Assign ε value to each pixel according to measured *C*, i.e. to solve inverse problem

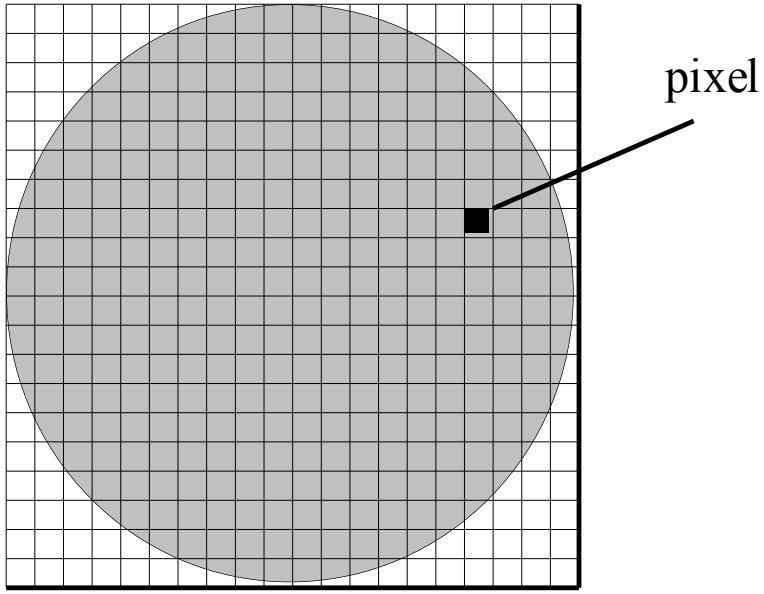

64x64 pixels (≈4,000)

Image reconstruction algorithms

Simplified forward problem: $\mathbf{C} = \mathbf{S}\varepsilon$

Linear back-projection (LBP) $\varepsilon \approx \mathbf{S}^T\mathbf{C}$

Tikhonov $\varepsilon = \left(\mathbf{S^T S} + \mu\mathbf{I}\right)^{-1}\mathbf{S^T C}$

Landweber iteration, $\varepsilon_{k+1} = \varepsilon_k + \alpha S^T\left(\lambda - S\varepsilon_k\right)$

Modified Newton-Raphson $\varepsilon_{k+1} = \varepsilon_k + \left(S^T S + \mu I\right)^{-1} S^T\left(\lambda - S\varepsilon_k\right)$

AC-ECT system

- 16 measurement channels in parallel
- 300 frames/second
- 73 dB SNR

- Twin-plane
- Anti-electrostatics
- Real-time 3D imaging

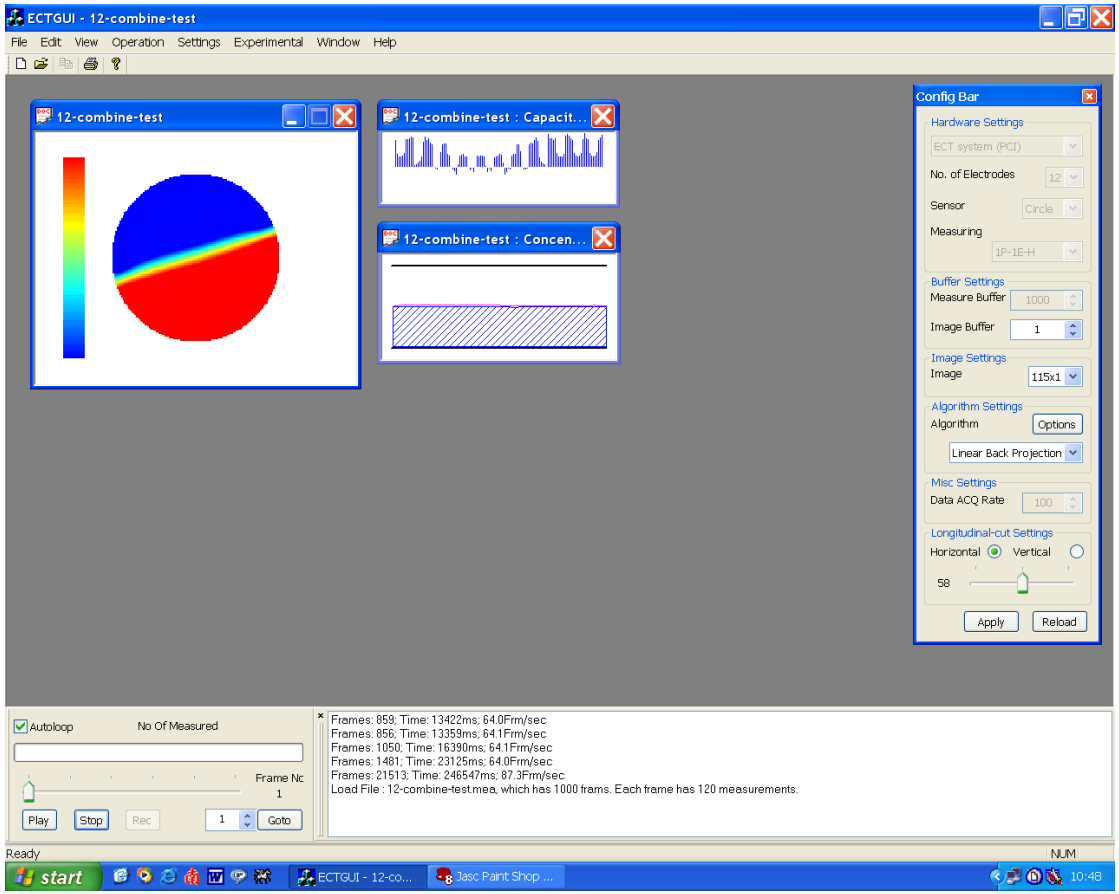


Schlumberger
PETRONAS
AIRBUS
Honeywell
NASA
AstraZeneca
GEA
Sherwood
Sherwood Scientific Ltd
DUPONT
The miracles of science
PŁ
JEJU
1952
NUS
National University
of Singapore
Tsinghua University
清華大學
中國科學院
CHINESE ACADEMY OF SCIENCES
ROLLS
ROYCE
Rolls-Royce
IET
AALBORG UNIVERSITY
DENMARK
CHIBA
UNIVERSITY
RUNMING UNIVERSITY OF SCIENCE AND TECHNOLOGY
中國科學院大連化學物理研究所
DALIAN INSTITUTE OF CHEMICAL PHYSICS,CHINESE ACADEMY OF SCIENCES
Institute of Coal Chemistry, Chinese Academy of Sciences

In-line measurement in pharmaceutical fluidized beds

- 4 last processes to make tablets: granulation, drying, compression, coating, 3 of them in fluidised beds

(a) Granulation

(b) Drying

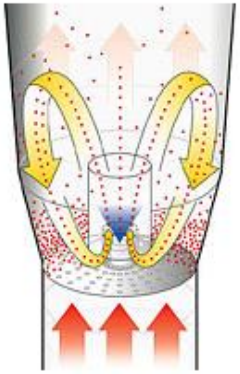

(c) Coating

- Problem in industry: Black box $\rightarrow$ trial-and-error
  $\rightarrow$ Less efficient, longer time, more energy, more pollution, poor product quality (e.g. agglomeration)
- ECT can provide images of gas/powder distribution, moisture distribution, dynamic process

Lab-scale (20 cm)

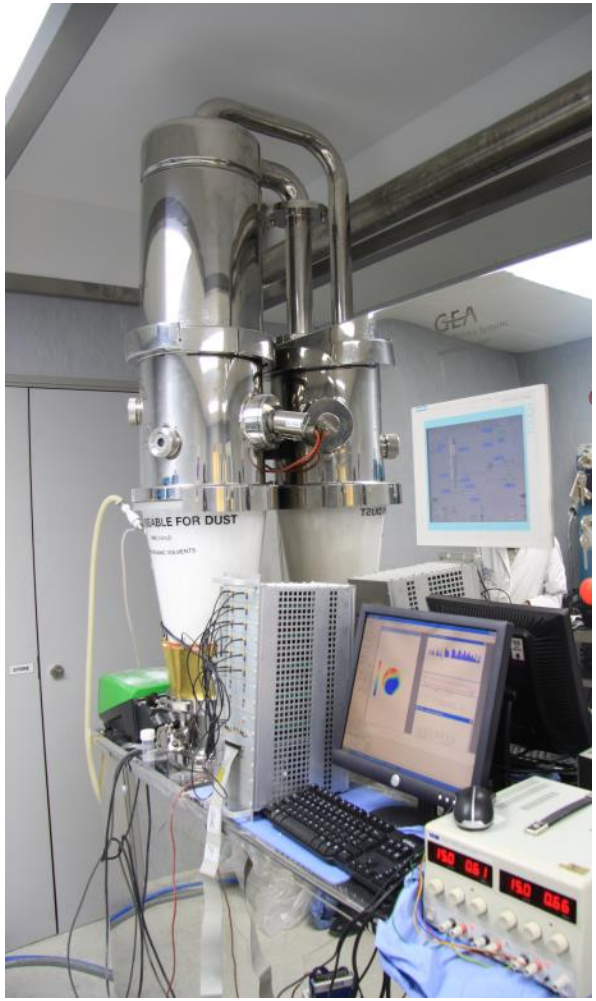

Semi-scale (50 cm)

Production-scale (1 meter)

Moisture measurements of drying process

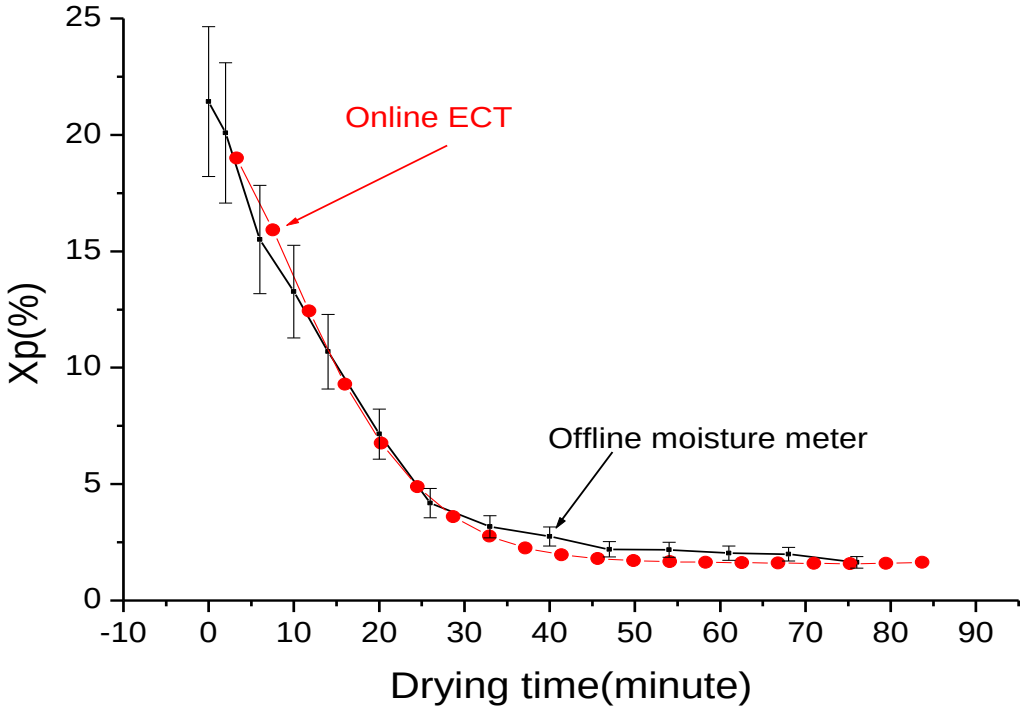

- Online ECT measurements vs. offline moisture meter
- In good agreement within 0.1%

Gas/powder flow

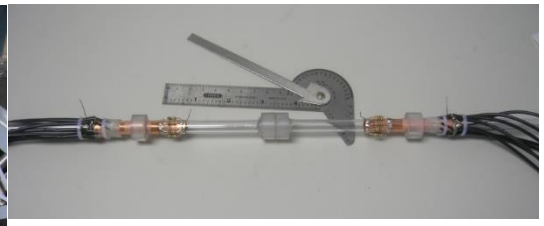

Gas/solids flow

Gas/solids cyclone

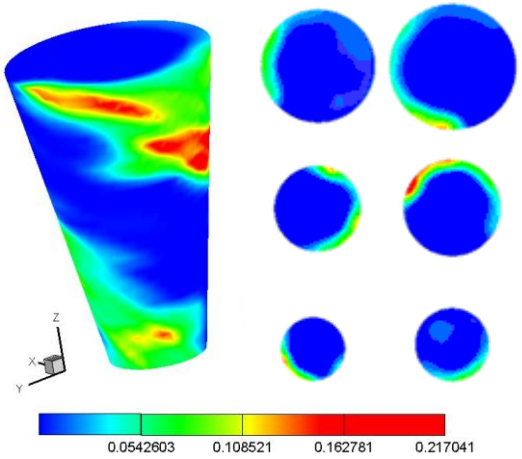

Multi-cyclone

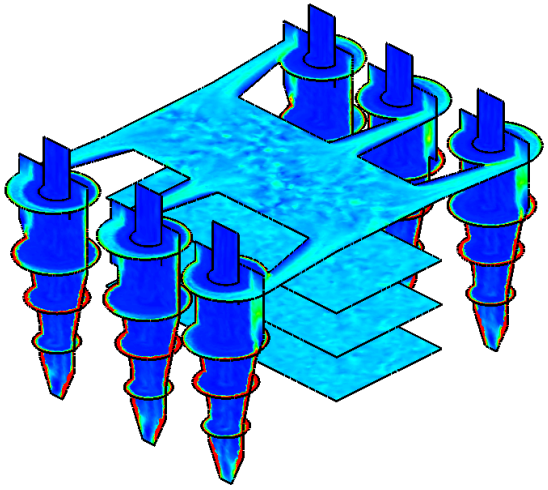

5. Summary